Corpora Non Agunt Nisi Fixata:

Ligand-Receptor Binding Kinetics in G Protein-Coupled Receptors

By Lizi Xia

The research described in this thesis was performed at the Division of Medicinal Chemistry of the Leiden Academic Centre for Drug Research (LACDR), Leiden University (Leiden, the Netherlands). The research was financially supported by EU/EFPIA Innovative Medicines Initiative Joint Undertaking, K4DD grant n^{o} 115366.

Printed by Gildprint. The cost of printing is sponsored by LACDR, Leiden University and PerkinElmer Nederland B.V..

Cover design: Yuejiao Cheng

Thesis layout: Lizi Xia

ISBN: 978-94-6233-953-8

Corpora Non Agunt Nisi Fixata:

Ligand Receptor Binding Kinetics in G Protein-Coupled Receptors

Proefschrift

Ter verkrijging van

de graad van Doctor aan de Universiteit Leiden,

op gezag van Rector Magnificus prof. mr. C. J. J. M. Stolker,

volgens besluit van het College voor Promoties

te verdedigen op woensdag 30 Mei 2018

klokke 13.15 uur

door

Lizi Xia

geboren te Luzhou, China

in 1983

Promotor: Prof. Dr. A. P. IJzerman

Co-promotor: Dr. L. H. Heitman

Promotiecommissie:

Prof. Dr. Hubertus Irth (Chair)

Prof. Dr. Joke Bouwstra (Secretary)

Prof. Dr. Steven Charlton/ University of Nottingham

Prof. Dr. Stephen Hill/ University of Nottingham

Prof. Dr. Bob van de Water

Prof. Dr. Mario van der Stelt

To my dear parents,

my wife,

my son,

and all my friends

献给我挚爱的亲朋好友

Content

Chapter 1

General Introduction

About this thesis

"A journey of a thousand miles begins with a single step (千里之行始于足下)". Similarly, pharmacological effects are triggered by the initial step of drug-target binding. This thesis focuses on the kinetics of binding interactions between ligands (drugs) and various G protein-coupled receptors (GPCR). GPCR are one of the largest and most important drug target families; many drugs in use today target these pharmaceutically relevant proteins.[1] However, many candidate drugs are still neither efficacious nor safe.[2] Thus the traditional affinity- or potency-based rationale in the early phases of drug discovery may need to be reconsidered. Although binding kinetics. i.e. the rate with which a ligand associates to and dissociates from the target, has been studied on a few drug target classes, the concept of binding kinetics has been emerging over the last decade as an additional and relevant selection criterion in the drug discovery pipeline.[3, 4]

To describe the importance and relevance of the research performed in this thesis, this chapter serves as a general introduction. First, the GPCR will be introduced. Second, the two families of human cannabinoid and human adenosine receptors will be mentioned; more specifically, both the human cannabinoid receptor 1 (hCB_1) and the human adenosine A_1 and A_3 (hA_1 and hA_3) receptors will be outlined as prototypical GPCR as well as potential drug targets. These targets are then the main "actors" in the subsequent experimental chapters of this thesis. Furthermore, the concept of binding kinetics will be presented in a chronological way, including some practical requirements for the early phase of drug discovery. Finally, the aim and scope of this thesis will be explained.

What are GPCR ?

GPCR are membrane bound proteins, composed of seven transmembrane helices with extracellular and intracellular loops and an extracellular (N-terminal) and intracellular (C-terminal) tail. They play key roles in physiology by detecting external stimuli (e.g. chemical small molecules, endogenous ligands, or photons) and activating internal signal transduction pathways and eventually physiological responses (**Figure 1A**). An agonist is able to bind to and activate a GPCR to produce a biological response. In contrast, a (neutral) antagonist blocks the action of the (endogenous) agonist, while an inverse agonist causes an action opposite to that of the agonist, i.e. decreasing the basal level of receptor activity (**Figure 1B**). Since GPCR are involved in various critical functions, it may not be surprising that GPCR are the target of about 30% of all drugs on the market.[5] Much of the current understanding of the structure and function of GPCR results from the pioneering research on the rhodopsin and β_2 adrenoceptor. As a result, Robert Lefkowitz and Brian Kobilka were awarded the 2012 Nobel prize in chemistry.[6, 7] However, key questions still remain unanswered in the GPCR field. For instance, although the ligand-GPCR complex can be observed, the detailed molecular recognition or complex stability is unknown.

A.

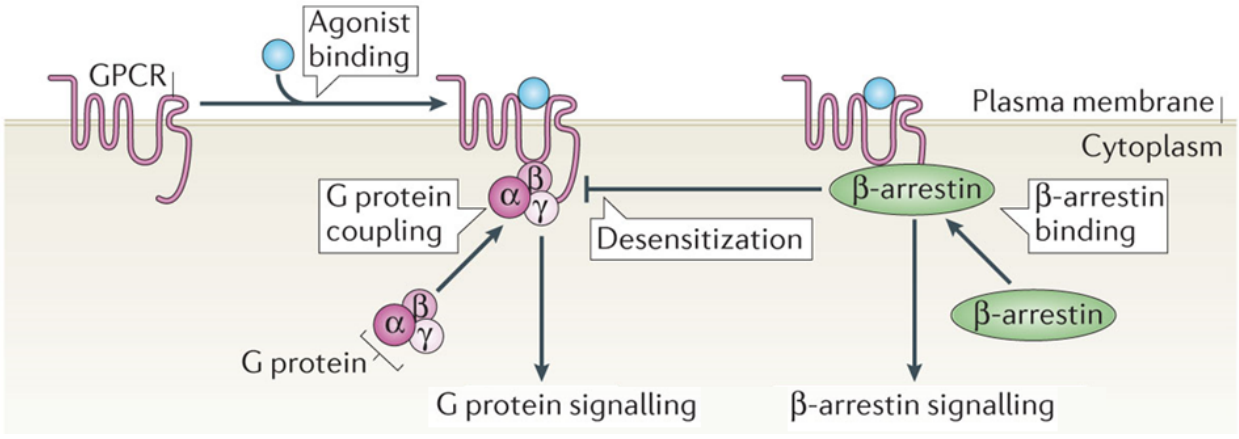

B.

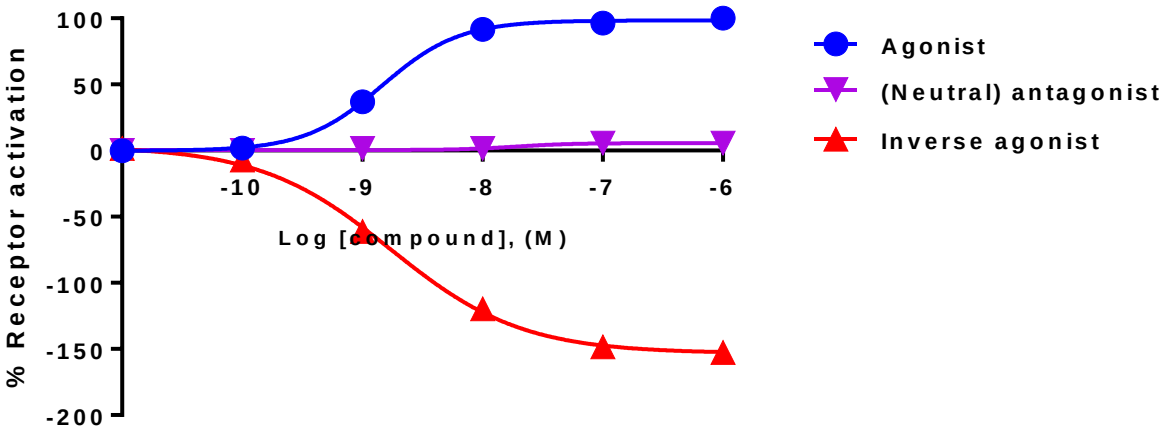

Figure 1: Panel **A**) A simplified schematic of GPCR signaling by agonist (activating ligand) binding. One GPCR can be activated through G protein-dependent (G protein coupling) and G protein-independent (β-arrestin binding) pathways, adapted from the review of Ghosh et al.[8] Panel **B**) Theoretical graph showing: 1) dose-dependent receptor activation by an agonist (blue curve); 2) a (neutral) antagonist that in this concept simply prevents the agonist from binding and, hence, from activating the receptor and more downstream signaling pathways (purple curve); and 3) an inverse agonist that in this concept also competes for binding with the agonist, however, it causes a subsequent decrease of basal receptor activity (red curve).

GPCR studied in this thesis

As recorded by the International Union of Basic and Clinical Pharmacology (IUPHAR) Committee on Receptor Nomenclature and Drug Classification, there are about 800 GPCR identified in the human body; The largest GPCR class is the one of rhodopsin-like GPCR, also known as class A GPCR.[8] It would be a daunting task to study all of them. As a result, this thesis is focused on a few, as prototypical examples.

Human cannabinoid 1 (hCB_1) receptor

Within the endocannabinoid system (ECS) two human cannabinoid receptor subtypes have been identified: the human CB_1 (hCB_1) receptor and the human CB_2 (hCB_2) receptor. They are primarily activated by endogenous cannabinoids (endocannabinoids, ECs), including anandamide (or N-

arachidonylethanolamine, AEA) and 2-arachidonoylglycerol (2-AG).[9, 10] The hCB_1 and hCB_2 receptors show 44% overall sequence homology, and display different pharmacological profiles.[11] Due to the long history of *Cannabis sativa* use,[12] a diversity of effects initiated through hCB_1 receptor activation by the plant's main psychoactive component, Δ^9-THC, has been described. These effects include feeling high, alteration of time perception, an increase in body sway and the munchies (i.e. the extreme desire for and enjoyment of food-intake).[13] It has been shown that the latter can also be triggered through activation of the hCB_1 receptor by endocannabinoids (ECs) from breast milk or other food products.[14-16]

The hCB_1 receptor is expressed in the central nervous system (CNS) and is also widely distributed in the peripheral nervous system (PNS) and peripheral tissues,[10, 17] including heart, liver, lung, gastrointestinal tract, pancreas and adipose tissue.[18, 19] The broad presence of the hCB_1 receptor in a variety of complex physiological systems provides numerous opportunities for the development of new medications. In the particular case of obesity, the ECS, including the hCB_1 receptor, is overactive with increased levels of endocannabinoids in plasma, and in central and peripheral tissues.[20] Therefore, blockade of the hCB_1 receptor is a potential approach for the treatment of obesity.

Rimonabant, a hCB_1 receptor inverse agonist, was developed by Sanofi-Aventis and introduced on the market in Europe in 2006. However, it was quickly withdrawn from the market due to the risk of unacceptable psychiatric side effects.[21-23] Many other hCB_1 receptor antagonists entered clinical trials, such as taranabant [24] and otenabant,[25] however, they were not developed further due to similar psychiatric side effects despite their different chemical structures. Although researchers have experienced many setbacks on this drug target, the intensive drug discovery efforts have never been terminated. Since 2016, a series of crystal-structures of the hCB_1 receptor have been resolved with antagonists (i.e. AM6538 and taranabant, [26, 27] **Figure 2A** and **2B**) or agonists (i.e. AM11542 and AM841,[28] **Figure 2C** and **2D**). Therefore, those hCB_1 receptor structures provide a molecular basis for

predicting the binding modes of hCB1 ligands, and may help in the future development of better drug candidates for the hCB_1 receptor.

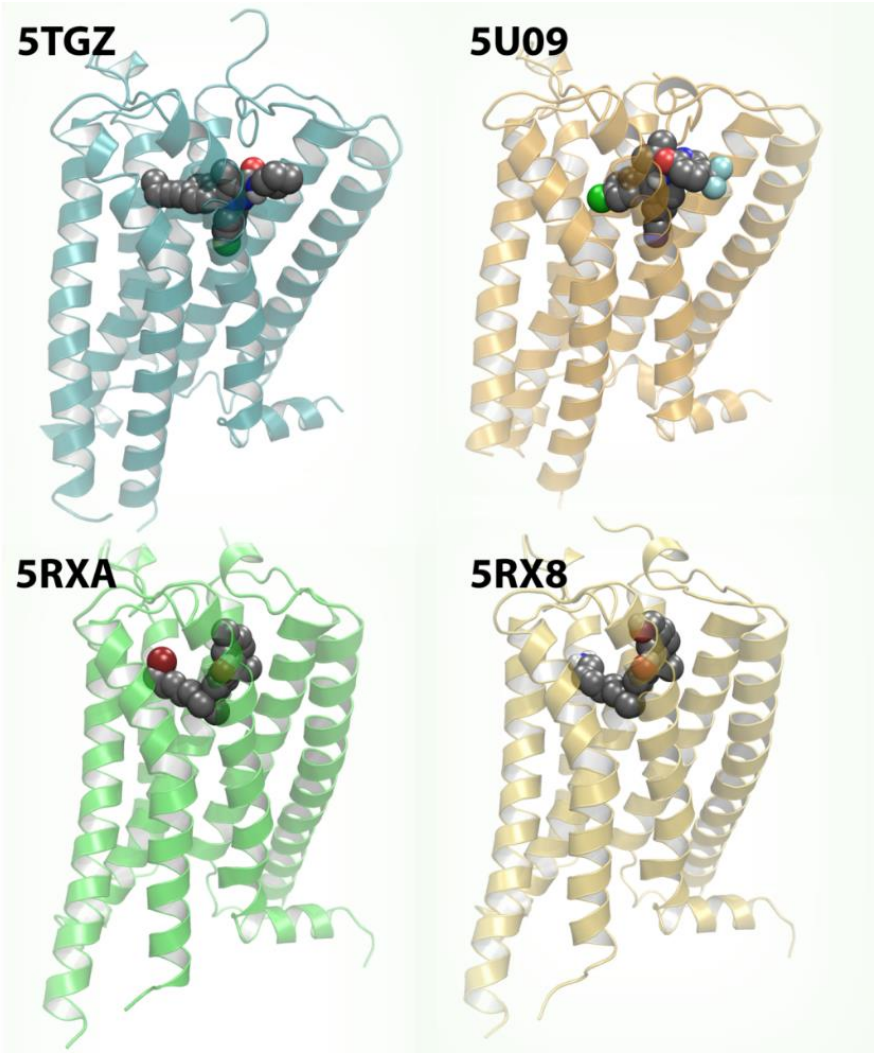

Figure 2: Crystal structures of hCB_1 receptor with various ligands. The typical seven helices of hCB_1 receptors are shown as ribbons and the intracellular and extracellular domains are present as loops. Panel **A** (upper left): Global structure of the hCB_1 receptor in complex with the antagonist AM6538[26] (PDB: 5TGZ). The receptor is shown in cyan cartoon representation. Panel **B** (upper right): Global structure of the hCB_1 receptor in complex with the antagonist taranabant[27] (PDB: 5U09). The receptor is represented as a yellow cartoon. Panel **C** (lower left): Global structure of the hCB_1 receptor in complex with the agonist AM11542[28] (PDB: 5XRA). The receptor is represented as a green cartoon. Panel **D** (lower right): Global structure of hCB_1 receptor in complex with the agonist AM841 [28] (PDB: 5XR8). The receptor is represented as a light yellow cartoon. All the ligands are presented in a space-filling style and their atoms color coded: black = carbon, red = oxygen, blue = nitrogen, green = chlorine, cyan = fluorine.

Human adenosine A_1 and A_3 (hA_1 and hA_3) receptor

Human adenosine A_1 and A_3 receptors belong to the family of human adenosine receptors with four distinct subtypes (hA_1, hA_{2A}, hA_{2B} and hA_3).[29] Although all subtypes are activated by the endogenous and ubiquitous local hormone adenosine, these purinergic receptors differ in their distribution and to which G protein they are coupled. Classically, following agonist activation hA_1 and hA_3 receptors induce a decrease in cyclic adenosine monophosphate (cAMP) levels due to their primary coupling to G_i proteins, while hA_{2A} and hA_{2B} receptors couple to G_s proteins and stimulate cAMP formation.[30]

Both hA_1 and hA_3 receptors have similar clinical potential for the treatment of ischemia-reperfusion injury,[31] renal disease,[32] and neuropathic pain.[33, 34] Besides, two hA_3 agonists have moved forward into a series of clinical trials: for IB-MECA, in total twelve completed or planned trials have been reported related to inflammatory conditions (e.g. keratoconjunctivitis sicca, rheumatoid arthritis, psoriasis, uveitis, etc.); for 2-Cl-IB-MECA, four trials have been registered for liver diseases (e.g. hepatocellular carcinoma, hepatitis C).[35, 36] Nevertheless, distinct pharmacological effects related to hA_1 and hA_3 receptors (i.e. cardioprotection[31, 37, 38] and neuroprotection[39]) can be ascribed to their different downstream effectors. For cardioprotection, the hA_1 receptor is linked to the atrial cardiac myocyte potassium channel and to phospholipase C, while the hA_3 receptor has been found to couple to not only phospholipase C but also phospholipase D; such plausible "hA_1 receptor – PLC" and "hA_3 receptor – PLD" signaling pathways may indicate distinct effects in the heart.[40, 41] For neuroprotection, the hA_1 receptor is activated acutely to inhibit neuronal calcium transients;[42] whereas hA_3 receptor activation in astrocytes results in a release of neuroprotective CCL2.[43]

Last but not least, the crystal structure of hA_1 receptor has been resolved quite recently (**Figure 3**).[44] Such progress suggests that the binding interaction of ligands on the hA_1 receptor will be better understood in the near future. Moreover, this structure also aids in understanding the binding modes of hA_3 receptor ligands, since this receptor is quite similar to hA_1 receptors.[29]

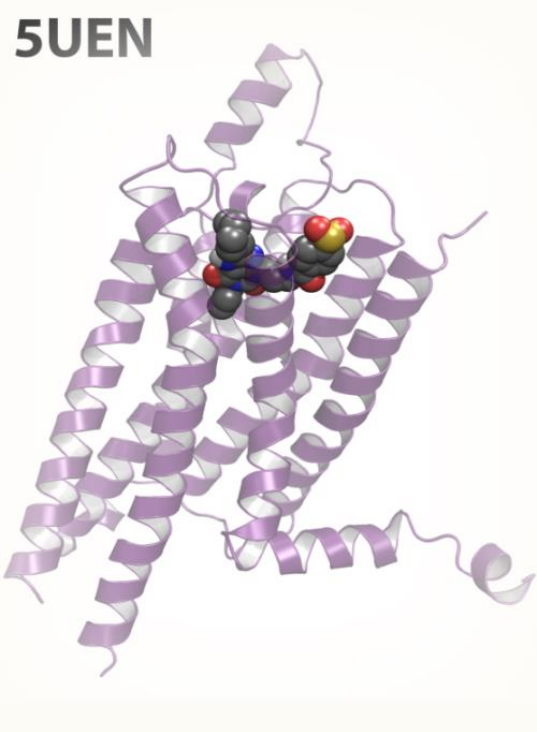

Figure 3: Global crystal structure of hA_1 receptor in complex with the antagonist DU172 (PDB: 5UEN).[44] The typical seven helices of hA_1 receptors are shown as ribbons and the intracellular and extracellular domains are present as loops. The receptor is represented as a purple cartoon. DU172 is presented in a space-filling style and its atoms are color coded: black = carbon, red = oxygen, blue = nitrogen, yellow = sulfur.

The concept of binding kinetics at these representative GPCR is not completely new. For example, a hCB_1 antagonist and negative allosteric modulators have been studied in this context,[45, 46] as are the human adenosine receptors.[47] However, key questions are remaining:

- Can we characterize ligands with a "good" kinetic profile on these receptors?
- Can we establish structure-kinetics relationships (SKR) of ligands for these receptors?
- Can we improve the technology of the kinetic assays on these receptors?
- Can we confirm that a ligand with "good" kinetic profile leads to target selectivity and clinical efficacy and/or safety?

To answer these questions, the concept of binding kinetics shall be introduced.

Historical aspects of drug-target binding kinetics

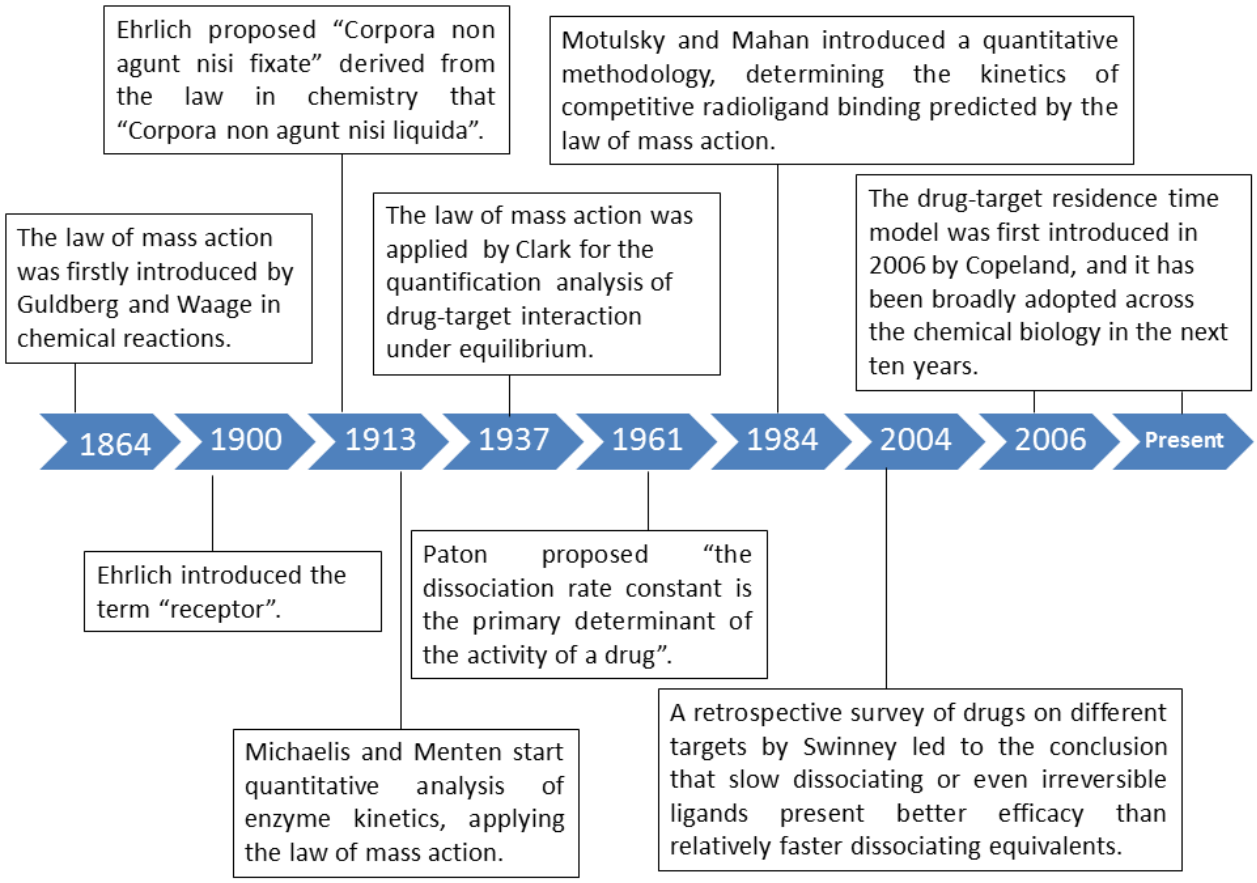

Figure 4: The emergence of binding kinetics studies.

The concept and study of drug-target binding kinetics have emerged since the evolution of modern pharmacology (**Figure 4**). In the 19th century, the law of mass action was firstly described in chemical reactions, while in the year 1900, Paul Ehrlich introduced the term "receptor", symbolizing the era of modern pharmacology. Later in 1913, Ehrlich also coined the phrase "corpora non agunt nisi fixata" (a drug will not work unless it is bound).[48, 49] From then on, drug action in the human body is described as a kinetic event, not only in terms of transport of drug molecules to the environment of targets (e.g., receptors), but also with respect to the drug-target interaction itself. In other words, the lifetime of the drug-target complex is relevant to drug action. More specifically, the law of mass action is the fundamental descriptor of drug-target interactions [50-52]:

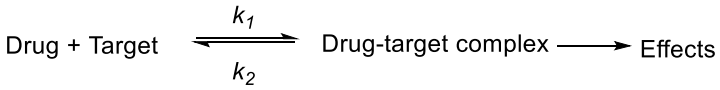

in which k_1 and k_2 represent the association (k_{on}) and dissociation (k_{off}) rate constant of a drug to and from its target, respectively. This mathematical application was first reported in enzyme kinetics (since 1913) and, later (1937) more emphasis was placed on equilibrium parameters of drug-target binding interactions. It lasted until 1961, when Paton proposed that "the dissociation rate constant is the primary determinant of the activity of a drug".[53, 54] Kinetic and affinity parameters were intertwined as drug activity (i.e. affinity), which is the ratio of both association and dissociation rate constants:[55]

$$\text{Kinetic } K_D \text{ (an affinity parameter)} = k_2/k_1$$

Methodologies to determine kinetics (presented as various rate constants) have been explored and improved over the decades. One example is the invention of patch clamp technology in the late 1970s which allowed (gating) kinetics of ion channels to be measured.[56] Another active research field is enzyme kinetics which was pushed forward by the study of catalytic mechanisms.[57] However, kinetics in the field of GPCR has often been overlooked or neglected. In 2004, a retrospective survey of 50 drugs on 17 different drug targets led to the conclusion that slowly dissociating or even irreversible ligands present better efficacy than relatively faster dissociating equivalents.[58] Noteworthy, GPCR were only a small fraction (~18%) among the investigated drug targets, in contrast to the fact that GPCR are one of the largest classes of drug targets.

Steady-state potency metrics (i.e. K_i and IC_{50}) are often used to characterize drugs targeting GPCR in a traditional early-phase drug discovery endeavor. However, there is mounting evidence to show that high affinity drug candidates cannot prevent high attrition rates in clinical trials.[2] This may, among others, be due to the dynamic, non-equilibrium, conditions *in vivo* (like in the human body) that often are in contrast to the equilibrium conditions applied in *in vitro* assays.[59] Therefore, other, better *in vivo* effect-predicting parameters should be taken into account. Binding kinetics as a term

collectively stands for the association (k_{on}) and dissociation (k_{off}) rate constants of a drug to and from its target. Particularly, over the last ten years, drug-target residence time (RT) has emerging as an additional parameter to assess the therapeutic potential of drug candidates with respect to drug efficacy and safety. RT is defined as the reciprocal of k_{off} and is an indication for the life-time of a drug-target complex. [59-61] In the field of GPCR, a number of structure-kinetics relationships (SKR) studies has been published, and the results suggest that including binding kinetics data (or kinetics profiles) when triaging compounds can improve the resulting decision process.[62-64] Following such rationale, appropriate binding kinetics experiments shall be incorporated in an early stage (*in vitro*) of drug design and discovery. Classical radioligand kinetic association and dissociation assays enable straightforward determination of association ($k_{on} = k_1$) and dissociation ($k_{off} = k_2$) rate constants. However, (radio)labeling every ligand of interest is impractical. In 1984, Motulsky and Mahan introduced an alternative strategy in which the kinetics of unlabeled ligands (cold ligands) can be quantified by using only one labeled tracer (hot ligand).[65] Such so-called competition association assay was validated by a further developed mathematic model obeying the law of mass action:

$$\text{Hot ligand} + \text{Receptor} \underset{k_2}{\overset{k_1}{\rightleftharpoons}} \text{Hot ligand-receptor complex}$$

$$\text{Cold ligand} + \text{Receptor} \underset{k_4}{\overset{k_3}{\rightleftharpoons}} \text{Cold ligand-receptor complex}$$

In brief, both a cold ligand of interest and a well-characterized (i.e. k_1 and k_2) hot ligand can competitively bind to the same receptor; the competitor may delay the time-dependent ascent of hot ligand binding or even produce a time-dependent decrease in hot ligand binding after an initial 'overshoot'.[65] This method has been used to quantify the binding kinetics of cold ligands (i.e. k_3 and k_4) to several GPCR.[62, 63, 66, 67] However, the competition association assay described above is quite laborious and time-consuming. Therefore, a so-called "dual-point competition association assay" was established, and validated for the hA_1 receptor.[68] By using only two time points of hot ligand specific

binding, a semi-quantitative measurement yielded a so-called kinetic rate index (KRI) of the cold ligand. Thereby, the throughput of kinetics assays can be improved greatly.

Objectives and outline of this thesis

Investigating ligand-GPCR binding kinetics is a leading theme in this thesis, which will be explored using hCB_1, hA_1 and hA_3 receptors. Currently, the drug discovery paradigm is shifting from studying structure-affinity relationships (SAR) alone, to a combination of SAR and extensive structure-kinetics relationships (SKR). This strategy is firstly exemplified in a study of hCB_1 receptor antagonists (**Chapter 2**). We provide evidence that, next to affinity, additional knowledge of binding kinetics is useful for selecting new hCB_1 receptor antagonists in the early phases of drug discovery. Following this, another selection of hCB_1 receptor antagonists with divergent residence times (RTs) was observed to have distinct modes of functional antagonism, in both G-protein dependent and G protein-independent signaling (**Chapter 3**).

The other research chapters (**Chapter 4-6**) are devoted to adenosine receptors. Firstly, an SKR study on a series of hA_3 receptor antagonists is performed in **Chapter 4**; furthermore, a "k_{on}-k_{off}-K_D" kinetic map enables the division of the antagonists into three subgroups, providing a possible direction for further development of hA_3 receptor antagonists. On the other hand, binding kinetics of hA_3 receptor agonists is reported in **Chapter 5**, providing binding kinetics insights of GPCR agonists. In **Chapter 6**, the application of a novel radio-isotopic technology in binding kinetics is described for the hA_1 receptor. Its robustness and potential for high-throughput screening may render this technology a preferred choice for further kinetics studies.

Last but not least, **Chapter 7** provides a general conclusion of the novel findings presented in this thesis, and future perspectives and opportunities for this field of research. Hopefully, this thesis will contribute to broadening the implementation of kinetics studies in drug discovery.

References

1. Alexander, S. P. H.; Kelly, E.; Marrion, N.; Peters, J. A.; Benson, H. E.; Faccenda, E.; Pawson, A. J.; Sharman, J. L.; Southan, C.; Buneman, O. P.; Catterall, W. A.; Cidlowski, J. A.; Davenport, A. P.; Fabbro, D.; Fan, G.; McGrath, J. C.; Spedding, M.; Davies, J. A.; Collaborators, C. The concise guide to pharmacology 2015/16: G protein-coupled receptors. *Br. J. Pharmacol.* **2015** *172*, 5744-5869.
2. Waring, M. J.; Arrowsmith, J.; Leach, A. R.; Leeson, P. D.; Mandrell, S.; Owen, R. M.; Pairaudeau, G.; Pennie, W. D.; Pickett, S. D.; Wang, J.; Wallace, O.; Weir, A. An analysis of the attrition of drug candidates from four major pharmaceutical companies. *Nat. Rev. Drug Discovery* **2015,** *14*, 475-486.
3. Copeland, R. A. The drug-target residence time model: a 10-year retrospective. *Nat. Rev. Drug. Discov.* **2016,** *15*, 87-95.
4. Copeland, R. A.; Pompliano, D. L.; Meek, T. D. Drug-target residence time and its implications for lead optimization. *Nat. Rev. Drug Discovery* **2006,** *5*, 730-739.
5. Overington, J. P.; Al-Lazikani, B.; Hopkins, A. L. How many drug targets are there? *Nat. Rev. Drug Discovery* **2006,** *5*, 993-996.
6. Lefkowitz, R. J. A brief history of G-protein coupled receptors (Nobel lecture). *Angew. Chem., Int. Ed.* **2013,** *52*, 6366-6378.
7. Kobilka, B. The structural basis of G-protein-coupled receptor signaling (Nobel lecture). *Angew. Chem., Int. Ed.* **2013,** *52*, 6380-6388.
8. Alexander, S. P. H.; Davenport, A. P.; Kelly, E.; Marrion, N.; Peters, J. A.; Benson, H. E.; Faccenda, E.; Pawson, A. J.; Sharman, J. L.; Southan, C.; Davies, J. A.; Collaborators, C. The concise guide to pharmacology 2015/16: G protein-coupled receptors. *Br. J. Pharmacol.* **2015,** *172*, 5744-5869.
9. Maccarrone, M.; Bab, I.; Bíró, T.; Cabral, G. A.; Dey, S. K.; Di Marzo, V.; Konje, J. C.; Kunos, G.; Mechoulam, R.; Pacher, P.; Sharkey, K. A.; Zimmer, A. Endocannabinoid signaling at the periphery: 50 years after THC. *Trends Pharmacol. Sci.* **2015,** *36*, 277-296.
10. Pertwee, R. G.; Howlett, A. C.; Abood, M. E.; Alexander, S. P. H.; Di Marzo, V.; Elphick, M. R.; Greasley, P. J.; Hansen, H. S.; Kunos, G.; Mackie, K.; Mechoulam, R.; Ross, R. A. International union of basic and clinical pharmacology. LXXIX. cannabinoid receptors and their ligands: beyond CB_1 and CB_2. *Pharmacol. Rev.* **2010,** *62*, 588-631.
11. Munro, S.; Thomas, K. L.; Abu-Shaar, M. Molecular characterization of a peripheral receptor for cannabinoids. *Nature* **1993,** *365*, 61-65.
12. Touw, M. The Religious and Medicinal Uses of Cannabis in China, India and Tibet. *Journal of Psychoactive Drugs* **1981,** 13, 23-34.
13. Melamede, R. Harm reduction-the cannabis paradox. *Harm Reduction Journal* **2005,** *2*, 1-13.
14. Di Marzo, V.; Sepe, N.; De Petrocellis, L.; Berger, A.; Crozier, G.; Fride, E.; Mechoulam, R. Trick or treat from food endocannabinoids? *Nature* **1998,** *396*, 636-636.
15. Di Tomaso, E.; Beltramo, M.; Piomelli, D. Brain cannabinoids in chocolate. *Nature* **1996,** *382*, 677-678.
16. Koch, M.; Varela, L.; Kim, J. G.; Kim, J. D.; Hernandez-Nuno, F.; Simonds, S. E.; Castorena, C. M.; Vianna, C. R.; Elmquist, J. K.; Morozov, Y. M.; Rakic, P.; Bechmann, I.; Cowley, M. A.; Szigeti-Buck, K.; Dietrich, M. O.; Gao, X.-B.; Diano, S.; Horvath, T. L. Hypothalamic POMC neurons promote cannabinoid-induced feeding. *Nature* **2015,** *519*, 45-50.
17. Abood, M.; Barth, F.; Bonner, T. I.; Cabral, G.; Casellas, P.; Cravatt, B. F.; Devane, W. A.; Elphick, M. R.; Felder, C. C.; Herkenham, M.; Howlett, A. C.; Kunos, G.; Mackie, K.; Mechoulam, R.; Pertwee, R. G. Cannabinoid receptors: CB_1 receptor. Last modified on May 16, **2017**. Accessed on July 20, 2017. *IUPHAR/BPS Guide to Pharmacology*, <http://www.guidetopharmacology.org/GRAC/ObjectDisplayForward?objectId=56.>
18. Pacher, P.; BÁTkai, S.; Kunos, G. The endocannabinoid system as an emerging target of pharmacotherapy. *Pharmacol. Rev.* **2006,** *58*, 389-462.

19. Bermudez-Silva, F. J.; Viveros, M. P.; McPartland, J. M.; Rodriguez de Fonseca, F. The endocannabinoid system, eating behavior and energy homeostasis: the end or a new beginning? *Pharmacol., Biochem. Behav.* **2010,** *95*, 375-382.
20. Perkins, J. M.; Davis, S. N. Endocannabinoid system overactivity and the metabolic syndrome: prospects for treatment. *Curr. Diabetes Rep.* **2008,** *8*, 12-19.
21. *FDA briefing document NDA 21-888 zimulti (rimonabant) tablets, 20 mg sanofi aventis advisory committee. Published on June 13, 2007. Accessed on July 20, 2017.* <*http://www.fda.gov/ohrms/dockets/ac/07/briefing/2007-4306b1-fda-backgrounder.pdf*>.
22. Boekholdt, S. M.; Peters, R. J. G. Rimonabant: obituary for a wonder drug. *Lancet* **2010,** *376*, 489-490.
23. Topol, E. J.; Bousser, M.-G.; Fox, K. A. A.; Creager, M. A.; Despres, J.-P.; Easton, J. D.; Hamm, C. W.; Montalescot, G.; Steg, P. G.; Pearson, T. A.; Cohen, E.; Gaudin, C.; Job, B.; Murphy, J. H.; Bhatt, D. L. Rimonabant for prevention of cardiovascular events (CRESCENDO): a randomised, multicentre, placebo-controlled trial. *Lancet* **2010,** *376*, 517-523.
24. Proietto, J.; Rissanen, A.; Harp, J. B.; Erondu, N.; Yu, Q.; Suryawanshi, S.; Jones, M. E.; Johnson-Levonas, A. O.; Heymsfield, S. B.; Kaufman, K. D.; Amatruda, J. M. A clinical trial assessing the safety and efficacy of the CB_1R inverse agonist taranabant in obese and overweight patients: low-dose study. *Int. J. Obes.* **2010,** *34*, 1243-1254.
25. Aronne, L. J.; Finer, N.; Hollander, P. A.; England, R. D.; Klioze, S. S.; Chew, R. D.; Fountaine, R. J.; Powell, C. M.; Obourn, J. D. Efficacy and safety of CP-945,598, a selective cannabinoid CB_1 receptor antagonist, on weight loss and maintenance. *Obesity* **2011,** *19*, 1404-1414.
26. Hua, T.; Vemuri, K.; Pu, M.; Qu, L.; Han, G. W.; Wu, Y.; Zhao, S.; Shui, W.; Li, S.; Korde, A.; Laprairie, R. B.; Stahl, E. L.; Ho, J.-H.; Zvonok, N.; Zhou, H.; Kufareva, I.; Wu, B.; Zhao, Q.; Hanson, M. A.; Bohn, L. M.; Makriyannis, A.; Stevens, R. C.; Liu, Z.-J. Crystal structure of the human cannabinoid receptor CB_1. *Cell* **2017,** *167*, 750-762.
27. Shao, Z.; Yin, J.; Chapman, K.; Grzemska, M.; Clark, L.; Wang, J.; Rosenbaum, D. M. High-resolution crystal structure of the human CB_1 cannabinoid receptor. *Nature* **2016,** *540*, 602-606.
28. Hua, T.; Vemuri, K.; Nikas, S. P.; Laprairie, R. B.; Wu, Y.; Qu, L.; Pu, M.; Korde, A.; Jiang, S.; Ho, J.-H.; Han, G. W.; Ding, K.; Li, X.; Liu, H.; Hanson, M. A.; Zhao, S.; Bohn, L. M.; Makriyannis, A.; Stevens, R. C.; Liu, Z.-J. Crystal structures of agonist-bound human cannabinoid receptor CB_1. *Nature* **2017,** *547*, 468-471.
29. IJzerman, A. P.; Fredholm, B. B.; Frenguelli, B. G.; Jacobson, K. A.; Klotz, K.-N.; Linden, J.; Müeller, C. E.; Schwabe, U.; Stiles, G. L.; Rebecca, H. Adenosine receptors, introduction. . http://www.guidetopharmacology.org/GRAC/FamilyIntroductionForward?familyId=3 (16/08/2017).
30. Fredholm, B. B.; IJzerman, A. P.; Jacobson, K. A.; Klotz, K.-N.; Linden, J. International union of pharmacology. XXV. nomenclature and classification of adenosine receptors. *Pharmacol. Rev.* **2001,** *53*, 527-552.
31. Hochhauser, E.; Leshem, D.; Kaminski, O.; Cheporko, Y.; Vidne, B. A.; Shainberg, A. The protective effect of prior ischemia reperfusion adenosine A_1 or A_3 receptor activation in the normal and hypertrophied heart. *Interactive CardioVascular and Thoracic Surgery* **2007,** *6*, 363-368.
32. Yap, S. C.; Lee, H. T. Adenosine and protection from acute kidney injury. *Curr. Opin. Nephrol. Hypertens.* **2012,** *21*, 24-32.
33. Sawynok, J. Adenosine receptor activation and nociception. *Eur. J. Pharmacol.* **1998,** *347*, 1-11.
34. Janes, K.; Esposito, E.; Doyle, T.; Cuzzocrea, S.; Tosh, D. K.; Jacobson, K. A.; Salvemini, D. A_3 adenosine receptor agonist prevents the development of paclitaxel‐induced neuropathic pain by modulating spinal glial‐restricted redox‐dependent signaling pathways. *Pain* **2014,** *155*, 2560-2567.
35. National center for biotechnology information. Pubchem compound database; CID=123683, https://pubchem.ncbi.nlm.nih.gov/compound/123683 (accessed June 30, 2017).
36. National center for biotechnology information. PubChem compound database; CID=3035850, https://pubchem.ncbi.nlm.nih.gov/compound/3035850 (accessed June 30, 2017).

37. Hill, R. J.; Oleynek, J. J.; Magee, W.; Knight, D. R.; Tracey, W. R. Relative importance of adenosine $A_1$and A_3 receptors in mediating physiological or pharmacological protection from ischemic myocardial injury in the rabbit heart. *J. Mol. Cell. Cardiol.* **1998,** *30*, 579-585.
38. Shneyvays, V.; Leshem, D.; Zinman, T.; Mamedova, L. K.; Jacobson, K. A.; Shainberg, A. Role of adenosine A_1 and A_3 receptors in regulation of cardiomyocyte homeostasis after mitochondrial respiratory chain injury. *Am. J. Physiol. Heart Circ. Physiol.* **2005,** *288*, 2792-2801.
39. Galvao, J.; Elvas, F.; Martins, T.; Cordeiro, M. F.; Ambrósio, A. F.; Santiago, A. R. Adenosine A_3 receptor activation is neuroprotective against retinal neurodegeneration. *Exp. Eye Res.* **2015,** *140*, 65-74.
40. Liang, B. T.; Stewart, D.; Jacobson, K. A. Adenosine A_1 and A_3 receptors: distinct cardioprotection. *Drug Dev. Res.* **2001,** *52*, 366-378.
41. Vladimir Shneyvays; Noam Safran; Irit Halili-Rutman; Shainberg, A. Insights into adenosine A_1 and A_3 receptors function: cardiotoxicity and cardioprotection. *Drug Dev. Res.* **2000,** *50*, 324-337.
42. Fredholm, B. B.; Chen, J.-F.; Cunha, R. A.; Svenningsson, P.; Vaugeois, J.-M. Adenosine and Brain Function. In *International Review of Neurobiology*, Academic Press: 2005; Vol. *63*, pp 191-270.
43. Wittendorp, M. C.; Boddeke, H. W. G. M.; Biber, K. Adenosine A3 receptor-induced CCL2 synthesis in cultured mouse astrocytes. *Glia* **2004,** *46*, 410-418.
44. Glukhova, A.; Thal, D. M.; Nguyen, A. T.; Vecchio, E. A.; Jörg, M.; Scammells, P. J.; May, L. T.; Sexton, P. M.; Christopoulos, A. Structure of the adenosine A_1 receptor reveals the basis for subtype selectivity. *Cell* **2017,** *168*, 867-877.
45. Wennerberg, M.; Cheng, L.; Hjorth, S.; Clapham, J. C.; Balendran, A.; Vauquelin, G. Binding properties of antagonists to Cannabinoid receptors in intact cells. *Fundam. Clin. Pharmacol.* **2011,** *25*, 200-210.
46. Cawston, E. E.; Redmond, W. J.; Breen, C. M.; Grimsey, N. L.; Connor, M.; Glass, M. Real-time characterization of cannabinoid receptor 1 (CB_1) allosteric modulators reveals novel mechanism of action. *Br. J. Pharmacol.* **2013,** *170*, 893-907.
47. Guo, D.; Heitman, L. H.; IJzerman, A. P. Kinetic aspects of the interaction between ligand and G protein-coupled receptor: the case of the adenosine receptors. *Chem. Rev.* **2017,** *117*, 38-66.
48. Kaufmann, S. H. E. Paul Ehrlich: founder of chemotherapy. *Nat. Rev. Drug Discovery* **2008,** *7*, 373-373.
49. Address in pathology on chemotherapeutics: scientific principles, methods, and results. *Lancet* **1913,** *182*, 445-451.
50. Waud, D. R. Pharmacological receptors. *Pharmacol. Rev.* **1968,** *20*, 49-88.
51. Clark, A. J. *Mode Of Action Of Drugs On Cells*. Williams and Wilkins Company, : Baltimore, Md., 1933.
52. Waage, P.; Gulberg, C. M. Studies concerning affinity. *J. Chem. Educ.* **1986,** *63*, 1044.
53. van Ginneken, C. A. M. Kinetics of Drug-Receptor Interaction. In *Kinetics of Drug Action*, van Rossum, J. M., Ed. Springer Berlin Heidelberg: Berlin, Heidelberg, 1977; pp 357-411.
54. Paton, W. D. M. A theory of drug action based on the rate of drug-receptor combination. *Proc. R. Soc. Lond. B Biol Sci.* **1961,** *154*, 21-69.
55. Hulme, E. C.; Trevethick, M. A. Ligand binding assays at equilibrium: validation and interpretation. *Br. J. Pharmacol.* **2010,** *161*, 1219-1237.
56. Bauer, R. J.; Bowman, B. F.; Kenyon, J. L. Theory of the kinetic analysis of patch-clamp data. *Biophys. J.* **1987,** *52*, 961-978.
57. Johnson, K. A. A century of enzyme kinetic analysis, 1913 to 2013. *FEBS Lett.* **2013,** *587*, 2753-2766.
58. Swinney, D. C. Biochemical mechanisms of drug action: what does it take for success? *Nat. Rev. Drug Discovery* **2004,** *3*, 801-808.
59. Guo, D.; Hillger, J. M.; IJzerman, A. P.; Heitman, L. H. Drug-target residence time—a case for G protein-coupled receptors. *Med. Res. Rev.* **2014,** *34*, 856-892.
60. Copeland, R. A. The drug-target residence time model: a 10-year retrospective. *Nat. Rev. Drug Discovery* **2016,** *15*, 87-95.

61. Swinney, D. C.; Haubrich, B. A.; van Liefde, I.; Vauquelin, G. The role of binding kinetics in GPCR drug discovery. *Curr. Top. Med. Chem.* **2015,** *15*, 2504-2522.
62. Vilums, M.; Zweemer, A. J. M.; Yu, Z.; de Vries, H.; Hillger, J. M.; Wapenaar, H.; Bollen, I. A. E.; Barmare, F.; Gross, R.; Clemens, J.; Krenitsky, P.; Brussee, J.; Stamos, D.; Saunders, J.; Heitman, L. H.; IJzerman, A. P. Structure–kinetic relationships—an overlooked parameter in hit-to-lead optimization: a case of cyclopentylamines as chemokine receptor 2 antagonists. *J. Med. Chem.* **2013,** *56*, 7706-7714.
63. Guo, D.; Xia, L.; van Veldhoven, J. P. D.; Hazeu, M.; Mocking, T.; Brussee, J.; IJzerman, A. P.; Heitman, L. H. Binding kinetics of ZM241385 derivatives at the human adenosine A_{2A} receptor. *ChemMedChem* **2014,** *9*, 752-761.
64. Louvel, J.; Guo, D.; Agliardi, M.; Mocking, T. A. M.; Kars, R.; Pham, T. P.; Xia, L.; de Vries, H.; Brussee, J.; Heitman, L. H.; IJzerman, A. P. Agonists for the adenosine A_1 receptor with tunable residence time. A case for nonribose 4-amino-6-aryl-5-cyano-2-thiopyrimidines. *J. Med. Chem.* **2014,** *57*, 3213-3222.
65. Motulsky, H. J.; Mahan, L. C. The kinetics of competitive radioligand binding predicted by the law of mass action. *Mol. Pharmacol.* **1984,** *25*, 1-9.
66. Dowling, M. R.; Charlton, S. J. Quantifying the association and dissociation rates of unlabelled antagonists at the muscarinic M_3 receptor. *Br. J. Pharmacol.* **2006,** *148*, 927-937.
67. Guo, D.; Mulder-Krieger, T.; IJzerman, A. P.; Heitman, L. H. Functional efficacy of adenosine A_{2A} receptor agonists is positively correlated to their receptor residence time. *Br. J. Pharmacol.* **2012,** *166*, 1846-1859.
68. Guo, D.; van Dorp, E. J. H.; Mulder-Krieger, T.; van Veldhoven, J. P. D.; Brussee, J.; IJzerman, A. P.; Heitman, L. H. Dual-point competition association assay: a fast and high-throughput kinetic screening method for assessing ligand-receptor binding kinetics. *J. Biomol. Screening* **2013,** *18*, 309-320.

Chapter 2

Structure-affinity Relationships and Structure-kinetic Relationships of 1,2-Diarylimidazol-4-carboxamide Derivatives as Human Cannabinoid 1 Receptor Antagonists

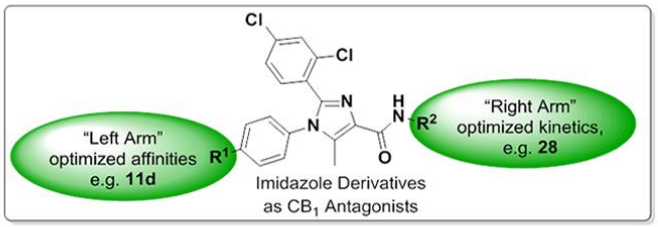

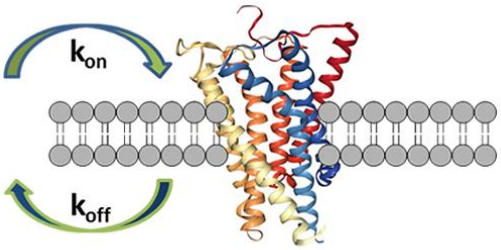

Lizi Xia, Henk de Vries, Eelke B. Lenselink, Julien Louvel, Michael J. Waring, Leifeng Cheng, Sara Pahlén, Maria J. Petersson, Peter Schell, Roine I. Olsson, Laura H. Heitman, Robert J. Sheppard, and Adriaan P. IJzerman

Adapted from: *J. Med. Chem.*, **2017**, 60(23): 9545–9564

About this chapter

Despite the plethora of human cannabinoid 1 (hCB_1) receptor antagonists active *in vitro* that have been synthesized as potential antiobesity drugs, the withdrawal from the market of rimonabant caused the termination of virtually all clinical programs of such antagonists. This was due to rimonabant's class-related serious central nervous system side effects. A better understanding of the molecular mechanisms of hCB_1 antagonist action may, albeit retrospectively, shed some light on what went wrong. It is now emerging that drug target binding kinetics, next to traditional potency measures, may indeed contribute to a better understanding of drug action. Therefore, we now report on the synthesis and biological evaluation of a series of 1,2-diarylimidazol-4-carboxamide derivatives developed as hCB_1 receptor antagonists. These were evaluated in a radioligand displacement binding assay, a [^{35}S]GTPγS binding assay, and in a competition association assay that enables the relatively fast kinetic screening of multiple compounds. The compounds show high affinities and a diverse range of kinetic profiles at the hCB_1 receptor, and their structure-kinetic relationships (SKR) were established. Using the recently resolved hCB_1 receptor crystal structures, we also performed a modelling study that sheds light on the crucial interactions for both the affinity and dissociation kinetics of this family of ligands. We provide evidence that, next to affinity, additional knowledge of binding kinetics is useful for selecting new hCB_1 receptor antagonists in the early phases of drug discovery.

Introduction

Within the endocannabinoid system (ECS) two human cannabinoid receptor subtypes have been identified: the human CB_1 (hCB_1) receptor and the human CB_2 (hCB_2) receptor.[1] They are members of the rhodopsin-like class A G-protein-coupled receptors (GPCR), and are primarily activated by endogenous cannabinoids (endocannabinoids, ECs), including anandamide (or N-arachidonylethanolamine, AEA) and 2-arachidonoylglycerol (2-AG).[1, 2] The hCB_1 and hCB_2 receptors show 44% overall sequence homology, and display different pharmacological profiles.[3] The hCB_1 receptor is present in the central nervous system (CNS) and is widely distributed in the peripheral nervous system (PNS) and peripheral tissues,[2, 4] including heart, liver, lung, gastrointestinal tract, pancreas and adipose tissue.[5, 6] The presence of the hCB_1 receptor within both the CNS and PNS mediates neurotransmitter release and controls various cognitive, motor, emotional and sensory functions. Furthermore, activation in the peripheral tissues contributes to energy balance and metabolic processes.[6-9]

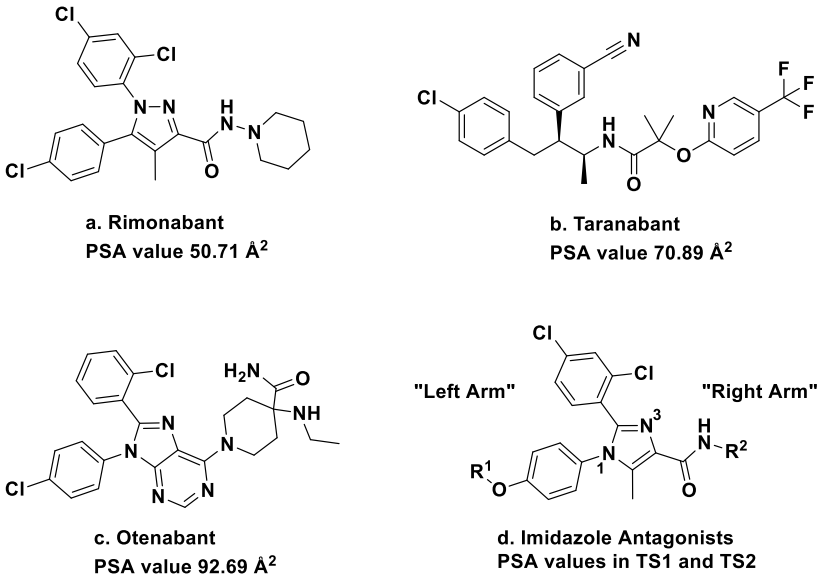

Figure 1: Structure of **a**) Rimonabant; **b**) Taranabant; **c**) Otenabant and **d**) the scaffold of 1,2-diarylimidazol-4-carboxamides as hCB_1 receptor antagonists; the R^1 substitution is defined as the "Left arm" of the scaffold while the R^2 substitution defines the "Right arm" of the scaffold. The calculation of PSA values are reported in supporting information.

The broad presence of the hCB_1 receptor in a variety of complex physiological systems provides numerous opportunities for therapeutic intervention. In the particular case of obesity, the ECS, including the hCB_1 receptor, is overactive with increased levels of endocannabinoids in plasma, both in central and peripheral tissues.[10] Therefore, blockade of the hCB_1 has been explored for the treatment of obesity. With this in mind, rimonabant (SR141716A, **Figure 1a**), a hCB_1 receptor inverse agonist, was developed by Sanofi-Aventis and introduced in Europe in 2006. However, it was quickly withdrawn from the market due to unacceptable psychiatric side effects.[11-13] Many other hCB_1 receptor antagonists entered into clinical trials, such as taranabant (MK-0364, **Figure 1b**)[14] and otenabant (CP945598, **Figure 1c**).[15] However, they were not developed further due to similar psychiatric side effects, despite their diverse chemical structures.

In order to avoid the CNS side effects, peripherally acting hCB_1 receptor antagonists with physicochemical features that reduce brain penetration have been developed.[16] Another approach has been the development of hCB_1 receptor neutral antagonists, because it has been postulated that the CNS side effects of rimonabant were due to its inverse agonism.[17-19]

Drug target binding kinetic parameters are receiving increasing attention, alongside classical affinity (K_i) and potency (IC_{50}) values, as has been discussed for several other class A GPCR. In particular the receptor-ligand residence time (RT) is emerging as an additional parameter to assess the therapeutic potential of drug candidates with respect to drug efficacy and safety.[20-22] In the research field of GPCR, a number of structure-kinetic relationship (SKR) studies have been published, and the results suggest that the strategic combination of SKR with classic structure-affinity relationships (SAR) can improve the resulting decision process.[23-26] By doing so, ligand-receptor interactions can be better understood, as together they not only comprise the equilibrium state of a ligand-receptor interaction but also its metastable intermediates and/or transition states.[27] The binding kinetics

driven drug discovery approach for the hCB_1 receptor has been validated in some aspects already by its application in the development of allosteric modulators of the hCB_1 receptor.[28, 29]

In the current study we report the synthesis and evaluation of 1,2-diarylimidazol-4-carboxamide derivatives (**Figure 1d**), as human CB_1 receptor antagonists with more polar characteristics than rimonabant.[30, 31] Together with rimonabant they were evaluated in a radioligand displacement assay, a [^{35}S]GTPγS binding assay, and a dual-point competition association assay that enables the relatively fast kinetic screening of compounds.[32] Selected compounds were progressed to a full competition association assay. The compounds show high affinities and a diverse range of kinetic profiles at the hCB_1 receptor, which allowed their structure-kinetic relationships (SKR) to be established. Their putative binding mode was analyzed using the recently resolved crystal structures of the hCB_1 receptor,[33,34] shedding light on key structural features of the receptor binding site that are involved in ligand recognition and dissociation. Thus we provide evidence that, in additional to affinity, knowledge of binding kinetics is useful for selecting new hCB_1 receptor antagonists in the early phases of drug discovery.

Results and discussion

Chemistry.

The synthesis of the 1,2-diarylimidazol-4-carboxamide scaffold commenced from commercially available 4-(benzyloxy)aniline **1**, which was converted to the 2,4-dichlorobenzamidine **2** (**Scheme 1**). After a one-pot condensation and cyclization sequence, the core-imidazole **3** was obtained. Afterwards, either saponification of the ethyl ester or acidic hydrolysis of the benzyl ether of **3** led to intermediates **4** and **5**, respectively. Subsequently, Mitsunobu reaction on intermediate **5** yielded mono- and tri-fluoropropyl ether derivatives **6a** and **6b**. After saponification of the ethyl esters of **6a** and **6b**, the corresponding carboxylic acids (**7a** and **7b**) were transformed to acid chlorides and

reacted with piperidin-1-amine to yield the corresponding amides (**8a** and **8b**). Alternatively, the rest of the series was produced from intermediate **4** by first introducing the piperidin-1-amide. Lewis acid-catalyzed cleavage of benzyl ether **9** followed by substitution of the released alcohol **10** with various alkyl halides gave the corresponding ethers **11a**-**11h**, completing the "left arm" series of antagonists (**Table 1**).

Scheme 1. Synthesis of antagonists **8a**, **8b** and **11a**-**h**.

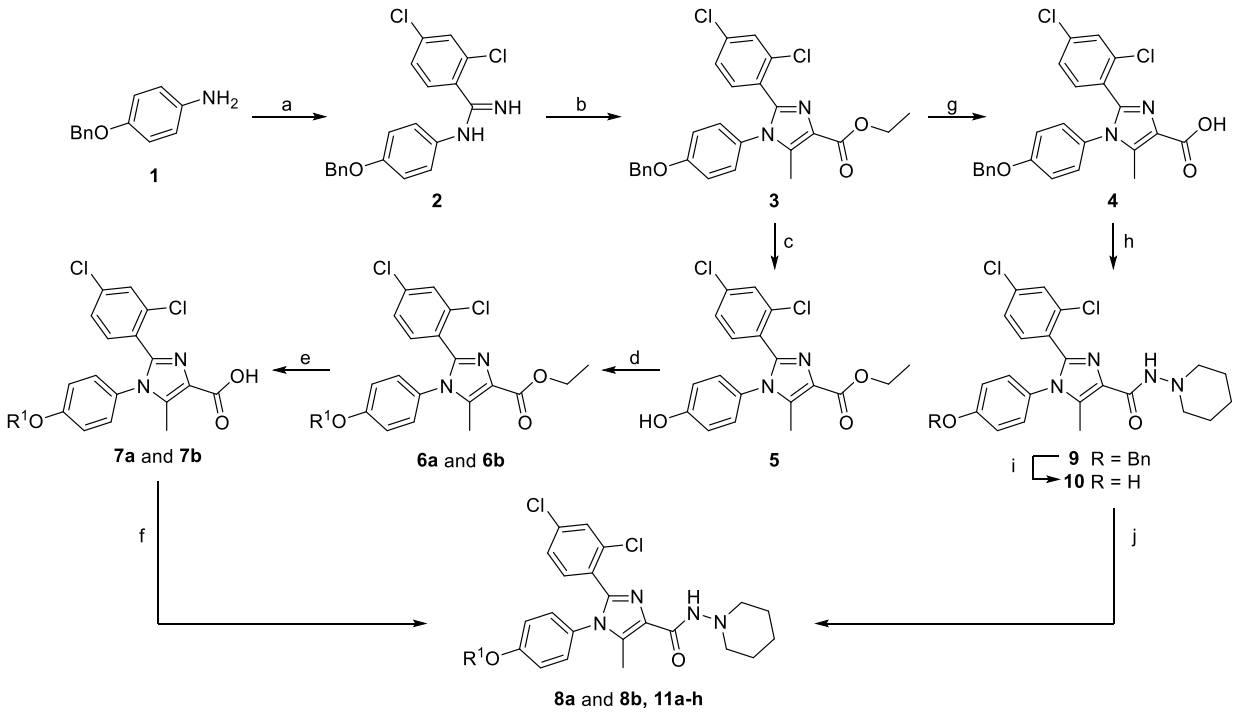

Reagents and conditions: **a**) EtMgBr, 2,4-diClPhCN, THF, r.t., 20 h, 98%; **b**) i. $EtO_2CC(O)CH(Br)CH_3$, K_2CO_3, THF, r.t. 66 h, ii. AcOH, reflux, 1 h, 65%; **c**) HBr, AcOH, r.t., 15 h, 63%; **d**) R^1-OH, DEAD, Ph_3P, THF, Toluene, r.t., 15h, 77%; **e**) KOH, EtOH:THF:H_2O 2:2:1, 50 °C, 3.5 h, 95%; **f**) i. $(COCl)_2$, DMF cat., CH_2Cl_2, r.t., 90 min, ii. Piperidin-1-amine.HCl, pyridine, CH_2Cl_2, r.t., 2 h, 55% (2 steps); **g**) KOH, MeOH:H_2O 3:1, reflux, 2 h, 99%; **h**) i. $(COCl)_2$, DMF cat., CH_2Cl_2, reflux, 2 h, ii. Piperidin-1-amine, NEt_3, CH_2Cl_2, 0 °C to r.t., 2 h, 74%; **i**) BBr_3, CH_2Cl_2, r.t., 1 h, 58%; **j**) R^1-X, base, CH_2Cl_2. 56-90% Corresponding R^1 substitutions are listed in **Table 1**.

The synthesis of the "right arm" series of antagonists was started from intermediate **4** (**Scheme 2**). Using various amines and the aforementioned acid chloride introduction/ amide formation sequence,

amides **12a**-**12h** were obtained, as well as racemic (±) **20**. Deprotection of the aromatic alcohol on **12a**-**12h** and subsequent sulfonylation using 3,3,3-trifluoropropane-1-sulfonylchloride gave compounds **14a**-**14h**.

Scheme 2. Synthesis of antagonists **14a**-**h**, **19**, (±)**22**, (±)**25** and **28**.

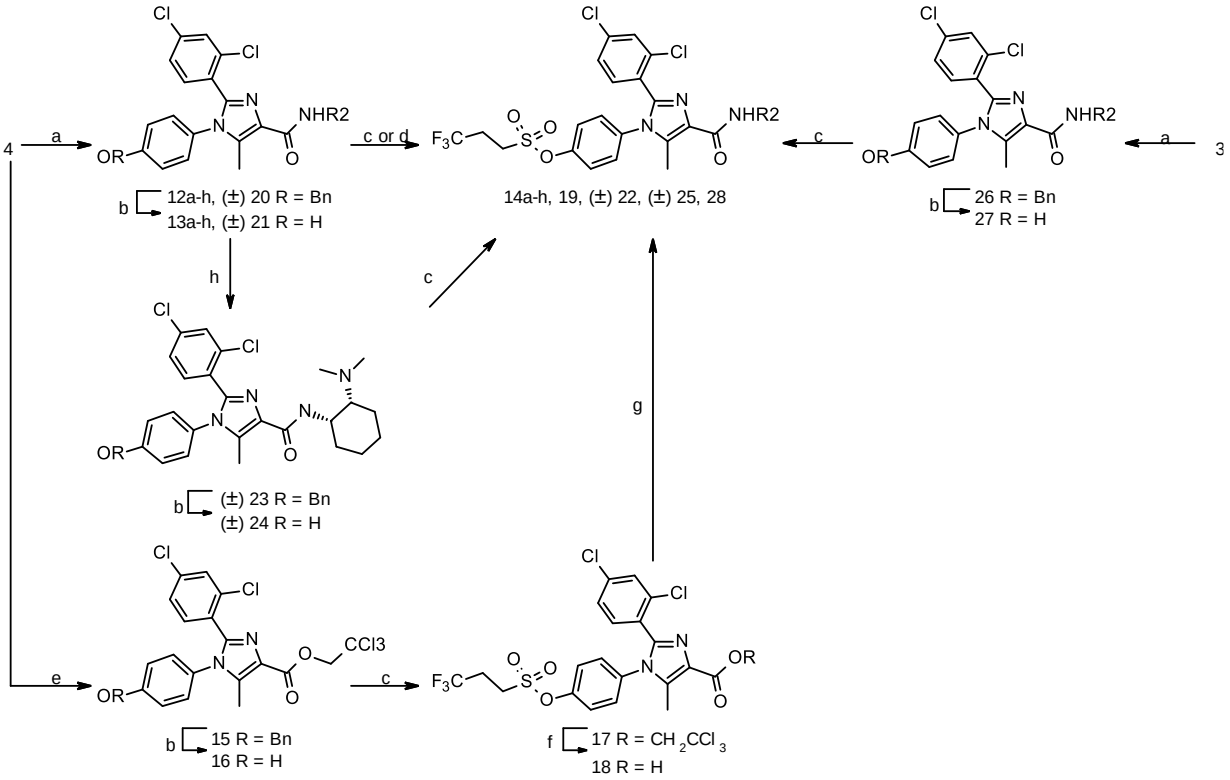

Reagents and conditions: **a**) i. $SOCl_2$, reflux; or $(COCl)_2$, DMF cat., CH_2Cl_2, r.t.; ii. R^2-NH_2, NEt_3, CH_2Cl_2, 17-98 % (2 steps); or 2-amino-5-trifluoromethylpyridine, Me_3Al, CH_2Cl_2, r.t. to 45 °C, 16 h, 64%; **b**) $BF_3.OEt_2$, Me_2S, CH_2Cl_2, r.t.; or HBr, AcOH, r.t. 20-97 %; **c**) Et_3N, $F_3CCH_2CH_2SO_2Cl$, CH_2Cl_2, -78 °C, 25-97 %; **d**) i. TBDMSCl, Et_3N, CH_2Cl_2, r.t., 22 h; ii. Boc_2O, THF, r.t., 4 h, 70% (4 steps, a, b, d i. & ii.); iii. TBAF, THF, r.t., 90 min; iv. $F_3CCH_2CH_2SO_2Cl$, Et_3N, CH_2Cl_2, -78 °C, 3 h; v. $SOCl_2$, MeOH, 0 °C to r.t., 1 h, 56% (3 steps, d iii., iv. & v.); **e**) i. $(COCl)_2$, DMF cat., CH_2Cl_2, r.t., 2 h, ii. Cl_3CCH_2OH, NEt_3, CH_2Cl_2, r.t., 3 h, 95% (2 steps, e, b); **f**) Zn, AcOH, 3 h; **g**) i. $(COCl)_2$, DMF cat., CH_2Cl_2, r.t., 2 h, ii. 4-aminocyclohexanol, NaOH, H_2O:CH_2Cl_2 2:1, r.t., 2 h, 54% (2 steps, f, g); **h**) CH_2O, $NaBH_4$, $NaBH_3CN$, CH_3CN, H_2O, AcOH, r.t., 48 h, 32%; . Corresponding R^2 substitutions are listed in **Table 2**.

After deprotection of racemic (±) **20** however, it was found that direct substitution was not possible, therefore a series of protecting group manipulations was executed on (±) **21** to end up with (±) **22**. Towards (±) **25**, (±) **20** was first di-methylated and subsequently debenzylated and sulfonylated

giving (±) **25**. Exploring alternative synthesis routes, compound **19** was synthesized, with a few extra steps, by first esterifying **4** with 2,2,2-trichloroethanol, followed by deprotection of the aromatic alcohol. Sulfonylation of the released alcohol, saponification of the trichloroethylester, acid chloride formation and subsequent amide formation gave **19**. To obtain trifluoromethylpyridine derivative **28**, conventional methods as described for the industrial production of rimonabant were applied,[35] starting with the direct amidation of ethyl ether **3** followed by debenzylation and sulfonylation.

Biology.

All 1,2-diarylimidazol-4-carboxamide derivatives were evaluated as antagonists in an *in vitro* [^{35}S]GTPγS binding assay on HEK-293 cells membrane fractions overexpressing the human CB_1 receptor. We also determined the functional activity of nine representative antagonists on the human CB_2 receptor. The data in **Table 1** and **S1** shows that all compounds tested had higher functional activity for the human CB_1 receptor over the human CB_2 receptor, with approximately 110 to 570-fold selectivity.

Likewise they were also tested in a [^{3}H]CP55940 radioligand displacement assay on membrane fractions of CHO cells overexpressing the recombinant human CB_1 receptor. These results are reported in **Tables 1** and **2**. We found that, although using different cellular background and assay systems, there is a significant correlation (r^2 = 0.49, P = 0.0001) between the affinity (pK_i) values from the radioligand binding assay and the potencies (pIC_{50}) determined in the [^{35}S]GTPγS binding assay (**Figure 2**). We subsequently determined the binding kinetics of the 1,2-diarylimidazol-4-carboxamide derivatives in a competition association assay with [^{3}H]CP55940 as the probe after a validation step.

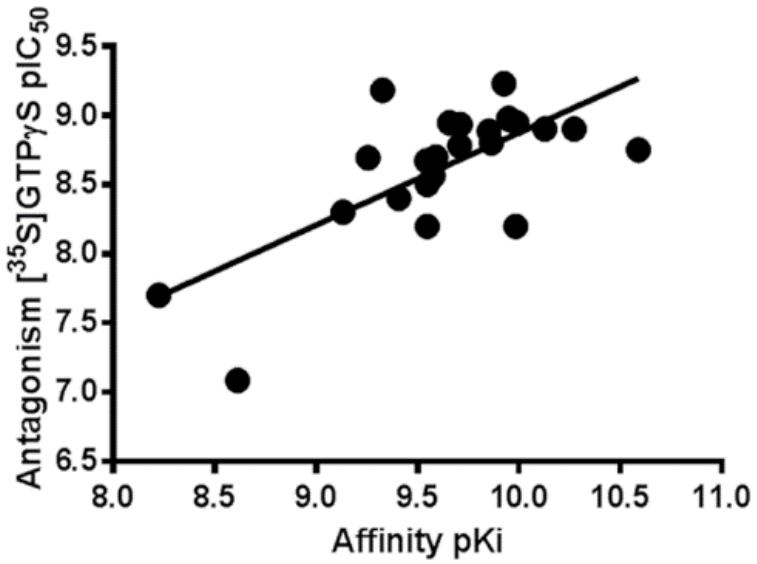

Figure 2: The correlation between the affinities/potencies of the CB_1 receptor antagonists measured in a radioligand binding assay (X-axis) and in a GTPγS binding assay (Y-axis) (r^2 = 0.49, *P* = 0.0001). Data taken from **Tables 1** and **2**.

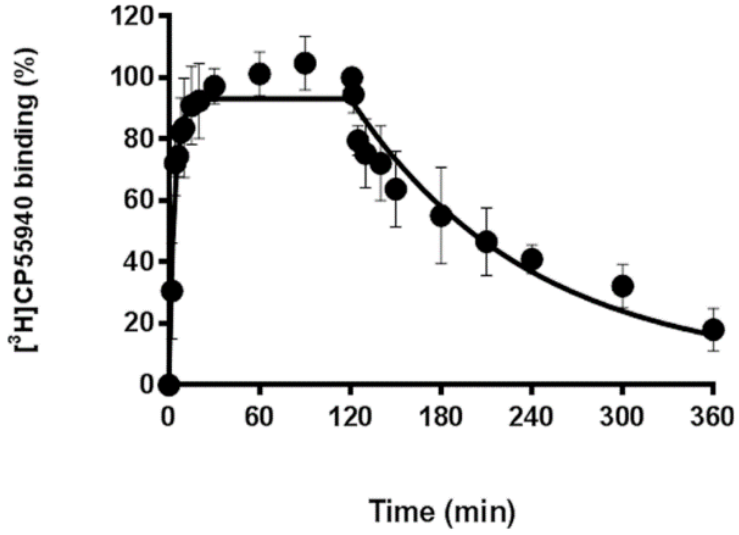

Figure 3: Association and dissociation profile of [^{3}H]CP55940 (2.9 nM) at recombinant hCB_1 receptors stably expressed on CHO cell membranes at 30 °C. After 120 min of association, unlabeled rimonabant (10 µM) was added to initiate the dissociation. Association data was fitted in Prism 6 using one-phase exponential association (n=3, combined and normalized). Dissociation data was fitted using one-phase exponential decay (n=4, combined and normalized). Data are shown as mean ± SEM from at least three separate experiments each performed in duplicate.

Table 1. In vitro pharmacology data, including conventional antagonism, binding affinities and KRI values, for human CB_1 receptor antagonists with various "left arm" R^1 substitutions.

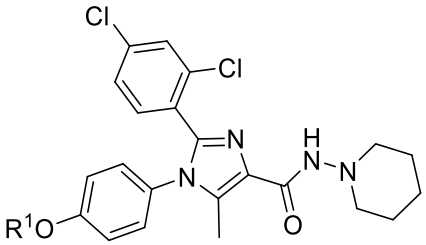

Code	R^1	[^{35}S]GTPγS binding pIC_{50}± SD or SEM (mean IC_{50} in nM) [a]	pK_i [b] ± SEM (mean K_i in nM)	KRI [c]
8a	$-CH_2CH_2CF_3$	8.3 ± 0.1 (5.6)[d]	9.1 ± 0.2 (1.26)	0.90 (0.90;0.89)
8b	$-CH_2CH_2CH_2F$	8.2 ± 0.01 (6.0) [d]	10 ± 0.2 (0.34)	1.09 (1.34;0.84)
9	$-CH_2Ph$	7.7 ± 0.1 (18)[d]	8.2 ± 0.1 (6.28)	0.90 ± 0.20
11a	$-CH_2CH_2CH_2CF_3$	8.9 ± 0.1 (1.2)	9.7 ± 0.1 (0.32)	0.80 (0.85;0.75)
11b	$-SO_2CH_2CH_2CH_3$	8.7 ± 0.03 (1.8) [d]	9.6 ± 0.1 (0.28)	0.59 ± 0.06
11c	$-SO_2CH_2CH_2CH_2F$	8.5 ± 0.2 (3.1)[d]	9.5 ± 0.2 (0.32)	0.88 (1.00;0.75)
11d	$-SO_2CH_2CH_2CF_3$	9.0 ± 0.03 (1.1)	9.9 ± 0.1 (0.11)	1.02 (1.08; 0.96)
11e	$-SO_2CH_2CH_2CH_2CH_3$	8.9 ± 0.05 (1.3) [d]	9.9 ± 0.1 (0.18)	0.77 ± 0.25
11f	$-SO_2CH_2CH_2CH_2CF_3$	8.9 ± 0.1 (1.2)	10 ± 0.2 (0.062)	0.93 (0.89;0.97)
11g	$-SO_2CH_2CH_2CH(CH_3)_2$	8.9 ± 0.1(1.3)	9.7 ± 0.1 (0.20)	1.02 (1.06;0.97)
11h	$-SO_2CH_2CH_2C(CH_3)_3$	8.7 ± 0.1 (2.4)	9.3 ± 0.1 (0.60)	0.73 (0.68;0.78)

[a] pIC_{50} ± SD (n=2) or SEM (n ≥ 3), obtained from [^{35}S]GTPγS binding on recombinant human CB_1 receptors stably expressed on HEK-293 cell membranes.

[b] pK_i ± SEM (n=3), obtained from radioligand binding assays with [^{3}H]CP55940 on recombinant human CB_1 receptors stably expressed on CHO cell membranes.

[c] KRI ± SEM (n = 3) or KRI (n1, n2) (n = 2), obtained from dual-point competition association assays with [^{3}H]CP55940 on recombinant human CB1 receptors stably expressed on CHO cell membranes.

[d] n = 2.

Table 2. In vitro pharmacology data, including conventional antagonism, binding affinity and KRI values, for human CB_1 receptor antagonists with various "right arm" R^2 substituents.

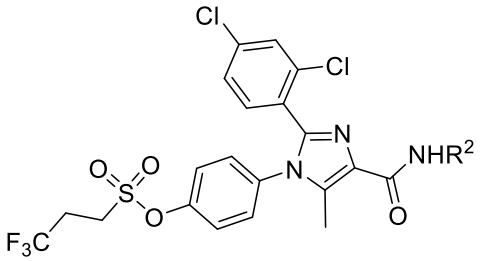

Code	R^2	[^{35}S]GTPγS binding pIC_{50}± SD or SEM (mean IC_{50} in nM) [a]	pK_i [b] ± SEM (mean K_i in nM)	KRI [c]
11d	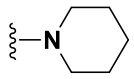	9.0 ± 0.03 (1.1)	9.9 ± 0.1 (0.11)	1.02 (1.08;0.96)
14a (±)	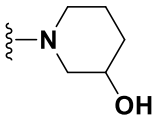	8.6 ± 0.1 (2.7) [d]	9.6 ± 0.1 (0.27)	0.71 ± 0.17
14b (±) *trans*	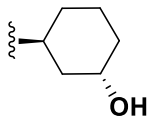	8.9 ± 0.04 (1.1)	10 ± 0.04 (0.10)	0.89 ± 0.12
14c (-) *trans*	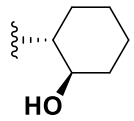	8.8 ± 0.2 (1.7) [d]	9.7 ± 0.2 (0.30)	0.74 ± 0.15
14d (+) *cis*	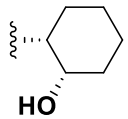	8.8 ± 0.03 (1.8)	11 ± 0.1 (0.027)	1.06 (1.09;1.02)
19 cis : trans (0.3:1)	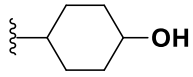	8.4 ± 0.01 (3.8) [d]	9.4 ± 0.1 (0.37)	0.88 ± 0.17
22 (±) *cis*	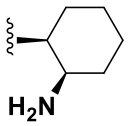	8.2 ± 0.1 (7.1)	9.5 ± 0.2 (0.52)	0.79 (0.65;0.93)
25 (±)*cis*	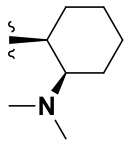	7.1 ± 0.1 (83) [d]	8.6 ± 0.2 (3.3)	0.74 (0.74;0.73)

14e	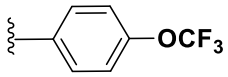	9.2 ± 0.1 (0.66) [d]	9.3 ± 0.4 (0.22)	1.29 ± 0.35
14f	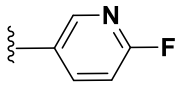	8.9 ± 0.01 (1.2) [d]	10 ± 0.4 (0.13)	0.70 (0.61;0.79)
14g	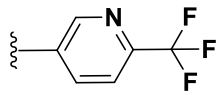	8.7 ± 0.1 (2.2) [d]	9.5 ± 0.2 (0.31)	1.12 ± 0.35
14h	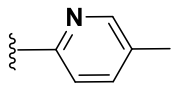	8.8 ± 0.03 (1.7)	9.9 ± 0.1 (0.14)	0.92 ± 0.16
28	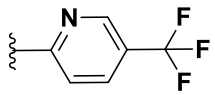	9.2 ± 0.06 (0.61)	9.9 ± 0.1 (0.19)	1.39 ± 0.34

[a] pIC_{50} ± SD (n=2) or SEM (n ≥ 3), obtained from [^{35}S]GTPγS binding on recombinant human CB_1 receptors stably expressed on HEK-293 cell membranes.

[b] pK_i ± SEM (n=3), obtained from radioligand binding assays with [^{3}H]CP55940 on recombinant human CB_1 receptors stably expressed on CHO cell membranes.

[c] KRI ± SEM (n = 3) or KRI (n_1, n_2) (n = 2), obtained from dual-point competition association assays with [^{3}H] CP55940 on recombinant human CB_1 receptors stably expressed on CHO cell membranes.

[d] n = 2.

[^{3}H]CP55940 binding kinetic assay.

Receptor association and dissociation rate constants of [^{3}H]CP55940 were directly determined in classic radioligand association and dissociation experiments at 30 °C. The binding of [^{3}H]CP55940 approached equilibrium after approximately 25 min (**Figure 3**), yielding a k_{on} (k_1) value of (1.4 ± 0.08) x 10^6 $M^{-1}s^{-1}$. Binding of the radioligand was reversible after the addition of rimonabant (10 µM), although the dissociation was rather slow. Even 240 min after the addition of rimonabant residual receptor binding (~15%) of [^{3}H]CP55940 was observed. The dissociation rate constant, k_{off} (k_2), of [^{3}H]CP55940 from the hCB_1 receptor was (1.5 ± 0.2) x 10^{-4} s^{-1}. The kinetic K_D value (k_{off}/k_{on}) of [^{3}H]CP55940 was 0.12 ± 0.03 nM (**Table 3**). The residence time (RT) of [^{3}H]CP55940 was calculated as 114 ± 16 min.

Table 3. Comparison of equilibrium binding and kinetic parameters of CP55940 determined using different methods[a)].

Assay	K_i or K_D (nM)	k_{on} ($M^{-1} \cdot s^{-1}$)	k_{off} (s^{-1})
Displacement [b)]	0.56 ± 0.04	N.A.[c)]	N.A.
Association & Dissociation [d)]	0.12 ± 0.03	(1.4 ± 0.08) x 10^6	(1.5 ± 0.2) x 10^{-4}
Competition association [e)]	0.54 ± 0.10	(1.2 ± 0.1) x 10^6	(6.5 ± 1.0) x 10^{-4}

[a]: Data are presented as means ± standard error of the mean (SEM) of at least three independent experiments performed in duplicate.

[b]: Equilibrium displacement of [^{3}H]CP55940 from hCB_1 receptor at 30 °C.

[c]: Not applicable.

[d]: Classic association and dissociation parameters of [^{3}H]CP55940 measured in standard kinetic assays at 30 °C.

[e]: Association and dissociation parameters of CP55940 measured in competition association assays at 30 °C.

Validation of the [^{3}H]CP55940 competition association assay for human CB_1 receptor.

With the k_{on} (k_1) and k_{off} (k_2) values of [^{3}H]CP55940 binding established from classical association and dissociation experiments, k_{on} (k_3) and k_{off} (k_4) of unlabeled CP55940 were determined by fitting the values based on the mathematical model as described in the experimental.[36] In this validation experiment we tested three different concentrations of unlabeled CP55940, corresponding to IC_{25}, IC_{50} and IC_{75} (**Figure 4A**). Values for k_{on} and k_{off} determined by this competition association method were (1.2 ± 0.1) x 10^6 $M^{-1} \cdot s^{-1}$ and (6.5 ± 1.0) x 10^{-4} s^{-1}, respectively. The k_{on} value was in good

agreement with the k_{on} (k_1) value determined in the classical association experiment (**Table 3**). The k_{off} value obtained by this method was also similar to that found in the classical kinetic dissociation experiments with [^{3}H]CP55940, with just a four-fold difference between the values (**Table 3**). In order to confirm the robustness of the assay with unlabeled human CB_1 receptor antagonists, an experiment was performed using rimonabant (**Figure 4B**, **Table 4**). The k_{on} and k_{off} values determined by this competition association method were (2.3 ± 0.3) x 10^5 $M^{-1}{\cdot}s^{-1}$ and (1.4 ± 0.2) x 10^{-3} s^{-1}, respectively, demonstrating that rimonabant behaves as a short residence time antagonist (14 ± 2.0 min), in good agreement with findings reported earlier.[37, 38]

Screening of hCB_1 receptor antagonists using the dual-point competition association assay.

The competition association assay described above is quite laborious and time-consuming. Therefore, a so-called "dual-point competition association assay" for the hCB_1 receptor was developed, according to the concept that we had previously established for the adenosine A_1 receptor.[32] To this end, [^{3}H]CP55940 and unlabeled antagonists were co-incubated at concentrations equal to, or 2 to 3-fold higher than, their K_i/IC_{50} values which had been determined in the [^{3}H]CP55940 displacement assay. The so-called kinetic rate index (KRI) was calculated by dividing the specific radioligand binding at 30 min (t_1) by the binding at 240 min (t_2). Antagonists with a KRI value larger than 1 indicate a slower dissociation rate, and thus a longer RT, than [^{3}H]CP55940, and *vice versa.* Furthermore, it was observed that the KRI values of the hCB_1 receptor antagonists had no obvious correlation with their affinities (**Figure 5A**).

A.

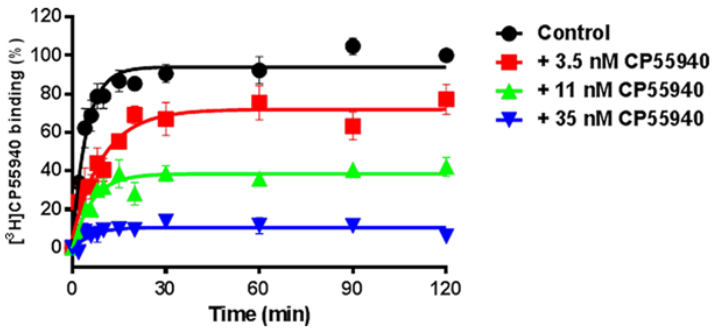

B.

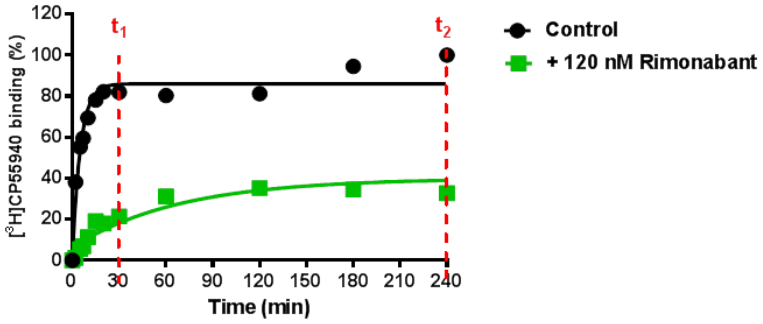

Figure 4: A) Competition association experiments with [^{3}H]CP55940 binding to recombinant hCB$_1$ receptors stably expressed on CHO cell membranes (30 °C) in the absence or presence of 3.5, 11, and 35 nM of unlabeled CP55940 (n=3, combined and normalized); **B**) Competition association experiments with [^{3}H]CP55940 binding to recombinant hCB$_1$ receptors stably expressed on CHO cell membranes (30 °C) in the absence or presence of 120 nM of unlabeled rimonabant (n=6, representative graph). t_1 is the radioligand binding at 30 min, while t_2 is the radioligand binding at 240 min.

Table 4. Kinetic parameters (k_{on}, k_{off} and RT) of selected human CB$_1$ receptor antagonists.

Code	k_{on} [a] ($M^{-1}s^{-1}$)	k_{off} [b] (s^{-1})	RT [c] (min)
11b	(3.0 ± 0.5)x10^5	(2.2 ± 0.2) x 10^{-4}	78 ± 5
14f	(7.2 ± 3.2)x10^5	(2.7 ± 0.5) x 10^{-4}	62 ± 10
28	(3.5 ± 0.7)x10^5	(7.8 ± 0.3) x 10^{-5}	260 ± 56
rimonabant	(2.3 ± 0.3)x10^5	(1.4 ± 0.2) x 10^{-3}	14 ± 2.0

[a] k_{on} ± SEM (n = 3), obtained from competition association assays with [^{3}H]CP55940 on recombinant human CB$_1$ receptors stably expressed on CHO cell membranes.

[b] k_{off} ± SEM (n = 3), obtained from competition association assays with [^{3}H]CP55940 on recombinant human CB$_1$ receptors stably expressed on CHO cell membranes.

[c] RT = 1/(60 * k_{off}); RT is expressed in min, whereas k_{off} is expressed in s^{-1}.

A.

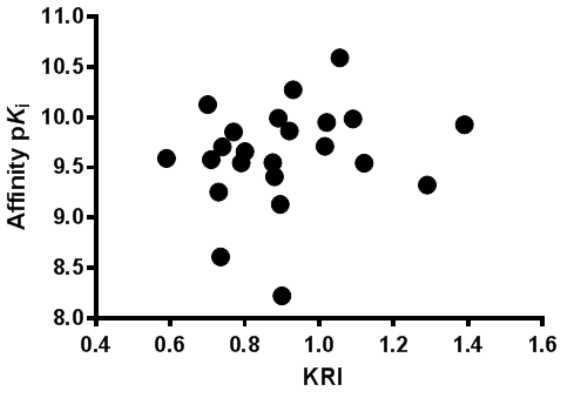

B.

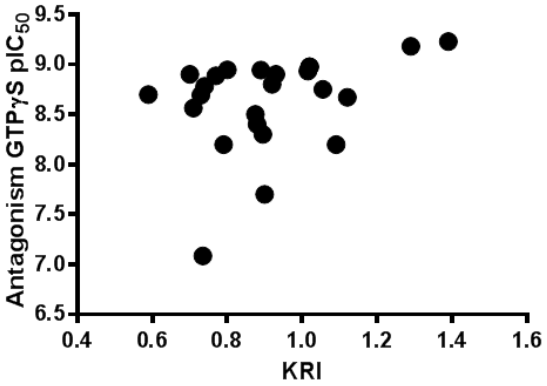

Figure 5: **A**) The negative logarithm of the affinities of the hCB_1 receptor antagonists used in this study had no obvious linear correlation with their KRI values (r^2 = 0.04, *P* = 0.33); **B**) The negative logarithm of [^{35}S]GTPγS IC_{50} values of the hCB_1 receptor antagonists in this study had no obvious linear correlation with their KRI values (r^2 = 0.12, *P* = 0.10).

Structure–Affinity Relationships (SAR) versus Structure–Kinetic Relationships (SKR).

The 1,2-diarylimidazol-4-carboxamide derivatives are rimonabant bioisosteres, in which the 2,4-dichlorophenyl, amide, aryl, and methyl moieties are maintained on an alternative heterocyclic diazo core (**Figure 1a** and **1d**). The derivatives included in this study differ in their substituents at the R^1 and R^2 positions, which are at the "left" and "right" arms of the scaffold, respectively (**Figure 1d**).

We were conscious that compound polarity may influence the activity parameters being studied, so polarity was determined by both calculated and experimental methods. Calculated methods

included Polar Surface Area (PSA),[39] ACDlogD7.4 with pK_a correction[40] and AZlogD7.4,[41] which were supplemented with experimentally determined Log*D* values. A PSA of 90 Å^2 has been described as a threshold value below which penetration of the blood–brain barrier is more likely, and thus serves as an indicator for potential to have CNS activity.[42] The calculated PSA values (**Tables S2** and **S3**) of most of the compounds in this study were above 90 Å^2, suggesting that they would have low blood-brain barrier penetration, and be better suited for peripheral antagonism of the hCB_1 receptor. We observed that neither affinities nor KRI values of the CB_1 receptor antagonists in this study had any obvious linear correlation with their lipophilicity or PSA values (**Figures S1** and **S2**).

"Left arm" optimization.

Fixing the right arm as a piperidine moiety, as in rimonabant, various ethers with different carbon chain lengths were introduced on the left arm (**Table 1**). Extension of the trifluoromethylalkyl chain from three carbons (**8a**, 1.26 nM) to four atoms (**11a**, 0.32 nM) increased affinity by about four-fold. Reducing the level of fluorination on the terminal carbon of the linear ether side-chain from three atoms (**8a**, 1.26 nM) to one atom (**8b**, 0.34 nM) also increased the affinity. By contrast, the analogue possessing a benzyl substituent on the left arm (**9**, 6.28 nM) displayed the weakest affinity of the analogues studied. The aforementioned modifications did not seem to have a drastic effect on KRI, with all compounds giving values around unity (0.80 to 1.09). As part of a strategy to increase PSA a sulfonyl-containing side-chain was introduced. The ligand bearing an *n*-propyl-sulfonyl moiety (**11b**) displayed a good affinity of 0.28 nM and a rather low KRI value of 0.59. Mono-fluorinating the terminal position led to no change in affinity (**11c**, 0.32 nM). In contrast to the ether substituents, trifluorination resulted in an almost three-fold increase (**11d**, 0.11 nM) relative to the mono-fluoro analogue. A slight increase in affinity was observed when the linear sulfonyl side-chain was extended from three carbon atoms (**11b**, 0.28 nM) to four (**11e**, 0.18 nM). Combination of this chain length with trifluoro-substitution, to give the side chain found in the CB_1 receptor agonist (-)-(R)-3-(2-hydroxymethylindanyl-4-oxy)phenyl-4,4,4-trifluoro-1-sulfonate (BAY 38-7271), [43, 44] led to a very

potent antagonist of the human CB_1 receptor (**11f**, 62 pM). Branching the chain from *n*-butyl to *i*-pentyl did not change the affinity (**11g** *vs.* **11e**), while introducing an additional methyl group led to a decrease in affinity (**11h**, *t*-hex chain, 0.60 nM). None of these ligands had a KRI value higher than 1, indicating their dissociation from the hCB_1 receptor was faster than CP55940. The analogue with the lowest KRI value (**11b**, 0.59) was selected for full-curve measurement (**Figure 6**, **Table 4**). As expected, its residence time (78 min) was shorter than that of CP55940 (114 min, see above) (**Table 4**). This result also serves as evidence that a KRI value seems to reliably reflect the corresponding dissociation rate constant.

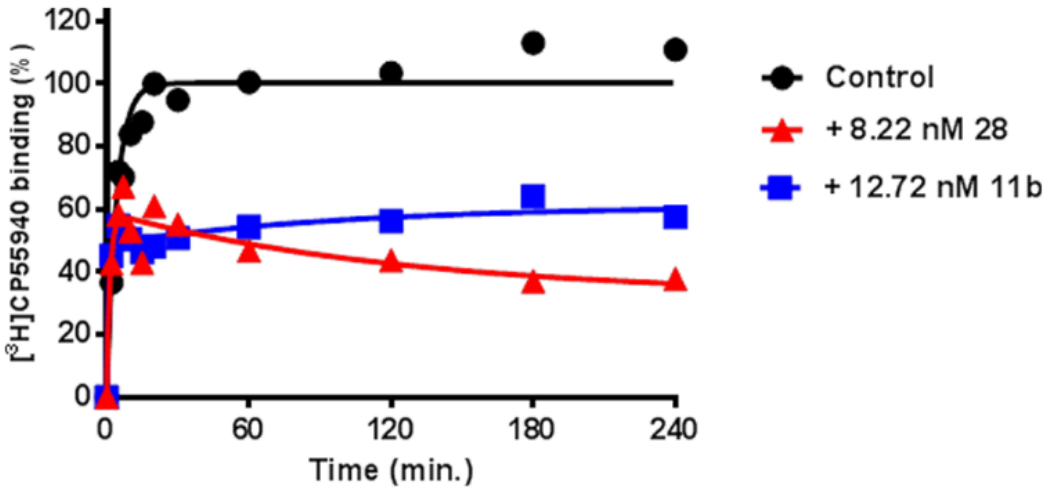

Figure 6: Competition association experiments with [^{3}H]CP55940 binding to recombinant hCB_1 receptors stably expressed on CHO cell membranes (30 °C) in the absence or presence of unlabeled long residence time compound **28** (8.22 nM, red, representative curve) or short residence time compound **11b** (12.72 nM, blue, representative curve). Data are shown as mean values from one representative experiment. At least three separate experiments each performed in duplicate.

All the linear side-chain antagonists had high affinities in the nanomolar to sub-nanomolar range, with **11f** (60 pM) as the most potent derivative. However, from the perspective of drug-target kinetic studies, despite giving a range of KRIs (0.59-1.09), none of these antagonists showed a KRI value significantly higher than 1, suggesting that none had longer residence times than CP55940.

"Right arm" optimization.

To explore the "right arm" of the 1,2-diarylimidazol-4-carboxamides, we chose to fix the "left arm" as a trifluoropropyl sulfonyl moiety (**11d**), since this group delivered high affinity (0.11 nM) and demonstrated a residence time similar to CP55940 (KRI = 1.02, **Table 1**). Introducing a hydroxyl at the 3-position of the piperidine ring yielded a ligand with lower affinity and KRI value (**14a**, K_i = 0.27 nM, KRI = 0.71) than **11d** (**Table 2**).

Efforts then focused on a series of ligands bearing cyclohexyl substituents instead of a piperidine. A carbocyclic analogue of **14a**, bearing a *trans*-hydroxyl on the 3-position of the cyclohexyl ring **14b** (racemic), delivered an approximately three-fold improvement in affinity and a slightly larger KRI value relative to the piperidine **14a** (**Table 2**). Moving the hydroxyl to the 4-position gave 4-hydroxycyclohexyl analogue (**19**), as a mixture of cis and trans diastereoisomers in a ratio of 0.3:1, and resulted in an approximately four-fold reduction in affinity (0.37 nM), whilst the KRI was unchanged (0.88); having a mixture does not allow any further conclusions, though. Interestingly, the *cis*- and *trans*-2-hydroxycyclohexyl antagonists (**14d** and **14c**, respectively) showed a substantial 10-fold difference in affinity, while their KRI values were quite similar. The more potent *cis*-isomer (**14d**, (+)) displayed an affinity of 27 pM and a KRI value close to unity. Switching the 2-substituent of the cyclohexane ring to an amine was detrimental, resulting in ligands with lower affinities. However, it is of note that the unsubstituted *cis*-amino group (**22**, (±), 0.52 nM) was less detrimental to affinity than a *cis*-dimethylamino substituent (**25**, (±), 3.3 nM), whilst the dissociation rates were very similar, as judged by their KRI values (**Table 2**). At this stage, on the basis of affinity alone, **14d** with an affinity of 27 pM seems an even better lead than **11f** with an affinity of 62 pM.

Last but not least, we found that by introducing an aromatic moiety, the compounds retain affinity in the sub-nanomolar range and, more importantly, their kinetic profiles were rather diverse. The analogue which bears a 4-trifluoromethoxyphenyl substituent (**14e**) showed high affinity (0.22 nM) and its KRI value was one of the highest measured (**Table 2**). Introduction of a pyridine moiety was

then studied. The 3-pyridyl analogues **14f** and **14g**, bearing a 6-fluoro or trifluoromethyl group, respectively, showed similar affinities (0.13 nM vs. 0.31 nM, respectively), although the latter had a much higher KRI value (1.12 vs. 0.70, respectively). This effect on KRI was increased further when the position of the nitrogen atom in the ring was switched to give the 5-substituted 2-pyridyl analogue (**28**, KRI = 1.39), which displayed the highest KRI value of all the compounds presented in this study. Finally, defluorinating this latter compound did not change the affinity, but gave rise to a marked reduction in KRI (**14h**, K_i = 0.14 nM, KRI = 0.92).

The compounds with high (**28**) and low (**11b** and **14f**) KRI values were tested in a full competition association assay to determine their association and dissociation rate constants (**Figure 6** and **Table 4**). According to the full curves, the compound with KRI > 1 (**28**) displayed an "overshoot" in the competition association curve, indicating its slow dissociation and yielding the longer residence time of 260 min, as compared to 114 min of the radioligand. By contrast, the compounds with KRI < 1 produced gradually ascending curves, suggesting faster dissociation and consequently shorter residence times of 78 min (**11b**) and 62 min (**14f**) (**Figure 6**, **Table 4**). Additionally, we determined their affinities on the human CB_2 receptor. From **Table 1 and S1** it shows that they all had higher affinity for the human CB_1 receptor, where approximately 12 to 125-fold selectivity over human CB_2 receptors was observed.

Functional assays.

As mentioned above, the antagonism in the [^{35}S]GTPγS binding assay compares quite well with the affinities derived from the [^{3}H]CP55940 displacement studies (**Figure 2**), while the KRI values of the compounds did not show any meaningful correlation with the pIC_{50} values from the GTPγS binding assay (**Figure 5B**). Since **28** showed slow dissociation, we decided to study this compound further in a more elaborate [^{35}S]GTPγS binding experiment, in which its functional activity in the inhibition of

CP55940 action was characterized and compared with rimonabant. Pretreatment of CHOK1 hCB_1 receptor membranes with rimonabant for 1h, prior to stimulation by the CB_1 receptor agonist CP55940 for 30 min, induced surmountable antagonism (a rightward shift of the agonist curve with little suppression of the maximum effect) as reported before.[45] In the case of **28** insurmountable antagonism was observed; the agonist concentration-effect curve was shifted to the right with a concomitant decrease (~50%) in its maximal response (**Figure 7**). In both cases inverse agonism by the compounds alone (in the absence of CP55940) was also apparent (negative values at Y-axis in **Figure 7**).

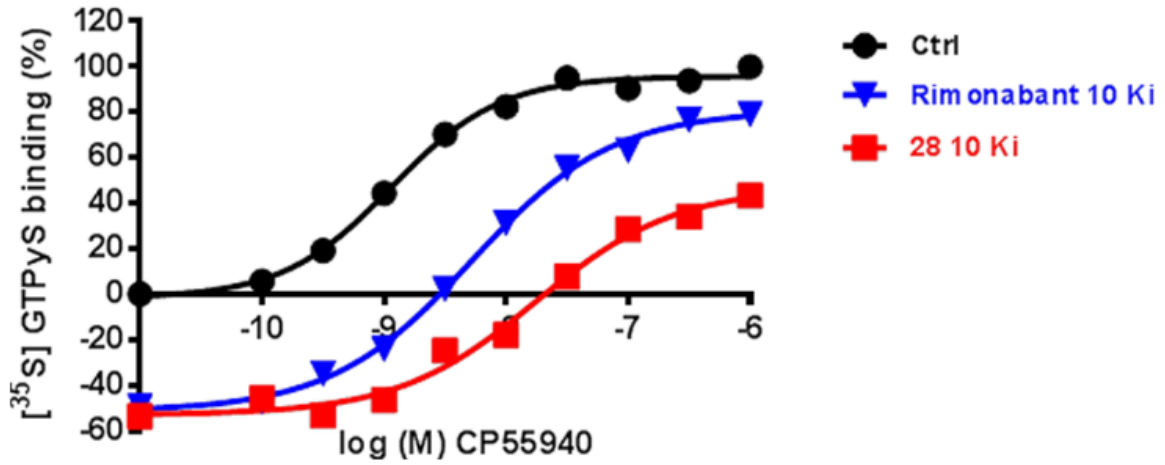

Figure 7: CP55940-stimulated [^{35}S]GTPγS binding to recombinant hCB_1 receptors stably expressed on CHO cell membranes (25 °C) in the absence (black, representative curve) or presence of long-residence-time compound **28** (red, representative curve) or rimonabant (blue, representative curve). Compound **28** or rimonabant was pre-incubated with the membranes for 1h prior to the challenge of agonist. [^{35}S]GTPγS was subsequently added and incubated for another 0.5 h. Plates were then filtered and the radioactivity counted. Curves were fitted to a four parameter logistic dose-response equation. Data were normalized according to the maximal response (100%) produced by CP55940. At least three separate experiments each performed in duplicate.

Computational studies.

Finally, we investigated the ligand-receptor interactions using the recently disclosed X-ray crystal structure of hCB_1 in complex with **29** [4-(4-(1-(2,4-dichlorophenyl)-4-methyl-3-(piperidin-1-ylcarbamoyl)-1H-pyrazol-5-yl)phenyl)but-3-ynyl nitrate, AM6538], crystal structure code:

PDB:5TGZ).[32] By docking **28** into the hCB_1 receptor it can be seen that, like **29**, it lies quite deep in the binding pocket of hCB_1 in the docked pose, immediately above the conserved Trp356$^{6.48}$ (**Figures 8A** and **B**). The main scaffold of the imidazole core and the 2,4-dichlorophenyl ring form a π-π interaction with the side chains of Phe102$^{N\text{-term}}$ and Phe170$^{2.57}$ respectively (**Figure 8B**). Unsurprisingly, and consistent with the SAR reported in **Table 1**, the "left arm" of our ligand docks into the same place as "Arm 2" of **29** in the crystal structure. This "left arm" extends into a long, narrow, and highly lipophilic channel formed by helices III, V, VI and ECL2 (**Figure 8A**). By contrast, the "right arm" of our ligands, which resemble "Arm 3" of **29** dock into an open cavity formed by various hydrophobic amino acid residues,[33] irrespective of whether a cyclohexyl, piperidine, or pyridine moiety is present. In the case of a pyridine moiety (**14e**-**14h** and **28**), the crystal structure suggests that there may be a π-π stacking interaction with His178$^{2.65}$. Further support for the docked pose of **28** comes from the higher resolution x-ray structure of taranabant bound to hCB1 (PDB: 5U09),[34] since both compounds share a trifluoromethylpyridine moiety on their "right arm".

A.

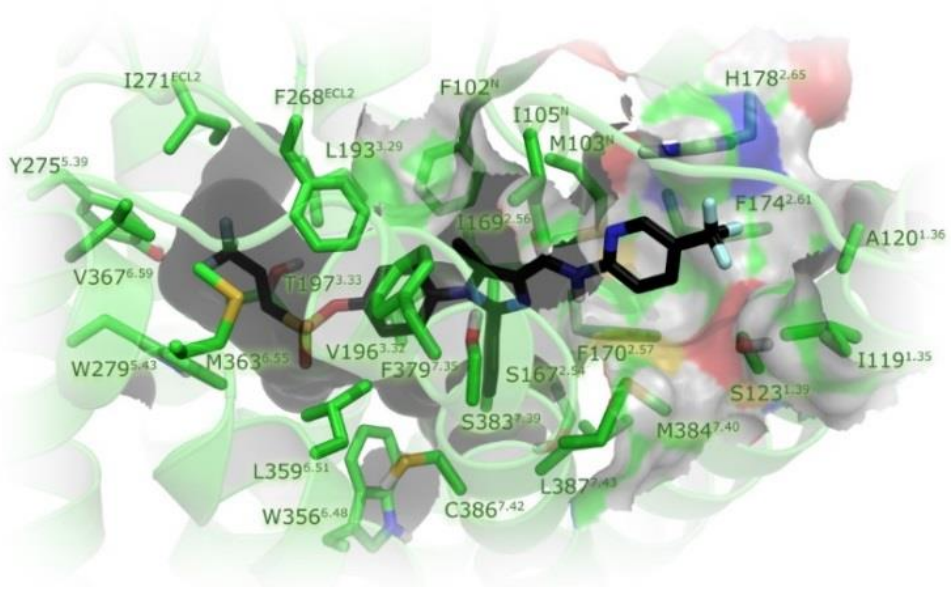

B.

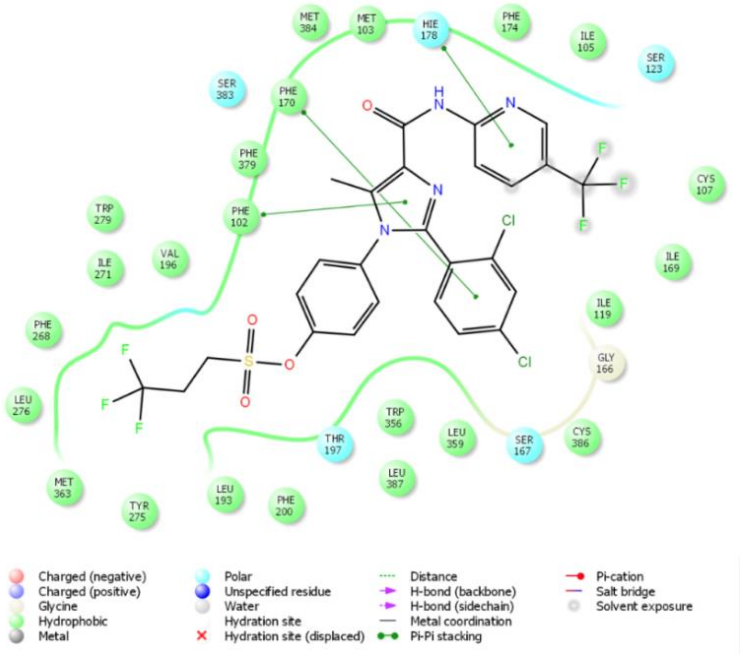

C.

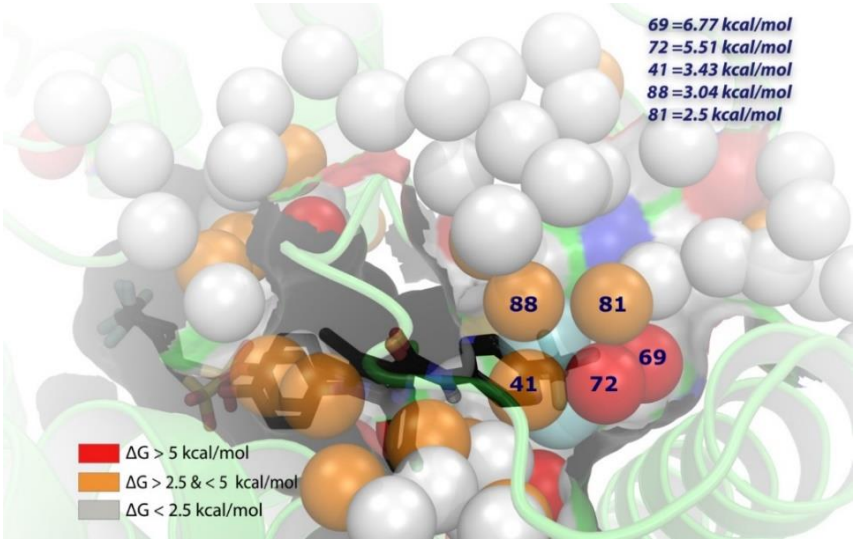

Figure 8: A) Docking of antagonist **28** into the binding site of the crystal structure of the CB_1 receptor (PDB: 5TGZ)[33] co-crystalized with **29** (not shown). Compound **28** is represented by black sticks, and residues within 5 Å of **28** are visualized as green sticks. The protein is represented by green ribbons, and relevant binding site confinements are indicated by white-grey (hydrophobic), red (electronegative), and blue (electropositive) layers. Ligand and residues atoms color code: yellow = sulfur, red = oxygen, blue = nitrogen, cyan = fluorine, white = hydrogen. **B)** 2-D interaction map of **28** docking into the CB1 receptor co-crystalized with **29** (PDB: 5TGZ),[33] demonstrating π- π stacking between imidazole core of **28** and $Phe102^{N\text{-}term}$, 2,4-dichlorophenyl ring and $Phe170^{2.57}$, pyridine and $His178^{2.65}$. **C)** Docking of **14f** and **28** into the binding site of the crystal structure of

the CB1 receptor co-crystalized with **29** (PDB: 5TGZ)[33] showing the overlay of numbered consecutively hydration sites of **14f** (colored spheres; for color code, see below) calculated by WaterMap. Hydration sites shown as red and orange spheres represent "unstable" water molecules. White spheres symbolize "stable" water molecules, which should not be displaced by **14f** or **28**. For the key hydration sites (41, 69, 72, 81, 88) surrounding the –F atom of **14f**, calculated ΔG values (in kcal/mol) with respect to bulk solvent are shown.

Using the crystal structure of the hCB_1-**29** complex, we performed WaterMap calculations to try and understand the differences in residence times observed for the ligands studied, with the hypothesis that unfavorable hydration might provide an explanation.[46-48] We focused on the pyridine ring substituents on the "right arm", and ligands **14f** and **28** in particular, because of their similar binding affinities but differing residence times. The smaller of the two ligands (**14f**, -F substitution, relatively short RT) was docked into the hCB_1 receptor, and a WaterMap was calculated for the complex. Around the –F substituent we found unstable water molecules (41, 69, 72, 81 and 88 in **Figure 8C**); these water molecules are coined unhappy waters.[49] By contrast, ligand **28** was able to displace these water molecules with its larger $-CF_3$ substituent, a process which might raise the energy of the transition state for dissociation. We postulate that this destabilization of the transition state may contribute to the prolonged residence time observed with this compound.

Conclusions

We have demonstrated that, in addition to affinity, knowledge of binding kinetics is useful for selecting and developing new hCB_1 receptor antagonists in the early phases of drug discovery. In the specific case of the hCB_1 receptor, a long residence time compound may be beneficial for a peripherally selective antagonist. We explored SAR and SKR parameters in a series of 1,2-diarylimidazol-4-carboxamide derivatives by examining the influence of substitutions at both "arms" of the molecules.

By introducing more polar linear sulfonyl side chains on the "left arm", affinity could be modulated, however the KRI values indicative for the compounds' kinetic properties were less than or similar to CP55940. Substitution of the "right arm" maintained or increased affinity, and with the introduction of an aromatic ring system KRI values >1 were obtained. With a residence time of 260 min, which is substantially longer than CP55940 (114 min.) or rimonabant (14 min.), 4-(2-(2,4-dichlorophenyl)-5-methyl-4-((5-(trifluoromethyl)pyridin-2-yl)carbamoyl)-1*H*-imidazol-1-yl)phenyl 3,3,3-trifluoropropane-1-sulfonate (**28**) stood out from the ligands studied. This slowly dissociating hCB_1 receptor antagonist also showed insurmountability in a functional GTPγS binding assay. Using the recently resolved hCB_1 crystal structures we analyzed the putative interactions of **28** with the receptor, from which we speculate that displacement of 'unhappy' water molecules may provide a plausible explanation for its slow dissociation. Therefore, compound **28**, or derivatives with similar characteristics, may be a useful tool to test whether prolonged blockade of the (peripheral) hCB_1 receptor has a beneficial effect on CB_1 receptor related disorders, such as obesity.

Experimental section

Chemistry. All solvents and reagents were purchased from commercial sources and were of analytical grade. Demineralized water is simply referred to as water or H_2O, as was used in all cases unless stated otherwise (i.e., brine). Thin-layer chromatography (TLC) was routinely consulted to monitor the progress of reactions, using aluminum-coated Merck silica gel F_{254} plates. Purification was performed on a semi-preparative high performance liquid chromatography (HPLC) with a mass triggered fraction collector, Shimadzu QP 8000 single quadrupole mass spectrometer equipped with 19 x 100 mm C8 column. The mobile phase used was, if nothing else is stated, acetonitrile and buffer (aqueous NH_4OAc (0.1 M) : acetonitrile 95 : 5). For isolation of isomers, a Kromasil CN E9344 (250 x 20 mm i.d.) column was used. A mixture of heptane/ethyl acetate/diethylamine 95 : 5 : 0.1 was used as mobile phase (1 mL/min). Fraction collection was guided using a UV-detector (330 nm). Analytical

purity of the final products was determined by Waters Acquity I-class ultra-performance liquid chromatography (UPLC) consisting of a binary solvent system, ultra-violet (UV) photo-diode array (PDA) detector, column temperature control manager and sample manager modules, coupled with in-line and mass spectrometry detection. The sample was injected onto, and separated by, a Waters Acquity BEH (C18) 1.7 mm (150x3 mm) UPLC column maintained at 40°C and eluted with 0.1% ammonium hydroxide in water (A) and acetonitrile (B) at a flow rate of 1 mL/min, using a linear gradient. Initial conditions started at 3% B, which was increased to 97% over 1.3 min, maintained for 0.2 min before returning to initial conditions over 0.2 min prior to the next injection. Eluent containing UPLC-separated analytes then flowed via the UV PDA detector scanning between 220-320 nm wavelengths at a resolution of 1.2 nm sampling at 40 points/s, into a Waters SQD single quadrupole mass spectrometer (MS) fitted with an electrospray source. All MS analyses were acquired for a total run time of 2 min, with mass scanning from 100-1000 u in both positive and negative ion modes alternately, using electrospray ionization (ESI). Typical MS settings included capillary voltage - 1kV, cone voltage - 25V, source temperature - 150°C, and desolvation temperature - 350°C. The data were acquired via a PC running MassLynx v4.1 in open access mode and processed and reported via OpenLynx software application. For each sample the purity is determined by integration of the UV absorption chromatogram. All final compounds show a single peak and are at least 95% pure.

^{1}H NMR measurements were performed on either a Varian Mercury 300 or a Varian Inova 500, operating at ^{1}H frequencies of 300 and 500 MHz respectively at ambient temperature. Chemical shifts are reported in parts per million (ppm), are designated by δ, and are downfield to the internal standard tetramethylsilane (TMS) in $CDCl_3$. Coupling constants are reported in Hz and are designated as *J*. High-resolution mass spectra were recorded on either a Micromass ZQ single quadrupole or a Micromass LCZ single quadrupole mass spectrometer both equipped with a pneumatically assisted electrospray interface (LC-MS). Melting points were determined on a Reichert melting point microscope and are uncorrected.

*N-(4-(Benzyloxy)phenyl)-2,4-dichlorobenzamidine (**2**).* Compound **1** (5.0 g, 21.2 mmol) was added dropwise to a solution of ethyl magnesium bromide (44.5 mL, 1 M in THF, 44.5 mmol) in dry THF (25 mL) under a nitrogen atmosphere. After stirring for 20 minutes a solution of 2,4-dichlorobenzonitrile (3.65 g, 21.2 mmol) in THF (25 mL) was added. The reaction mixture was stirred for 20 hours at r.t.. Water (50 mL) was carefully added. Extraction with EtOAc (2 x 100 mL), drying (Na_2SO_4), filtration and evaporation to dryness afforded the crude title compound (7.7 g, 98%).

*Ethyl 1-(4-(benzyloxy)phenyl)-2-(2,4-dichlorophenyl)-5-methyl-1H-imidazole-4-carboxylate (**3**).* To a solution of compound **2** (6.88 g, 18.5 mmol) in THF (50 mL) was added potassium carbonate (2.56 g, 18.5 mmol) and the suspension was stirred for 10 minutes. Ethyl-3-bromo-2-oxobutanoate (4.65 g, 22.2 mmol) was added dropwise over 1 hour, and the mixture was stirred for 66 hours at r.t.. The solution was filtered and evaporated to dryness. The residue was dissolved in AcOH and refluxed for 1 hour. The mixture was cooled to r.t., water (100 mL) added and the product extracted with EtOAc (2 x 200 mL). The combined organic phases were washed with saturated aqueous sodium hydrogen carbonate, dried (Na_2SO_4), filtered, and concentrated *in vacuo*. Flash chromatography (silica, 30-40% EtOAc in hexane) afforded the title compound (5.75 g, 65%) as a pale yellow solid. ^{1}H NMR ($CDCl_3$): δ 7.50-7.20 (m, 8H), 7.10-6.90 (m, 4H), 5.10 (s, 2H), 4.50 (q, 2H), 2.5 (s, 3H), 1.5 (t, 3H).

*1-(4-(Benzyloxy)phenyl)-2-(2,4-dichlorophenyl)-5-methyl-1H-imidazole-4-carboxylic acid (**4**).* To a suspension of compound **3** (3.62 g, 7.5 mmol) in MeOH (60 mL) was added potassium hydroxide (4.05 g, 72 mmol) in water (20 mL), and the reaction mixture heated to reflux. After 2 h the mixture was cooled to r.t., acidified to pH~2 with HCl (1 M) and extracted with ethyl acetate (2 x 200 mL). The combined organic phases were dried (Na_2SO_4), filtered and concentrated *in vacuo* to give the crude title compound (3.38 g, 99%).

*Ethyl 2-(2,4-dichlorophenyl)-1-(4-hydroxyphenyl)-5-methyl-1H-imidazole-4-carboxylate (**5**).* compound **3** (4.82 g, 10 mmol) was dissolved in HBr (33% in AcOH, 80 mL) and stirred overnight at r.t. with exclusion of light. The solvents were evaporated and the residue co-evaporated with EtOH. The

residue was dissolved in EtOH, HCl (4 M in dioxane, 5 mL) and $MgSO_4$ were added, and the resulting mixture heated under reflux for 2.5 h. The reaction mixture was cooled to r.t., filtered, and concentrated *in vacuo*. The residue was dissolved in EtOAc and washed with water basified with triethylamine and then brine. The organic layer was dried over Na_2SO_4 and concentrated *in vacuo* to give the crude title compound (4.74 g) as a brown, viscous oil of sufficient purity for the next step.

*Ethyl 2-(2,4-dichlorophenyl)-5-methyl-1-(4-(3,3,3-trifluoropropoxy)phenyl)-1H-imidazole-4-carboxylate (**6a**).* A solution of compound **5** (978 mg, 2.5 mmol), 3,3,3-trifluoro-1-propanol (428 mg, 3.75 mmol) and triphenylphosphine (984 mg, 3.75 mmol) in anhydrous THF (12 mL) were treated with DEAD (40% in toluene, 1.72 mL, 3.75 mmol). The resulting mixture was stirred at r.t. for 30 h, then heated to 50 °C overnight. After cooling to r.t., additional 3,3,3-trifluoro-1-propanol (428 mg, 3.75 mmol) and triphenylphosphine (984 mg, 3.75 mmol) were added, followed by di-*tert*-butylazodicarboxylate (863 mg, 3.75 mmol), and the resulting mixture stirred at r.t. overnight. Again, additional 3,3,3-trifluoro-1-propanol (428 mg, 3.75 mmol) and triphenylphosphine (984 mg, 3.75 mmol) were added, followed by di-*tert*-butyl azodicarboxylate (863 mg, 3.75 mmol), and the resulting mixture stirred at r.t. overnight. The mixture was concentrated *in vacuo* and the residue purified by column chromatography (silica gel, 10-50% EtOAc in hexanes) to yield the title compound (880 mg, 68%) as a yellowish foam of sufficient purity for the next transformation. ^{1}H NMR (500 MHz, $CDCl_3$) δ 7.22-7.16 (m, 3H), 7.01 (d, J = 8.7 Hz, 2H), 6.83 (d, J = 8.7 Hz, 2H), 4.40 (q, J = 7.1 Hz, 2H), 4.22-4.10 (m, 2H), 2.66-2.54 (m, 2H), 2.40 (s, 3H), 1.40 (t, J = 7.1 Hz, 3H).

*Ethyl 2-(2,4-dichlorophenyl)-1-(4-(3-fluoropropoxy)phenyl)-5-methyl-1H-imidazole-4-carboxylate (**6b**).* A solution of compound **5** (978 mg, 2.5 mmol), 3-fluoropropan-1-ol (293 mg, 3.75 mmol) and triphenylphosphine (984 mg, 3.75 mmol) in anhydrous THF (9 mL) were treated with DEAD (40% solution in toluene, 1.72 mL, 3.75 mmol). The resulting mixture was stirred at r.t. overnight. The residue was purified by column chromatography (silica gel, 20-40% EtOAc in hexanes). The product containing fractions were combined and concentrated *in vacuo*. The residue was dissolved in CH_2Cl_2,

then an equal amount of hexane was added. The resulting solid was filtered off, and the filtrate concentrated *in vacuo* to yield the title compound (1.07 g, 85%) as a colorless foam of *ca.* 90% purity which was used in the next transformation without further purification. ^{1}H NMR (500 MHz, $CDCl_3$) δ 7.35-7.20 (m, 3H), 7.03 (d, *J* = 8.7 Hz, 2H), 6.87 (d, *J* = 8.7 Hz, 2H), 4.73-4.60 (m, 2H), 4.44 (q, *J* = 7.1 Hz, 2H), 4.11-4.07 (m, 2H), 2.44 (s, 3H), 2.24-2.13 (m, 2H), 1.44 (t, *J* = 7.1 Hz, 3H).

*2-(2,4-Dichlorophenyl)-5-methyl-1-(4-(3,3,3-trifluoropropoxy)phenyl)-1H-imidazole-4-carboxylic acid (**7a**).* A stirred solution of compound **6a** (880 mg, 1.72 mmol), in a mixture of THF (15 mL) and EtOH (15 mL), was treated with KOH (1.07 g, 19 mmol) dissolved in water (10 mL) and the resulting mixture stirred at 50 °C. After 3 h 30 min the reaction mixture was cooled to r.t. then concentrated *in vacuo*. The residue was partitioned between CH_2Cl_2 and HCl (1 M) and, after phase separation, the aqueous layer was extracted two more times with CH_2Cl_2. The combined organic extracts were dried over $MgSO_4$ and concentrated *in vacuo* to give the title compound (714 mg, 90%) as a yellowish foam. ^{1}H NMR (500 MHz, $CDCl_3$) δ 7.32-7.18 (m, 3H), 7.00 (d, *J* = 8.7 Hz, 2H), 6.85 (d, *J* = 8.7 Hz, 2H), 4.18-4.14 (m, 2H), 2.66-2.55 (m, 2H), 2.42 (s, 3H).

*2-(2,4-Dichlorophenyl)-1-(4-(3-fluoropropoxy)phenyl)-5-methyl-1H-imidazole-4-carboxylic acid (**7b**).* A solution of compound **6b** (1.07 g, 2.13 mmol, ca. 90% pure), in a mixture of THF (20 mL) and EtOH (20 mL), was treated with KOH (1.40 g, 25 mmol) dissolved in water (10 mL) and the resulting mixture stirred at 50 °C. After 3 h 30 min the reaction mixture was cooled to r.t. then concentrated *in vacuo*. The residue was partitioned between CH_2Cl_2 and HCl (1 M) and, after phase separation, the aqueous layer extracted with CH_2Cl_2 and twice with EtOAc. The combined organic extracts were dried over $MgSO_4$ and concentrated *in vacuo* to give the title compound (856 mg, 95%) as a yellowish foam which was sufficiently pure for the next step. ^{1}H NMR (500 MHz, $CDCl_3$) δ 7.35-7.22 (m, 3H), 7.04 (d, *J* = 8.7 Hz, 2H), 6.88 (d, *J* = 8.7 Hz, 2H), 4.72-4.60 (m, 2H), 4.12-4.09 (m, 2H), 2.46 (s, 3H), 2.25-2.14 (m, 2H).

*2-(2,4-Dichlorophenyl)-5-methyl-N-(piperidin-1-yl)-1-(4-(3,3,3-trifluoropropoxy)phenyl)-1H-imidazole-4-carboxamide (**8a**).* A solution of compound **7a** (643 mg, 1.4 mmol) in CH_2Cl_2 (10 mL) was treated with oxalyl chloride (200 µL, 2.36 mmol), followed by 10 µL DMF. The resulting mixture was stirred for 90 min at r.t., then concentrated *in vacuo*. The residue was dried under vacuum as a yellowish foam which was used without further purification. Subsequently, to a mixture of piperidin-1-amine hydrochloride (0.3 mmol) and pyridine (100 µL) in CH_2Cl_2 (1 mL) was added a portion of crude intermediate (2-(2,4-dichlorophenyl)-5-methyl-1-(4-(3,3,3-trifluoropropoxy)phenyl)-1*H*-imidazole-4-carbonyl chloride (96 mg, 0.2 mmol)) in CH_2Cl_2 (1 mL) and the resulting mixture stirred at r.t. for 2 h 30 min. The reaction mixture was washed with saturated aqueous $NaHCO_3$ (2 mL) and, after phase separation, filtered through a phase separator. The solvents were evaporated and the residue purified by preparative HPLC eluting on a reverse-phase column (5-100% acetonitrile in aqueous NH_4OAc (0.1 M)) to give the title compound (45 mg, 41%) as a colorless solid. ^1H NMR (500 MHz, $CDCl_3$) δ 7.90 (s, 1H), 7.35 (d, *J* = 1.9 Hz, 3H), 7.29 (d, *J* = 8.3 Hz, 1H), 7.23 (dd, *J* = 1.9, 8.3 Hz, 1H), 7.03 (d, *J* = 8.9 Hz, 2H), 6.87 (d, *J* = 8.9 Hz, 2H), 4.19 (t, *J* = 6.6 Hz, 2H), 2.94-2.81 (m, 4H), 2.69-2.60 (m, 2H), 2.47 (s, 3H), 1.82-1.73 (m, 4H), 1.49-1.41 (m, 2H); HRMS Calcd for [$C_{25}H_{25}Cl_2F_3N_4O_2$+H]: 541.1385. Found: 541.1366. HPLC: 100%.

*2-(2,4-Dichlorophenyl)-1-(4-(3-fluoropropoxy)phenyl)-5-methyl-N-(piperidin-1-yl)-1H-imidazole-4-carboxamide (**8b**).* A solution of compound **7b** (732 mg, 1.55 mmol) in CH_2Cl_2 (20 mL) was treated with oxalyl chloride (200 µL, 2.36 mmol), followed by DMF (10 µL). The resulting mixture was stirred for 90 min at r.t., then concentrated *in vacuo*. The residue was dried under vacuum as a yellowish foam which was used without further purification. Subsequently, to a mixture of piperidin-1-amine hydrochloride (0.39 mmol) and pyridine (100 µL) in CH_2Cl_2 (2 mL) was added a portion of crude 2-(2,4-dichlorophenyl)-1-(4-(3-fluoropropoxy)phenyl)-5-methyl-1*H*-imidazole-4-carbonyl chloride (115 mg, 0.26 mmol) in CH_2Cl_2 (2 mL) and the resulting mixture was stirred at r.t. for 2 h. The reaction mixture was washed with saturated aqueous $NaHCO_3$ (2 mL) and, after phase separation, filtered through a phase separator. The solvents were evaporated and the residue purified by preparative

HPLC eluting on a reverse-phase column (5-100% CH_3CN in aqueous NH_4OAc (0.1 M)) to give the title compound (74 mg, 56%) as a colorless solid. ^1H NMR (500 MHz, $CDCl_3$) δ 7.90 (s, 1H), 7.35 (d, *J* = 2.0 Hz, 1H), 7.28 (d, *J* = 8.2 Hz, 1H), 7.23 (dd, *J* = 2.0, 8.2 Hz, 1H), 7.01 (d, *J* = 8.9 Hz, 2H), 6.86 (d, *J* = 8.9 Hz, 2H), 4.66 (dt, *J* = 5.7, 47.0 Hz, 2H), 4.09 (t, *J* = 6.1 Hz, 2H), 2.95-2.82 (m, 4H), 2.47 (s, 3H), 2.25-2.13 (m, 2H), 1.81-1.73 (m, 4H), 1.49-1.40 (m, 2H); HRMS Calcd for [$C_{25}H_{27}Cl_2FN_4O_2$+H]: 505.1573. Found: 505.1572. HPLC: 100%.

*1-(4-(Benzyloxy)phenyl)-2-(2,4-dichlorophenyl)-5-methyl-N-(piperidin-1-yl)-1H-imidazole-4-carboxamide (**9**).* To a solution of compound **4** (3.38 g, 7.5 mmol) in CH_2Cl_2 (60 mL) were added 3 drops of DMF, followed by oxalyl chloride (1.3 mL, 14.9 mmol). The mixture was refluxed for 2 hours, then cooled to r.t. and evaporated to dryness. The residue was dissolved in CH_2Cl_2 (50 mL) and cooled to 0 °C. Triethylamine (2.1 mL, 14.9 mmol) was added, followed by piperidin-1-amine (0.9 mL, 8.2 mmol), and the mixture stirred at r.t. for 2 hours. Water (300 mL) was added and the mixture extracted with CH_2Cl_2 (3 x 100 mL). The organic extracts were dried (Na_2SO_4), filtered, and concentrated *in vacuo*. Flash chromatography (silica, 66-100% EtOAc in hexane) afforded the title compound (2.94 g, 74%) as a white solid. ^1H NMR (400 MHz, $CDCl_3$) δ 7.71 (d, *J* = 8.3 Hz, 1H), 7.42-7.32 (m, 7H), 7.29 (dd, *J* = 1.9, 8.3 Hz, 1H), 7.24 (d, *J* = 9.0 Hz, 2H), 6.98 (d, *J* = 9.0 Hz, 2H), 5.04 (s, 2H), 4.05-3.52 (m, 4H), 2.54 (s, 3H), 2.29-2.16 (m, 4H), 1.78-1.57 (m, 2H); HRMS Calcd for [$C_{29}H_{28}Cl_2N_4O_2$+H]: 535.1667. Found: 535.1667. HPLC: 96.9%.

*2-(2,4-Dichlorophenyl)-1-(4-hydroxyphenyl)-5-methyl- N-(piperidin-1-yl)-1H-imidazole-4-carboxamide (**10**).* A solution of compound **9** (2.78 g, 5.2 mmol) in CH_2Cl_2 (80 mL) was cooled to 0 °C then treated dropwise with boron tribromide (1 M in CH_2Cl_2, 10.4 mL, 10.4 mmol). The reaction mixture was stirred at r.t. for 1 hour then treated with water (200 mL). The mixture was extracted with EtOAc (3 x 200 mL). The combined organic phases were dried (Na_2SO_4), filtered, and concentrated *in vacuo*. Flash chromatography (silica, 75-100% EtOAc in hexane) afforded the title compound (1.34 g, 58%) as a white solid. ^1H NMR (400 MHz, $CDCl_3$) δ 8.66 (br s, 1H), 7.94 (br s, 1H), 7.31 (d, *J* = 1.9 Hz, 1H),

7.23 (d, *J* = 8.3 Hz, 1H), 7.18 (dd, *J* = 1.9, 8.3 Hz, 1H), 6.92-6.85 (m, 4H), 2.90-2.67 (m, 4H), 2.43 (s, 3H), 1.69-1.56 (m, 4H), 1.43-1.30 (m, 2H).

*2-(2,4-Dichlorophenyl)-5-methyl-N-(piperidin-1-yl)-1-(4-(4,4,4-trifluorobutoxy)-phenyl)-1H-imidazole-4-carboxamide (**11a**).* A suspension of compound **10** (351 mg, 0.79 mmol) and K_2CO_3 (218 mg, 1.58 mmol) in acetone (50 mL) was treated dropwise with 1-iodo-4,4,4-trifluorobutane (376 mg, 1.58 mmol). The reaction mixture was refluxed overnight then cooled, filtered, and concentrated *in vacuo*. Flash chromatography (silica, hexane : EtOAc 1:2) afforded the title compound (200 mg, 46%) as a white solid. ^{1}H NMR (400 MHz, $CDCl_3$) δ 7.91 (br s, 1H), 7.32 (d, *J* = 1.9 Hz, 1H), 7.27 (d, *J* = 8.3 Hz, 1H), 7.21 (dd, *J* = 2.0, 8.3 Hz, 1H), 7.00 (d, *J* = 8.9 Hz, 2H), 6.83 (d, *J* = 8.9 Hz, 2H), 3.99 (t, *J* = 6.0 Hz, 2H), 3.13-2.67 (m, 4H), 2.45 (s, 3H), 2.38-2.23 (m, 2H), 2.10-2.00 (m, 2H), 1.84-1.71 (m, 4H), 1.50-1.38 (m, 2H); MS *m/z* 578 (M+Na); HRMS Calcd for [$C_{26}H_{27}Cl_2F_3N_4O_2$+H]: 555.1541. Found: 555.1504. HPLC: 100%.

*4-(2-(2,4-Dichlorophenyl)-5-methyl-4-(piperidin-1-ylcarbamoyl)-1H-imidazol-1-yl)phenyl propane-1-sulfonate (**11b**).* A solution of compound **10** (320 mg, 0.72 mmol) in CH_2Cl_2 (10 mL) was cooled to 0 °C. Et_3N (100 µL, 0.72 mmol) was added followed by 1-propanesulfonyl chloride (81 µL, 0.72 mmol) and the reaction mixture was stirred at room temperature overnight. Water was added, the mixture extracted with CH_2Cl_2 (3 x 20 mL), dried (Na_2SO_4), filtered and concentrated. Flash chromatography (silica, hexane : EtOAc 1 : 2) afforded the title compound (220 mg, 56%) as a white solid. ^{1}H NMR (400 MHz, $CDCl_3$) δ 7.82 (br s, 1H), 7.29-7.15 (m, 5H), 7.10-7.03 (m, 2H), 3.23-3.14 (m, 2H), 2.90-2.70 (m, 4H), 2.42 (s, 3H), 2.01-1.88 (m, 2H), 1.75-1.65 (m, 4H), 1.41-1.31 (m, 2H), 1.06 (t, *J* = 7.5 Hz, 3H); ^{13}C NMR (126 MHz, $CDCl_3$) δ 160.8, 149.0, 142.3, 136.8, 135.3, 135.0, 133.8, 133.4, 130.6, 129.9, 129.1, 128.2, 127.4, 123.1, 57.2, 52.9, 25.4, 23.3, 17.5, 13.0, 10.9; HRMS Calcd for [$C_{25}H_{28}Cl_2N_4O_4S$+H]: 551.1287. Found: 551.1313. HPLC: 100%.

*4-(2-(2,4-Dichlorophenyl)-5-methyl-4-(piperidin-1-ylcarbamoyl)-1H-imidazol-1-yl)phenyl 3-fluoropropane-1-sulfonate (**11c**).* A suspension of compound **10** (200 mg, 0.45 mmol) in dry CH_2Cl_2 (3

mL) was treated with Et_3N (45 mg, 0.45 mmol) at r.t.. The resulting mixture was cooled to -78 °C and 3-fluoropropane-1-sulfonyl chloride (72 mg, 0.45 mmol) in dry CH_2Cl_2 (0.5 mL) was added dropwise. After 1 h 40 min at -78 °C was added 3-fluoropropane-1-sulfonyl chloride (72 mg, 0.45 mmol) and after a total of 4 h 40 min was added Et_3N (55 mg, 0.54 mmol). The reaction was allowed to reach r.t. overnight. It was then cooled to 0 °C and Et_3N (55 mg, 0.54 mmol) was added, followed by 3-fluoropropane-1-sulfonyl chloride (72 mg, 0.45 mmol) after a total of 19 h. After 1 h the reaction mixture was washed with water and concentrated *in vacuo*. The product was purified by HPLC (30-100% CH_3CN in aqueous NH_4OAc (0.1 M) over 40 min) to yield the title compound as a white solid (160 mg, 63%). ^1H NMR (400 MHz, $CDCl_3$) δ 7.88 (br s, 1H), 7.39-7.17 (m, 5H), 7.11 (d, J = 8.8 Hz, 2H), 4.58 (dt, J = 5.5, 46.8 Hz, 2H), 3.53-3.33 (m, 2H), 2.92-2.71 (m, 4H), 2.45 (s, 3H), 2.40-2.23 (m, 2H), 1.83-1.62 (m, 4H), 1.46-1.33 (m, 2H). HRMS Calcd for $[C_{25}H_{27}Cl_2FN_4O_4S+H]$: 569.119. Found: 569.1192. HPLC: 100%.

*4-(2-(2,4-Dichlorophenyl)-5-methyl-4-(piperidin-1-ylcarbamoyl)-1H-imidazol-1-yl)phenyl 3,3,3-trifluoropropane-1-sulfonate methanesulfonic acid salt (**11d**).* A solution of compound **10** (0.89 g, 2.00 mmol) in CH_2Cl_2 (20 mL) was cooled to 0 °C then treated with Et_3N (0.35 mL, 2.4 mmol), followed by 3,3,3-trifluoropropanesulfonyl chloride (prepared by an analogous method to that described in WO00/010968 for the butyl homologue) (0.35 mL, 2.40 mmol). The reaction mixture was stirred at r.t. overnight. TLC showed remaining starting material and so another portion of Et_3N and 3,3,3-trifluoropropanesulfonyl chloride was added and the reaction mixture stirred for additional 2 h. Water was added and the product was extracted with CH_2Cl_2, dried (Na_2SO_4), filtered, and concentrated *in vacuo*. Flash chromatography (33-100% EtOAc in hexane) followed by recrystallisation (hexane : EtOAc) afforded the title compound (700 mg, 59%) as a colorless solid. ^1H NMR (400 MHz, $CDCl_3$) δ 7.92 (s, 1H), 7.34-7.24 (m, 5H), 7.20-7.13 (m, 2H), 3.54-3.48 (m, 2H), 3.00-2.82 (m, 4H), 2.84-2.73 (m, 2H), 2.50 (s, 3 H), 1.83-1.72 (m, 4 H), 1.49-1.39 (m, 2H); HRMS Calcd for $[C_{26}H_{29}Cl_2F_3N_4O_7S_2+H]$: 605.1004. Found: 605.1012. HPLC: 100%.

*4-(2-(2,4-Dichlorophenyl)-5-methyl-4-(piperidin-1-ylcarbamoyl)-1H-imidazol-1-yl)phenyl butane-1-sulfonate (**11e**).* A solution of compound **10** (320 mg, 0.72 mmol) in CH_2Cl_2 (10 mL) was cooled to 0 °C. Et_3N (100 µL, 0.72 mmol) was added followed by 1-butanesulfonyl chloride (93 µL, 0.72 mmol) and the reaction mixture was stirred at r.t. overnight. Water was added and the mixture extracted with CH_2Cl_2 (3 x 20 mL), dried (Na_2SO_4), filtered, and concentrated *in vacuo*. Flash chromatography (silica, hexane : EtOAc 1:2) afforded the title compound (230 mg, 57%) as a white solid. ^{1}H NMR (400 MHz, $CDCl_3$) δ 7.82 (br s, 1H), 7.27-7.16 (m, 5H), 7.09-7.04 (m, 2H), 3.23-3.17 (m, 2H), 2.92-2.68 (m, 4H), 2.42 (s, 3H), 1.93-1.84 (m, 2H), 1.74-1.66 (m, 4H), 1.50-1.40 (m, 2H), 1.40-1.33 (m, 2H), 0.91 (t, *J* = 7.4 Hz, 3H) ; MS *m/z* 588 (M+Na); HRMS Calcd for [$C_{26}H_{30}Cl_2N_4O_4S$+H]: 565.1443. Found: 565.1450. HPLC: 100%.

*4-(2-(2,4-Dichlorophenyl)-5-methyl-4-(piperidin-1-ylcarbamoyl)-1H-imidazol-1-yl)-phenyl 4,4,4-trifluorobutane-1-sulfonate (**11f**).* A solution of compound **10** (0.49 g, 1.20 mmol) in CH_2Cl_2 (20 mL) was cooled to 0 °C and treated with Et_3N (0.67 mL, 4.8 mmol), followed by 4,4,4-trifluorobutane-1-sulfonyl chloride (prepared as described in WO00/010968) (0.38 g, 1.80 mmol). The reaction mixture was stirred at r.t. for 3 h. TLC showed remaining starting material so another portion of Et_3N and 4,4,4-trifluorobutane-1-sulfonyl chloride was added and the reaction mixture stirred overnight. Water was added, then the mixture was extracted with CH_2Cl_2. The organic extracts were dried (Na_2SO_4), filtered, and concentrated *in vacuo*. Flash chromatography (33-100% EtOAc in hexane) followed by recrystallisation (hexane : EtOAc) afforded the title compound (0.45 g, 61%) as a colorless solid. ^{1}H NMR (400 MHz, $CDCl_3$) δ 7.92 (br s, 1H), 7.34-7.22 (m, 5H), 7.15 (d, *J* = 8.7 Hz, 2H), 3.38 (t, *J* = 7.3 Hz, 2H), 3.12-2.74 (m, 4H), 2.49 (s, 3H), 2.43-2.32 (m, 2H), 2.32-2.22 (m, 2H), 1.82-1.74 (m, 4H), 1.50-1.40 (m, 2H); HRMS Calcd for [$C_{26}H_{27}Cl_2F_3N_4O_4S$+H]: 619.1160. Found: 619.1148. HPLC: 96.9%.

*4-(2-(2,4-Dichlorophenyl)-5-methyl-4-(piperidin-1-ylcarbamoyl)-1H-imidazol-1-yl)phenyl 3-methylbutane-1-sulfonate (**11g**).* A solution of compound **10** (50 mg, 0.11 mmol) in CH_2Cl_2 (3 mL) was

cooled to 0 °C then treated with Et_3N (20 µL, 0.13 mmol). The resulting mixture was cooled to -78 °C, then 3-methylbutane-1-sulfonyl chloride (23 mg, 0.13 mmol) carefully added. The reaction was stirred at -78 °C for 1.5 h. Water was added, then the mixture was extracted with CH_2Cl_2. The organic extracts were dried, filtered, and concentrated *in vacuo* to give a residue which was purified by HPLC to deliver the title compound (46 mg, 71%) as a solid. ^{1}H NMR (400 MHz, $CDCl_3$) δ 7.86 (s, 1H), 7.31-7.20 (m, 5H), 7.14-7.08 (m, 2H), 3.27-3.20 (m, 2H), 2.89-2.76 (m, 4H), 2.46 (s, 3H), 1.87-1.79 (m, 2H), 1.78-1.68 (m, 5H), 1.44-1.36 (m, 2H), 0.93 (d, *J* = 6.5 Hz, 6H); HRMS Calcd for [$C_{26}H_{27}Cl_2F_3N_4O_4S$+H]: 579.1600. Found: 579.1584. HPLC: 100%.

*4-(2-(2,4-Dichlorophenyl)-5-methyl-4-(piperidin-1-ylcarbamoyl)-1H-imidazol-1-yl)phenyl 3,3-dimethylbutane-1-sulfonate (**11h**).* A solution of compound **10** (50 mg, 0.11 mmol) in CH_2Cl_2 (3 mL) was cooled to 0 °C and treated with Et_3N (20 µL, 0.13 mmol). The resulting mixture was cooled to -78 °C and 3,3-dimethylbutane-1-sulfonyl chloride (25 mg, 0.13 mmol) was carefully added. The reaction was stirred at -78 °C for 2 h. Water was added, then the mixture extracted with CH_2Cl_2. The organic extracts were dried, filtered, and concentrated *in vacuo* to give a residue which was purified by preparative HPLC to deliver the title compound (46 mg, 69%) as a solid. ^{1}H NMR (400 MHz, $CDCl_3$) δ 7.85 (s, 1H), 7.32-7.17 (m, 5H), 7.11-7.09 (d, *J* = 8.7 Hz, 2H), 3.26-3.15 (m, 2H), 2.92-2.74 (m, 4H), 2.46 (s, 3H), 1.87-1.78 (m, 2H), 1.77-1.68 (m, 5H), 1.46-1.34 (m, 2H), 0.92 (s, 9H); HRMS Calcd for [$C_{28}H_{34}Cl_2N_4O_4S$+H]: 593.1756. Found: 593.1755. HPLC: 100%.

*racemic 1-(4-(Benzyloxy)phenyl)-2-(2,4-dichlorophenyl)-N-(3-hydroxypiperidin-1-yl)-5-methyl-1H-imidazole-4-carboxamide (**12a**).* Compound **4** (752 mg, 1.66 mmol) and $SOCl_2$ (33.2 mmol) were mixed and the resulting mixture was refluxed for 1.5 h. Excess $SOCl_2$ was removed under reduced pressure and the residue was azeotroped with toluene. 3-Hydroxy-1-aminopiperidine (6.64 mmol) was mixed with CH_2Cl_2 (15 mL) and THF (2 mL) and Et_3N (13.28 mmol). The mixture was cooled to -20 °C under a nitrogen atmosphere. A THF (5 mL) mixture of the acid chloride from above was added dropwise during 20 minutes. The resulting mixture was allowed to slowly warm to r.t. and stirred

overnight. Aqueous NaOH (1 M, 5 mL) and EtOH (15 mL) were added and the mixture was heated to 40 °C for 15 minutes. The reaction mixture was then diluted to 50 mL with CH_2Cl_2 and washed with water (2 x 20 mL) and brine (20 mL). The organic layer was dried ($MgSO_4$), filtered, and concentrated *in vacuo*. The residue was purified by flash chromatography (8% EtOH in CH_2Cl_2) and then by reverse phase HPLC (Kromasil C8, 60% CH_3CN in aqueous NH_4OAc (0.1 M)). The product fraction was concentrated *in vacuo* and then dissolved in CH_2Cl_2 and washed with water several times and then brine. The organic layer was dried ($MgSO_4$), filtered and concentrated *in vacuo* to give the title compound (160 mg, 17% yield). ^{1}H NMR (400 MHz, $CDCl_3$) δ 7.99 (s, 1H), 7.33-7.19 (m, 6H), 7.18-7.07 (m, 2H), 6.90 (d, J = 8.8 Hz, 2H), 6.81 (d, J = 8.8 Hz, 2H), 5.18 (s, 1H), 4.92 (s, 2H), 3.94-3.85 (m, 1H), 3.06-2.97 (m, 1H), 2.85-2.66 (m, 3H), 2.34 (s, 3H), 1.87-1.77 (m, 1H), 1.63-1.50 (m, 2H), 1.46-1.34 (m, 1H); MS *m/z* 551 (M+H).

*racemic 1-(4-(Benzyloxy)phenyl)-2-(2,4-dichlorophenyl)-N-(3-hydroxycyclohexyl)-5-methyl-1H-imidazole-4-carboxamide (**12b**).* A suspension of compound **4** (2.00 g, 4.41 mmol) in CH_2Cl_2 (50 mL) was treated with oxalyl chloride (2.80 g, 22.1 mmol) at r.t., followed by one drop of DMF. The mixture was stirred at r.t. for 15 min after which the solvent was removed *in vacuo*. The acid chloride was suspended in CH_2Cl_2 (10 mL) and added dropwise to a mixture of 3-aminocyclohexanol (610 mg, 5.29 mmol), aqueous NaOH (1 M, 30 mL) and CH_2Cl_2 (30 mL). After stirring at r.t. for 2 h, adding more 3-aminocyclohexanol after 1 h 25 min (67 mg, 0.58 mmol) and 1 h 45 min (58 mg, 0.50 mmol), water and CH_2Cl_2 were added and the phases separated. The organic phase was washed with aqueous HCl (10%) and brine, then dried ($MgSO_4$), filtered, and concentrated *in vacuo* to yield the crude title compound (2.79 g). ^{1}H NMR (400 MHz, $CDCl_3$) δ 7.40-7.16 (m, 8H), 7.03-6.88 (m, 4H), 5.01 (s, 2H), 4.44-4.32 (m, 0.5H), 4.18-4.11 (m, 0.5 H), 4.06-3.94 (m, 0.5 H), 3.76-3.66 (m, 0.5 H), 2.46 (s, 3H), 2.03-1.10 (m, 8H); MS *m/z* 550 (M+H).

*racemic 1-(4-(Benzyloxy)phenyl)-2-(2,4-dichlorophenyl)-N-((trans)-2-hydroxycyclohexyl)-5-methyl-1H-imidazole-4-carboxamide (**12c**).* A suspension of compound **4** (2.00 g, 4.41 mmol) in CH_2Cl_2 (100 mL)

was treated with oxalyl chloride (2.80 g, 22.1 mmol) at r.t., followed by one drop of DMF. The mixture was stirred at r.t. for 35 min after which the mixture was concentrated *in vacuo*. The acid chloride was suspended in CH_2Cl_2 (10 mL) and added dropwise to a mixture of *trans*-2-aminocyclohexanol hydrochloride (802 mg, 5.29 mmol), aqueous NaOH (1 M, 30 mL) and CH_2Cl_2 (30 mL). After stirring at r.t. for 2 h, water/CH_2Cl_2 were added and the phases were separated. The organic phase was washed with aqueous HCl (10%) and brine, dried ($MgSO_4$), filtered, and concentrated *in vacuo* to yield the crude title compound (2.69 g). ^{1}H NMR (400 MHz, $CDCl_3$) δ 7.94 (s, 1H), 7.37-7.25 (m, 6H), 7.23-7.17 (m, 2H), 6.97 (d, *J* = 8.6 Hz, 2H), 6.89 (d, *J* = 8.6 Hz, 2H), 5.23 (s, 1H), 4.98 (s, 2H), 3.80-3.62 (m, 1H), 3.59-3.42 (m, 1H), 2.42 (s, 3H), 2.14-1.93 (m, 2H), 1.75-1.59 (m, 2H), 1.39-1.14 (m, 4H); MS *m/z* 550 (M+H).

*racemic 1-(4-(Benzyloxy)phenyl)-2-(2,4-dichlorophenyl)-N-((cis)-2-hydroxycyclohexyl)-5-methyl-1H-imidazole-4-carboxamide (**12d**).* A suspension of compound **4** (2.00 g, 4.41 mmol) in CH_2Cl_2 (100 mL) was treated with oxalyl chloride (2.85 g, 22.5 mmol) at r.t., followed by one drop of DMF. The mixture was stirred at r.t. for 20 min after which the solvents were evaporated under reduced pressure. The acid chloride was suspended in CH_2Cl_2 (10 mL) and added dropwise to a mixture of *cis*-2-aminocyclohexanol hydrochloride (816 mg, 5.38 mmol), aqueous NaOH (1M, 30 mL) and CH_2Cl_2 (30 mL). After stirring at r.t. for 2 h water was added and the phases were separated. The organic phase was washed with aqueous HCl (0.1 M) and brine, dried ($MgSO_4$), filtered, and concentrated *in vacuo* to yield the title compound (2.40 g, 99%). ^{1}HNMR (400 MHz, $CDCl_3$) δ 7.45 (d, *J* = 7.8 Hz, 1H), 7.41-7.16 (m, 8H), 6.98 (d, *J* = 8.8 Hz, 2H), 6.90 (d, *J* = 8.8 Hz, 2H), 5.01 (s, 2H), 4.16-4.08 (m, 1H), 4.03-3.96 (m, 1H), 2.89 (br s, 1H), 2.43 (s, 3H), 1.83-1.54 (m, 6H), 1.47-1.32 (m, 2H); MS *m/z* 550 (M+H).

*1-(4-(Benzyloxy)phenyl)-2-(2,4-dichlorophenyl)-5-methyl-N-(4-(trifluoromethoxy)phenyl)-1H-imidazole-4-carboxamide (**12e**).* A suspension of compound **4** (1.00 g, 2.21 mmol) in CH_2Cl_2 (15 mL) was treated with oxalyl chloride (1.40 g, 11.0 mmol) at r.t., followed by one drop of DMF. The

mixture was stirred at r.t. for 15 min after which the solvents were evaporated under reduced pressure. A mixture of 4-trifluoromethoxy-phenylamine (469 mg, 2.65 mmol), Et_3N (313 mg, 3.09 mmol) and CH_2Cl_2 (5 mL) was added dropwise to the acid chloride suspended in CH_2Cl_2 (15 mL). The reaction mixture was stirred at r.t. for 2 h and 10 min. CH_2Cl_2 was added and the resulting mixture was washed with aqueous HCl (10%) and brine, dried ($MgSO_4$), filtered, and evaporated to yield the crude title compound (1.42 g). ^{1}H NMR (400 MHz, $CDCl_3$) δ 9.37 (br s, 1H), 7.76-7.74 (m, 2H), 7.39-7.16 (m, 10H), 7.05-6.93 (m, 4H), 5.03 (s, 2H), 2.50 (s, 3H); MS *m/z* 612 (M+H).

*1-(4-(Benzyloxy)phenyl)-2-(2,4-dichlorophenyl)-N-(6-fluoropyridin-3-yl)-5-methyl-1H-imidazole-4-carboxamide (**12f**).* A suspension of compound **4** (1.00 g, 2.21 mmol) in CH_2Cl_2 (15 mL) was treated with oxalyl chloride (1.40 g, 11.0 mmol) at r.t., followed by one drop of DMF. The mixture was stirred at r.t. for 5 min after which the solvents were removed *in vacuo*. The acid chloride was suspended in CH_2Cl_2 (8 mL) then treated dropwise with a mixture of 6-fluoro-pyridin-3-ylamine (297 mg, 2.65 mmol), Et_3N (313 mg, 3.09 mmol) and CH_2Cl_2 (7 mL). Stirring was continued at r.t. for 75 min, after which CH_2Cl_2 was added and the resulting mixture washed with aqueous HCl (10%) and brine. The organic extracts were dried ($MgSO_4$), filtered, and concentrated *in vacuo* to yield the crude title compound (1.19 g). ^{1}H NMR (400 MHz, $CDCl_3$) δ 9.24 (s, 1H), 8.39-8.33 (m, 2H), 7.39-6.89 (m, 3H), 5.02 (s, 2H), 2.49 (s, 3H); MS *m/z* 547 (M+H).

*1-(4-(Benzyloxy)phenyl)-2-(2,4-dichlorophenyl)-5-methyl-N-(6-(trifluoromethyl)pyridin-3-yl)-1H-imidazole-4-carboxamide (**12g**).* A suspension of compound **4** (1.00 g, 2.21 mmol) in CH_2Cl_2 (15 mL) was treated with oxalyl chloride (1.40 g, 11.03 mmol) at r.t., followed by one drop of DMF. The mixture was stirred at r.t. for 5 min after which the solvents were removed *in vacuo*. The acid chloride was suspended in CH_2Cl_2 (8 mL) then treated dropwise with a solution of 6-trifluoromethyl-pyridin-3-ylamine (407 mg, 2.51 mmol) and Et_3N (360 mg, 3.56 mmol) in CH_2Cl_2 (7 mL). The reaction mixture was stirred at r.t. for 1.5 h then diluted with CH_2Cl_2 and washed with aqueous HCl (10% w/w) and brine. The organic extracts were dried ($MgSO_4$), filtered, and concentrated *in vacuo* to yield the

crude title product (1.32 g). ^{1}H NMR (400 MHz, $CDCl_3$) δ 9.50 (s, 1H), 8.82 (d, *J* = 2.0 Hz, 1H), 8.55 (dd, *J* = 2.0, 8.6 Hz, 1H), 7.65 (d, *J* = 8.6 Hz, 1H), 7.40-7.21 (m, 7H), 7.06-6.89 (m, 5H), 5.03 (s, 2H), 2.50 (s, 3H); MS *m/z* 597 (M+H).

*1-(4-(Benzyloxy)phenyl)-2-(2,4-dichlorophenyl)-5-methyl-N-(5-methylpyridin-2-yl)-1H-imidazole-4-carboxamide (**12h**).* A suspension of compound **4** (3.00 g, 6.62 mmol) in CH_2Cl_2 (70 mL) was treated with oxalyl chloride (4.20 g, 33.1 mmol) at r.t., followed by one drop of DMF. The mixture was stirred at r.t. for 5 min after which the solvents were evaporated under reduced pressure. A mixture of 5-methyl-pyridin-2-ylamine (816 mg, 7.54 mmol), Et_3N (890 mg, 8.80 mmol) and CH_2Cl_2 (20 mL) was added dropwise to the acid chloride suspended in CH_2Cl_2 (20 mL). The reaction mixture was stirred at r.t. for 30 min. CH_2Cl_2 was added and the resulting mixture was washed with aqueous HCl (10%) and brine, dried ($MgSO_4$), filtered and evaporated. The residue was purified by flash chromatography (20-30% EtOAc in heptane) to yield the title compound as a white solid (980 mg, 27%). ^{1}H NMR (400 MHz, Pyridine-d_5) δ 10.11 (s, 1H), 8.52 (s, 1H), 8.04 (s, 1H), 7.40-6.88 (m, 3H), 4.80 (s, 2H), 2.39 (s, 3H), 1.88 (s, 3H); MS *m/z* 543 (M+H).

*racemic 2-(2,4-Dichlorophenyl)-1-(4-hydroxyphenyl)-N-(3-hydroxypiperidin-1-yl)-5-methyl-1H-imidazole-4-carboxamide (**13a**).* A mixture of *racemic* 1-(4-(benzyloxy)phenyl)-2-(2,4-dichlorophenyl)-*N*-(3-hydroxypiperidin-1-yl)-5-methyl-1*H*-imidazole-4-carboxamide (160 mg, 0.29 mmol) and dimethyl sulfide (1.45 mmol) in CH_2Cl_2 under nitrogen atmosphere were treated dropwise with $BF_3{\cdot}OEt_2$ (1.45 mmol). The resulting mixture was stirred for 4 days at ambient temperature while continuously adding small volumes of CH_2Cl_2 and 1,4-dioxane. EtOH was added and the mixture was stirred for 30 mins and then concentrated *in vacuo*. The residue was dissolved in EtOAc (50 mL) and washed with water (2 x 20 mL) and brine (20 mL). The organic layer was dried (Na_2SO_4), filtered and concentrated *in vacuo* to give the title compound (127 mg, 95%) as a white solid. MS *m/z* 461 (M+H).

*racemic 2-(2,4-Dichlorophenyl)-N-(3-hydroxycyclohexyl)-1-(4-hydroxyphenyl)-5-methyl-1H-imidazole-4-carboxamide (**13b**).* A suspension of crude 1-(4-(benzyloxy)phenyl)-2-(2,4-dichlorophenyl)-*N*-(3-hydroxycyclohexyl)-5-methyl-1*H*-imidazole-4-carboxamide (2.79 g, 5.07 mmol) in CH_2Cl_2 (50 mL) and dimethyl sulfide (3.15 g, 50.7 mmol) was treated with boron trifluoride diethyl etherate (5.77 g, 50.7 mmol). The reaction mixture was stirred at r.t. for 36 h (dark), adding more dimethyl sulfide (3.15 g, 50.7 mmol) and boron trifluoride (5.77 g, 50.7 mmol) after 16 h. The solvent was evaporated and the residue dissolved in EtOAc/water. The phases were separated and the organic phase dried ($MgSO_4$), filtered, and concentrated *in vacuo* to yield the crude title compound (2.54 g). MS *m/z* 460 (M+H).

*racemic 2-(2,4-Dichlorophenyl)-N-((trans)-2-hydroxycyclohexyl)-1-(4-hydroxyphenyl)-5-methyl-1H-imidazole-4-carboxamide (**13c**).* Crude *racemic* 1-(4-(benzyloxy)phenyl)-2-(2,4-dichlorophenyl)-*N*-((*trans*)-2-hydroxycyclohexyl)-5-methyl-1*H*-imidazole-4-carboxamide (2.68 g, 4.87 mmol) was suspended in HBr (33% in AcOH, 60 mL). The mixture was stirred at r.t., in the dark, for 1 h 20 min. EtOH was added and the mixture concentrated *in vacuo*. The residue was dissolved in MeOH and neutralized with $NaHCO_3$ (1 M, aq). One spoon of K_2CO_3 was added and the mixture was stirred at r.t. for 1 h. The solvent was evaporated and the resulting mixture extracted with toluene followed by THF. The combined organic phases were washed with aqueous HCl (10%) and brine, dried ($MgSO_4$), filtered and evaporated. The product was purified by HPLC (30-100% CH_3CN in aqueous NH_4OAc (0.1 M) over 40 min) to yield the title compound as a white solid (829 mg, yield over 2 steps 41%). ^{1}H NMR (400 MHz, $CDCl_3$) δ 7.36-7.18 (m, 4H), 6.86-6.66 (m, 4H), 5.28 (s, 1H), 4.60 (br s, 1H), 3.85-3.74 (m, 1H), 3.52-3.41 (m, 1H), 2.37 (s, 3H), 2.13-1.97 (m, 2H), 1.78-1.67 (m, 2H), 1.44-1.15 (m, 4H); MS *m/z* 460 (M+H).

*racemic 2-(2,4-Dichlorophenyl)-N-((cis)-2-hydroxycyclohexyl)-1-(4-hydroxyphenyl)-5-methyl-1H-imidazole-4-carboxamide (**13d**).* A suspension of racemic 1-(4-(benzyloxy)phenyl)-2-(2,4-dichlorophenyl)-*N*-((*cis*)-2-hydroxycyclohexyl)-5-methyl-1*H*-imidazole-4-carboxamide (2.38 g, 4.33 mmol) in HBr (33% in AcOH, 50 mL). The reaction mixture was stirred at r.t., in the dark, for 1 h.

EtOH was added and the solvents were evaporated under reduced pressure. The residue was dissolved in MeOH and neutralized with aqueous $NaHCO_3$ (1 M). The solvent was evaporated and the mixture dissolved in water/CH_2Cl_2. The phases were separated and the organic phase was washed with brine, dried ($MgSO_4$), filtered and evaporated. The residue was dissolved in MeOH and one spoon of K_2CO_3 was added, and the resulting mixture was stirred at r.t. for 1 h before the solvent was evaporated. The residue was resuspended in CH_2Cl_2 and washed with aqueous HCl (10%), and the solvents were evaporated. The residue was dissolved in THF, dried ($MgSO_4$), filtered and evaporated to yield the crude title compound (2.10 g). ^{1}H NMR (400 MHz, THF-d_8) δ 8.65 (d, J = 7.3 Hz, 1H), 7.66 (d, J = 8.3 Hz, 1H), 7.55 (d, J = 1.7 Hz, 1H), 7.25 (dd, J = 1.7, 8.3, 1H), 7.18 (d, J = 8.6 Hz, 2H), 6.79 (d, J = 8.6 Hz, 2H), 3.99-3.91 (m, 1H), 3.91-3.82 (m, 1H), 3.64-3.55 (m, 1H), 2.47 (s, 3H), 1.86-1.63 (m, 5H), 1.58-1.44 (m, 1H), 1.38-1.28 (m, 2H); MS *m/z* 460 (M+H).

*2-(2,4-Dichlorophenyl)-1-(4-hydroxyphenyl)-5-methyl-N-(4-(trifluoromethoxy)pheny1)-1H-imidazole-4-carboxamide (**13e**).* Crude **12e** (1.35 g, 2.20 mmol) was suspended in HBr (33% in AcOH, 25 mL). The reaction mixture was stirred at r.t., in the dark, for 1 h. EtOH was added and the solvents were evaporated at reduced pressure. The residue was dissolved in MeOH and neutralized with aqueous $NaHCO_3$ (1 M). The solvent was evaporated and the mixture dissolved in water/CH_2Cl_2. The phases were separated and the organic phase was washed with brine, dried ($MgSO_4$), filtered, and concentrated *in vacuo* to yield the crude title compound (1.10 g). ^{1}H NMR (400 MHz, $CDCl_3$) δ 7.73-7.71 (m, 2H), 7.39-7.16 (m, 5H), 6.94-6.76 (m, 4H), 2.45 (s, 3H); MS *m/z* 522 (M+H).

*2-(2,4-Dichlorophenyl)-N-(6-fluoropyridin-3-yl)-1-(4-hydroxyphenyl)-5-methyl-1H-imidazole-4-carboxamide (**13f**).* Compound **12f** (1.15 g, 2.10 mmol) was suspended in HBr (33% in AcOH, 25 mL). The reaction mixture was stirred at r.t., in the dark, for 2 h 30 min. EtOH was added and the solvents were evaporated under reduced pressure. The residue was dissolved in MeOH and neutralized with aqueous $NaHCO_3$ (1 M). The solvent was evaporated and the mixture dissolved in water/CH_2Cl_2. The phases were separated and the organic phase was washed with brine, dried ($MgSO_4$), filtered, and

concentrated *in vacuo* to give a residue which was purified by HPLC (30-60% CH_3CN in NH_4OAc (0.1 M) over 40 min, then 100% CH_3CN) to yield the title compound as a white solid (519 mg, yield over 2 steps 53%). ^{1}H NMR (400 MHz, $CDCl_3$) δ 9.14 (s, 1H), 8.37-8.30 (m, 2H), 7.34 (s, 1H), 7.25-7.20 (m, 2H), 6.96-6.90 (m, 3H), 6.79-6.77 (m, 2H), 2.48 (s, 3H); MS *m/z* 457 (M+H).

*2-(2,4-Dichlorophenyl)-1-(4-hydroxyphenyl)-5-methyl-N-(6-(trifluoromethyl)pyridin-3-yl)-1H-imidazole-4-carboxamide (**13g**).* A suspension of crude **12g** (1.17 g, 1.96 mmol) in CH_2Cl_2 (6 mL) and dimethyl sulfide (1.22 g, 19.6 mmol) was treated with boron trifluoride (2.78 g, 19.6 mmol). The reaction mixture was stirred at r.t. for 31 h (dark). Water and CH_2Cl_2 were added and the phases separated. The organic phase was washed with water (x4) and concentrated *in vacuo*. The residue was dissolved in MeOH and stirred at r.t. for 20 h before water was added and the MeOH removed *in vacuo*. The resulting mixture was extracted with Et_2O (x 2) and the combined organic phases were washed with brine, dried ($MgSO_4$), filtered, and concentrated *in vacuo* to yield the crude title compound (776 mg). ^{1}H NMR (400 MHz, $CDCl_3$) δ 9.29 (s, 1H), 8.75 (d, *J* = 2.1 Hz, 1H), 8.54 (dd, *J* = 2.1, 8.6 Hz, 1H), 7.64 (d, *J* = 8.6 Hz, 1H), 7.33 (d, *J* = 1.7 Hz, 1H), 7.27-7.19 (m, 2H), 6.96 (d, *J* = 8.7 Hz, 2H), 6.78 (d, *J* = 8.7 Hz, 1H), 5.51 (br s, 1H), 2.48 (s, 3H); MS *m/z* 507 (M+H).

*2-(2,4-Dichlorophenyl)-1-(4-hydroxyphenyl)-5-methyl-N-(5-methylpyridin-2-yl)-1H-imidazole-4-carboxamide (**13h**).* Compound **12h** (958 mg, 1.76 mmol) was suspended in HBr (33% in AcOH, 25 mL). The reaction mixture was stirred at r.t., in the dark, for 1 h. EtOH was added and the solvents were evaporated under reduced pressure. The residue was dissolved in MeOH and neutralized with aqueous $NaHCO_3$ (1 M). The solvent was evaporated and the mixture dissolved in water/CH_2Cl_2. The phases were separated and the organic phase was washed with brine, dried ($MgSO_4$), filtered and evaporated to yield the title compound (772 mg, 97%). ^{1}H NMR (400 MHz, Pyridine-d_5) δ 10.12 (s, 1H), 8.52 (s, 1H), 8.03 (s, 1H), 7.40-6.89 (m, 8H), 2.42 (s, 3H), 1.88 (s, 3H); MS *m/z* 453 (M+H).

*racemic 4-(2-(2,4-Dichlorophenyl)-4-(3-hydroxypiperidin-1-ylcarbamoyl)-5-methyl-1H-imidazol-1-yl)phenyl 3,3,3-trifluoropropane-1-sulfonate (**14a**).* A solution of 2-(2,4-dichlorophenyl)-1-(4-

hydroxyphenyl)-*N*-(3-hydroxypiperidin-1-yl)-5-methyl-1*H*-imidazole-4-carboxamide (118 mg, 0.25 mmol) in CH_2Cl_2 (1 mL), and THF (1 mL) was treated with Et_3N (0.25 mmol) under a nitrogen atmosphere. The solution was cooled to -78 °C and a solution of 3,3,3-trifluoropropane-1-sulfonyl chloride in CH_2Cl_2 (1 mL) was added slowly while monitoring the progress with LC-MS. The reaction mixture was quenched by addition of EtOH. The reaction mixture was concentrated *in vacuo* and the residue was purified by reverse phase HPLC (Kromasil C8, 5-100% CH_3CN in aqueous NH_4OAc (0.1 M)) and by flash chromatography (8% EtOH in CH_2Cl_2). The product was freeze-dried to give the title compound (40 mg, 25%) as a white powder. ^{1}H NMR (CD_3OD) δ 7.52-7.44 (m, 2H), 7.44-7.34 (m, 5H), 3.91-3.82 (m, 1H), 3.77-3.69 (m, 2H), 3.11 (dd, *J* = 3.0, 10.1 Hz, 1H), 2.95-2.80 (m, 3H), 2.74-2.58 (m, 2H), 2.46 (s, 3H), 1.95-1.75 (m, 2H), 1.73-1.62 (m, 1H), 1.44-1.31 (m, 1H); MS *m/z* 621 (M+H); HRMS Calcd for [$C_{25}H_{25}Cl_2F_3N_4O_5S$+H]: 621.0954. Found: 621.0919. HPLC: 100%.

*racemic 4-(2-(2,4-Dichlorophenyl)-4-((trans)-3-hydroxycyclohexylcarbamoyl)-5-methyl-1H-imidazol-1-yl)phenyl 3,3,3-trifluoropropane-1-sulfonate (**14b**).* A suspension of crude 2-(2,4-dichlorophenyl)-*N*-(3-hydroxycyclohexyl)-1-(4-hydroxyphenyl)-5-methyl-1*H*-imidazole-4-carboxamide (2.53 mg, 5.49 mmol) in dry CH_2Cl_2 (20 mL) was treated with Et_3N (667 mg, 6.59 mmol) at r.t.. The resulting mixture was cooled to -78 °C and 3,3,3-trifluoropropane-1-sulfonyl chloride (1.30 mg, 6.59 mmol) was added dropwise. After stirring at -78 °C for 2 h 45 min, the reaction mixture was allowed to reach r.t., upon which it was washed with water and evaporated. The stereoisomers were separated by HPLC (30-100% CH_3CN in aqueous NH_4OAc (0.1 M)) to yield the *trans*-hydroxycyclohexyl product (205 mg, 7.5% over 3 steps) as a white solid. ^{1}H NMR (400 MHz, $CDCl_3$) δ 7.34-7.23 (m, 5H), 7.20-7.10 (m, 3H), 4.45-4.33 (m, 1H), 4.17-4.10 (m, 1H), 3.55-3.47 (m, 2H), 2.87-2.73 (m, 2H), 2.49 (s, 3H), 2.05-1.51 (m, 8H), 1.48-1.36 (m, 1H); HRMS Calcd for [$C_{26}H_{26}Cl_2F_3N_3O_5S$+H]: 620.1001. Found: 620.1028. HPLC: 100%.

*(-) 4-(2-(2,4-Dichlorophenyl)-4-((trans)-2-hydroxycyclohexylcarbamoyl)-5-methyl-1H-imidazol-1-yl)phenyl 3,3,3-trifluoropropane-1-sulfonate (**14c**).* A suspension of *racemic* 2-(2,4-dichlorophenyl)-*N*-((*trans*)-2-hydroxycyclohexyl)-1-(4-hydroxyphenyl)-5-methyl-1*H*-imidazole-4-carboxamide (829 mg,

1.80 mmol) in dry CH_2Cl_2 (10 mL) was treated with Et_3N (182 mg, 1.80 mmol) at r.t.. The resulting mixture was cooled to -78 °C and 3,3,3-trifluoropropane-1-sulfonyl chloride (354 mg, 1.80 mmol) dry CH_2Cl_2 (1 mL) was added dropwise. After stirring at -78 °C for 1 h the reaction mixture was washed with water and evaporated. The racemic product was purified by HPLC (30-100% CH_3CN in aqueous NH_4OAc (0.1 M) over 40 min) to yield the title compound as a white solid (710 mg, 64 %). ^{1}H NMR (400 MHz, $CDCl_3$) *δ* 7.29-7.06 (m, 8H), 3.82-3.62 (m, 2H), 3.50-3.41 (m, 2H), 3.41-3.31 (m, 1H), 2.81-2.65 (m, 2H), 2.43 (s, 3H), 2.09-1.90 (m, 2H), 1.75-1.61 (m, 2H), 1.34-1.12 (m, 4H); HRMS Calcd for [$C_{26}H_{26}Cl_2F_3N_3O_5S$+H): 620.1001. Found: 620.1011. The (-)-enantiomer was separated from the racemate (535 mg, 0.86 mmol) by chiral chromatography (Chiralpak AD, heptane : *i*PrOH 85 : 15) to afford the title compound (220 mg) (95.6% *ee*) as white solid after freeze drying. $[\alpha]_D$ = -2.9 (*c* 1.04, CH_3CN); ^{1}H NMR (400 MHz, $CDCl_3$) *δ* 7.29-7.06 (m, 8H), 3.82-3.62 (m, 2H), 3.50-3.41 (m, 2H), 3.41-3.31 (m, 1H), 2.81-2.65 (m, 2H), 2.43 (s, 3H), 2.09-1.90 (m, 2H), 1.75-1.61 (m, 2H), 1.34-1.12 (m, 4H); HRMS Calcd for [$C_{26}H_{26}Cl_2F_3N_3O_5S$+H]: 620.1001. Found: 620.0956. HPLC: 100%. Vibrational Circular Dichroism experiments were unable to unambiguously assign the absolute stereochemistry of the (+) and (-) enantiomers.

*(+) 4-[2-(2,4-Dichlorophenyl)-4-({[cis-2-hydroxycyclohexyl] amino}carbonyl)-5-methyl-1H-imidazol-1-yl]phenyl-3,3,3-trifluoropropane-1-sulfonate (**14d**).* A suspension of crude racemic 2-(2,4-dichlorophenyl)-*N*-((*cis*)-2-hydroxycyclohexyl)-1-(4-hydroxyphenyl)-5-methyl-1*H*-imidazole-4-carboxamide (2.00 g, 4.34 mmol) in dry CH_2Cl_2 (30 mL) was treated with Et_3N (440 mg, 4.34 mmol) at r.t.. The resulting mixture was cooled to -78 °C and 3,3,3-trifluoropropane-1-sulfonyl chloride (854 mg, 4.34 mmol) was added dropwise. After stirring at -78 °C for 2 h 20 min, more Et_3N (2 x (73 mg, 0.72 mmol)) and 3,3,3-trifluoropropane-1-sulfonyl chloride (2 x (110 mg, 0.56 mmol)) were added (2nd addition after 1 h). After 2 h the reaction mixture was washed with water and evaporated. The racemic product was purified by HPLC (30-100% CH_3CN in aqueous NH_4OAc (0.1 M) over 40 min) to yield the title compounds as a white solid (1.31 g, yield over 2 steps 51%). ^{1}H NMR (400 MHz, $CDCl_3$) *δ* 7.38 (d, *J* = 7.7 Hz, 1H), 7.28-7.16 (m, 5H), 7.09 (d, *J* = 8.7 Hz, 2H), 4.13-4.02 (m, 1H), 4.00-3.89 (m,

1H), 3.49-3.38 (m, 2H), 2.80-2.65 (m, 2H), 2.42 (s, 3H), 1.78-1.47 (m, 6H), 1.44-1.28 (m, 2H); HRMS Calcd for [$C_{26}H_{26}Cl_2F_3N_3O_5S$+H]: 620.1001. Found: 620.1025. The (+)-enantiomer was separated from the racemate (1.00 g, 1.61 mmol) by Chiral chromatography (Chiralpak AD, heptane/*i*PrOH 80/20) to yield the title compound (444 mg) (> 99.9% *ee*) as a white powder after freeze drying. $[\alpha]_D$ = +9.9 (*c* 1.02, CH_3CN); ^{1}H NMR (400 MHz, $CDCl_3$) δ 7.38 (d, *J* = 7.7 Hz, 1H), 7.28-7.16 (m, 5H), 7.09 (d, *J* = 8.7 Hz, 2H), 4.13-4.02 (m, 1H), 4.00-3.89 (m, 1H), 3.49-3.38 (m, 2H), 2.80-2.65 (m, 2H), 2.63-2.53 (m, 1H), 2.42 (s, 3H), 1.78-1.47 (m, 6H), 1.44-1.28 (m, 2H); HRMS Calcd for [$C_{26}H_{26}Cl_2F_3N_3O_5S$+H] 620.1001. Found: 620.0945. HPLC: 100%. Vibrational Circular Dichroism experiments were unable to unambiguously assign the absolute stereochemistry of the (+) and (-) enantiomers.

*4-(2-(2,4-Dichlorophenyl)-5-methyl-4-(4-(trifluoromethoxy)phenylcarbamoyl)-1H-imidazol-1-yl)phenyl 3,3 ,3-trifluoropropane-1-sulfonate (**14e**).* A suspension of **13e** (150 mg, 0.29 mmol) in dry CH_2Cl_2 (2 mL) was treated with Et_3N (38 mg, 0.37 mmol) at r.t.. The resulting mixture was cooled to -78 °C and 3,3,3-trifluoropropane-1-sulfonyl chloride (79 mg, 0.40 mmol) in 0.5 mL dry CH_2Cl_2 was added dropwise. After stirring at -78 °C for 70 min, the reaction mixture was washed with water and evaporated. The product was purified by HPLC (30-100% CH_3CN in aqueous NH_4OAc (0.1 M) over 35 min) to yield the title compound as a white solid (84 mg, yield over 3 steps 43%). ^{1}H NMR (400 MHz, $CDCl_3$) δ 9.10 (s, 1H), 7.71 (d, *J* = 9.0 Hz, 2H), 7.36-7.24 (m, 9H), 7.22-7.15 (m, 4H), 3.54-3.47 (m, 2H), 2.86-2.72 (m, 2H), 2.53 (s, 3H); HRMS Calcd for [$C_{27}H_{19}Cl_2F_6N_3O_5S$+H]: 682.0405. Found: 682.0403. HPLC: 100%.

*4-(2-(2,4-Dichlorophenyl)-4-(6-fluoropyridin-3-ylcarbamoyl)-5-methyl-1H-imidazol-1-yl)phenyl 3,3,3-trifluoropropane-1-sulfonate (**14f**).* A suspension of 2-(2,4-dichlorophenyl)-*N*-(6-fluoropyridin-3-yl)-1-(4-hydroxyphenyl)-5-methyl-1*H*-imidazole-4-carboxamide (150 mg, 0.33 mmol) in dry CH_2Cl_2 (2 mL) was treated with Et_3N (43 mg, 0.43 mmol) at r.t.. The resulting mixture was cooled to -78°C and 3,3,3-trifluoropropane-1-sulfonyl chloride (90 mg, 0.46 mmol) in dry CH_2Cl_2 (0.5 mL) was added dropwise. After stirring at -78 °C for 2 h 30 min, more 3,3,3-trifluoropropane-1-sulfonyl chloride (14

mg, 0.07 mmol) was added and the mixture stirred for another 2 h. The reaction mixture was washed with water and evaporated. The product was purified by HPLC (30-100% CH_3CN in aqueous NH_4OAc (0.1 M) over 35 min) to yield the title compound as a white solid (133 mg, 66%). ^1H NMR (400 MHz, $CDCl_3$) δ 9.09 (s, 1H), 8.40-8.31 (m, 2H), 7.37-7.24 (m, 5H), 7.19 (d, *J* = 8.8 Hz, 2H), 6.95-6.88 (m, 1H), 3.55-3-46 (m, 2H), 2.86-2.72 (m, 2H), 2.53 (s, 3H). ^{13}C NMR (126 MHz, $CDCl_3$) δ 161.5, 160.7, 158.9, 148.7, 142.6, 138.4 (d, *J* = 15.1), 137.2, 135.5 (d, *J* = 38.6), 134.0, 133.3, 133.0 (d, *J* = 4.5), 132.7 (d, *J* = 7.5), 130.8, 130.0, 129.4, 127.7, 127.6, 125.1 (q, *J* = 276.6), 123.2, 109.5 (d, *J* = 38.8), 44.6 (q, *J* = 3.3), 29.3 (q, *J* = 31.9), 11.0.; HRMS Calcd for $[C_{25}H_{18}Cl_2F_4N_4O_4S+H]$: 617.0440. Found: 617.0473. HPLC: 100%.

*4-(2-(2,4-Dichlorophenyl)-5-methyl-4-(6-(trifluoromethyl)pyridin-3-ylcarbamoyl)-1H-imidazol-1-yl)phenyl 3,3,3-trifluoropropane-1-sulfonate (**14g**).* A suspension of crude **13g** (150 mg, 0.30 mmol) in dry CH_2Cl_2 (2 mL) was treated with Et_3N (39 mg, 0.38 mmol) at r.t. then cooled to -78 °C. To this was added dropwise 3,3,3-trifluoropropane-1-sulfonyl chloride (91 mg, 0.46 mmol) in dry CH_2Cl_2 (0.5 mL). After stirring at -78 °C for 70 min, the mixture was washed with water and concentrated *in vacuo* to give a residue which was purified by HPLC (30-100% CH_3CN in aqueous NH_4OAc (0.1 M) over 40 min) to yield the title compound as a white solid (131 mg, yield over 3 steps 52%). ^1H NMR (400 MHz, $CDCl_3$) δ 9.29 (s, 1H), 8.77 (d, *J* = 2.1 Hz, 1H), 8.56 (dd, *J* = 2.1, 8.6 Hz, 1H), 7.66 (d, *J* = 8.6 Hz, 1H), 7.37-7.16 (m, 7H), 3.55-3.46 (m, 2H), 2.86-2.72 (m, 2H), 2.53 (s, 3H); HRMS Calcd for $[C_{26}H_{18}Cl_2F_6N_4O_4S+H]$: 667.0408. Found: 667.0389. HPLC: 100%.

*4-(2-(2,4-Dichlorophenyl)-5-methyl-4-(5-methylpyridin-2-ylcarbamyl)-1H-imidazol-1-yl)phenyl 3,3,3-trifluoropropane-1-sulfonate (**14h**).* A suspension of **13h** (150 mg, 0.33 mmol) in dry CH_2Cl_2 (2 mL) was treated with Et_3N (44 mg, 0.43 mmol) at r.t.. The resulting mixture was cooled to -78 °C and 3,3,3-trifluoropropane-1-sulfonyl chloride (94 mg, 0.48 mmol) in dry CH_2Cl_2 (0.5 mL) was added dropwise. After stirring at -78 °C for 80 min, the reaction mixture was washed with water and evaporated. The product was purified by HPLC (30-100% CH_3CN in aqueous NH_4OAc (0.1 M) over 40

min) to yield the title compound as a white solid (132 mg, 65%). ^{1}H NMR (400 MHz, $CDCl_3$) δ 9.63 (s, 1H), 8.23 (d, *J* = 8.4 Hz, 1H), 8.11 (d, *J* = 1.4 Hz, 1H), 7.51 (dd, *J* = 2.1, 8.4 Hz, 1H), 7.34-7.24 (m, 5H), 7.18 (d, *J* = 8.9 Hz, 2H), 3.55-3.44 (m, 2H), 2.86-2.71 (m, 2H), 2.53 (s, 3H), 2.28 (s, 3H). HRMS Calcd for [$C_{26}H_{21}Cl_2F_3N_4O_4S$+H]: 613.0691. Found: 613.0702. HPLC: 100%.

*2,2,2-Trichloroethyl-1-(4-(benzyloxy)phenyl)-2-(2,4-dichlorophenyl)-5-methyl-1H-imidazole-4-carboxylate (**15**).* A solution of compound **4** (10.0 g, 22.1 mmol) in CH_2Cl_2 (210 mL) was treated with oxalyl chloride (18.5 g, 145 mmol), followed by a few drops of DMF. The mixture was stirred at r.t. for 2 h after which the solvents were evaporated. The residue was dissolved in CH_2Cl_2 (80 mL) and the mixture was cooled to 0 °C, upon which 2,2,2-trichloroethanol (3.63 g, 24.3 mmol) was added followed by DIPEA (3.42 g, 26.5 mmol). The ice bath was then removed and the reaction mixture was stirred at r.t. for 3 h, adding DMAP (279 mg, 2.28 mmol) after 1 h 40 min. The reaction mixture was diluted with CH_2Cl_2, washed with water, dried ($MgSO_4$), filtered and concentrated *in vacuo* to yield the crude title compound (14.9 g). ^{1}H NMR (400 MHz, $CDCl_3$) δ 7.40-7.14 (m, 8H), 7.04-6.98 (m, 2H), 6.94-6.88 (m, 2H), 5.01 (4H, s), 2.45 (s, 3H); MS *m/z* 583 (M+H).

*2,2,2-Trichloroethyl-2-(2,4-dichlorophenyl)-1-(4-hydroxyphenyl)-5-methyl-1H-imidazole-4-carboxylate (**16**).* Crude **15** (14.77 g) was dissolved in HBr (33% in AcOH, 200 mL). After having stirred at r.t. for an additional hour the reaction mixture was cooled to 0 °C and EtOH was added. The mixture was stirred for 10 min before the solvents were evaporated. The residue was dissolved in MeOH and neutralized with aqueous $NaHCO_3$ (1 M). The solvent was evaporated and the mixture dissolved in CH_2Cl_2. The organic phase was washed with brine and water, dried ($MgSO_4$), filtered and concentrated *in vacuo* to yield the title compound (10.4 g, 95% over 2 steps). ^{1}H NMR (400 MHz, $CDCl_3$) δ 8.63 (br s, 1H), 7.25-7.08 (m, 3H), 6.86-6.68 (m, 4H), 4.95 (s, 2H), 2.43 (s, 3H); MS *m/z* 493 (M+H).

*2,2,2-Trichloroethyl-2-(2,4-dichlorophenyl)-5-methyl-1-(4-(3,3,3- trifluoropropylsulfonyloxy)phenyl)-1H-imidazole-4-carboxylate (**17**).* A suspension of **16** (5.01 g, 10.13 mmol) in dry CH_2Cl_2 (100 mL)

under nitrogen was treated with Et_3N (1.23 g, 12.2 mmol) at r.t.. The resulting mixture was cooled to -78 °C and 3,3,3-trifluoropropane-1-sulfonyl chloride (2.19 g, 11.1 mmol) was added dropwise. The reaction mixture was stirred at -78 °C for 3 h, adding more 3,3,3-trifluoropropane-1-sulfonyl chloride (0.28 g 1.43 mmol) after 2 h. Water was added and the phases were separated on a phase separator. The organic phase was concentrated *in vacuo* to yield the title compound (6.43 g, 97%). ^{1}H NMR (400 MHz, $CDCl_3$) δ 7.37-7.15 (m, 7H), 5.01 (s, 2H), 3.53-3.45 (m, 2H), 2.84-2.70 (m, 2H), 2.48 (s, 3H); MS *m/z* 653 (M+H).

*2-(2,4-Dichlorophenyl)-5-methyl-1-(4-(3,3,3-trifluoropropylsulfonyloxy)phenyl)-1H-imidazole-4-carboxylic acid (**18**).* A solution of **17** (6.43 g, 9.82 mmol) in AcOH (100 mL) was treated with zinc dust (9.74 g, 148.91 mmol). The reaction mixture was stirred at r.t. for 3 h after which it was filtered through celite and evaporated. The residue was dissolved in CH_2Cl_2 and washed with aqueous HCl (0.1 M), dried, filtered, and concentrated *in vacuo* to yield the crude title compound (5.28 g). MS *m/z* 523 (M+H).

*4-(2-(2,4-Dichlorophenyl)-4-(4-hydroxycyclohexylcarbamoyl)-5-methyl-1H-imidazol-1-yl)phenyl 3,3,3-trifluoropropane-1-sulfonate (**19**).* A solution of **18** (crude 528 mg) in CH_2Cl_2 (25 mL) was treated with oxalyl chloride (641 mg, 5.00 mmol). A precipitate formed immediately after the addition so more CH_2Cl_2 (15 mL) was added, followed by a few drops of DMF. The reaction mixture was stirred at r.t. for 2 h after which more oxalyl chloride (641 mg, 5.00 mmol) was added. After another 10 min the solvents were evaporated. Half of the crude material was suspended in CH_2Cl_2 (5 mL) and added dropwise to a mixture of 4-aminocyclohexanol (74 mg, 0.64 mmol), NaOH (1 M, 10 mL) and CH_2Cl_2 (5 mL). The reaction mixture was stirred at r.t. for 2 h after which water/CH_2Cl_2 were added and the phases separated. The organic phase was washed with aqueous HCl (0.1 M) and concentrated *in vacuo*. The product was purified by HPLC to yield the title compound as a white solid after freeze drying (164 mg, 54% over 2 steps). Note that the title compound is a mixture of *cis*- and *trans*-isomers in a ratio of 0.3 : 1. ^{1}H NMR (400 MHz, $CDCl_3$) δ 7.33-7.19 (m, 6H), 7.17-7.11 (m, 2H), 7.02 (d,

J = 8.4 Hz, 0.6H), 4.07-3.99 (m, 0.3H), 3.99-3.86 (1H, m), 3.66-3.56 (m, 0.6H), 3.52-3.45 (m, 2H), 2.85-2.71 (m, 2H), 2.48 and 2.47 (2 x s, 3H), 2.12-1.95 (m, 2.6H), 1.81-1.65 (m, 3.8H), 1.49-1.26 (m, 2.7H); HRMS Calcd for [$C_{26}H_{26}Cl_2F_3N_3O_5S$+H]: 620.1001. Found: 620.1002. HPLC: 100%.

*racemic N-((cis)-2-Aminocyclohexyl)-1-[4-(benzyloxy)phenyl)-2-(2,4-dichlorophenyl)-5-methyl-1H-imidazole-4-carboxamide (**20**).* A suspension of compound **4** (2.00 g, 4.41 mmol) in CH_2Cl_2 (50 mL) was treated with oxalyl chloride (2.80 mg, 22.1 mmol) at r.t., followed by one drop of DMF. The mixture was stirred at r.t. for 30 min after which the solvents were evaporated under reduced pressure. Half of the amount of the acid chloride (1.04 mg, 2.20 mmol) suspended in CH_2Cl_2 (250 mL) was added dropwise during 31 h to a mixture of (*cis*)-cyclohexane-1,2-diamine (5.00 mg, 43.79 mmol), aqueous NaOH (1 M, 50 mL) and CH_2Cl_2 (50 mL). After the addition was complete water was added and the phases were separated. The organic phase was washed with aqueous HCl (10%) and brine, dried ($MgSO_4$), filtered and evaporated to yield the crude title compound (1.31 mg). ^{1}H NMR (400 MHz, $CDCl_3$) δ 8.57 (br s, 2H), 7.69 (br s, 1H), 7.37-6.90 (m, 2H), 5.00 (s, 2H), 4.41 (br s, 1H), 3.72 (br s, 1H), 2.42 (s, 3H), 2.18-1.40 (m, 8H); MS *m/z* 549 (M+H).

*racemic N-((cis)-2-Aminocyclohexyl)-2-(2,4-dichlorophenyl)-1-(4-hydroxyphenyl)-5-methyl-1H-imidazole-4-carboxamide (**21**).* A suspension of crude racemic **20** (791 mg, 1.44 mmol) in CH_2Cl_2 (5 mL) and dimethyl sulfide (894 mg, 14.39 mmol) was treated with boron trifluoride (2.04 g, 14.4 mmol). The reaction mixture was stirred at r.t. for 2.5 days (dark). Water and EtOAc were added and the phases separated. The organic phase was dried ($MgSO_4$), filtered and evaporated to yield the crude title compound (715 mg). MS *m/z* 459 (M+H).

*racemic 4-(4-((cis)-2-Aminocyclohexylcarbamoyl-2-(2,4-dichlorophenyl)-5-methyl-1H-imidazol-1-yl)phenyl 3,3,3-trifluoropropane-1-sulfonate (**22**).* A suspension of crude racemic **21** (715 mg, 1.56 mmol) in CH_2Cl_2 (15 mL) and Et_3N (0.987 g, 9.76 mmol) was treated with TBDMSCl (0.985 g, 6.53 mmol). The reaction mixture was stirred at r.t. for 22 h. CH_2Cl_2 and water were added and the phases separated. The organic phase was dried ($MgSO_4$), filtered and evaporated to yield the crude silylated

intermediate an oil (1.14 g, 1.99 mmol). MS *m/z* 573 (M+H). A solution of the crude intermediate (1.14 g, 1.99 mmol) in THF (10 mL) was treated with $(Boc)_2O$ (444 mg, 2.03 mmol). The reaction mixture was stirred at r.t. for 4 h after which the solvent was evaporated at reduced pressure and the residue dissolved in CH_2Cl_2. The organic phase was washed with water, dried ($MgSO_4$), filtered, and concentrated *in vacuo*. The residue was purified by flash chromatography (10-100% EtOAc in heptane) to yield the Boc-protected intermediate (620 mg, yield over 4 steps 70%). ^{1}H NMR (400 MHz, $CDCl_3$) δ 7.37 (d, *J* = 8.2 Hz, 1H), 7.24-7.08 (m, 3H), 6.85 (d, *J* = 8.7 Hz, 2H), 6.70 (d, *J* = 8.7 Hz, 2H), 5.12 (d, *J* = 4.5 Hz, 1H), 4.32-4.19 (m, 1H), 3.83-3.74 (m, 1H), 2.38 (s, 3H), 1.79-1.39 (m, 8H), 1.33 (s, 9H), 0.87 (s, 9H), 0.11 (s, 6H); MS *m/z* 673 (M+H). A suspension of the fully protected intermediate (610 mg, 0.91 mmol) in dry THF (3 mL) was treated with TBAF (1.0 M THF, 237 mg, 0.91 mmol). The reaction mixture was stirred at r.t. for 1 h 45 min. The solvent was evaporated and the residue dissolved in CH_2Cl_2, washed with water, dried ($MgSO_4$), filtered and evaporated. The residue was dissolved in EtOAc and some silica gel was added. The suspension was filtered through a plug of silica gel and eluted with EtOAc. The solvent was evaporated to yield the crude desilylated intermediate (529 mg). ^{1}H NMR (400 MHz, $CDCl_3$) δ 7.36 (d, *J* = 8.1 Hz, 1H), 7.21 (d, *J* = 1.6 Hz, 1H), 7.13 (d, *J* = 8.3 Hz, 1H), 7.09 (dd, *J* = 1.6, 8.3 Hz, 1H), 6.80 (d, *J* = 8.6 Hz, 2H), 6.68 (d, *J* = 8.6 Hz, 2H), 5.07 (d, *J* = 6.6 Hz, 1H), 4.28-4.16 (m, 1H), 3.84-3.72 (m, 1H), 2.32 (s, 3H), 1.55-1.37 (m, 8H), 1.31 (9H, s); MS *m/z* 559 (M+H). A suspension of the crude intermediate (506 mg, 0.91 mmol) in dry CH_2Cl_2 (6 mL) was treated with Et_3N (110 mg, 1.09 mmol) at r.t.. The resulting mixture was cooled to -78 °C and 3,3,3-trifluoropropane-1-sulfonyl chloride (181 mg, 0.92 mmol) in dry CH_2Cl_2 (0.2 mL) was added dropwise. After stirring at -78 °C for 3 h (including extra additions of 3,3,3-trifluoro-propane-1-sulfonyl chloride (2 x 43 mg, 0.22 mmol) after 1.5 h and 2.5 h), the reaction mixture was washed with water and evaporated to yield the crude intermediate (655 mg). MS *m/z* 719 (M+H). To a suspension of the Boc-protected intermediate (655 mg, 0.91 mmol) in MeOH (10 mL) at 0 °C was added dropwise a solution of thionyl chloride in MeOH (prepared by dropwise addition of thionyl chloride (5.41 g, 45.5 mmol) to MeOH (10 mL) at -40 °C). After the addition the ice bath was removed. The

reaction mixture was stirred at r.t. for 1 h after which the solvents were evaporated. The product was purified by HPLC (30-100% CH_3CN (with 0.1 % formic acid) in 0.1% formic acid (aq) during 40 min). The CH_3CN was evaporated and the resulting mixture extracted with CH_2Cl_2. The organic phase was washed with aqueous $NaHCO_3$ (1 M), dried ($MgSO_4$), filtered, and concentrated *in vacuo* to yield the title compound as a slightly yellow solid (315 mg yield over 3 steps 56%). ^1H NMR (400 MHz, $CDCl_3$) δ 7.51 (d, *J* = 8.7 Hz, 1H), 7.32-7.20 (m, 5H), 7.14 (d, *J* = 8.8 Hz, 2H), 4.20-4.09 (m, 1H), 3.52-3.44 (m, 2H), 3.15-3.06 (m, 1H), 2.84-2.71 (m, 2H), 2.47 (s, 3H), 1.70-1.39 (m, 10H); HRMS Calcd for $[C_{26}H_{27}Cl_2F_3N_4O_4S+H]$: 619.1160. Found: 619.1216. HPLC: 95.4%.

*racemic 1-(4-(Benzyloxy)phenyl)-2-(2,4-dichlorophenyl)-N-((cis)-2-(dimethylamino)cyclohexyl)-5-methyl-1H-imidazole-4-carboxamide (**23**).* To a suspension of racemic **20** (493 mg, 0.90 mmol) in CH_3CN (10 mL) was added formaldehyde, 36% (135 mg, 4.49 mmol) and sodium borohydride (75 mg, 1.97 mmol) in portions. The suspension was stirred at r.t. for 2 days adding after 2.5 h sodium borohydride (77 mg, 2.04 mmol), 3.5 h formaldehyde (36% in H_2O, 67 mg, 2.24 mmol), 18.5 h formaldehyde (36% in H_2O, 67 mg, 2.24 mmol) and sodium borohydride (77 mg, 2.04 mmo1) (the temperature was increased to 40 °C for 4.5 h), 23 h AcOH (1.85 mL) at r.t., 28 h formaldehyde (36% in H_2O, 135 mg, 4.49 mmol) followed by sodium cyanoborohydride (112 mg, 1.78 mmol), 42 h formaldehyde (36% in H_2O, (135 mg, 4.49 mmol) followed by sodium cyano borohydride (126 mg, 2.01 mmol). The reaction mixture was diluted with CH_2Cl_2, washed with NaOH (1 M) and brine, dried ($MgSO_4$), filtered and evaporated. The residue was purified by HPLC (30-100% CH_3CN in aqueous NH_4OAc (0.1 M) over 30 min). The CH_3CN was evaporated and the resulting mixture extracted with CH_2Cl_2, dried ($MgSO_4$), filtered and evaporated to yield the title compound (163 mg, 32%). MS *m/z* 577 (M+H).

*racemic 2-(2,4-Dichlorophenyl)-N-((cis)-2-(dimethylamino)cyclohexyl)-1-(4-hydroxyphenyl)-5-methyl-1H-imidazole-4-carboxamide (**24**).* A suspension of racemic **23** (163 mg, 0.28 mmol) in CH_2Cl_2 (2 mL) and dimethyl sulfide (351 mg, 5.64 mmol) was treated with boron trifluoride (801 mg, 5.64 mmol).

The reaction mixture was stirred at r.t. for 2 days (dark) adding more of dimethyl sulfide (176 mg, 2.82 mmol) and boron trifluoride (401 mg, 2.82 mmol) after 17 h. Water and CH_2Cl_2 were added and the phases separated. The organic phase was washed with water, dried ($MgSO_4$), filtered, and concentrated *in vacuo* to yield the crude title compound (104 mg). MS *m/z* 487 (M+H).

*racemic 4-(2-(2,4-Dichlorophenyl)-4-((cis)-2-(dimethylamino)cyclohexylcarbamoyl)-5-methyl-1H-imidazol-1-yl]phenyl 3,3,3-trifluoropropane-1-sulfonate (**25**).* A suspension of racemic **24** (104 mg, 0.21 mmol) in dry CH_2Cl_2 (1.5 mL) was treated with Et_3N (26 mg, 0.26 mmol) at r.t.. The resulting mixture was cooled to -78 °C and 3,3,3-trifluoropropane-1-sulfonyl chloride (50 mg, 0.26 mmol) in dry CH_2Cl_2 (0.5 mL) was added dropwise. After stirring at -78 °C for 6.5 h (and adding more 3,3,3-trifluoropropane-1-sulfonyl chloride (2 x 50 mg, 0.26 mmol) after 2 h and 4 h, and Et_3N (26 mg, 0.26 mmol) after 4 h), the reaction mixture was washed with water and evaporated. The residue was purified by HPLC (30-100% CH_3CN (with 0.1% formic acid) in 0.1% formic acid over 40 min) and freeze dried. The product was dissolved in CH_2Cl_2 and washed with $NaHCO_3$ (1 M) and water, dried ($MgSO_4$), filtered and concentrated *in vacuo* to yield the title compound as a slightly yellow oil (37 mg yield over 2 steps 20%). ^{1}H NMR (400 MHz, $CDCl_3$) δ 7.54 (d, *J* = 7.6 Hz, 1H), 7.37 (d, *J* = 8.3 Hz, 1H), 7.31 (d, *J* = 2.0 Hz, 1H), 7.29 (d, *J* = 8.9 Hz, 1H), 7.26 (dd, *J* = 2.0, 8.3 Hz, 1H), 7.17 (d, *J* = 8.9 Hz, 1H), 4.59-4.51 (m, 1H), 3.56-3.48 (m, 2H), 2.86-2.76 (m, 2H), 2.51 (s, 3H), 2.31 (s, 6H), 2.26-2.19 (m, 1H), 2.07 (dt, *J* = 3.8, 11.8 Hz, 1H), 2.04-1.96 (m, 2H), 1.85-1.77 (m, 1H), 1.54-1.25 (m, 5H); HRMS Calcd for [$C_{28}H_{31}Cl_2F_3N_4O_4S$+H]: 647.1473. Found: 647.1472. HPLC: 100%.

*1-(4-(Benzyloxy)phenyl)-2-(2,4-dichlorophenyl)-5-methyl-N-(5-(trifluoromethyl)pyridin-2-yl)-1H-imidazole-4-carboxamide (**26**).* A solution of 2-amino-5-(trifluoromethyl)pyridine (404 mg, 2.49 mmol) in CH_2Cl_2 (2.5 mL) under argon was carefully treated with trimethylaluminium (2.0 M in toluene, 1.25 mL, 2.5 mmol) over 5 min. The solution was stirred at r.t. for 1.5 h to give a 0.66 M solution of the amidation reagent. A portion of this solution (3.75 mL, 2.5 mmol) was added to compound **3** (400 mg, 0.83 mmol). After stirring at 45 °C overnight the mixture was cooled to 0 °C and quenched with HCl

(aq, 2 M, 7.5 mL). The mixture was diluted with dichloromethane and neutralized by addition of KOH (aq, 2 M). The organic phase was separated and the aqueous phase was extracted further with dichloromethane. The collected organic phases were washed with H_2O, dried (Na_2SO_4), filtered, and concentrated *in vacuo* to give a residue which was purified by preparative HPLC to give the title compound (319 mg, 64%) as a solid. ^{1}H NMR (400 MHz, $CDCl_3$) δ 9.91 (s, 1H), 8.57 (s, 1H), 8.52 (d, *J* = 8.8 Hz, 1H), 7.92 (dd, *J* = 2.1, 8.8 Hz, 1H), 7.44-7.32 (m, 6H), 7.30-7.21 (m, 2H), 7.04 (d, *J* = 8.9 Hz, 2H), 6.95 (d, *J* = 8.9 Hz, 2H), 5.05 (s, 2H), 2.52 (s, 3H); MS *m/z* 597 (M+H).

*2-(2,4-Dichlorophenyl)-1-(4-hydroxyphenyl)-5-methyl-N-(5-(trifluoromethyl)pyridin-2-yl)-1H-imidazole-4-carboxamide (**27**).* Compound **26** (319 mg, 0.53 mmol) was dissolved in HBr (4.1 M in acetic acid, 7.5 mL, 30.8 mmol) and the mixture stirred at r.t. for 4 h. The acetic acid was co-evaporated with EtOH, the residue neutralized with ammonia and dissolved in methanol. Purification by flash chromatography gave the title compound (266 mg, 98%). ^{1}H NMR (400 MHz, DMF-d7) δ 10.36 (s, 1H), 10.09 (s, 1H), 8.89 (d, *J* = 1.0 Hz, 1H), 8.69 (d, *J* = 8.9 Hz, 1H), 8.45 (dd, *J* = 1.0, 8.9 Hz, 1H), 7.85 (d, *J* = 8.3 Hz, 1H), 7.80 (s, 1H), 7.67 (d, *J* = 8.3 Hz, 1H), 7.40 (d, *J* = 8.4 Hz, 2H), 7.06 (d, *J* = 8.4 Hz, 2H), 2.65 (s, 3H); MS *m/z* 507 (M+H).

*4-(2-(2,4-Dichlorophenyl)-5-methyl-4-(5-(trifluoromethyl)pyridin-2-ylcarbamoyl)-1H-imidazol-1-yl)phenyl 3,3,3-trifluoropropane-1-sulfonate (**28**).* A mixture of **27** (136 mg, 0.27 mmol) and Et_3N (40 µL, 0.32 mmol) in CH_2Cl_2 (4.0 mL) was cooled to -78 °C then carefully treated with 3,3,3-trifluoropropane-1-sulfonyl chloride (63 mg, 0.32 mmol). The resulting mixture was stirred at -78 °C for 1 h, then allowed to reach room temperature. Water was added to the reaction, and the phases were separated. The organic phase was washed with $NaHCO_3$, and brine, then dried (Na_2SO_4), filtered, and concentrated *in vacuo* to give a residue which was purified by preparative HPLC to give the title compound (88 mg, 49%) as a solid. ^{1}H NMR (400 MHz, $CDCl_3$) δ 9.87 (s, 1H), 8.55 (s, 1H), 8.49 (d, *J* = 8.8 Hz, 1H), 7.91 (dd, *J* = 2.1, 8.8 Hz, 1H), 7.36-7.21 (m, 5H), 7.19 (d, J = 8.8 Hz, 2H), 3.55-3.46 (m, 2H), 2.87-2.71 (m, 2H), 2.54 (s, 3H); ^{13}C NMR (126 MHz, $CDCl_3$) δ 162.0, 154.3, 148.6, 145.6

(q, *J* = 4.1), 142.7, 137.0, 136.2, 135.6 (q, *J* = 3.2), 135.2, 134.1, 133.4, 131.0, 130.0, 129.3, 127.9, 127.5, 125.1 (q, *J* = 277.1), 123.8 (q, *J* = 271.3), 123.2, 122.1 (q, *J* = 32.7), 113.1, 44.5 (q, *J* = 3.3), 29.3 (q, *J* = 31.5), 11.1. HRMS Calcd for [$C_{26}H_{18}Cl_2F_6N_4O_4S$ +H]: 667.0408. Found: 667.0540. HPLC: 100%.

Biology. *Chemicals and Reagents.* [^{3}H]CP55940 (specific activity 141.2 Ci/mmol) was purchased from Perkin Elmer (Waltham, MA). Bicinchoninic acid (BCA) and BCA protein assay reagent were obtained from Pierce Chemical Company (Rochford, IL). Rimonabant was from Cayman Chemical Company (Ann Arbor, MI). CHOK1hCB_1_bgal cells (catalog number 93-0959C2) were obtained from DiscoveRx (Fremont, CA). The membranes (catalog number RBHCB1M400UA) used for [^{35}S]GTPγS antagonism experiment were purchased from Perkin Elmer (Waltham, MA). All other chemicals were of analytical grade and obtained from standard commercial sources.

Cell Culture and Membrane Preparation. CHOK1hCB_1_bgal cells were cultured in Ham's F12 Nutrient Mixture supplemented with 10% fetal calf serum, 1 mM glutamine, 50 µg/mL penicillin, 50 µg/ml streptomycin, 300 mg/mL hygromycin and 800 µg/mL geneticin in a humidified atmosphere at 37 °C and 5% CO_2. Cells were subcultured twice a week at a ratio of 1:10 on 10-cm ø plates by trypsinization. For membrane preparation the cells were subcultured 1:10 and transferred to large 15-cm ø plates. Membrane fractions were prepared exactly as described before.[50]

Equilibrium Radioligand Displacement Assays. [^{3}H]CP55940 displacement assays on 96-well plate were used for the determination of affinity (IC_{50} and K_i) values of antagonists for the cannabinoid CB_1 receptors. The displacement experiments were performed using 6 concentrations of competing antagonists in 25 µL of assay buffer (50 mM Tris–HCl, 5 mM $MgCl_2$, 0.1% BSA, pH 7.4) in the presence of another 25 µL of assay buffer with a final concentration of 3.5 nM [^{3}H]CP55940. At this concentration, total radioligand binding did not exceed 10% of that added to prevent ligand depletion. Membrane aliquots containing 5 µg of CHOK1hCB_1_bgal membrane in 100 µL assay buffer were incubated at 30 °C for 60 min. Nonspecific binding (NSB) was determined in the presence of 10 µM rimonabant. Incubation was terminated by rapid filtration performed on 96-well GF/C filter

plates (Perkin Elmer, Groningen, the Netherlands), presoaked for 30 min with 0.25% PEI (PolyEthyleneImine), using a PerkinElmer Filtermate-harvester (Perkin Elmer, Groningen, the Netherlands). After 30 min of dehydration of the filter plate at 50 °C, the filter-bound radioactivity was determined by scintillation spectrometry using the 2450 MicroBeta^2 Plate Counter. The binding values were recorded in both counts per minute (CPM) and disintegrations per minute (DPM). Each antagonist was measured in duplicate and at least 3 individual experiments were performed.

Classic Radioligand Kinetic Assays. Association experiments were performed by incubating membrane aliquots containing 5 µg of CHOK1hCB_1_bgal membrane in a total volume of 100 µL of assay buffer at 30 °C with 3.5 nM [^{3}H]CP55940. The amount of radioligand bound to the receptor was measured at different time intervals during a total incubation of 120 min. Dissociation experiments were performed by preincubating membrane aliquots containing 5 µg of protein in a total volume of 100 µL of assay buffer for 60 min. After the preincubation, radioligand dissociation was initiated by the addition of 10 µM unlabeled rimonabant. The amount of radioligand still bound to the receptor was measured at various time intervals for a total of 240 min. to ensure that full dissociation from cannabinoid CB_1 receptor was reached. Incubation was terminated by rapid filtration performed on GF/C filters (Whatman International, Maidstone, UK), presoaked for 30 min with 0.25% PEI, using a Brandel harvester (Brandel, Gaithersburg, MD). Filter-bound radioactivity was determined by scintillation spectrometry using a Tri-Carb 2900 TR liquid scintillation counter (Perkin Elmer, Boston, MA).

Competition Association Assays. Kinetic Rate Index (KRI) values are an average of at least two independent experiments, each consisting of two replicates. Kinetic rate constant values are an average of at least three independent experiments, each consisting of two replicates. The binding kinetics of unlabeled ligands was quantified using the competition association assay based on the theoretical framework by Motulsky and Mahan.[36] A concentration of 1 to 3-fold of the IC_{50} value was used to determine the binding kinetics of unlabeled CB_1 receptor antagonists. The competition

association assay was initiated by adding membrane aliquots (5 µg/well) at different time points for a total of 240 min to a total volume of 100 µL of assay buffer at 30 °C with 3.5 nM [^{3}H]CP55940 in the absence or presence of competing CB_1 receptor antagonists (1 to 3-fold IC_{50}). Incubations were terminated, and samples were obtained as described under *Equilibrium Radioligand* Displacement *Assay*. The "dual-point" competition association assays[32] were run similarly, with only two time points, at 30 and 240 min, respectively.

[^{35}S]GTPγS Binding Assays. Antagonism assay: The antagonism of all tested compounds was evaluated at 30 °C in a [^{35}S]GTPγS binding assay as reported earlier.[51] Insurmountability assay: Membrane homogenates containing the CB_1 receptor (5 µg) were equilibrated in the assay buffer (50 mM Tris–HCl, 5 mM $MgCl_2$, 1 mM EDTA, 100 mM NaCl, 0.05% BSA, pH7.4) supplemented with 1 µM GDP, 1 mM DTT and 5 µg saponin. Membrane preparations were pre-incubated with or without antagonists (10-fold K_i values on the CB_1 receptor) for 1 h prior to the challenge of a CB_1 receptor agonist, CP55940 at 25 °C with concentrations ranging from 1 µM to 0.1 nM. Subsequently, [^{35}S]GTPγS (final concentration 0.3 nM) was added and incubation continued for another 30 min at 25 °C. Incubations were terminated and samples were obtained as described under *Equilibrium Radioligand Displacement Assays*.

Data analysis. All experimental data were analyzed using the nonlinear regression curve fitting program GraphPad Prism 6.0 (GraphPad Software, Inc., San Diego, CA). From displacement assays, IC_{50} values were obtained by non-linear regression analysis of the displacement curves. The obtained IC_{50} values were converted into K_i values using the Cheng-Prusoff equation to determine the affinity of the ligands.[52] The k_{on} and k_{off} values for radiolabeled and unlabeled ligands were fitted and calculated, and the k_{on} and k_{off} values were used to calculate residence times (in min) and kinetic dissociation binding constants (kinetic K_D). Association and dissociation rates for unlabeled compounds were calculated by fitting the data into the competition association model using "kinetics of competitive binding":[36]

$$K_A = k_1[L]\cdot 10^{-9} + k_2$$

$$K_B = k_3[I]\cdot 10^{-9} + k_4$$

$$S = \sqrt{(K_A - K_B)^2 + 4\cdot k_1 \cdot k_3 \cdot L \cdot I \cdot 10^{-18}}$$

$$K_F = 0.5(K_A + K_B + S)$$

$$K_S = 0.5(K_A + K_B - S)$$

$$Q = \frac{B_{\max} \cdot k_1 \cdot L \cdot 10^{-9}}{K_F - K_S}$$

$$Y = Q \cdot \left(\frac{k_4 \cdot (K_F - K_S)}{K_F \cdot K_S} + \frac{k_4 - K_F}{K_F} e^{(-K_F \cdot X)} - \frac{k_4 - K_S}{K_S} e^{(-K_S \cdot X)}\right)$$

Where k_1 is the k_{on} of the radioligand ($M^{-1}s^{-1}$), k_2 is the k_{off} of the radioligand (s^{-1}), L is the radioligand concentration (nM), I is the concentration of the unlabeled competitor (nM), X is the time (min) and Y is the specific binding of the radioligand (DPM). During a competition association these parameters are set, obtaining k_1 from the control curve without competitor and k_2 from previously performed dissociation assays described under *Traditional Radioligand Kinetic Assays*. With that the k_3, k_4 and B_{max} can be calculated, where k_3 represents the k_{on} ($M^{-1}s^{-1}$) of the unlabeled ligand, k_4 stands for the k_{off} (s^{-1}) of the unlabeled ligand and B_{max} equals the total binding (DPM). All competition association data were globally fitted. Residence times (RT, expressed in min) were calculated as RT = $1/(60*k_{off})$.

Computational studies. All computational studies were performed in the Schrödinger suite,[53] and based on the crystal structure of the CB_1 receptor co-crystalized with **29** (PDB: 5TGZ).[33] The crystal structure was prepared with the protein preparation wizard.[53] Ligands were docked using induced fit docking,[54] with core constraints on the 2,4-dichlorophenyl ring of **29** (all ligands share this moiety). To study whether the difference in RTs among **11d**, **14f** and **28** could be explained by unfavorable hydration, we generated a WaterMap around **14f**.[47, 48] Figures were rendered using PyMol.[55]

References

1. Maccarrone, M.; Bab, I.; Bíró, T.; Cabral, G. A.; Dey, S. K.; Di Marzo, V.; Konje, J. C.; Kunos, G.; Mechoulam, R.; Pacher, P.; Sharkey, K. A.; Zimmer, A. Endocannabinoid signaling at the periphery: 50 years after THC. *Trends Pharmacol. Sci.* **2015,** *36*, 277-296.

2. Pertwee, R. G.; Howlett, A. C.; Abood, M. E.; Alexander, S. P. H.; Di Marzo, V.; Elphick, M. R.; Greasley, P. J.; Hansen, H. S.; Kunos, G.; Mackie, K.; Mechoulam, R.; Ross, R. A. International union of basic and clinical pharmacology. LXXIX. cannabinoid receptors and their ligands: beyond CB_1 and CB_2. *Pharmacol. Rev.* **2010,** *62*, 588-631.
3. Munro, S.; Thomas, K. L.; Abu-Shaar, M. Molecular characterization of a peripheral receptor for cannabinoids. *Nature* **1993,** *365*, 61-65.
4. Abood, M.; Barth, F.; Bonner, T. I.; Cabral, G.; Casellas, P.; Cravatt, B. F.; Devane, W. A.; Elphick, M. R.; Felder, C. C.; Herkenham, M.; Howlett, A. C.; Kunos, G.; Mackie, K.; Mechoulam, R.; Pertwee, R. G. Cannabinoid receptors: CB1 receptor. Last modified on May 16, **2017**. Accessed on July 20, 2017. *IUPHAR/BPS Guide to Pharmacology*, http://www.guidetopharmacology.org/GRAC/ObjectDisplayForward?objectId=56.
5. Pacher, P.; BÁTkai, S.; Kunos, G. The endocannabinoid system as an emerging target of pharmacotherapy. *Pharmacol. Rev.* **2006,** *58*, 389-462.
6. Bermudez-Silva, F. J.; Viveros, M. P.; McPartland, J. M.; Rodriguez de Fonseca, F. The endocannabinoid system, eating behavior and energy homeostasis: the end or a new beginning? *Pharmacol., Biochem. Behav.* **2010,** *95*, 375-382.
7. Pertwee, R. G. The pharmacology of cannabinoid receptors and their ligands: an overview. *Int. J. Obes.* **2006,** *30*, S13-S18.
8. Pellicoro, A.; Ramachandran, P.; Iredale, J. P.; Fallowfield, J. A. Liver fibrosis and repair: immune regulation of wound healing in a solid organ. *Nat. Rev. Immunol.* **2014,** *14*, 181-194.
9. Cinar, R.; Iyer, M. R.; Liu, Z.; Cao, Z.; Jourdan, T.; Erdelyi, K.; Godlewski, G.; Szanda, G.; Liu, J.; Park, J. K.; Mukhopadhyay, B.; Rosenberg, A. Z.; Liow, J.-S.; Lorenz, R. G.; Pacher, P.; Innis, R. B.; Kunos, G. Hybrid inhibitor of peripheral cannabinoid-1 receptors and inducible nitric oxide synthase mitigates liver fibrosis. *JCI Insight* **2016,** *1*, e87336.
10. Perkins, J. M.; Davis, S. N. Endocannabinoid system overactivity and the metabolic syndrome: prospects for treatment. *Curr. Diabetes Rep.* **2008,** *8*, 12-19.
11. FDA briefing document NDA 21-888 zimulti (rimonabant) tablets, 20 mg sanofi aventis advisory committee. Published on June 13, 2007. Accessed on July 20, 2017. <http://www.fda.gov/ohrms/dockets/ac/07/briefing/2007-4306b1-fda-backgrounder.pdf>.
12. Boekholdt, S. M.; Peters, R. J. G. Rimonabant: obituary for a wonder drug. *Lancet* **2010,** *376*, 489-490.
13. Topol, E. J.; Bousser, M.-G.; Fox, K. A. A.; Creager, M. A.; Despres, J.-P.; Easton, J. D.; Hamm, C. W.; Montalescot, G.; Steg, P. G.; Pearson, T. A.; Cohen, E.; Gaudin, C.; Job, B.; Murphy, J. H.; Bhatt, D. L. Rimonabant for prevention of cardiovascular events (CRESCENDO): a randomised, multicentre, placebo-controlled trial. *Lancet* **2010,** *376*, 517-523.
14. Proietto, J.; Rissanen, A.; Harp, J. B.; Erondu, N.; Yu, Q.; Suryawanshi, S.; Jones, M. E.; Johnson-Levonas, A. O.; Heymsfield, S. B.; Kaufman, K. D.; Amatruda, J. M. A clinical trial assessing the safety and efficacy of the CB_1R inverse agonist taranabant in obese and overweight patients: low-dose study. *Int. J. Obes.* **2010,** *34*, 1243-1254.
15. Aronne, L. J.; Finer, N.; Hollander, P. A.; England, R. D.; Klioze, S. S.; Chew, R. D.; Fountaine, R. J.; Powell, C. M.; Obourn, J. D. Efficacy and safety of CP-945,598, a selective cannabinoid CB_1 receptor antagonist, on weight loss and maintenance. *Obesity* **2011,** *19*, 1404-1414.
16. Kloet, A. D. d.; Woods, S. C. Endocannabinoids and their receptors as targets for obesity therapy. *Endocrinology* **2009,** *150*, 2531-2536.
17. Sharma, M. K.; Murumkar, P. R.; Barmade, M. A.; Giridhar, R.; Yadav, M. R. A comprehensive patents review on cannabinoid 1 receptor antagonists as antiobesity agents. *Expert Opin. Ther. Pat.* **2015,** *25*, 1093-1116.
18. Storr, M. A.; Bashashati, M.; Hirota, C.; Vemuri, V. K.; Keenan, C. M.; Duncan, M.; Lutz, B.; Mackie, K.; Makriyannis, A.; Macnaughton, W. K.; Sharkey, K. A. Differential effects of CB_1 neutral antagonists and inverse agonists on gastrointestinal motility in mice. *Neurogastroenterol. Motil.* **2010,** *22*, 787-e223.

19. Tudge, L.; Williams, C.; Cowen, P. J.; McCabe, C. Neural effects of cannabinoid CB_1 neutral antagonist tetrahydrocannabivarin on food reward and aversion in healthy volunteers. *Int. J. Neuropsychopharmacol.* **2015,** *18*, pyu094.
20. Copeland, R. A. The drug-target residence time model: a 10-year retrospective. *Nat. Rev. Drug Discovery* **2016,** *15*, 87-95.
21. Swinney, D. C.; Haubrich, B. A.; van Liefde, I.; Vauquelin, G. The role of binding kinetics in GPCR drug discovery. *Curr. Top. Med. Chem.* **2015,** *15*, 2504-2522.
22. Guo, D.; Hillger, J. M.; IJzerman, A. P.; Heitman, L. H. Drug-target residence time—a case for G protein-coupled receptors. *Med. Res. Rev.* **2014,** *34*, 856-892.
23. Vilums, M.; Zweemer, A. J. M.; Yu, Z.; de Vries, H.; Hillger, J. M.; Wapenaar, H.; Bollen, I. A. E.; Barmare, F.; Gross, R.; Clemens, J.; Krenitsky, P.; Brussee, J.; Stamos, D.; Saunders, J.; Heitman, L. H.; IJzerman, A. P. Structure–kinetic relationships—an overlooked parameter in hit-to-lead optimization: a case of cyclopentylamines as chemokine receptor 2 antagonists. *J. Med. Chem.* **2013,** *56*, 7706-7714.
24. Guo, D.; Xia, L.; van Veldhoven, J. P. D.; Hazeu, M.; Mocking, T.; Brussee, J.; IJzerman, A. P.; Heitman, L. H. Binding kinetics of ZM241385 derivatives at the human adenosine A_{2A} receptor. *ChemMedChem* **2014,** *9*, 752-761.
25. Louvel, J.; Guo, D.; Agliardi, M.; Mocking, T. A. M.; Kars, R.; Pham, T. P.; Xia, L.; de Vries, H.; Brussee, J.; Heitman, L. H.; IJzerman, A. P. Agonists for the adenosine A_1 receptor with tunable residence time. A case for nonribose 4-amino-6-aryl-5-cyano-2-thiopyrimidines. *J. Med. Chem.* **2014,** *57*, 3213-3222.
26. Xia, L.; Burger, W. A. C.; van Veldhoven, J. P. D.; Kuiper, B. J.; van Duijl, T. T.; Lenselink, E. B.; Paasman, E.; Heitman, L. H.; IJzerman, A. P. Structure–affinity relationships and structure–kinetics relationships of pyrido[2,1-f]purine-2,4-dione derivatives as human adenosine A_3 receptor antagonists. *J. Med. Chem.* **2017,** *60*, 7555-7568.
27. Guo, D.; Heitman, L. H.; IJzerman, A. P. The role of target binding kinetics in drug discovery. *ChemMedChem* **2015,** *10*, 1793-1796.
28. Cawston, E. E.; Redmond, W. J.; Breen, C. M.; Grimsey, N. L.; Connor, M.; Glass, M. Real-time characterization of cannabinoid receptor 1 (CB_1) allosteric modulators reveals novel mechanism of action. *Br. J. Pharmacol.* **2013,** *170*, 893-907.
29. Cawston, E. E.; Connor, M.; Di Marzo, V.; Silvestri, R.; Glass, M. Distinct temporal fingerprint for cyclic adenosine monophosphate (cAMP) signaling of indole-2-carboxamides as allosteric modulators of the cannabinoid receptors. *J. Med. Chem.* **2015,** *58*, 5979-5988.
30. Cheng, L. Midazole-4-carboxamide derivatives for use as cb modulators. In WO 2007031721 A1: **2007**.
31. Ahlqvist, M.; Cheng, L.; Lundqvist, R.; Sörensen, H. 1,2-diarylimidazoles for use as cb1 modulators. In WO 2007031720 A1: **2007**.
32. Guo, D.; van Dorp, E. J. H.; Mulder-Krieger, T.; van Veldhoven, J. P. D.; Brussee, J.; IJzerman, A. P.; Heitman, L. H. Dual-point competition association assay: a fast and high-throughput kinetic screening method for assessing ligand-receptor binding kinetics. *J. Biomol. Screening* **2013,** *18*, 309-320.
33. Hua, T.; Vemuri, K.; Pu, M.; Qu, L.; Han, Gye W.; Wu, Y.; Zhao, S.; Shui, W.; Li, S.; Korde, A.; Laprairie, Robert B.; Stahl, Edward L.; Ho, J.-H.; Zvonok, N.; Zhou, H.; Kufareva, I.; Wu, B.; Zhao, Q.; Hanson, Michael A.; Bohn, Laura M.; Makriyannis, A.; Stevens, Raymond C.; Liu, Z.-J. Crystal structure of the human cannabinoid receptor CB_1. *Cell* **2016,** *167*, 750-762.e714.
34. Shao, Z.; Yin, J.; Chapman, K.; Grzemska, M.; Clark, L.; Wang, J.; Rosenbaum, D. M. High-resolution crystal structure of the human CB_1 cannabinoid receptor. *Nature* **2016,** *540*, 602-606.
35. Gustafsson, T.; Ponten, F.; Seeberger, P. H. Trimethylaluminium mediated amide bond formation in a continuous flow microreactor as key to the synthesis of rimonabant and efaproxiral. *Chem. Commun.* **2008**, 1100-1102.

36. Motulsky, H. J.; Mahan, L. C. The kinetics of competitive radioligand binding predicted by the law of mass action. *Mol. Pharmacol.* **1984,** *25*, 1-9.
37. Packeu, A.; Wennerberg, M.; Balendran, A.; Vauquelin, G. Estimation of the dissociation rate of unlabelled ligand–receptor complexes by a 'two-step' competition binding approach. *Br. J. Pharmacol.* **2010,** *161*, 1311-1328.
38. Wennerberg, M.; Cheng, L.; Hjorth, S.; Clapham, J. C.; Balendran, A.; Vauquelin, G. Binding properties of antagonists to cannabinoid receptors in intact cells. *Fundam. Clin. Pharmacol.* **2011,** *25*, 200-210.
39. Labute, P. A widely applicable set of descriptors. *J. Mol. Graphics Modell.* **2000,** *18*, 464-477.
40. Advanced Chemistry Development, I., Toronto, On, Canada, www.acdlabs.com. *The ACD software* 12; **2015**.
41. Davis, A. M.; Wood, D. J. Quantitative structure–activity relationship models that stand the test of time. *Mol. Pharmaceutics* **2013,** *10*, 1183-1190.
42. Hitchcock, S. A.; Pennington, L. D. Structure−brain exposure relationships. *J. Med. Chem.* **2006,** *49*, 7559-7583.
43. De Vry, J.; Rüdiger Jentzsch, K. Discriminative stimulus effects of BAY 38-7271, a novel cannabinoid receptor agonist. *Eur. J. Pharmacol.* **2002,** *457*, 147-152.
44. Mauler, F.; Mittendorf, J.; Horváth, E.; de Vry, J. Characterization of the Diarylether Sulfonylester (−)-(R)-3-(2-Hydroxymethylindanyl-4-oxy)phenyl-4,4,4-trifluoro-1-sulfonate (BAY 38-7271) as a Potent Cannabinoid Receptor Agonist with Neuroprotective Properties. *J. Pharmacol. Exp. Ther.* **2002,** *302*, 359-368.
45. Horswill, J. G.; Bali, U.; Shaaban, S.; Keily, J. F.; Jeevaratnam, P.; Babbs, A. J.; Reynet, C.; Wong Kai In, P. PSNCBAM-1, a novel allosteric antagonist at cannabinoid CB_1 receptors with hypophagic effects in rats. *Br. J. Pharmacol.* **2007,** *152*, 805-814.
46. Segala, E.; Guo, D.; Cheng, R. K. Y.; Bortolato, A.; Deflorian, F.; Doré, A. S.; Errey, J. C.; Heitman, L. H.; IJzerman, A. P.; Marshall, F. H.; Cooke, R. M. Controlling the dissociation of ligands from the adenosine A_{2A} receptor through modulation of salt bridge strength. *J. Med. Chem.* **2016,** *59*, 6470-6479.
47. Abel, R.; Young, T.; Farid, R.; Berne, B. J.; Friesner, R. A. Role of the active-site solvent in the thermodynamics of Factor Xa ligand binding. *J. Am. Chem. Soc.* **2008,** *130*, 2817-2831.
48. Young, T.; Abel, R.; Kim, B.; Berne, B. J.; Friesner, R. A. Motifs for molecular recognition exploiting hydrophobic enclosure in protein–ligand binding. *Proc. Natl. Acad. Sci. U. S. A.* **2007,** *104*, 808-813.
49. Mason, J. S.; Bortolato, A.; Weiss, D. R.; Deflorian, F.; Tehan, B.; Marshall, F. H. High end GPCR design: crafted ligand design and druggability analysis using protein structure, lipophilic hotspots and explicit water networks. *In Silico Pharmacology* **2013,** *1*, 23.
50. Xia, L.; Vries, H.; IJzerman, A. P.; Heitman, L. H. Scintillation proximity assay (SPA) as a new approach to determine a ligand's kinetic profile. A case in point for the adenosine A1 receptor. *Purinergic Signalling* **2015,** 12, 115-126.
51. Ryberg, E.; Larsson, N.; Sjögren, S.; Hjorth, S.; Hermansson, N. O.; Leonova, J.; Elebring, T.; Nilsson, K.; Drmota, T.; Greasley, P. J. The orphan receptor GPR55 is a novel cannabinoid receptor. *Br. J. Pharmacol.* **2007,** *152*, 1092-1101.
52. Cheng, Y.-C.; Prusoff, W. H. Relationship between the inhibition constant (K_i) and the concentration of inhibitor which causes 50 percent inhibition (IC_{50}) of an enzymatic reaction. *Biochem. Pharmacol.* **1973,** *22*, 3099-3108.
53. Schrödinger, L. L. C., New York. *Schrödinger Release 2016-4: MS Jaguar*, **2016**.
54. Sherman, W.; Day, T.; Jacobson, M. P.; Friesner, R. A.; Farid, R. Novel procedure for modeling ligand/receptor induced fit effects. *J. Med. Chem.* **2006,** *49*, 534-553.
55. Schrödinger, L. L. C., New York. *The PyMOL molecular graphics system*, 1.8.3.2; **2016**.

Supporting information

Determination of target selectivity between human CB_1 and CB_2 receptors and physicochemical properties for human CB1 receptor antagonists Contents.

1. Selectivity data for representative human CB_1 receptor antagonists at human CB_2 receptor

Method: The antagonism of all tested compounds was evaluated at 30 °C in a [^{35}S]GTPγS binding assay as reported earlier.[51]

Table S1. Selectivity data for representative human CB_1 receptor antagonists at human CB_2 receptor.

Antagonist	[^{35}S]GTPγS binding pIC_{50} ± SD or SEM (mean IC_{50} in nM) [a]	pK_i ± SEM (mean K_i in nM) [b]
11b	N. D. [c]	7.5 ± 0.01 (35)
11d	6.6 ± 0.05 (288)	N. D. [c]
11f	6.5 (320)	N. D. [c]
11g	6.6 ± 0.01 (271) [d]	N. D. [c]
11h	5.9 ± 0.03 (1358)	N. D. [c]
14b (±) *trans*	6.4 ± 0.1 (425) [d]	N. D. [c]
14d (+) *cis*	6.4 ± 0.2 (440) [d]	N. D. [c]
22 (±) *cis*	6.1 ± 0.03 (805) [d]	N. D. [c]
14f	N. D. [c]	8.9 ± 0.1 (1.4)
14h	6.4 ± 0.05 (400) [d]	N. D. [c]
28	6.9 ± 0.04 (133) [d]	8.3 ± 0.1 (4.9)

[a] pIC_{50} ± SD (n=2) or SEM (n ≥ 3), except **11f** was n=1, obtained from [^{35}S]GTPγS binding on recombinant human CB_2 receptors stably expressed on HEK-293 cell membranes.

[b] pK_i ± SEM (n=3), obtained from radioligand binding assays with [^{3}H]CP55940 on recombinant human CB_2 receptors stably expressed on CHO cell membranes.

[c] N.D. = Not determined.

[d] n=2.

2. Calculating Polar Surface Area (PSA)

Method: PSA is an in-house implementation (AstraZeneca, Vladimir Sherbukin) of a literature model.[39] In brief, Van der Waals surface area around polar atoms (N, O and H attached either to N or O), all other atoms are treated as non-polar. The algorithm sums up atomic contributions and subtracts buried surfaces where two atomic spheres intersect making a bond. Parameters for the following elements are available: H, C, N, O, S, F and Cl. If any other element occurs in the molecule, the value will be missing.

3. Calculating ACDlogD7.4 with pKa correction

Method: the values of ACDLogD7.4 with pKa correction were calculated using the ACD software, version 12 (www.acdlabs.com) with utilization of in house pKa data (AstraZeneca) as a pKa correction library.

4. Calculating AZlogD7.4

Method: the values of AZlogD7.4 were obtained from AstraZeneca's Auto-QSAR method.[41]

5. LogD determination

Method: measurement of $LogD_{O/W}$ is based on the traditional shake flask technique, but with the modification of measuring compounds in mixtures of ten at a time using UPLC with quantitative mass spectrometry (MS) as a method to measure the relative octanol and aqueous concentrations. Two quality control (QC) samples (Cyclobenzaprine with moderate LogD, and Nicardipine with high LogD) are used in all pools to ensure good quality. Caffeine, with low LogD, is used as an additional QC sample and is randomly placed in all runs. The method has been thoroughly validated against the previous shake flask methodologies. The range of LogD values that can be determined by this method is dependent on the solubility of the compound in octanol and buffer, as well as the MS response of the individual compounds, and varies typically between approximately 0 to 4.

Equipment:

Robot, samples: Hamilton Star
Robot, optimization: BRAVO Velocity11, Biomek FX
Mass spectrometer: Waters Micromass TQS with MassLynx 4.1
LC-system: Waters Acquity Ultra Performance LC
Column: Acquity UPLC HSS T3 1.8 µm, 2.1·50 mm or Acquity UPLC BEH C18 1.7 µm, 2.1·50 mm
Vortexer: IKA-VIBRAX-VXR
Shaker: Edmund Bühler SM25
Centrifuge: Eppendorf Centrifuge 5810 R
Plates: 2 ml U96 deep well plate PP (Nunc Cat No 278752)
1.3 ml U96 deep well plate PP (Nunc Cat No 260252)
Nunc microtiter plate 96-well V-bottom PP (Nunc Cat No 249944).

Phosphate buffer:
$Na_2HPO_4x2H_2O$ (p.a grade) and $NaH_2PO_4xH_2O$ (p.a grade) purchased from Merck or other vendor. A stock solution of 100 mM (pH approximately 7.2) is prepared by dissolving 12.731 g $Na_2HPO_4x2H_2O$ and 3.929 g $NaH_2PO_4xH_2O$ in 1 L of water. This stock solution can be stored in room temperature for at least one year.

The stock solution is diluted ten times and pH adjusted to 7.4. Thereafter, equal parts of buffer and 1-octanol are vigorously mixed in a separation funnel three times (at least 15 minutes between each mixing) to saturate the solutions. The mixture is left overnight to separate the upper octanol phase from the lower buffer phase before being used in experiments.

All the physicochemical properties are summarized in **Table S2** and **S3**. Their correlations with affinities and KRI values are summarized in **Figure S1** and **S2**.

Table S2. Physicochemical parameters of "left arm" (R^1) compounds.

Code	R^1	Calculated PSA ($Å^2$)	ACDlogD7.4 with pKa correction	AZ logD7.4	LogD
8a	$-CH_2CH_2CF_3$	56.91	5.482	4.4	5.40
8b	$-CH_2CH_2CH_2F$	56.91	5.347	3.96	5.30
9	$-CH_2Ph$	56.91	6.073	4.6	> 5.30
11a	$-CH_2CH_2CH_2CF_3$	56.91	5.876	4.83	> 5.50
11b	$-SO_2CH_2CH_2CH_3$	94.14	5.053	3.64	4.60
11c	$-SO_2CH_2CH_2CH_2F$	94.14	4.704	3.46	4.15

11d	$-SO_2CH_2CH_2CF_3$	94.14	5.039	4.07	4.90
11e	$-SO_2CH_2CH_2CH_2CH_3$	94.14	5.563	3.97	5.10
11f	$-SO_2CH_2CH_2CH_2CF_3$	94.14	5.333	4.15	5.30
11g	$-SO_2CH_2CH_2CH(CH_3)_2$	94.14	5.916	4.29	5.30
11h	$-SO_2CH_2CH_2C(CH_3)_3$	94.14	6.327	4.56	> 5.80

Table S3. Physicochemical parameters of "right arm" (R^2) compounds.

Code	R^2	Calculated PSA (Å²)	ACDlogD7.4 with pKa correction	AZ logD7.4	LogD
11d	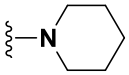	94.14	5.039	4.07	4.90
14a (±)	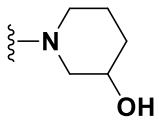	116.7	3.844	3.42	3.80
14b (±) *trans*	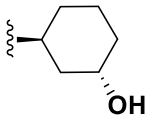	112.2	4.303	4.64	4.60
14c (-) *trans*	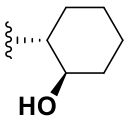	112.2	4.557	4.74	> 4.40
14d (+) *cis*	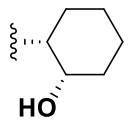	112.2	4.557	4.74	> 4.30
19 *cis : trans* (0.3:1)	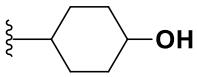	112.2	4.395	4.38	4.20
22 (±) *cis*	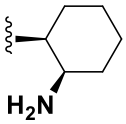	117.7	2.416	3.67	3.35
25 (±)*cis*	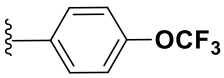	90.87	3.001	4.23	3.80
14e	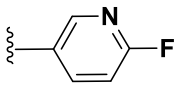	98.49	6.51	6.04	> 4.00

14f	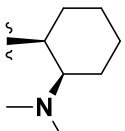	99.63	3.33	4.78	> 4.30
14g	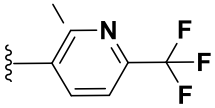	99.63	3.745	5.45	> 4.90
14h	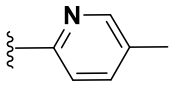	99.63	4.914	5.37	5.80
28	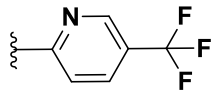	99.63	4.256	5.52	> 5.00

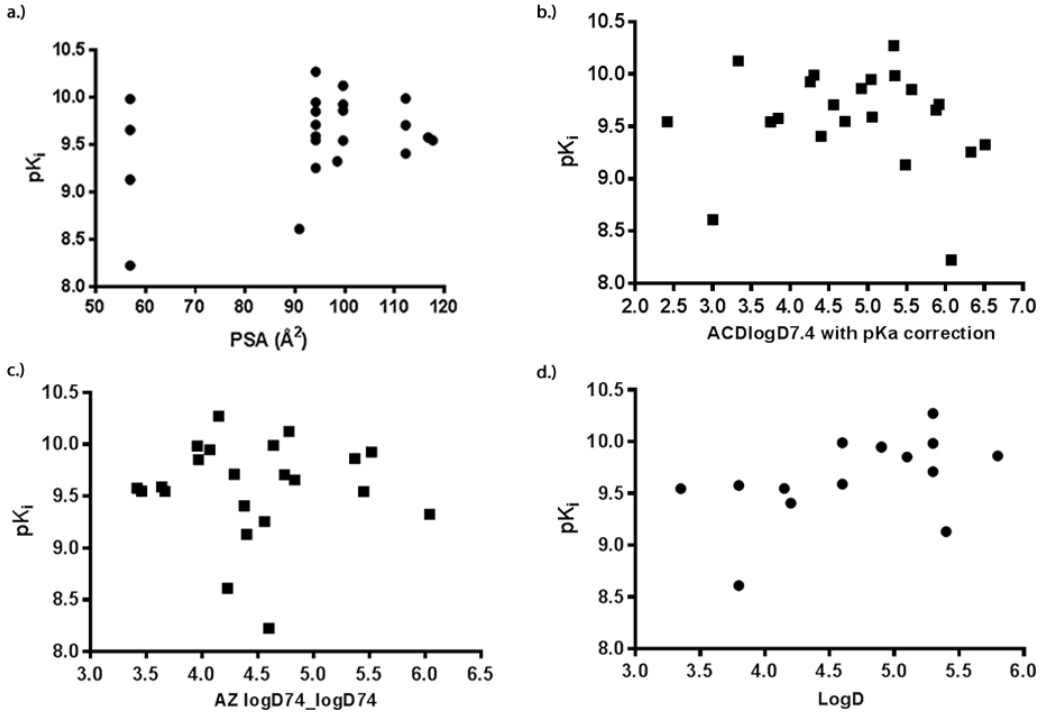

Figure S1: Absence of correlation between physicochemical parameters and affinities **a)** The calculated PSA values (X-axis) had no obvious linear correlation with the negative logarithm of affinity values (pK_i, Y-axis) of the hCB_1 receptor antagonists (r^2 = 0.14, *P* = 0.068); **b)** The calculated LogD values (X-axis, ACDlogD7.4 with pKa correction) had no obvious linear correlation with the negative logarithm of affinity values (pK_i, Y-axis) of the hCB_1 receptor antagonists (r^2 = 0.012, *P* = 0.62); **c)** The calculated LogD values (X-axis, AZ logD74) had no obvious linear correlation with the negative logarithm of affinity values (pK_i, Y-axis) of the CB_1 receptor antagonists (r^2 = 8.2e-006; *P* = 0.99); **d)** The experimentally determined LogD values (X-axis, LogD) had no obvious linear correlation with the negative logarithm of affinity values (pK_i, Y-axis) of the hCB_1 receptor antagonists (r^2 = 0.24, *P* = 0.065).

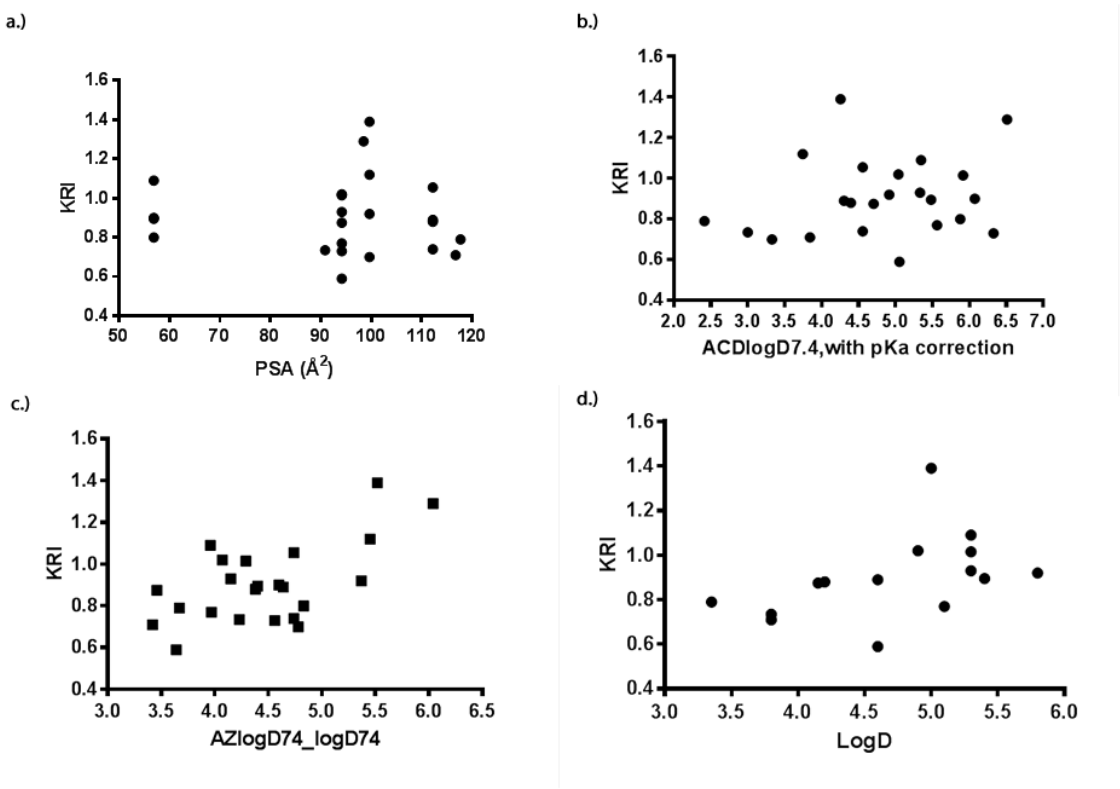

Figure S2: Absence of correlation between physicochemical parameters and KRI values **a)** The calculated PSA values (X-axis) had no obvious linear correlation with the KRI values (Y-axis) of the hCB_1 receptor antagonists (r^2 = 0.0044, *P* = 0.76); **b)** The calculated LogD values (X-axis, ACDlogD7.4 with pKa correction) had no obvious linear correlation with the KRI values (Y-axis) of the hCB_1 receptor antagonists (r^2 = 0.045, *P* = 0.32); **c)** The calculated LogD values (X-axis, AZ logD74) had no obvious linear correlation with the KRI values (Y-axis) of the hCB_1 receptor antagonists (r^2 = 0.38; *P* = 0.0029); **d)** The experimentally determined LogD values (X-axis,LogD) had no obvious linear correlation with the KRI values (Y-axis) of the hCB_1 receptor antagonists (r^2 = 0.22, *P* = 0.070).

References

1. Ryberg, E.; Larsson, N.; Sjögren, S.; Hjorth, S.; Hermansson, N. O.; Leonova, J.; Elebring, T.; Nilsson, K.; Drmota, T.; Greasley, P. J. The orphan receptor GPR55 is a novel cannabinoid receptor. *Br. J. Pharmacol.* **2007,** *152*, 1092-1101.
2. Labute, P. A widely applicable set of descriptors. *J. Mol. Graphics Modell.* **2000,** *18*, 464-477.
3. Davis, A. M.; Wood, D. J. Quantitative structure–activity relationship models that stand the test of time. *Mol. Pharmaceutics* **2013,** *10*, 1183-1190.

Chapter 3

Kinetics of human Cannabinoid 1 (CB_1) receptor antagonists: structure-kinetics relationships (SKRs) and implications for insurmountable antagonism

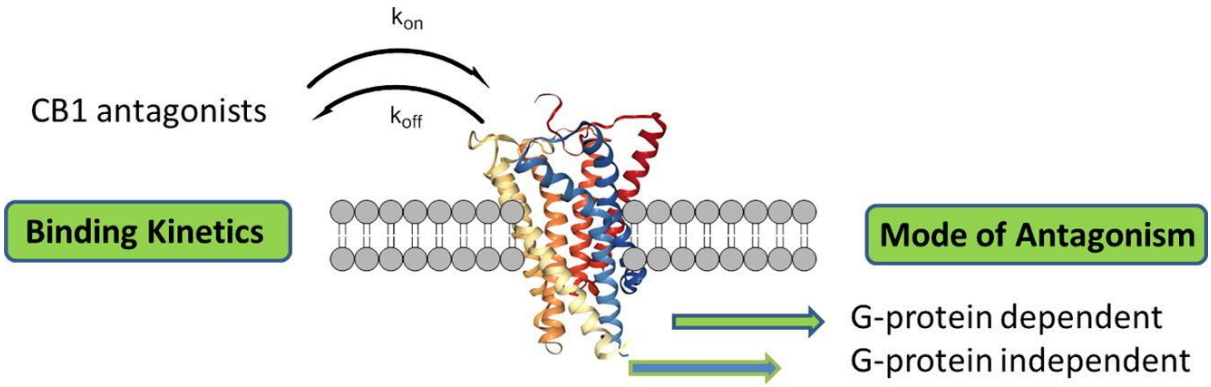

Binding kinetics of CB1 antagonists defines their mode of functional antagonism

Lizi Xia, Henk de Vries, Xue Yang, Eelke B. Lenselink, Athina Kyrizaki, Francis Barth, Julien Louvel, Matthias K. Dreyer, Daan van der Es, Adriaan P. IJzerman, Laura H. Heitman

Adapted from: *Biochem. Pharmacol.* **2017** doi: 10.1016/j.bcp.2017.10.014. [Epub ahead of print]

About this chapter

While equilibrium binding affinities and *in vitro* functional antagonism of human CB_1 receptor antagonists have been studied in detail, little is known on the kinetics of their receptor interaction. In this study, we therefore conducted kinetic assays for nine 1-(4,5-diarylthiophene-2-carbonyl)-4-phenylpiperidine-4-carboxamide derivatives and included the CB_1 antagonist rimonabant as a comparison. For this we newly developed a dual-point competition association assay with [^{3}H]CP55940 as the radioligand. This assay yielded Kinetic Rate Index (KRI) values from which structure-kinetics relationships (SKR) of hCB_1 receptor antagonists could be established. The fast dissociating antagonist **6** had a similar receptor residence time (RT) as rimonabant, i.e. 19 and 14 min, respectively, while the slowest dissociating antagonist (**9**) had a very long RT of 2222 min, i.e. pseudo-irreversible dissociation kinetics. In functional assays, **9** displayed insurmountable antagonism, while the effects of the shortest RT antagonist **6** and rimonabant were surmountable. Taken together, this study shows that hCB_1 receptor antagonists can have very divergent RTs, which are not correlated to their equilibrium affinities. Furthermore, their RTs appear to define their mode of functional antagonism, i.e. surmountable vs. insurmountable. Finally, based on the recently resolved hCB_1 receptor crystal structure, we propose that the differences in RT can be explained by a different binding mode of antagonist **9** from short RT antagonists that is able to displace unfavorable water molecules. Taken together, these findings are of importance for future design and evaluation of potent and safe hCB_1 receptor antagonists.

Introduction

The human cannabinoid 1 (hCB_1) receptor is categorized as a "lipid G protein-coupled receptor (GPCR)" due to its hydrophobic endogenous ligands, such as anandamide (AEA) and 2-arachidonoylglycerol (2-AG), which are crucial components of the endocannabinoid system (ECS).[1, 2] The CB_1 receptor belongs to the class A GPCR family, and has been shown to signal through inhibitory $G_{\alpha i/o}$ heterotrimeric G proteins,[3] and to interact with β-arrestin.[4] Nowadays, it is widely acknowledged that the hCB_1 receptor is not only present in the central nervous system (CNS), but also widely distributed in the peripheral nervous system (PNS) and peripheral tissues,[5] including the heart, lung, liver, gastrointestinal tract, pancreas and adipose tissue.[6, 7] The ECS, including the hCB_1 receptor, has been shown to be overactive in metabolic disorders where increased endocannabinoid levels are found in plasma, in central and peripheral tissues.[8] Therefore, blockade of the hCB_1 receptor is seen as a potential approach for the treatment of metabolic disorders such as obese dyslipidemia, liver disease and diabetes.[9]

Rimonabant, as an anti-obesity drug, was the first hCB_1 receptor antagonist to reach the market in Europe, but was withdrawn in 2008 by the manufacturer because of the risk of serious psychiatric adverse effects, such as depression.[10-13] As a result, many research programs in this field were terminated. Afterwards, the development of peripherally-restricted hCB_1 antagonists gained attention, as they may not have CNS-related side-effects. The general strategy was to introduce more polar or even ionic functional groups to a ligand's scaffold. However, some recent clinical and pre-clinical reports on this type of compounds either show no antiobesity effect at all [14] or no improved effect in comparison to rimonabant.[14-17]

Most recently, the concept of drug target binding kinetics is receiving increased attention. In particular the receptor-ligand residence time (RT) is emerging as an additional parameter to assess the therapeutic potential of drug candidates with respect to drug efficacy and safety.[18-20] The strategic combination of structure-kinetic relationship (SKR) with classic structure-affinity

relationship (SAR) analyses results in a better understanding of a ligand-receptor interaction, as together this not only comprises the equilibrium state of a ligand-receptor interaction but also its metastable intermediates and/or transition states. Recently, a number of structure-kinetic relationship (SKR) studies have been published in the field of GPCR.[21-24] These suggest that including binding kinetic data when triaging compounds can change, and hopefully improve, the resulting decision process as a compound's target affinity and residence time are not always correlated.

In the current study, a series of 9 previously reported peripherally-selective 1-(4,5-diarylthiophene-2-carbonyl)-4-phenylpiperidine-4-carboxamide derivatives were selected for a structure-kinetics relationships (SKR) study, next to structure-affinity relationships (SAR). These compounds arose from so-called scaffold hopping, where the pyrazole ring of rimonabant was replaced by a five-membered thiophene ring.[25, 26] In addition, some polar substituents were introduced on the thiophene and phenyl rings, as well as a carboxamide moiety; all to increase the ligands' polar surface area, and thus to reduce brain penetration (**Table 1**). Together with rimonabant as a reference, they were evaluated in equilibrium and kinetic radioligand binding assays yielding affinity values and kinetic binding parameters, which resulted in traditional SAR and novel SKR, respectively. All compounds had high affinities, but possessed diverse kinetic profiles at the hCB_1 receptor. This "kinetic screening campaign" led to the identification of a very long (**9,** 2222 min) and short RT hCB_1 receptor antagonist (**6,** 19 min), while rimonabant was determined to have a RT of 14 min. Subsequently, we applied two other radioligand binding experiments (i.e. "two-step incubation" and "wash-out" equilibrium displacement experiments) to characterize the pseudo-irreversible binding kinetics of antagonist **9**, compared to the reversible binding kinetics of antagonist **6** and rimonabant. With such large differences in RT (~185 fold), we decided to further investigate their concomitant functional effects in both G protein-dependent and -independent (i.e. β-arrestin recruitment) signaling. Their putative binding mode was analyzed using the recently resolved crystal structures of the hCB_1 receptor,[27] shedding light on key structural features of the receptor binding site that are involved in dissociation or pseudo-irreversible binding. In summary, we provide evidence that, next to affinity,

additional knowledge of a compound's binding kinetics is useful for selecting and developing new and, potentially, improved hCB_1 receptor antagonists in the early phases of drug discovery.

Method

Chemicals and reagents. The syntheses of antagonists **1**-**9** have been described previously.[25, 26] All compounds were fully characterized by HPLC and ^{1}H NMR. For compounds **1**, **2**, **3**, **4**, **8** and **9**, purity was analyzed by a Symmetry C18 column (50 x 2.1 mm ; 3.5 µm), with a 15 minute gradient of acetonitrile/water (0 % -> 90 % CH_3CN). For compound **5**, purity was analyzed by an XTerra MS C18 column (50 x 2.1 mm ; 3.5 µm), with a 15 minute gradient of acetonitrile/10mM ammonium acetate with 3% CH_3CN (0 % -> 90 % CH_3CN). For compound **6** and **7**, purity was analyzed by an Acquity BEH C18 column (50 x 2.1 mm ; 1.7 µm), with a 3 minute gradient of acetonitrile/water with 3% CH_3CN (1 % -> 95 % CH_3CN). All antagonists were found to have a purity of 95% or higher. The compound characterization details for the nine antagonists are shown below.

*1-[[5-(2,4-Dichlorophenyl)-4-[4-(2-hydroxyethoxy)phenyl]-2-thienyl]carbonyl]-4-phenyl-4-piperidinecarboxamide (**1**).* ^{1}H NMR (600 MHz, DMSO-d_6) δ 7.72 (s, 1H), 7.59 (s, 1H), 7.48 (s, 2H), 7.43 (d, J = 7.6 Hz, 2H), 7.35 (t, J = 7.7 Hz, 2H), 7.28 – 7.22 (m, 2H), 7.14 – 7.08 (m, 3H), 6.85 (d, J = 8.8 Hz, 2H), 4.83 (t, J = 5.5 Hz, 1H), 4.15 (d, J = 12.5 Hz, 2H), 3.94 (t, J = 4.9 Hz, 2H), 3.68 (q, J = 5.2 Hz, 2H), 2.54 (d, J = 8.7 Hz, 2H), 1.89 (t, J = 10.7 Hz, 2H). Purity: 99%. Retention Time: 9.26 min.

*1-[[4-[4-[(2-Aminoethyl)thio]phenyl]-5-(2,4-dichlorophenyl)-2-thienyl]carbonyl]-4-phenyl-4-piperidinecarboxamide (**2**).* ^{1}H NMR (600 MHz, DMSO-d_6) δ 7.88 (bs, 3H), 7.75 (d, J = 1.8 Hz, 1H), 7.64 (s, 1H), 7.54 – 7.48 (m, 2H), 7.42 (d, J = 7.4 Hz, 2H), 7.36 (t, J = 7.8 Hz, 2H), 7.30 (d, J = 8.5 Hz, 2H), 7.25 (t, J = 7.3 Hz, 2H), 7.19 (d, J = 8.4 Hz, 2H), 7.11 (s, 1H), 4.15 (d, J = 11.2 Hz, 2H), 3.17 (t, J = 7.3 Hz, 2H), 2.95 (t, J = 7.3 Hz, 2H), 2.55 (d, J = 14.1 Hz, 2H), 1.96 – 1.83 (m, 2H). Purity: 99 %. Retention Time: 7.34 min.

*1-[[5-(2,4-Dichlorophenyl)-4-[4-[[2-[(methylsulfonyl)amino]ethyl]thio]phenyl]-2-thienyl]carbonyl]-4-phenyl-4-piperidinecarboxamide (**3**).* ^{1}H NMR (600 MHz, DMSO-d_6) δ 7.74 (d, *J* = 1.3 Hz, 1H), 7.65 (s, 1H), 7.54 – 7.47 (m, 2H), 7.43 (d, *J* = 7.4 Hz, 2H), 7.35 (t, *J* = 7.8 Hz, 2H), 7.27 (s, 1H), 7.25 (d, *J* = 4.5 Hz, 4H), 7.16 (d, *J* = 8.5 Hz, 2H), 7.10 (s, 1H), 4.16 (d, *J* = 12.6 Hz, 2H), 3.15 – 3.10 (m, 2H), 3.10 – 3.03 (m, 2H), 2.89 (s, 3H), 2.55 (d, *J* = 13.5 Hz, 2H), 1.89 (t, *J* = 10.6 Hz, 2H). Purity: 100 %. Retention Time: 9.79 min.

*1-[[5-(2,4-Dichlorophenyl)-4-[4-[3-(methylsulfonyl)propoxy]phenyl]-2-thienyl]carbonyl]-4-phenyl-4-piperidinecarboxamide (**4**).* ^{1}H NMR (600 MHz, DMSO-d_6) δ 7.73 (s, 1H), 7.60 (s, 1H), 7.48 (d, *J* = 1.0 Hz, 2H), 7.42 (d, *J* = 7.4 Hz, 2H), 7.35 (t, *J* = 7.8 Hz, 2H), 7.28 – 7.22 (m, 2H), 7.13 (d, *J* = 8.8 Hz, 2H), 7.10 (s, 1H), 6.86 (d, *J* = 8.8 Hz, 2H), 4.16 (d, *J* = 14.0 Hz, 2H), 4.05 (t, *J* = 6.2 Hz, 2H), 3.26 – 3.22 (m, 2H), 3.00 (sz, 3H), 2.55 (d, *J* = 13.6 Hz, 2H), 2.16 – 2.07 (m, 2H), 1.89 (t, *J* = 11.2 Hz, 2H). Purity: 95 %. Retention Time: 9.64 min.

*1-[[5-(2,4-Dichlorophenyl)-4-[4-[(3-hydroxypropyl)thio]phenyl]-2-thienyl]carbonyl]-4-phenyl-4-piperidinecarboxamide (**5**).* ^{1}H NMR (600 MHz, DMSO-d_6) δ 7.73 (d, *J* = 0.9 Hz, 1H), 7.63 (s, 1H), 7.49 (d, *J* = 1.7 Hz, 2H), 7.42 (d, *J* = 7.4 Hz, 2H), 7.36 (t, *J* = 7.8 Hz, 2H), 7.25 (t, *J* = 7.2 Hz, 2H), 7.21 (d, *J* = 8.5 Hz, 2H), 7.14 (d, *J* = 8.5 Hz, 2H), 7.10 (s, 1H), 4.55 (t, *J* = 5.2 Hz, 1H), 4.15 (d, *J* = 13.4 Hz, 2H), 3.47 (q, *J* = 6.0 Hz, 2H), 2.98 (t, *J* = 7.3 Hz, 2H), 2.57 – 2.52 (m, 2H), 1.89 (t, *J* = 12.4 Hz, 2H), 1.69 (p, *J* = 6.6 Hz, 2H). Purity: 100 %. Retention Time: 9.28 min.

*1-[[5-(2,4-Dichlorophenyl)-4-[4-[(3-hydroxypropyl)sulfonyl]phenyl]-2-thienyl]carbonyl]-4-phenyl-4-piperidinecarboxamide (**6**).* ^{1}H NMR (600 MHz, DMSO-d_6) δ 7.81 (d, *J* = 8.4 Hz, 2H), 7.76 – 7.73 (m, 2H), 7.55 (d, *J* = 8.3 Hz, 1H), 7.52 (dd, *J* = 8.3, 2.0 Hz, 1H), 7.48 (d, *J* = 8.5 Hz, 2H), 7.43 (d, *J* = 7.5 Hz, 2H), 7.36 (t, *J* = 7.8 Hz, 2H), 7.25 (t, *J* = 7.2 Hz, 2H), 7.10 (s, 1H), 4.63 (t, *J* = 5.3 Hz, 1H), 4.17 (d, *J* = 13.3 Hz, 2H), 3.40 (q, *J* = 6.0 Hz, 2H), 3.30 – 3.24 (m, 2H), 2.54 (d, *J* = 14.2 Hz, 2H), 1.90 (t, *J* = 12.3 Hz, 2H), 1.70 – 1.60 (m, 2H). Purity: 100 %. Retention Time: 1.52 min.

*1-[[5-(2,4-Dichlorophenyl)-4-[4-[(4-hydroxybutyl)thio]phenyl]-2-thienyl]carbonyl]-4-phenyl-4-piperidinecarboxamide (**7**).* ^{1}H NMR (600 MHz, DMSO-d_6) δ 7.73 (d, J = 0.8 Hz, 1H), 7.64 (s, 1H), 7.52 – 7.47 (m, 2H), 7.43 (d, J = 7.5 Hz, 2H), 7.36 (t, J = 7.8 Hz, 2H), 7.26 (t, J = 7.2 Hz, 2H), 7.21 (d, J = 8.4 Hz, 2H), 7.14 (d, J = 8.4 Hz, 2H), 7.11 (s, 1H), 4.42 (t, J = 5.1 Hz, 1H), 4.16 (d, J = 13.3 Hz, 2H), 2.95 (t, J = 7.2 Hz, 2H), 2.54 (d, J = 15.6 Hz, 2H), 1.90 (t, J = 12.6 Hz, 2H), 1.63 – 1.56 (m, 2H), 1.55 – 1.49 (m, 2H). Purity: 100 %. Retention Time: 1.79 min.

*4-[5-[(4-Carbamoyl-4-phenylpiperidin-1-yl)carbonyl]-2-(2,4-dichlorophenyl)thien-3-yl]phenyl propane-1-sulfonate (**8**).* ^{1}H NMR (600 MHz, DMSO-d_6) δ 7.74 (d, J = 2.0 Hz, 1H), 7.68 (s, 1H), 7.51 (dt, J = 8.3, 5.2 Hz, 2H), 7.43 (d, J = 7.4 Hz, 2H), 7.36 (t, J = 7.8 Hz, 2H), 7.33 – 7.29 (m, 2H), 7.29 – 7.23 (m, 4H), 7.11 (s, 1H), 4.16 (d, J = 13.3 Hz, 2H), 3.56 – 3.46 (m, 2H), 2.54 (d, J = 14.0 Hz, 2H), 1.90 (t, J = 12.2 Hz, 2H), 1.86 – 1.78 (m, 2H), 1.02 (t, J = 7.4 Hz, 3H). Purity: 98 %. Retention Time: 10.62 min.

*1-[[5-(2,4-Dichlorophenyl)-4-[4-[3-(methylthio)propoxy]phenyl]-2-thienyl]carbonyl]-4-phenyl-4-piperidinecarboxamide (**9**).* ^{1}H NMR (600 MHz, DMSO-d_6) δ 7.72 (s, 1H), 7.59 (s, 1H), 7.48 (d, J = 1.0 Hz, 2H), 7.43 (d, J = 7.4 Hz, 2H), 7.36 (t, J = 7.8 Hz, 2H), 7.25 (t, J = 7.2 Hz, 2H), 7.17 – 7.07 (m, 3H), 6.85 (d, J = 8.8 Hz, 2H), 4.15 (d, J = 12.2 Hz, 2H), 4.01 (t, J = 6.1 Hz, 2H), 2.59 (t, J = 7.2 Hz, 2H), 2.54 (d, J = 13.1 Hz, 2H), 2.05 (s, 3H), 1.97 – 1.91 (m, 2H), 1.91 – 1.83 (m, 2H). Purity: 98 %. Retention Time: 11.43 min.

[^{3}H]CP55940 (specific activity 141.2 Ci/mmol) and [^{35}S]GTPγS (specific activity 1250 Ci/mmol) were purchased from Perkin Elmer (Waltham, MA). Bicinchoninic acid (BCA) and BCA protein assay reagent was obtained from Pierce Chemical Company (Rochford, IL). Rimonabant (SR141716A) was from Cayman Chemical Company (Ann Arbor, MI). CHOK1hCB1_bgal and CHOK1hCB2_bgal cells (catalog number 93-0959C2 and 93-0706C2) and the Pathhunter® detection kit (catalog number 93-0001M) were obtained from DiscoveRx (Fremont, CA). All other chemicals were of analytical grade and obtained from standard commercial sources.

Cell culture and membrane preparation. CHOK1hCB1_bgal cells and CHOK1hCB2_bgal cells were cultured in Ham's F12 Nutrient Mixture supplemented with 10% fetal calf serum (FCS), 1 mM glutamine, 50 μg/ml penicillin, 50 μg/ml streptomycin, 300 mg/ml hygromycin and 800 μg/ml geneticin in a humidified atmosphere at 37°C and 5% CO_2. Cells were subcultured twice a week at a ratio of 1:10 on 10-cm ø plates by trypsinization. For membrane preparation the cells were subcultured 1:10 and transferred to large 15 cm ø plates. Membrane fractions were prepared as described before.[28]

Radioligand equilibrium displacement assays. Membrane aliquots containing 5 μg (CHOK1hCB1_bgal) or 1.5 μg (CHOK1hCB2_bgal) protein were incubated in a total volume of 100 μL assay buffer (50 mM Tris–HCl, 5 mM $MgCl_2$, 0.1% BSA, pH 7.4) at 30°C for 60 min. Displacement experiments were performed using 6 concentrations of competing antagonist in the presence of a final concentration of ~3 nM [^{3}H]CP55940 (CHOK1hCB1_bgal) or ~1.5 nM [^{3}H]CP55940 (CHOK1hCB2_bgal). At this concentration, total radioligand binding did not exceed 10% of that added to prevent ligand depletion. Nonspecific binding (NSB) was determined in the presence of 10 μM rimonabant (CHOK1hCB1_bgal) or 10 μM AM630 (CHOK1hCB2_bgal). For the "two-step incubation" assays, antagonists were first pre-incubated with membrane aliquots at 30 °C for 3 h, then ~3 nM of [^{3}H]CP55940 was added and coincubated for a further 60 min. For all experiments, incubation was terminated by rapid filtration performed on 96-well GF/C filter plates (Perkin Elmer, Groningen, the Netherlands), presoaked for 30 min with 0.25% PEI (PolyethyleneImine), using a PerkinElmer Filtermate-harvester (Perkin Elmer, Groningen, the Netherlands). After drying the filter plate at 50 °C for 30 min, the filter-bound radioactivity was determined by scintillation spectrometry using the 2450 MicroBeta^2 Plate Counter (Perkin Elmer, Boston, MA).

"Wash-out" assays. For washout experiments, 100 μl assay buffer containing either 1% DMSO (as blank control for total binding and non-specific binding) or antagonist (**9**, **6** or rimonabant, final concentration 1 μM stock in assay buffer) was added to 1.5-ml Eppendorf tubes containing 20 μg of

CHOK1hCB1_bgal protein. This mixture was brought to a total volume of 300 µL assay buffer, which was then incubated at 30 °C for 1 h. Subsequently, the mixture was centrifuged at 13,000 revolutions per minute (RPM) at 4 °C for 5 min to allow the removal of the supernatant containing unbound ligand. Then the membrane pellet was resuspended in 1 ml assay buffer by vortexing and spun at 13,000 RPM at 4 °C for 10 min. After three washing cycles, the membrane pellets were resuspended in 300 µl assay buffer and placed on ice. Subsequently, 100 µl [^{3}H] CP55940 (~3 nM) was added, followed by another incubation at 30 °C for 60 min. Incubation was terminated by rapid filtration performed on GF/C filters (Whatman International, Maidstone, UK), presoaked for 30 min with 0.25% PEI, using a Brandel harvester (Brandel, Gaithersburg, MD). Filter-bound radioactivity was determined by scintillation spectrometry using a Tri-Carb 2900 TR liquid scintillation counter (Perkin Elmer, Boston, MA).

Radioligand association and dissociation assays. Association experiments were performed by incubating membrane aliquots containing 5 µg of CHOK1hCB1_bgal membrane in a total volume of 100 µL of assay buffer at 30 °C with ~3 nM [^{3}H]CP55940. The amount of radioligand bound to the receptor was measured at different time intervals during a total incubation of 120 min. Dissociation experiments were performed by preincubating membrane aliquots containing 5 µg of protein in a total volume of 100 µL of assay buffer for 60 min. After the preincubation, radioligand dissociation was initiated by the addition of 5 µl 10 µM unlabeled rimonabant. The amount of radioligand still bound to the receptor was measured at various time intervals for a total of 240 min to ensure that full dissociation from hCB_1 receptor was reached. Incubations were terminated and samples were obtained as described under *Radioligand equilibrium displacement assays.*

Radioligand competition association assays. The binding kinetics of unlabeled ligands were quantified using the competition association assay based on the theoretical framework by Motulsky and Mahan.[29] The competition association assay was initiated by adding membrane aliquots (5 µg/well) at different time points for a total of 240 min to a total volume of 100 µl of assay buffer at

30 °C with ~3 nM [^{3}H]CP55940 in the absence or presence of a single concentration of competing hCB_1 receptor antagonists (1 to 3-fold IC_{50}). Incubations were terminated and samples were obtained as described under *Radioligand equilibrium displacement assays.* The "dual-point" competition association assays were designed as described previously,[30] where in this case the two time points were selected at 30 (t_1) and 240 min (t_2).

*[^{35}S]GTPγS binding assays for selected long and short RT antagonists (**9, 6,** rimonabant).* The assays were performed by incubating 5 µg of homogenized CHOK1CB1_bgal membranes in a total volume of 80 µl assay buffer (50 mM Tris-HCl buffer, 5 mM $MgCl_2$, 150 mM NaCl, 1 mM EDTA, 0.05% BSA and 1 mM DTT, pH 7.4) supplemented with 1 µM GDP and 5 µg saponin. The assays were performed in a 96-well plate format, where DMSO stock solutions of the compounds were added using a HP D300 Digital Dispenser (Tecan, Männedorf, Switserland). The final concentration of organic solvent per assay point was ≤0.1%. In all cases, the basal level of [^{35}S]GTPγS binding was measured in untreated membrane samples, whereas the maximal level of [^{35}S]GTPγS binding was measured by treatment of the membranes with 1 µM CP55940, unless stated otherwise. To determine the IC_{50} values (inverse agonism) of hCB_1 receptor antagonists, as well as EC_{50} values of CP55940 (a reference CB_1 receptor agonist), the membranes were incubated with increasing concentrations of ligand for 90 minutes at 30°C. To determine the IC_{50} (antagonism) values of hCB_1 receptor antagonists, membrane preparations were pre-incubated for 30 min at 30 °C with a range of concentrations of the antagonists prior to the addition of an EC_{80} concentration of CP55940 (3.8 nM) and 20 µL [^{35}S]GTPγS (final concentration ~0.3 nM) after which incubation continued for another 90 min at 30 °C. For the insurmountability experiments, membrane preparations were pre-incubated with or without antagonists (10-, 30-, 100-fold K_i values) for 60 min at 30 °C, prior to the addition of CP55940 (1 µM to 0.1 nM) and 20 µl [^{35}S]GTPγS (final concentration ~0.3 nM), after which incubation continued for another 30 min at 30 °C. For the surmountability (control) experiments, antagonists and CP55940 were co-incubated with [^{35}S]GTPγS for 30 min at 30 °C. For all experiments, incubations were

terminated and samples were obtained as described under *Radioligand equilibrium displacement assays,* by using GF/B filters (Whatman International, Maidstone, UK).

PathHunter® β*-arrestin recruitment assays for selected long and short RT antagonists (**9, 6,** rimonabant).* The PathHunter® protein complementation assay (Fremont, CA, USA) was performed according to the manufacturer's protocol.[31] CHOK1hCB1_bgal cells were seeded at a density of 5,000 cells per well of solid black-walled 384-well plates (Catalogue number 3712, Corning, NY, USA) in 20 µl cell culture medium and incubated overnight in a humidified atmosphere at 37 °C and 5% CO_2. DMSO stock solutions of the compounds were added using a HP D300 Digital Dispenser (Tecan, Männedorf, Switzerland). The final concentration of organic solvent per assay point was ≤0.1 %. The basal level of β-arrestin recruitment was measured in untreated cells, and the maximal level of β-arrestin recruitment was measured by treatment of cells with 1 µM CP55940, unless stated otherwise. To determine the IC_{50} values (inverse agonism) of hCB_1 receptor antagonists, as well as EC_{50} values of CP55940, the cells were stimulated with increasing concentrations of ligand and incubated for 90 min (standard duration) or 6 h (extended duration) in a humidified atmosphere at 37 °C and 5 % CO_2. To determine the IC_{50} (inhibition) values of hCB_1 receptor antagonists, the cells were exposed to increasing concentrations of each antagonist and preincubated for 30 min under the same condition, followed by the addition of an EC_{80} concentration of CP55940 (39 nM), after which the cells were incubated for 90 min in a humidified atmosphere at 37 °C and 5% CO_2. For the insurmountability assays, the cells were pre-incubated with or without antagonists (10-, 30-, 100-fold K_i values on the hCB_1 receptor) for 60 min, after that CP55940 (1 µM to 0.1 nM) was added and incubated for another 30 min. For the surmountability (control) experiments, antagonists and CP55940 were co-incubated for 30 min at 37 °C and 5% CO_2. For all the experiments, β-galactosidase enzyme activity was determined by using the PathHunter® detection mixture, according to the kit's protocol.[31] Detection mixture (12 µL per well) was added and the plate was incubated for 60 min in the dark at room temperature. Chemiluminescence, indicated as relative light units (RLU), was measured on an EnVision multilabel plate reader (Perkin Elmer, MA, USA).

*Computational studies on selected long and short RT antagonists (**9, 6,** rimonabant).* The computational studies were based on the crystal structure of the hCB_1 receptor co-crystalized with AM6538 (PDB: 5TGZ) [27] and prepared with the protein preparation wizard.[32] Since the antagonists **9**, **6** and rimonabant were similar to the co-crystalized AM6538, induced fit docking [33] was used with core constraints on the 2,4-dichlorophenyl ring of AM6538. To study to the potential differences in hydration between ligands, an apo (without ligand present) WaterMap was generated.[34, 35] Figures were rendered using PyMol,[36] for clarity the "cartoon" representation of residues 362 to 375 was hidden.

Data analysis. All experimental data were analyzed using the nonlinear regression curve fitting program GraphPad Prism 6.0 (GraphPad Software, Inc., San Diego, CA). From displacement assays, IC_{50} values were obtained by non-linear regression analysis of the displacement curves. The obtained IC_{50} values were converted into K_i values using the Cheng-Prusoff equation to determine the affinity of the ligands,[37] using a K_D value of 0.10 nM (CHOK1hCB1_bgal) and 0.33 nM (CHOK1hCB2_bgal).[38] The observed association rates (k_{obs}) derived from both assays were obtained by fitting association data using 'one phase exponential association'. The dissociation rate constants were obtained by fitting dissociation data to a 'one phase exponential decay' model. The k_{obs} values were converted into association rate constants (k_{on}) using the equation $k_{on} = (k_{obs} – k_{off})/[L]$, where [L] is the amount of radioligand used for the association experiments. The association and dissociation rate constants were used to calculate the kinetic K_D using the equation $K_D = k_{off}/k_{on}$. The residence time (RT, in min) was calculated using the equation $RT = 1/(60 * k_{off})$, as k_{off} is in s^{-1}. Association and dissociation rate constants for unlabeled compounds were calculated by fitting the data into the competition association model using "kinetics of competitive binding":[29]

$$K_A = k_1[L]\cdot 10^{-9} + k_2$$

$$K_B = k_3[I]\cdot 10^{-9} + k_4$$

$$S = \sqrt{(K_A - K_B)^2 + 4\cdot k_1 \cdot k_3 \cdot L \cdot I \cdot 10^{-18}}$$

$$K_F = 0.5(K_A + K_B + S)$$

$$K_S = 0.5(K_A + K_B - S)$$

$$Q = \frac{B_{\max} \cdot k_1 \cdot L \cdot 10^{-9}}{K_F - K_S}$$

$$Y = Q \cdot \left(\frac{k_4 \cdot (K_F - K_S)}{K_F \cdot K_S} + \frac{k_4 - K_F}{K_F} e^{(-K_F \cdot X)} - \frac{k_4 - K_S}{K_S} e^{(-K_S \cdot X)}\right)$$

where k_1 is the k_{on} of the radioligand ($M^{-1}s^{-1}$), k_2 is the k_{off} of the radioligand (s^{-1}), L is the radioligand concentration (nM), I is the concentration of the unlabeled competitor (nM), X is the time (s) and Y is the specific binding of the radioligand (DPM). The control curve (without competitor) from competition association assays generated the k_1 value, and the k_2 value was obtained in previous experiments (data not shown). With that the k_3, k_4 and B_{max} were calculated, where k_3 represents the k_{on} ($M^{-1}s^{-1}$) of the unlabeled ligand, k_4 stands for the k_{off} (s^{-1}) of the unlabeled ligand and B_{max} equals the total binding (DPM). All competition association data were globally fitted. [^{35}S]GTPγS binding and β-arrestin recruitment curves were analyzed by nonlinear regression using "log (agonist or inhibitor) vs response-variable slope" to obtain potency, inhibitory potency or efficacy values of agonists and inverse agonists (EC_{50}, IC_{50} or E_{max}, respectively). In the (in)surmountability assays, Gaddum/Schild EC_{50} shift equations were used to obtain Schild-slopes and *p*A_2 values; statistical analysis with two-way ANOVA with Tukey's post-test was applied. All values obtained are means of at least three independent experiments performed in duplicate, unless stated otherwise.

Results

Binding affinity (K_i) of hCB$_1$ receptor antagonists.

Table 1. Equilibrium binding affinity (K_i) and kinetic parameters (KRI, k_{on}, k_{off}, RT and K_D) for hCB_1 receptor antagonists

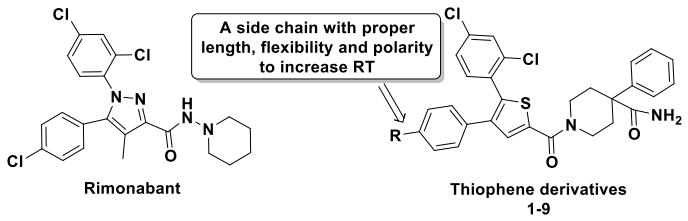

Antagonist	R	CB_1 binding						CB_2 binding
		pKi ± SEM (K_i in nM)[a]	KRI [b]	k_{on} [c] ($M^{-1}s^{-1}$)	k_{off} [d] (s^{-1})	RT [e] (min)	K_D [f] (nM)	pKi ± SEM (K_i in nM)[g]
Rimonabant	N.A.[h]	8.8 ± 0.1 (1.8)	0.65 ± 0.03	(2.3 ± 0.3) x 10^5	(1.4 ± 0.2) x 10^{-3}	14 ± 2.0	5.9 ± 0.3	N.D.[i]
1	$-OCH_2CH_2OH$	9.3 ± 0.1 (0.53)	0.81 ± 0.02	N.D.	N.D.	N.D.	N.D.	7.7 ± 0.1 (22)
2	$-SCH_2CH_2NH_2$	9.3 ± 0.04 (0.53)	1.30 ± 0.21	N.D.	N.D.	N.D.	N.D.	7.8 ± 0.5 (33)
3	$-SCH_2CH_2NHSO_2CH_3$	9.7 ± 0.03 (0.19)	1.39 (1.41; 1.36)	(1.5 ± 0.2) x 10^5	(3.0 ± 0.7) x 10^{-5}	556 ± 124	0.22 ± 0.07	8.8 ± 0.04 (1.6)
4	$-OCH_2CH_2CH_2SO_2CH_3$	9.3 ± 0.1 (0.50)	1.08 (1.10; 1.06)	N.D.	N.D.	N.D.	N.D.	7.3 ± 0.1 (58)
5	$-SCH_2CH_2CH_2OH$	9.6 ± 0.1 (0.28)	1.02 ± 0.31	N.D.	N.D.	N.D.	N.D.	8.2 ± 0.3 (9.7)
6	$-SO_2CH_2CH_2CH_2OH$	7.9 ± 0.01 (14)	0.70 ± 0.17	(5.2 ± 0.7) x 10^4	(8.8 ± 1.7) x 10^{-4}	19 ± 3.6	18 ± 3.1	7.2 ± 0.1 (74)
7	$-SCH_2CH_2CH_2CH_2OH$	9.6 ± 0.1 (0.24)	1.32 ± 0.15	(1.4 ± 0.2) x 10^5	(4.7 ± 0.7) x 10^{-5}	357 ± 51	0.34 ± 0.02	7.6 ± 0.1 (26)
8	$-OSO_2CH_2CH_2CH_3$	9.9 ± 0.03 (0.13)	1.51 ± 0.14	(2.0 ± 0.2) x 10^5	(3.8 ± 1.2) x 10^{-5}	435 ± 132	0.19 ±0.05	7.4 ± 0.02 (38)
9	$-OCH_2CH_2CH_2SCH_3$	8.9 ± 0.1 (1.4)	1.57 ± 0.39	(8.5 ± 0.8) x 10^4	(7.5 ± 3.0) x 10^{-6}	2222 ± 888	0.084 ± 0.026	7.3 ± 0.1 (54)

[a] pK_i ± SEM (n = 3), obtained from radioligand binding assays with [^{3}H] CP55940 on recombinant human CB_1 receptors stably expressed on CHO cell membranes.

[b] KRI ± SEM (n = 3) or KRI (n_1; n_2) (n = 2), obtained from dual-point competition association assays with [^{3}H] CP55940 on recombinant human CB_1 receptors stably expressed on CHO cell membranes.

[c] k_{on} ± SEM (n = 3), obtained from competition association assays with [^{3}H] CP55940 on recombinant human CB_1 receptors stably expressed on CHO cell membranes.

[d] k_{off} ± SEM (n = 3), obtained from competition association assays with [^{3}H] CP55940 on recombinant human CB_1 receptors stably expressed on CHO cell membranes.

[e] RT = 1/(60 * k_{off}); RT is expressed in min, whereas k_{off} is expressed in s-1.

[f] $K_D = k_{off}/k_{on}$.

[g] pK_i ± SEM (n = 3), obtained from radioligand binding assays with [^{3}H] CP55940 on recombinant human CB_2 receptors stably expressed on CHO cell membranes.

[h] N.A. not applicable.

[i] N.D. not determined.

The binding affinities of nine hCB_1 receptor antagonists were determined in equilibrium radioligand displacement studies. All antagonists were able to concentration-dependently inhibit specific [^{3}H]CP55940 binding to the human CB_1 receptor and their affinities are listed in **Table 1**. All antagonists had a high binding affinity, ranging from 0.13 nM for antagonist **8** to 14 nM for antagonist **6**, while the reference antagonist, rimonabant, had an affinity of 1.8 nM. Moreover, we determined the affinity of all nine compounds on the hCB_2 receptor. From **Table 1** it follows that they all had higher affinity for the hCB_1 receptor, where approximately 5-292-fold selectivity over hCB_2 receptors was observed.

Kinetic Rate Index (KRI) values of hCB_1 receptor antagonists.

Subsequently, these hCB_1 receptor antagonists were screened in the so-called "dual-point" competition association assay. The specific binding of [^{3}H]CP55940 was measured after 30 and 240 minutes in the absence and presence of a single concentration of unlabeled hCB_1 receptor antagonists, which yielded their Kinetic Rate Index (KRI). The KRI values of the hCB_1 receptor antagonists ranged from 0.65 to 1.57 (**Table 1**). Antagonists with a KRI value larger than 1.0 were considered to have a slower dissociation rate, and thus a longer RT, than the radioligand used, i.e.

[^{3}H]CP55940, and *vice versa.* Four antagonists (**3**, **7**, **8** and **9**) had KRI values ≥ 1.3, whereas two antagonists (**6** and rimonabant) had KRI values ≤ 0.7 (**Table 1**).

Structure−Affinity Relationships (SAR) and Structure−Kinetics Relationships (SKR) of hCB$_1$ receptor antagonists.

The obtained affinities (K_i values) and kinetic profiles (k_{on}, k_{off} values and RTs) permitted us to derive SAR and SKR for this series of antagonists. Different sidechains were examined as the R group (**Table 1**). On antagonist **1** the R_1 substituent was a 2-hydroxyethoxy, which resulted in a high affinity of 0.53 nM and a KRI-value of 0.81. When the side chain of antagonist **1** was replaced by a similar 2-mercaptoethylamine (**2**), its affinity was unchanged and its KRI value was substantially increased to 1.30. When the terminal amine of **2** was extended by methanesulfonyl ($-SO_2CH_3$) as in antagonist **3**, it yielded an approximately 3-fold increased affinity (0.53 nM vs 0.19 nM) and slightly higher KRI value (1.39). The slightly less polar side chain of antagonist **4** did not improve affinity in comparison to **2** but slightly reduced the KRI value (1.08). Next, a 3-mercapto-1-propanol side chain was introduced (**5**), which did not affect the affinity, but the compound's KRI value was close to unity (1.02). When the thio-ether of **5** was oxidized to sulfonyl (**6**), the affinity was decreased by 50-fold to 14 nM and the KRI value reduced to 0.70. When the propyl side chain of antagonist **5** was extended to a butyl (**7**), the affinity remained the same (0.28 nM vs. 0.24 nM), but its KRI value increased to 1.32. Lastly, antagonists **8** and **9** were obtained by slight variations of the linear side chains from antagonists **6** and **7**, respectively, which resulted in pronounced effects on both affinity and kinetics. From the 5-mercapto-1-pentanol side chain (**7**) to 3-(methylthio)propan-1-ol (**9**), the affinity dropped by approximately 6-fold (0.24 nM vs. 1.4 nM), while the KRI value increased from 1.32 to the highest of the series (1.57). From sulfonic 1-propanol (**6**) to alkyl sulfate (**8**), not only the affinity improved from 14 nM to 0.13 nM (107-fold), but also its KRI value increased from the lowest value of the series (0.70) to the second highest value (1.51, **Table 1**).

Binding kinetics of selected hCB$_1$ receptor antagonists using the competition association assay.

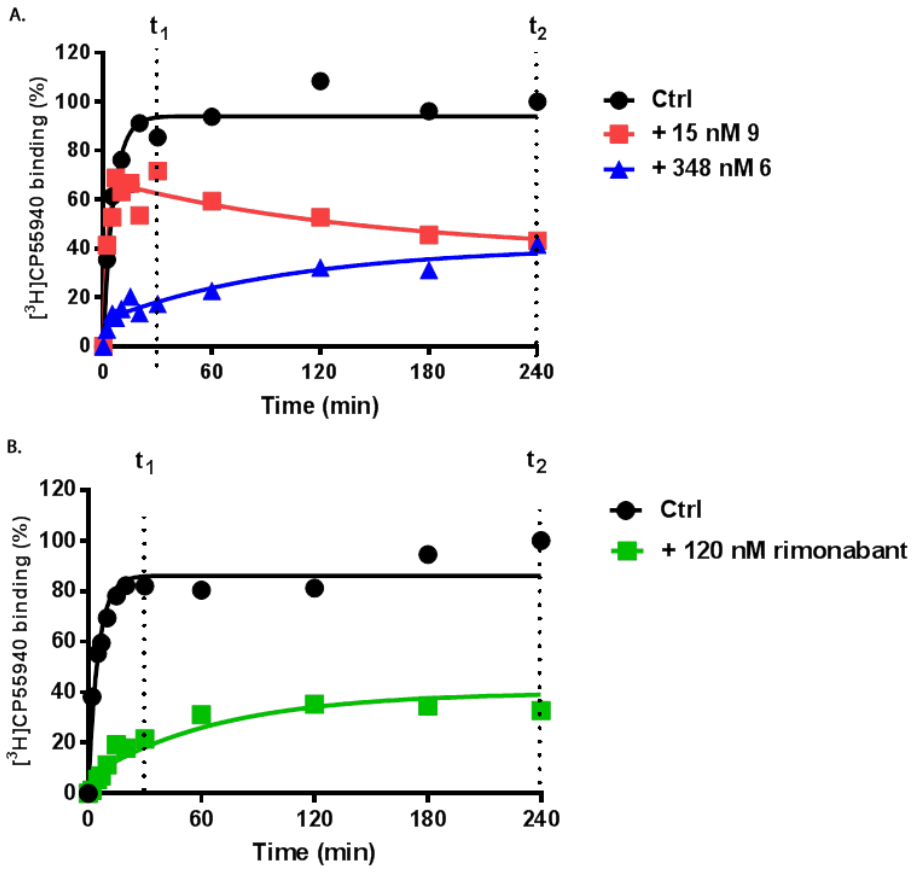

Figure 1. Competition association experiments with [^{3}H]CP55940 binding to recombinant hCB$_1$ receptors stably expressed on CHO cell membranes (30 °C) in the absence or presence of unlabeled long-residence-time antagonist **9** (**A**), short-residence-time antagonist **6** (**A**), or reference antagonist rimonabant (**B**). Representative graphs are shown from one experiment performed in duplicate. Note, t_1, t_2 are indicated, which were the two time points used in KRI determinations. Data are summarized in **Table 1**.

Next, the kinetic binding parameters of six antagonists that had either low or high KRI values (**3, 6, 7, 8, 9** and rimonabant) were determined using the competition association assay with [^{3}H]CP55940. Association rate constants varied by merely 4.5-fold, ranging from (5.2 ± 0.7) x 10^4 $M^{-1}s^{-1}$ for compound **6** to (2.3 ± 0.3) x 10^5 $M^{-1}s^{-1}$ for rimonabant (**Table 1**). There was a 180-fold difference in dissociation rate constants, in line with the divergent KRI values. Rimonabant had the fastest dissociation rate constant of (1.4 ± 0.2) x 10^{-3} s^{-1} and thus the shortest RT of 14 min, while compound **9** had the slowest dissociation rate constant of (7.5 ± 3.0) x 10^{-6} s^{-1} and thus the longest RT of 2222 min (**Table 1**). Of note, the long RT antagonist **9** (**Figure 1A**) displayed a typical "overshoot" in the association curve, indicative of a slower dissociation than [^{3}H]CP55940, while the short RT

antagonists, both antagonist **6** (**Figure 1A**) and rimonabant (**Figure 1B**), presented gradually ascending curves.

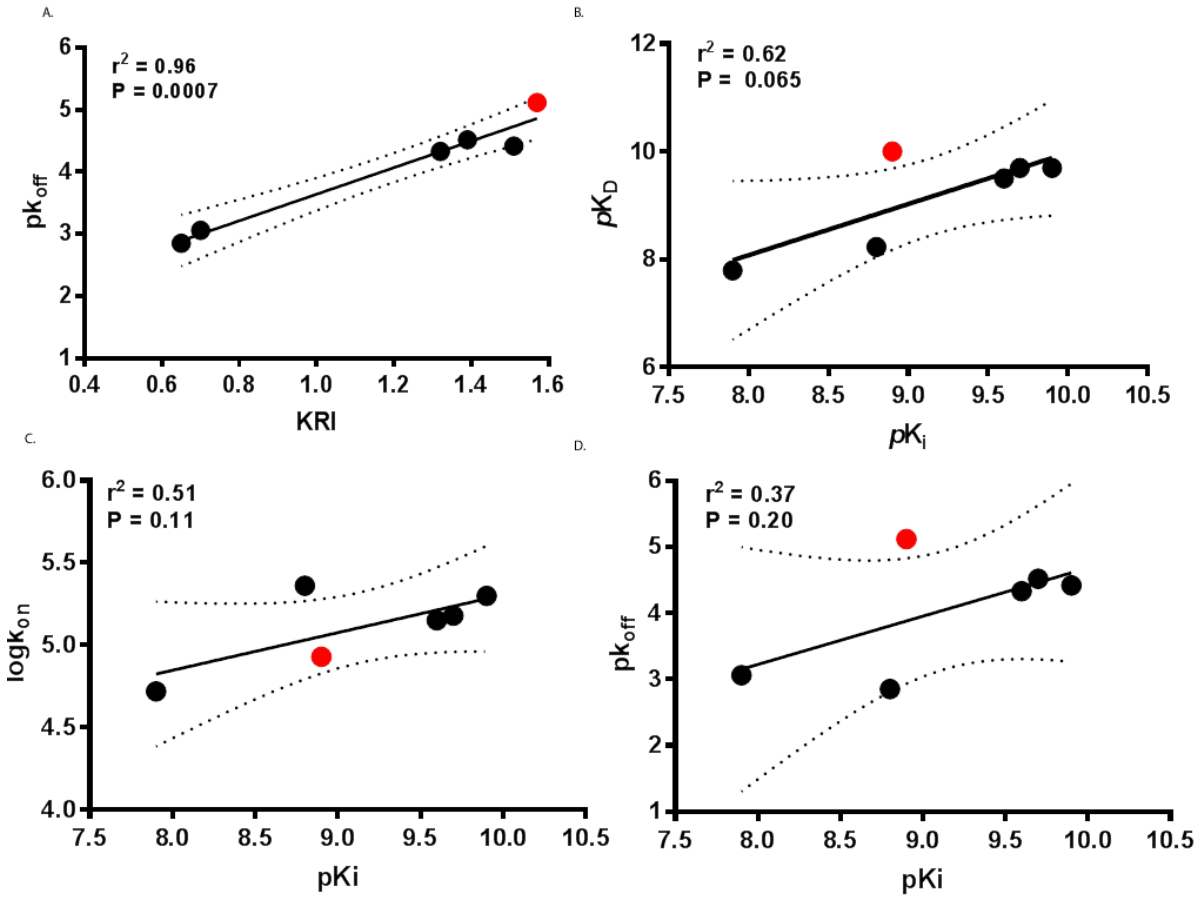

Figure 2. The correlations between the negative logarithm of the hCB$_1$ receptor antagonists' dissociation rate constants (pk$_{off}$) and their Kinetic Rate Index (KRI) (**A**), the CB$_1$ receptor antagonists' affinity (pK$_i$) and their "kinetic K$_D$" (pK$_D$) (**B**), association rate constants (log k$_{on}$) (**C**) and dissociation rate constants (pk$_{off}$) (**D**). The data point of the longest RT antagonist **9** is highlighted in red. Data used in these plots are detailed in **Table 1**. The central line corresponds to the linear regression of the data, the dotted lines represent the 95% confidence intervals for the regression.

Notably, a good correlation between the negative logarithm of the antagonist's dissociation rate constants and their KRI values derived from the kinetic assays was obtained (**Figure 2A**), which confirmed that a compound's KRI value is a good predictor for its dissociation rate constant. A significant correlation was also observed between the antagonist affinities (pK$_i$ values) determined in equilibrium displacement experiments and their pK$_D$ values derived from competition association

experiments (**Figure 2B**). In contrast, the kinetic parameters (log k_{on} or pk_{off} values) of the hCB_1R antagonists did not show a significant correlation with their affinities (**Figure 2C** and **2D**).

Binding kinetics of selected hCB_1 receptor antagonists using (pseudo-)equilibrium binding assays.

As another means to investigate differences in compound binding kinetics, "two-step incubation" equilibrium displacement experiments were performed for the long (**9**) and short RT antagonists (**6** and rimonabant), as shown in **Figure 3A**-**C**. When the displacement curves of the longest RT antagonist **9** were compared with the control and the two-step incubation, a significant one log-unit shift was observed (**Figure 3A**) resulting in a pK_i of 8.9 ± 0.1 to 9.8 ± 0.1, respectively. In contrast, no such affinity-shift was observed for either short RT antagonist (**Figure 3B** and **C, Table 2**), indicative of quick equilibration kinetics.

Table 2. Affinities of selected long (**9**) and short (**6**) RT hCB_1 receptor antagonists determined by the "two-step incubation" assays, using rimonabant as a reference.

Antagonists	"Two-step" incubation[a] (pK_i ± SEM)	Standard assay (Control)[b] (pK_i ± SEM)	"Affinity Shift"[c] (log unit)
9	9.8 ± 0.1 *	8.9 ± 0.1	+ 0.9
6	7.9 ± 0.04 ns	7.9 ± 0.01	0
Rimonabant	8.7 ± 0.1 ns	8.8 ± 0.1	- 0.1

[a] pK_i ± SEM (n = 3), obtained from radioligand binding assays with [^{3}H] CP55940 on recombinant human CB_1 receptors stably expressed on CHO cell membranes.

[b] pK_i ± SEM (n = 3), obtained from radioligand binding assays with [^{3}H] CP55940 on recombinant human CB_1 receptors stably expressed on CHO cell membranes (taken from **Table 1** for comparison).

[c] Affinity shift = pK_i (two-step incubation) - pK_i (standard assay).

Student's t-test was applied for the comparison of "affinity" obtained from "two-step" incubation by standard affinity, * $p < 0.05$, ns for not significant.

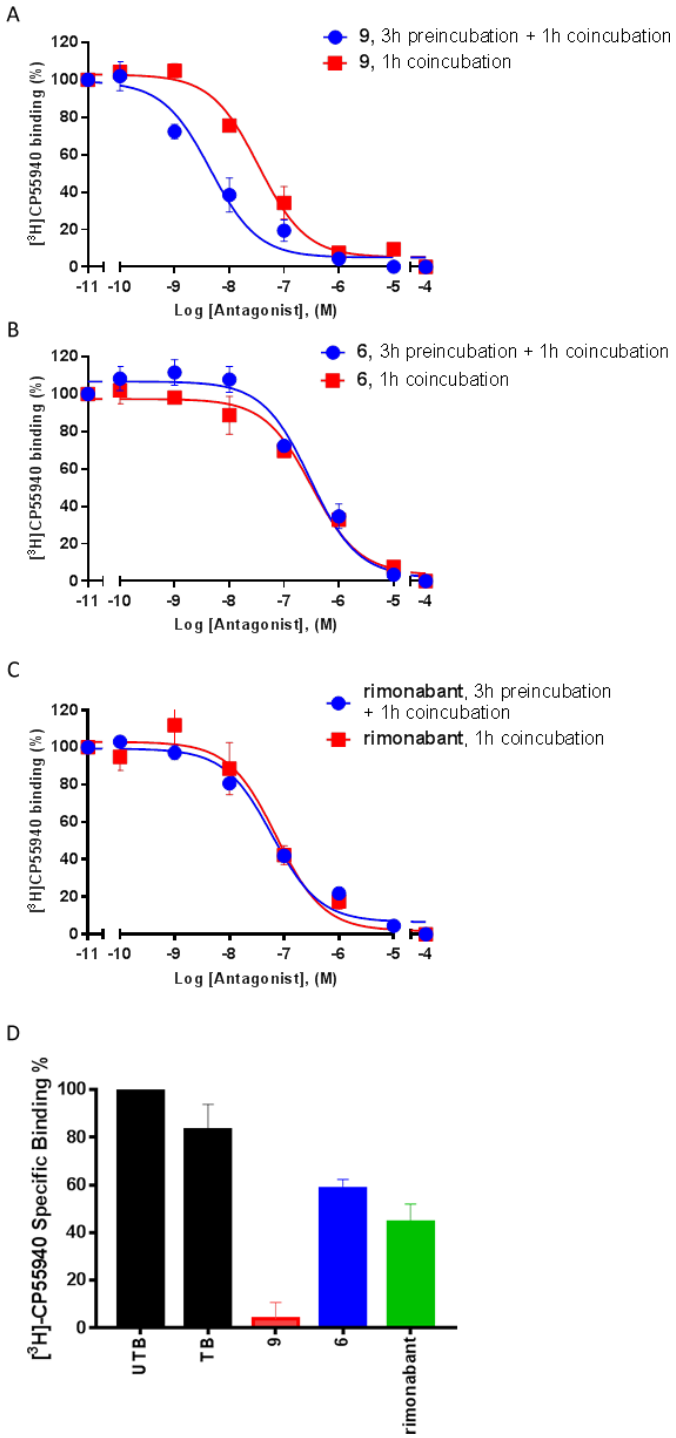

Figure 3. The "two-step incubation" experiments with [^{3}H]CP55940 binding to recombinant hCB$_1$ receptors stably expressed on CHO cell membranes (30 °C) in the absence or presence of unlabeled long-residence-time antagonist **9** (**A**), short-residence-time antagonist **6** (**B**), or reference antagonist rimonabant (**C**). Combined graphs are shown from three experiments performed in duplicate. The "wash-out" experiment with [^{3}H]CP55940 binding to recombinant hCB$_1$ receptors stably expressed on CHO cell membranes (30 °C) in the absence (UTB and TB) or presence of 1 µM of the longest RT antagonist **9** , the short RT antagonist **6** or reference antagonist rimonabant (**D**). The percentage of the specific radioligand binding relative to the unwashed blank control (UTB, 100%) is 83 ± 6.2 % for washed blank control (TB), 3.8 ± 4.1 % for antagonist **9** , 59 ± 2.2 % for antagonist **6** and 44 ± 4.4 % for rimonabant. Data are mean values ± SEM of three independent experiments in duplicate (see **Table 2** for pK$_i$ values).

The observed affinity-shift of the long RT antagonist **9** was further investigated in a "wash-out" experiment. As shown in **Figure 3D**, once the long RT antagonist **9** saturated hCB_1 receptors during pre-incubation, they could not be recovered by washing as indicated by a lack of [^{3}H]CP55940 binding, while for both short RT antagonists (**6** and rimonabant) washing of pre-saturated hCB_1 receptors did result in significant restoration of [^{3}H]CP55940 binding. Taken together, these two (pseudo-)equilibrium experiments yielded a qualitative indication that antagonist **9** had significantly slower dissociation kinetics from hCB_1 receptors than rimonabant and antagonist **6**. This was in agreement with the quantitative results obtained from the (dual-point) competition association experiments.

Computational studies on selected long and short RT antagonists.

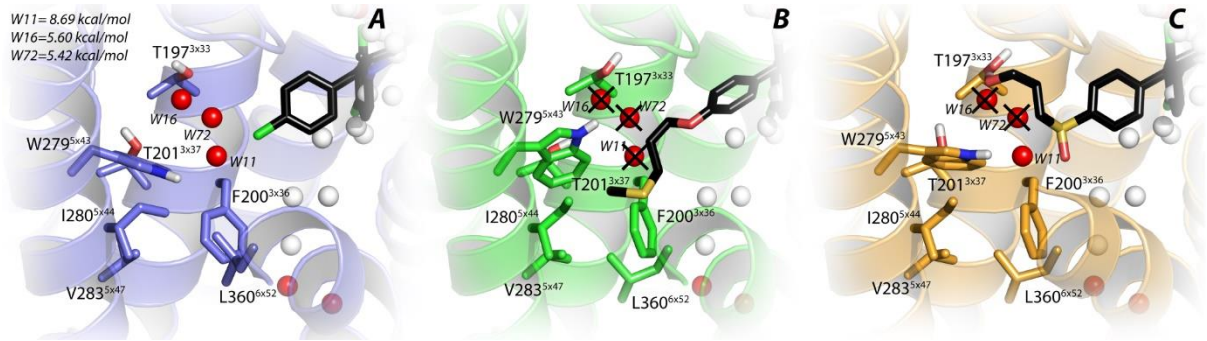

Figure 4. Docking of rimonabant (**A**), antagonist **9** (**B**) and antagonist **6** (**C**) into the binding site of the crystal structure of the hCB_1 receptor (PDB: 5TGZ)[27] co-crystalized with AM6538 (not shown), showing the overlay of numbered consecutively hydration sites of the apo-WaterMap. Hydration sites shown as red spheres represent "unstable" water molecules (>5 kcal/mol), whereas white spheres symbolize "stable" water molecules. For the unfavorable hydration centers ("unstable" water molecules) the ΔG is reported (**A**). Rimonabant is represented by black sticks, and residues within 5 Å of rimonabant are visualized as blue sticks. The protein is represented by blue ribbons (**A**). Antagonist **9** is represented by black sticks, and residues within 5 Å of **9** are visualized as green sticks. The protein is represented by green ribbons. The displaced unstable water molecule was covered with a cross (**B**). Antagonist **6** is represented by black sticks, and residues within 5 Å of **6** are visualized as yellow sticks. The displaced unstable water molecule was covered with a cross (**C**). The protein is represented by yellow ribbons. Ligand and residues atoms color code: yellow = sulfur, red = oxygen, blue = nitrogen, white = hydrogen.

In addition, to study differences between RT and binding modes, rimonabant, antagonist **6** and **9** were docked using induced-fit docking. An apo-WaterMap was generated on the basis that the small

cavity, formed by W279^{5x43}, I280^{5x44} and L360^{6x52}, could be occupied by unfavorable water molecules (W11, W16 and W72 in **Figure 4**). *W11* (ΔG = 8.69 kcal/mol) was one of the most unfavorable hydration centers in this WaterMap. This hydration center is neither displaced by rimonabant nor by the short RT antagonist **6** (**Figure 4A** and **C**). Interestingly, following from the proposed binding pose of the long RT antagonist **9**, this hydration center can be displaced by this antagonist (**Figure 4B**) as the pocket formed by the aforementioned residues is being opened.

Functional characterization of long and short RT antagonists.

Subsequently, the short RT antagonists (**6** and rimonabant) and long RT antagonist (**9**) were functionally characterized in hCB$_1$ receptor agonist-induced [^{35}S]GTPγS binding and G protein-independent (β-arrestin recruitment) assays. Firstly, their antagonistic behavior was revealed on both G protein-dependent and –independent signaling (**Table 3**), as all antagonists caused a dose-dependent decrease of agonist-induced signaling. The long RT antagonist **9** had the highest antagonistic potency in both [^{35}S]GTPγS binding and β-arrestin recruitment assays (3.0 ± 0.3 nM and 30 ± 2.7 nM, respectively), while potencies of the short RT antagonist **6** were the lowest (589 ± 96 nM and 8261 ± 179 nM, respectively). Interestingly, the antagonist potencies were significantly lower in β-arrestin recruitment compared to [^{35}S]GTPγS binding assays, where the potencies obtained from the latter were in closer agreement to the affinity values. Secondly, their mode of antagonism, i.e. surmountable or insurmountable, was investigated in both [^{35}S]GTPγS binding and β-arrestin recruitment assays. Pretreatment of CHOK1hCB1 receptor membranes ([^{35}S]GTPγS binding, **Figure 5A**) or cells (β-arrestin recruitment, **Figure 6A**) with increasing concentrations of the long RT antagonist **9** before stimulation by the CB$_1$ receptor agonist CP55940 induced insurmountable antagonism (**Figure 5A**). In other words, the CP55940 concentration-effect curves were shifted to the right with a concomitant decrease in the maximal response. Conversely, the short RT antagonists (**6** and rimonabant) displayed surmountable antagonism, i.e. shifting CP55940's curves to the right

without affecting its maximum effect ([^{35}S]GTPγS binding, **Figure 5C, E;** and β-arrestin recruitment, **Figure 6C, E**).

Table 3. Functional effects of selected long (**9**) and short (**6**) RT hCB$_1$ receptor antagonists determined by [^{35}S]GTPγS binding and β-arrestin recruitment assays, using rimonabant as a reference.

n ≥ 3		**Antagonist potency**	**Antagonist (in)surmountability**				**Inverse agonism**
			Preincubation		Coincubation		
	Antagonist	pIC$_{50}$ ± SEM (IC$_{50}$ in nM) [a]	*p*A$_2$ [b]	Schild slope [b]	*p*A$_2$ [b]	Schild slope [b]	pIC$_{50}$ ± SEM (IC$_{50}$ in nM) [c]
[^{35}S]GTPγS binding assays	**9**	8.5 ± 0.0 (3.0)	N.A.[d]	N.A.	8.9 ± 0.0	2.4 ± 0.2	8.6 ± 0.1 (2.7)
	6	6.3 ± 0.1 (589)	8.5 ± 0.5	1.0 ± 0.2	9.1 ± 0.2	1.1 ± 0.0	7.1 ± 0.1 (84)
	Rimonabant	8.0 ± 0.1 (11)	10 ± 0.2	1.3 ± 0.1	10 ± 0.3	1.2 ± 0.2	8.4 ± 0.1 (4.0)
β-arrestin recruitment assays	**9**	7.5 ± 0.0 (30)	N.A.	N.A.	8.1 ± 0.1	1.8 ± 0.0	6.8 ± 0.2 (165)
	6	5.1 ± 0.0 (8261)	6.4 ± 0.0	1.2 ± 0.2	7.7 ± 0.1	0.7 ± 0.2	6.8 ± 0.2 (179)
	Rimonabant	6.8 ± 0.1 (184)	8.0 ± 0.2	1.3 ± 0.3	8.2 ± 0.4	1.2 ± 0.3	6.3 ± 0.2 (627)

[a] pIC$_{50}$ ± SEM, obtained from either [^{35}S]GTPγS binding (n = 4) or β-arrestin recruitment (n = 3) assays on recombinant human CB$_1$ receptors stably expressed on CHO cell membranes or intact cell line.

[b] Obtained from Schild analyses, [^{35}S]GTPγS binding assays (n = 3) or β-arrestin recruitment assays (n=3, except for pre-incubation assays with Rimonabant n = 5).

[c] pIC$_{50}$ ± SEM, obtained from either [^{35}S]GTPγS binding (n = 3) or β-arrestin recruitment (n = 3) assays on recombinant human CB$_1$ receptors stably expressed on CHO cell membranes or intact cell line.

[d] N.A. not applicable.

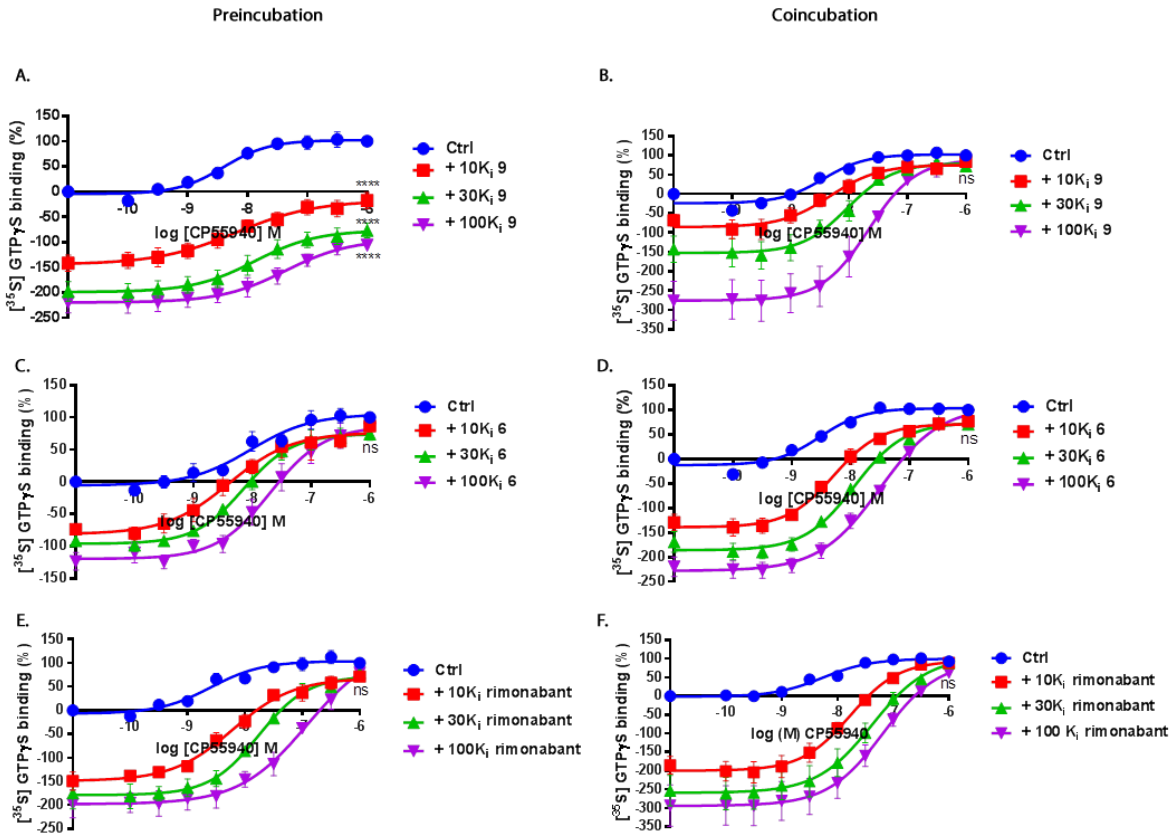

Figure 5. CP55940-stimulated [^{35}S]GTPγS binding to recombinant hCB$_1$ receptors stably expressed on CHO cell membranes (30 °C) in the absence or presence of long-residence-time antagonist **9** (**A** and **B)**, short-residence-time antagonist **6** (**C** and **D)** and reference antagonist rimonabant (**E** and **F**). Antagonist **9** (**A**), **6** (**C**) or rimonabant (**E**) were either incubated for 60 min prior to the challenge with the hCB$_1$ receptor agonist CP55940 or coincubated with CP55940 (antagonist **9, B**, antagonist **6, D** or rimonabant, **F**). The agonist curves were generated in the presence of increasing concentrations of antagonist, namely 10-, 30-, 100-fold their respective K_i values. The shift in agonist EC_{50} was determined to perform Schild analyses. Two-way ANOVA with Tukey's post-test was applied for the comparison of E_{max} by agonist control, **** $p < 0.0001$, ns for not significant. Data were normalized according to the maximal response (100%) produced by CP55940. Combined graphs are shown from three experiments performed in duplicate (see **Table 3** for pA_2 and Schild-slope values).

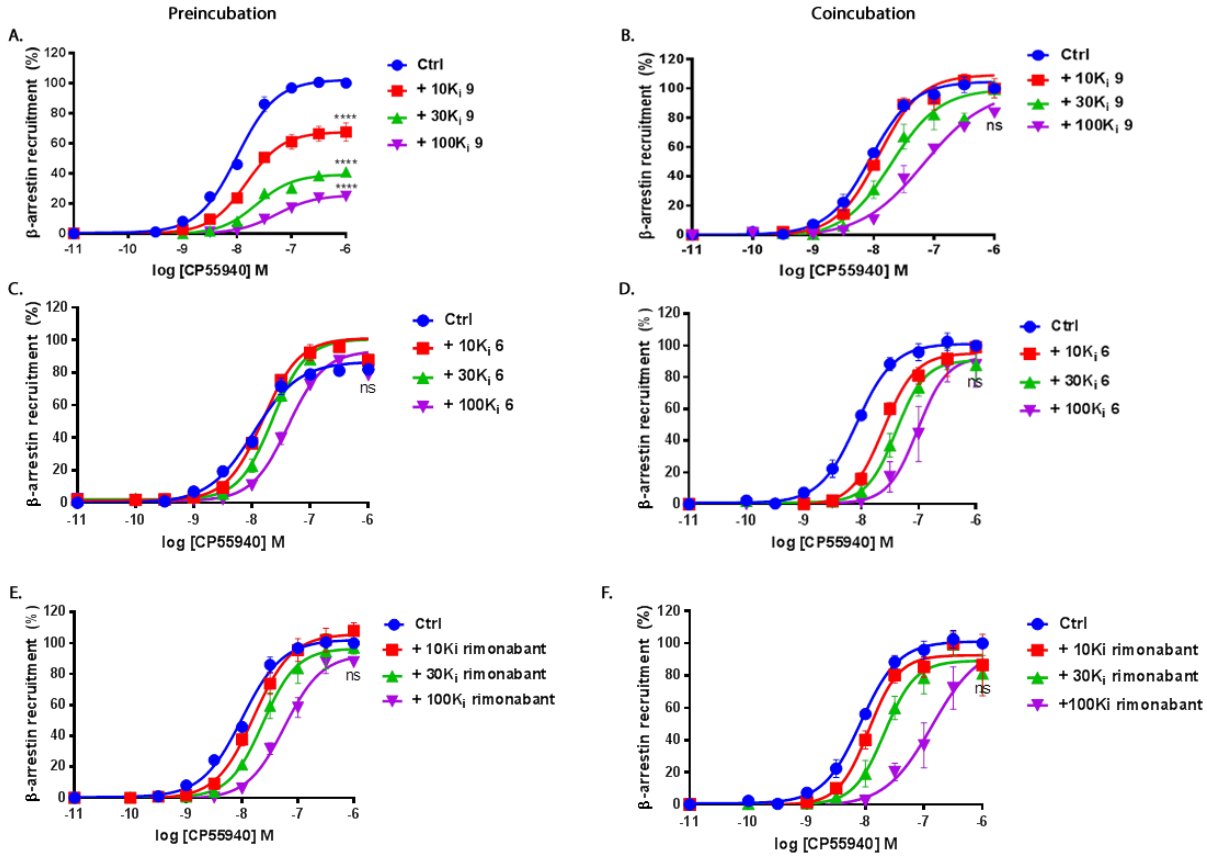

Figure 6. CP55940-stimulated β-arrestin recruitment to recombinant hCB_1 receptors stably expressed on CHO cells (37 °C and 5 % CO_2) in the absence or presence of long-residence-time antagonist **9** (**A** and **B**), short-residence-time antagonist **6** (**C** and **D**) and reference antagonist rimonabant (**E** and **F**). Antagonist **9** (**A**), **6** (**C**) or rimonabant (**E**) were either incubated for 60 min prior to the challenge of the hCB_1 receptor agonist CP55940 or were coincubated with CP55940 (antagonist **9, B**, antagonist **6, D** or rimonabant, **F**). The agonist curves were generated in the presence of increasing concentrations of antagonist, namely 10-, 30-, 100-fold their respective K_i values. The shift in agonist EC_{50} was determined to perform Schild analyses. Two-way ANOVA with Tukey's post-test was applied for the comparison of E_{max} by agonist control, **** $p < 0.0001$, ns for not significant. Data were normalized according to the maximal response (100%) produced by CP55940. Combined graphs are shown from at least three experiments performed in duplicate (n=3, except for pre-incubation assays with Rimonabant n=5). See **Table 3** for pA_2 and Schild-slope values.

Under such experimental set-up, the obtained Schild-slopes of both **6** and rimonabant were close to unity in either [^{35}S]GTPγS binding or β-arrestin recruitment assays (**Table 3**). Moreover, from [^{35}S]GTPγS binding assays the pA_2 value of **6** was close to its pK_i value (8.5 ± 0.5 from Table **3** vs 7.9 ±

0.01 from **Table 2**), while for rimonabant these were more divergent (10 ± 0.2 from **Table 3** vs 8.8 ± 0.1 from **Table 2**). In addition, pA_2 values derived from β-arrestin recruitment assays for **6** and rimonabant were less comparable with the corresponding pK_i values. Next, we performed co-incubation experiments with these antagonists in the presence of CP55940 ([^{35}S]GTPγS binding, **Figure 5B, D, F**; and β-arrestin recruitment, **Figure 6B, D, F**). In this experimental set-up, all antagonists produced a rightward shift in the CP55940 concentration-effect curves without a suppression of the maximal response. Notably, the Schild-slopes of the short RT antagonists (**6** and rimonabant) were close to unity in both [^{35}S]GTPγS binding (1.1 ± 0.0 for **6**, 1.2 ± 0.2 for rimonabant, **Table 3**) and β-arrestin recruitment assays (0.7 ± 0.2 for **6**, 1.2 ± 0.3 for rimonabant, **Table 3**). In contrast, for the long RT antagonist **9** the Schild-slope derived from both assays was well above unity (**Table 3**).

Inverse agonism of the selected CB_1 antagonists.

Finally, it became clear from the [^{35}S]GTPγS binding assays that the antagonists behaved as inverse agonists (**Figure 7A**). It follows that all antagonists caused a dose-dependent decrease of basal [^{35}S]GTPγS binding. The short RT antagonist **6** was 21-fold less potent as an inverse agonist than short RT rimonabant, while the latter was actually equally potent to the long RT antagonist **9** (**Table 3).** Furthermore, we decided to investigate the presence of inverse agonism in the β-arrestin recruitment assay. After adjusting the standard protocol (i.e. extending the incubation time from 90 min to 6 h) inverse agonism was observed for all antagonists (**Figure 7B** and **Table 3**), as in the [^{35}S]GTPγS binding assays. Rimonabant was the least potent inverse agonist in the β-arrestin recruitment assay (IC_{50} = 627 nM), while the short RT and long RT antagonist had a similar potency (**6:** IC_{50} = 179 nM and **9:** IC_{50} = 165 nM, respectively). Overall, the inverse agonistic potencies in β-arrestin recruitment assays were significantly lower than those obtained in the [^{35}S]GTPγS binding assays.

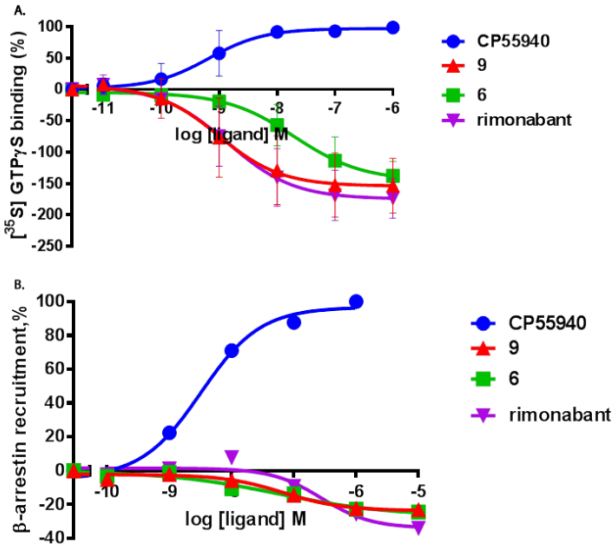

Figure 7. Characterization of inverse agonism for long RT antagonist **9**, short RT antagonist **6** and reference antagonist rimonabant. [^{35}S]GTPγS binding to recombinant hCB_1 receptors stably expressed on CHO cell membranes (**A**) or β-arrestin recruitment to recombinant hCB_1 receptors stably expressed on CHO cells (**B**) with ligand concentrations ranging from 0.1 nM to 10 µM. Data were normalized according to the maximal response (100%) produced by CP55940. Combined graphs are shown from three experiments performed in duplicate in **A**; a representative graph is shown from one experiment performed in duplicate in **B** (see **Table 3** for pIC_{50} values).

Discussion

Ligand optimization based on Structure–Kinetics Relationships (SKR).

Receptor binding kinetics is increasingly being recognized as an important parameter to understand a drug's mechanism of action and ultimately improve its *in vivo* efficacy and safety. Here we focused on the substitutions at the thiophene's 3-position (R group) in a series of rimonabant related antagonists (**Table 1**). Applying equilibrium and kinetic radioligand binding assays, we assayed the binding interactions of nine of such hCB_1 receptor antagonists together with the reference compound rimonabant. As a result, diverse affinity and KRI values were determined and both long and short RT antagonists were identified. Interestingly, the recent hCB_1 receptor crystal structures indicate that the aliphatic R-substitutions fit in the lipophilic "long and narrow channel" of the hCB_1 receptor.[27, 39] Apparently, targeting this channel with diversified chemical fragments is highly relevant

for the improvement of binding interactions at the hCB_1 receptor. Specifically from antagonists **6** (RT = 19 min) and **9** (RT = 2222 min) it seems that a longer (6- vs 5-atom) tail with less polarity contributes significantly to slow receptor dissociation kinetics and better affinity (1.4 nM of **9** vs 14 nM of **6**).Interestingly, the more than 100-fold gain in residence time is not fully reflected in the increase in affinity. This may in part be due to the entropic cost of the aliphatic chain when it has to adapt to the steric requirements of the hydrophobic channel of the binding site, resulting in a slower association rate.[40] Taken together, this limited SKR study proves that kinetic profiles should and can be taken into account during the lead optimization process in drug discovery.

The computational insights of the binding modes.

Using the crystal structure of the hCB_1-AM6538 complex (PDB: 5TGZ),[27] we performed WaterMap calculations to try and understand the differences in residence times observed for the hCB_1 receptor antagonists studied, with the hypothesis that unfavorable hydration might provide an explanation.[34, 35, 41, 42] We focused on antagonist **9** and **6**, and in particular the substitutions at the thiophene's 3-position (R-group) as this was the only structural difference (**Figure 4**). When the antagonist with the shorter and more hydrophilic side chain (**6**, $-SO_2CH_2CH_2CH_2OH$, short RT) was docked into the apo WaterMap, it was able to displace water molecules found in positions *W16* and *W72;* while unstable water molecule *W11* was still around its side chain (**Figure 4C**). We propose that the interaction with $T197^{3x33}$ forces **6** in an orientation where its sulfonyl further stabilized water molecules found in position *W11*. By contrast, antagonist **9** was able to displace all these water molecules (*W11*, *W16* and *W72*) with its longer and more hydrophobic side chain, a process which might raise the energy of the transition state for dissociation (**Figure 4B**). We postulate that this destabilization of the transition state may contribute to the prolonged RT observed with this compound. In contrast, rimonabant cannot displace those unhappy water similarly to antagonist **6**, due to its lack of the linear side chain reaching those energetically unfavorable or unhappy waters (**Figure 4A**).

Methodological aspects on radioligand binding assays.

A so-called dual-point competition association assay for hCB_1 receptor was applied for the "kinetic screening campaign" to increase throughput in comparison to the traditional competition association experiments as shown before.[30] A good correlation between the antagonists' KRI values and dissociation rate constants (k_{off}, k_4) corroborated the robustness of this assay (**Figure 2A**). In contrast, no significant correlations were found between the kinetic binding parameters, k_{on} (k_3) or k_{off} (k_4), and affinity values of these antagonists (**Figure 2 C, D**). Besides, the equilibrium K_i and kinetic K_D values were significantly correlated (**Figure 2B**). Noteworthy, the extraordinary long RT antagonist **9** (**Figure 3,** highlighted in red color) was observed as a significant "outlier" in the correlation plots involving the affinity values obtained from equilibrium assays (**Figure 2B, D**). This clearly indicates that equilibrium was not reached for this antagonist during the radioligand displacement assay where a relatively short incubation time is used. In general, equilibrium affinities of long RT antagonists might often be underestimated and this potentially results in ignoring such interesting compounds for further evaluation.

Subsequently, we designed a "two-step incubation" experiment for further investigation of the affinity-shift of short and long RT antagonists. The displacement curve of the long RT antagonists **9** was shifted leftward about 10-fold, compared to a standard affinity determination, which was then similar to its calculated kinetic K_D (**Table 1** and **2**). In contrast, the affinity of short RT antagonists (**6** and rimonabant) determined in the "two-step incubation" and standard experiments showed no such shift (**Table 2**). These results once more indicate that during a longer period of incubation in the absence of a competing ligand a larger fraction of antagonist **9** forms a tight and slowly dissociating ligand-receptor complex. During preincubation the antagonist **9** enjoys a binding "monopoly" to hCB_1 receptors and the occupied hCB_1 receptors are pseudo-irreversibly blocked, as antagonist **9** (with its extremely long RT) is unlikely to dissociate again. Such a potential two-step (or multi-step) bimolecular binding has also been reported for CCR5 antagonists, where a shift in the apparent affinity was also reported after pre-incubation.[43] Moreover, the pseudo-irreversible binding of long RT antagonist **9** was also confirmed in "wash-out" experiments, where its binding to hCB_1 receptors

was washing-resistant, while short RT antagonists **6** and rimonabant were washed away more easily (**Figure 3D**). A washing-resistant effect has been reported more often for covalently binding ligands to various targets.[44-46] While the current study was mostly focused on developing methodologies for investigating whether the addition of SKR would result in a different triaging of CB_1 antagonists, we are aware that the translation to native tissues should be made. For example, it is known that CB_1 receptors are the most highly expressed receptors in the brain, where they have been shown to form functional heteromers with other GPCR, such as adenosine A_{2A} receptors[47] and beta2 adrenergic receptors.[48] Although this has yet to be investigated for CB_1 receptors, a ligand's binding kinetics is likely to be very different on a monomer than a (hetero)dimer as was recently shown for homodimers of adenosine A_3 receptors.[49, 50]

The functional effects of long or short RT human CB_1 receptor antagonists.

Diverging dissociation rate constants of antagonists have been linked to differentiation in functional effects (i.e. surmountable vs insurmountable antagonism) and concomitant physiological relevance, even before the concept of kinetic studies was gaining acceptance.[51, 52] In our studies, the differences in binding interactions between long and short RT antagonists (**9** vs **6** and rimonabant) prompted us to further investigate potential differences in functional effects. In both [^{35}S]GTPγS binding and β-arrestin recruitment assays, long RT antagonist **9** generated an insurmountable effect when preincubated before stimulation with the agonist CP55940 (**Figure 5A** and **6A**). Importantly, when the preincubation was excluded, its effects became surmountable proving that (**Figure 5B** and **6B**) the long RT antagonist **9** prevents the agonist CP55940 to activate receptors by competitive pseudo-irreversible binding to hCB_1 receptors, as opposed to allosterically inhibiting CP55940 activation.[53, 54] Since the short RT antagonists (**6** and rimonabant) do not occupy hCB_1 receptors for that long, CP55940 was able to activate hCB_1 receptors in the presence of such antagonists under all experimental conditions, which resulted in surmountable antagonism (**Figure 5C-F** and **6C-F**). Moreover, the surmountable effect can be quantified through competitive Gaddum-Schild analysis.[55]

Here for the short RT antagonists (**6** and rimonabant) Schild-slopes close-to-unity were obtained, which indicated a one-to-one competition with the agonist CP55940 while equilibrium was reached. Interestingly, the Schild-slopes determined in the coincubation experiments of long RT antagonist **9** were above 1, i.e. the EC_{50} shifts were greater than predicted by such analysis. This effect can again be explained by its pseudo-irreversible binding to the hCB_1 receptor, where equilibrium was not reached at the chosen incubation times. Of note, in native systems (i.e. under non-equilibrium conditions) endocannabinoid exposure is high, but short due to metabolic degradation of the agonist.[56, 57] However, long and short RT antagonists will still differentiate under these circumstances, as an insurmountable antagonist (i.e. with long RT) can cope with the high local concentrations of the endogenous agonist , while the short RT antagonist cannot. One last note is on the applicability domain of a Schild-plot analysis. Strictly speaking this analysis was derived for systems without constitutive activity, while its use for other systems, i.e. displaying constitutive activity like in our study, has been (re)considered.[58] From Kenakin's reasoning it appears that a small overestimation of the potency of inverse agonists is possible.

Secondly, the selected long or short RT hCB_1 receptor antagonists (**9**, **6** and rimonabant[59]) behaved as inverse agonists in the standard [^{35}S]GTPγS binding assays (**Table 3, Figure 7A**). In the β-arrestin recruitment assay inverse agonism was only observed when the assay-kit manufacturer's protocol was adjusted to contain a longer incubation time (i.e. 6-hour instead of 90 min) (**Figure 7B**).[31] Of note, the cells tolerated this increased incubation time, since the potency of the reference agonist CP55940 did not change (data not shown). The inverse agonism at cannabinoid receptors (i.e. CB_1 and CB_2) in the β-arrestin recruitment assay has been seldom reported.[60] Importantly, although we have used a cell line that heterologously (and abundantly) expresses CB_1 receptors which might raise the question that the level of constitutive activity is an artefact, it is known that this receptor is the highest expressed GPCR in the brain.[61, 62] Moreover, the scientific community, including pharmaceutical industry, actually prompted that the inverse agonistic characteristic might be the

cause of adverse side effects seen with CB_1 antagonists and is therefore in pursuit of 'neutral' antagonists.[63, 64] Noteworthy, there was no correlation between inverse agonism and RTs.

Lastly, the CB_1 receptor is a class A GPCR and it has been reported that its down-stream signaling pathways involve both G protein-coupling and β-arrestin recruitment.[65] When comparing the functional results from [^{35}S]GTPγS binding and β-arrestin recruitment, we learned the antagonists were more potent in the former. Recently, it was reported that hCB_1 receptor activation can trigger 3 "waves" of signaling, G protein-coupling as the first, β-arrestin recruitment as the second, and a combination of the two as the last.[66] The possible correlation between binding kinetics and signaling effects on the CB_1 receptor merits further investigation.

In conclusion, we have evaluated the binding kinetics of nine 1-(4,5-diarylthiophene-2-carbonyl)-4-phenylpiperidine-4-carboxamide derivatives at the hCB_1 receptor, and described structure-kinetics relationships (SKR) defined by their Kinetic Rate Index (KRI) values and dissociation rate constants. The antagonist **9** was found to be a pseudo-irreversible hCB_1 receptor antagonist with a residence time of 2222 min at 30 ^{o}C. Moreover, the difference in receptor-ligand interaction (i.e. long vs short RT) was correlated with the mode of functional antagonism (insurmountable vs surmountable), as determined for both G protein-dependent and –independent signaling pathways. Following from docking studies and WaterMap calculations, we speculate that displacement of unfavorable water molecules may provide a plausible explanation for antagonist **9**'s slow dissociation, or even pseudo-irreversible binding at the hCB_1 receptor. These findings could be highly valuable for the further development of potent and safe CB_1 receptor antagonists for metabolic disorders such as obesity.

References

1. Maccarrone, M.; Bab, I.; Bíró, T.; Cabral, G. A.; Dey, S. K.; Di Marzo, V.; Konje, J. C.; Kunos, G.; Mechoulam, R.; Pacher, P.; Sharkey, K. A.; Zimmer, A. Endocannabinoid signaling at the periphery: 50 years after THC. *Trends Pharmacol. Sci.* **2015,** *36*, 277-296.

2. Pertwee, R. G.; Howlett, A. C.; Abood, M. E.; Alexander, S. P. H.; Di Marzo, V.; Elphick, M. R.; Greasley, P. J.; Hansen, H. S.; Kunos, G.; Mackie, K.; Mechoulam, R.; Ross, R. A. International union of basic and clinical pharmacology. LXXIX. cannabinoid receptors and their ligands: beyond CB_1 and CB_2. *Pharmacol. Rev.* **2010,** *62*, 588-631.
3. Howlett, A. C. Cannabinoid inhibition of adenylate cyclase. Biochemistry of the response in neuroblastoma cell membranes. *Mol. Pharmacol.* **1985,** 27, 429-436.
4. Jin, W.; Brown, S.; Roche, J. P.; Hsieh, C.; Celver, J. P.; Kovoor, A.; Chavkin, C.; Mackie, K. Distinct domains of the CB_1 cannabinoid receptor mediate desensitization and internalization. *J. Neurosci.* **1999,** 19, 3773-3780.
5. Abood, M.; Barth, F.; Bonner, T. I.; Cabral, G.; Casellas, P.; Cravatt, B. F.; Devane, W. A.; Elphick, M. R.; Felder, C. C.; Herkenham, M.; Howlett, A. C.; Kunos, G.; Mackie, K.; Martin, B. R.; Mechoulam, R.; Pertwee, R. G. Cannabinoid receptors: CB_1 receptor. http://www.guidetopharmacology.org/GRAC/ObjectDisplayForward?objectId=56. (December 8).
6. Pacher, P.; BÁTkai, S.; Kunos, G. The endocannabinoid system as an emerging target of pharmacotherapy. *Pharmacol. Rev.* **2006,** *58*, 389-462.
7. Bermudez-Silva, F. J.; Viveros, M. P.; McPartland, J. M.; Rodriguez de Fonseca, F. The endocannabinoid system, eating behavior and energy homeostasis: the end or a new beginning? *Pharmacol., Biochem. Behav.* **2010,** *95*, 375-382.
8. Perkins, J. M.; Davis, S. N. Endocannabinoid system overactivity and the metabolic syndrome: prospects for treatment. *Curr. Diabetes Rep.* **2008,** *8*, 12-19.
9. Lu, D.; Dopart, R.; Kendall, D. A. Controlled downregulation of the cannabinoid CB_1 receptor provides a promising approach for the treatment of obesity and obesity-derived type 2 diabetes. *Cell Stress Chaperones* **2016,** 21, 1-7.
10. FDA briefing document NDA 21-888 zimulti (rimonabant) tablets, 20 mg sanofi aventis advisory committee. Published on June 13, 2007. Accessed on July 20, 2017. <http://www.fda.gov/ohrms/dockets/ac/07/briefing/2007-4306b1-fda-backgrounder.pdf>.
11. Topol, E. J.; Bousser, M.-G.; Fox, K. A. A.; Creager, M. A.; Despres, J.-P.; Easton, J. D.; Hamm, C. W.; Montalescot, G.; Steg, P. G.; Pearson, T. A.; Cohen, E.; Gaudin, C.; Job, B.; Murphy, J. H.; Bhatt, D. L. Rimonabant for prevention of cardiovascular events (CRESCENDO): a randomised, multicentre, placebo-controlled trial. *Lancet* **2010,** *376*, 517-523.
12. Boekholdt, S. M.; Peters, R. J. G. Rimonabant: obituary for a wonder drug. *Lancet* **2010,** *376*, 489-490.
13. Mitchell, P. B.; Morris, M. J. Depression and anxiety with rimonabant. *Lancet* **2007,** 370, 1671-1672.
14. Röver, S.; Andjelkovic, M.; Bénardeau, A.; Chaput, E.; Guba, W.; Hebeisen, P.; Mohr, S.; Nettekoven, M.; Obst, U.; Richter, W. F.; Ullmer, C.; Waldmeier, P.; Wright, M. B. 6-Alkoxy-5-aryl-3-pyridinecarboxamides, a new series of bioavailable cannabinoid receptor type 1 (CB_1) antagonists including peripherally selective compounds. *J. Med. Chem.* **2013,** 56, 9874-9896.
15. Abdel-Magid, A. F. Treatment of metabolic disorders with CB_1 receptor inverse agonists. *ACS Med. Chem. Lett.* **2016,** 7, 874-875.
16. Klumpers, L. E.; Fridberg, M.; de Kam, M. L.; Little, P. B.; Jensen, N. O.; Kleinloog, H. D.; Elling, C. E.; van Gerven, J. M. A. Peripheral selectivity of the novel cannabinoid receptor antagonist TM38837 in healthy subjects. *Br. J. Clin. Pharmacol.* **2013,** 76, 846-857.
17. Dow, R. L.; Carpino, P. A.; Gautreau, D.; Hadcock, J. R.; Iredale, P. A.; Kelly-Sullivan, D.; Lizano, J. S.; O'Connor, R. E.; Schneider, S. R.; Scott, D. O.; Ward, K. M. Design of a potent CB_1 receptor antagonist series: potential scaffold for peripherally-targeted agents. *ACS Med. Chem. Lett.* **2012,** 3, 397-401.
18. Guo, D.; Hillger, J. M.; IJzerman, A. P.; Heitman, L. H. Drug-target residence time—A case for G protein-coupled receptors. *Med. Res. Rev.* **2014,** 34, 856-892.
19. Swinney, D. C.; Haubrich, B. A.; van Liefde, I.; Vauquelin, G. The role of binding kinetics in GPCR drug discovery. *Curr. Top. Med. Chem.* **2015,** *15*, 2504-2522.

20. Copeland, R. A. The drug-target residence time model: a 10-year retrospective. *Nat. Rev. Drug Discovery* **2016,** *15*, 87-95.
21. Vilums, M.; Zweemer, A. J. M.; Yu, Z.; de Vries, H.; Hillger, J. M.; Wapenaar, H.; Bollen, I. A. E.; Barmare, F.; Gross, R.; Clemens, J.; Krenitsky, P.; Brussee, J.; Stamos, D.; Saunders, J.; Heitman, L. H.; IJzerman, A. P. Structure–kinetic relationships—an overlooked parameter in hit-to-lead optimization: a case of cyclopentylamines as chemokine receptor 2 antagonists. *J. Med. Chem.* **2013,** *56*, 7706-7714.
22. Guo, D.; Xia, L.; van Veldhoven, J. P. D.; Hazeu, M.; Mocking, T.; Brussee, J.; IJzerman, A. P.; Heitman, L. H. Binding kinetics of ZM241385 derivatives at the human adenosine A_{2A} receptor. *ChemMedChem* **2014,** *9*, 752-761.
23. Louvel, J.; Guo, D.; Agliardi, M.; Mocking, T. A. M.; Kars, R.; Pham, T. P.; Xia, L.; de Vries, H.; Brussee, J.; Heitman, L. H.; IJzerman, A. P. Agonists for the adenosine A_1 receptor with tunable residence time. A case for nonribose 4-amino-6-aryl-5-cyano-2-thiopyrimidines. *J. Med. Chem.* **2014,** *57*, 3213-3222.
24. Xia, L.; Burger, W. A. C.; van Veldhoven, J. P. D.; Kuiper, B. J.; van Duijl, T. T.; Lenselink, E. B.; Paasman, E.; Heitman, L. H.; IJzerman, A. P. Structure–affinity relationships and structure–kinetics relationships of pyrido[2,1-f]purine-2,4-dione derivatives as human adenosine A_3 receptor antagonists. *J. Med. Chem.* **2017,** *60*, 7555-7568.
25. Barth, F.; Ducoux, J. P.; Gueule, P.; Rinaldi-Carmona, M.; Rouquette, A. Thiophene-2-carboxamide derivatives, preparation thereof and therapeutic use thereof (2010) Patent Application WO2010012964. In 2010.
26. Ducoux, J. P.; Rinaldi-Carmona, M.; Rouquette, A. Derives de 3-alcoxy-4,5-diarylthiophene-2-carboxamide, leur preparation et leur application en therapeutique (2010) Patent Application WO2010109150. In 2010.
27. Hua, T.; Vemuri, K.; Pu, M.; Qu, L.; Han, Gye W.; Wu, Y.; Zhao, S.; Shui, W.; Li, S.; Korde, A.; Laprairie, Robert B.; Stahl, Edward L.; Ho, J.-H.; Zvonok, N.; Zhou, H.; Kufareva, I.; Wu, B.; Zhao, Q.; Hanson, Michael A.; Bohn, Laura M.; Makriyannis, A.; Stevens, Raymond C.; Liu, Z.-J. Crystal Structure of the Human Cannabinoid Receptor CB_1. *Cell* **2016,** 167, 750-762.e714.
28. Xia, L.; Vries, H.; IJzerman, A. P.; Heitman, L. H. Scintillation proximity assay (SPA) as a new approach to determine a ligand's kinetic profile. A case in point for the adenosine A1 receptor. *Purinergic Signalling* **2015,** 12, 115-126.
29. Motulsky, H. J.; Mahan, L. C. The kinetics of competitive radioligand binding predicted by the law of mass action. *Molecular Pharmacology* **1984,** 25, 1-9.
30. Guo, D.; van Dorp, E. J. H.; Mulder-Krieger, T.; van Veldhoven, J. P. D.; Brussee, J.; IJzerman, A. P.; Heitman, L. H. Dual-point competition association assay: a fast and high-throughput kinetic screening method for assessing ligand-receptor binding kinetics. *J. Biomol. Screening* **2013,** 18, 309-320.
31. https://www.discoverx.com/DiscoveRx/media/ContentFiles/DataSheets/93-0001M.pdf.
32. Schrödinger Release 2017-2: Schrödinger Suite 2017-2 Protein Preparation Wizard; Epik, Schrödinger, LLC, New York, NY, 2017; Impact, Schrödinger, LLC, New York, NY, 2017; Prime, Schrödinger, LLC, New York, NY, 2017.
33. Sherman, W.; Day, T.; Jacobson, M. P.; Friesner, R. A.; Farid, R. Novel procedure for modeling ligand/receptor induced fit effects. *J. Med. Chem.* **2006,** *49*, 534-553.
34. Abel, R.; Young, T.; Farid, R.; Berne, B. J.; Friesner, R. A. Role of the active-site solvent in the thermodynamics of Factor Xa ligand binding. *J. Am. Chem. Soc.* **2008,** *130*, 2817-2831.
35. Young, T.; Abel, R.; Kim, B.; Berne, B. J.; Friesner, R. A. Motifs for molecular recognition exploiting hydrophobic enclosure in protein–ligand binding. *Proc. Natl. Acad. Sci. U. S. A.* **2007,** *104*, 808-813.
36. Schrödinger, L. L. C., New York. *The PyMOL molecular graphics system*, 1.8.3.2; **2016**.
37. Cheng, Y.-C.; Prusoff, W. H. Relationship between the inhibition constant (K_i) and the concentration of inhibitor which causes 50 percent inhibition (IC_{50}) of an enzymatic reaction. *Biochem. Pharmacol.* **1973,** 22, 3099-3108.

38. Soethoudt, M.; Grether, U.; Fingerle, J.; Grim, T. W.; Fezza, F.; de Petrocellis, L.; Ullmer, C.; Rothenhäusler, B.; Perret, C.; van Gils, N.; Finlay, D.; MacDonald, C.; Chicca, A.; Gens, M. D.; Stuart, J.; de Vries, H.; Mastrangelo, N.; Xia, L.; Alachouzos, G.; Baggelaar, M. P.; Martella, A.; Mock, E. D.; Deng, H.; Heitman, L. H.; Connor, M.; Di Marzo, V.; Gertsch, J.; Lichtman, A. H.; Maccarrone, M.; Pacher, P.; Glass, M.; van der Stelt, M. Cannabinoid CB_2 receptor ligand profiling reveals biased signalling and off-target activity. *Nat. Commun.* **2017,** 8, 13958-13972.
39. Shao, Z.; Yin, J.; Chapman, K.; Grzemska, M.; Clark, L.; Wang, J.; Rosenbaum, D. M. High-resolution crystal structure of the human CB_1 cannabinoid receptor. *Nature* **2016,** 540, 602-606.
40. Weiß, R. G.; Setny, P.; Dzubiella, J. Principles for tuning hydrophobic ligand–receptor binding kinetics. *J. Chem. Theory Comput.* **2017,** 10.1021/acs.jctc.1027b00216.
41. Segala, E.; Guo, D.; Cheng, R. K. Y.; Bortolato, A.; Deflorian, F.; Doré, A. S.; Errey, J. C.; Heitman, L. H.; IJzerman, A. P.; Marshall, F. H.; Cooke, R. M. Controlling the dissociation of ligands from the adenosine A_{2A} receptor through modulation of salt bridge strength. *J. Med. Chem.* **2016,** *59*, 6470-6479.
42. Pearlstein, R. A.; Sherman, W.; Abel, R. Contributions of water transfer energy to protein-ligand association and dissociation barriers: Watermap analysis of a series of p38α MAP kinase inhibitors. *Proteins: Struct., Funct., Bioinf.* **2013,** 81, 1509-1526.
43. Swinney, D. C.; Beavis, P.; Chuang, K.-T.; Zheng, Y.; Lee, I.; Gee, P.; Deval, J.; Rotstein, D. M.; Dioszegi, M.; Ravendran, P.; Zhang, J.; Sankuratri, S.; Kondru, R.; Vauquelin, G. A study of the molecular mechanism of binding kinetics and long residence times of human CCR5 receptor small molecule allosteric ligands. *Br. J. Pharmacol.* **2014,** 171, 3364-3375.
44. Yang, X.; Dong, G.; Michiels, T. J. M.; Lenselink, E. B.; Heitman, L.; Louvel, J.; IJzerman, A. P. A covalent antagonist for the human adenosine A_{2A} receptor. *Purinergic Signalling* **2016,** 13, 191-201.
45. Tan, L.; Wang, J.; Tanizaki, J.; Huang, Z.; Aref, A. R.; Rusan, M.; Zhu, S.-J.; Zhang, Y.; Ercan, D.; Liao, R. G.; Capelletti, M.; Zhou, W.; Hur, W.; Kim, N.; Sim, T.; Gaudet, S.; Barbie, D. A.; Yeh, J.-R. J.; Yun, C.-H.; Hammerman, P. S.; Mohammadi, M.; Jänne, P. A.; Gray, N. S. Development of covalent inhibitors that can overcome resistance to first-generation FGFR kinase inhibitors. *Proc. Natl. Acad. Sci. U. S. A.* **2014,** 111, E4869-E4877.
46. Leonti, M.; Casu, L.; Raduner, S.; Cottiglia, F.; Floris, C.; Altmann, K.-H.; Gertsch, J. Falcarinol is a covalent cannabinoid CB_1 receptor antagonist and induces pro-allergic effects in skin. *Biochem. Pharmacol.* **2010,** 79, 1815-1826.
47. Moreno, E.; Chiarlone, A.; Medrano, M.; Puigdellivol, M.; Bibic, L.; Howell, L. A.; Resel, E.; Puente, N.; Casarejos, M. J.; Perucho, J.; Botta, J.; Suelves, N.; Ciruela, F.; Gines, S.; Galve-Roperh, I.; Casado, V.; Grandes, P.; Lutz, B.; Monory, K.; Canela, E. I.; Lluis, C.; McCormick, P. J.; Guzman, M. Singular location and signaling profile of adenosine A_{2A}-cannabinoid CB_1 receptor heteromers in the dorsal striatum. *Neuropsychopharmacology* **2017**, 1-14.
48. Hudson, B. D.; Hébert, T. E.; Kelly, M. E. M. Physical and functional interaction between CB_1 cannabinoid receptors and β2-adrenoceptors. *Br. J. Pharmacol.* **2010,** 160, 627-642.
49. Hill, S. J.; May, L. T.; Kellam, B.; Woolard, J. Allosteric interactions at adenosine A_1 and A_3 receptors: new insights into the role of small molecules and receptor dimerization. *Br. J. Pharmacol.* **2014,** 171, 1102-1113.
50. May, L. T.; Bridge, L. J.; Stoddart, L. A.; Briddon, S. J.; Hill, S. J. Allosteric interactions across native adenosine-A(3) receptor homodimers: quantification using single-cell ligand-binding kinetics. *FASEB J.* **2011,** 25, 3465-3476.
51. Vauquelin, G. Determination of drug-receptor residence times by radioligand binding and functional assays: experimental strategies and physiological relevance. *MedChemComm* **2012,** 3, 645-651.
52. Sullivan, S. K.; Hoare, S. R. J.; Fleck, B. A.; Zhu, Y.-F.; Heise, C. E.; Struthers, R. S.; Crowe, P. D. Kinetics of nonpeptide antagonist binding to the human gonadotropin-releasing hormone receptor: Implications for structure–activity relationships and insurmountable antagonism. *Biochem. Pharmacol.* **2006,** 72, 838-849.

53. Ahn, K. H.; Mahmoud, M. M.; Kendall, D. A. Allosteric modulator ORG27569 induces CB_1 cannabinoid receptor high affinity agonist binding state, receptor internalization, and Gi protein-independent ERK1/2 kinase activation. *J. Biol. Chem.* **2012,** 287, 12070-12082.
54. Horswill, J. G.; Bali, U.; Shaaban, S.; Keily, J. F.; Jeevaratnam, P.; Babbs, A. J.; Reynet, C.; Wong Kai In, P. PSNCBAM-1, a novel allosteric antagonist at cannabinoid CB_1 receptors with hypophagic effects in rats. *Br. J. Pharmacol.* **2007,** 152, 805-814.
55. Colquhoun, D. Why the Schild method is better than Schild realised. *Trends Pharmacol. Sci.* **2007,** 28, 608-614.
56. Reggio, P. H. Endocannabinoid Binding to the Cannabinoid Receptors: What Is Known and What Remains Unknown. *Curr. Med. Chem.* **2010,** 17, 1468-1486.
57. Fowler, C. J.; Doherty, P.; Alexander, S. P. H. Chapter Two - Endocannabinoid Turnover. In *Advances in Pharmacology*, Kendall, D.; Alexander, S. P. H., Eds. Academic Press: 2017; Vol. 80, pp 31-66.
58. Kenakin, T. Orthosteric Drug Antagonism. In *A Pharmacology Primer: Techniques for More Effective and Strategic Drug Discovery (4th Edition)*. Academic Press: 2014; pp 128-131.
59. Rinaldi-Carmona, M.; Barth, F.; Héaulme, M.; Alonso, R.; Shire, D.; Congy, C.; Soubrié, P.; Brelière, J.-C.; Le Fur, G. Biochemical and pharmacological characterisatioN OF SR141716A, the first potent and selective brain cannabinoid receptor antagonist. *Life Sci.* **1995,** 56, 1941-1947.
60. McGuinness, D.; Malikzay, A.; Visconti, R.; Lin, K.; Bayne, M.; Monsma, F.; Lunn, C. A. Characterizing Cannabinoid CB_2 Receptor Ligands Using DiscoveRx PathHunter™ β-Arrestin Assay. *J. Biomol. Screening* **2008,** 14, 49-58.
61. Herkenham, M.; Lynn, A. B.; Little, M. D.; Johnson, M. R.; Melvin, L. S.; de Costa, B. R.; Rice, K. C. Cannabinoid receptor localization in brain. *Proc. Natl. Acad. Sci. U. S. A.* **1990,** 87, 1932-1936.
62. Miller, L. K.; Devi, L. A. The Highs and Lows of Cannabinoid Receptor Expression in Disease: Mechanisms and Their Therapeutic Implications. *Pharmacol. Rev.* **2011,** 63, 461-470.
63. Pertwee, R. G. Inverse agonism and neutral antagonism at cannabinoid CB_1 receptors. *Life Sci.* **2005,** 76, 1307-1324.
64. Erdozain, A. M.; Diez-Alarcia, R.; Meana, J. J.; Callado, L. F. The inverse agonist effect of rimonabant on G protein activation is not mediated by the cannabinoid CB_1 receptor: evidence from postmortem human brain. *Biochem. Pharmacol.* **2012,** 83, 260-268.
65. Turu, G.; Hunyady, L. Signal transduction of the CB_1 cannabinoid receptor. *J. Mol. Endocrinol.* **2010,** 44, 75-85.
66. Nogueras-Ortiz, C.; Yudowski, G. A. The multiple waves of cannabinoid 1 receptor signaling. *Mol. Pharmacol.* **2016,** 90, 620-626.

Chapter 4

Structure-Affinity Relationships and Structure-Kinetics Relationships of Pyrido[2,1-*f*]purine-2,4-dione Derivatives as Human Adenosine A_3 Receptor Antagonists

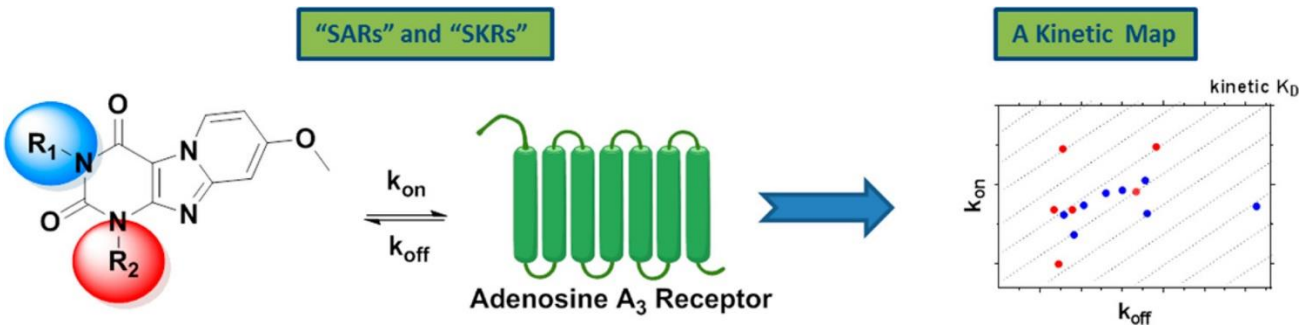

Lizi Xia, Wessel A. C. Burger, Jacobus P.D. van Veldhoven, Boaz J. Kuiper, Tirsa T. van Duijl, Eelke B. Lenselink, Ellen Paasman, Laura H. Heitman, and Adriaan P. IJzerman

Adapted from: *J. Med. Chem.*, **2017**, 60(17): 7555–7568

About this chapter

We expanded on a series of pyrido[2,1-*f*]purine-2,4-dione derivatives as human adenosine A_3 receptor (hA_3R) antagonists to determine their kinetic profiles and affinities. Many compounds showed high affinities and a diverse range of kinetic profiles. We found hA_3R antagonists with very short residence time (RT) at the receptor (2.2 min for **5**) and much longer RTs (e.g. 376 min for **27**, or 391 min for **31**). Two representative antagonists (**5** and **27**) were tested in [^{35}S]GTPγS binding assays, and their RTs appeared correlated to their (in)surmountable antagonism. From a k_{on}-k_{off}-K_D kinetic map we divided the antagonists into three subgroups, providing a possible direction for the further development of hA_3R antagonists. Additionally, we performed a computational modelling study that sheds light on the crucial receptor interactions dictating the compounds' binding kinetics. Knowledge of target binding kinetics appears useful for developing and triaging new hA_3R antagonists in the early phase of drug discovery.

Introduction

The adenosine A_3 receptor is the youngest member discovered in the family of adenosine receptors,[1] all of which belong to class A G-protein coupled receptors (GPCR) and fall into four distinct subtypes (A_1, A_{2A}, A_{2B} and A_3). Although all subtypes are activated by the endogenous ligand adenosine, these purinergic receptors differ from each other in their distribution and to which G protein they are coupled. Following agonist activation, the A_1 and A_3 adenosine receptors cause a decrease in cAMP levels as they primarily couple to G_i proteins. The A_{2A} and A_{2B} adenosine receptors on the other hand, are primarily linked to G_s proteins and this leads to increased levels of cAMP upon receptor activation.[2]

Although the pharmacological characterization of adenosine receptors has been well documented,[3] the human adenosine A_3 receptor (hA_3R) is less well characterized because of its "dichotomy" in different therapeutic applications.[4] Moreover, certain ligands have been described as cytoprotective or cytotoxic merely depending on the concentration employed, highlighting the difficulties that arise when characterizing novel hA_3R compounds.[5] Nevertheless, there is no doubt that the hA_3R has therapeutic potential in clinical indications (i.e. cardiovascular diseases,[6, 7] cancer,[7, 8] and respiratory diseases[7, 9-11]), due to its overexpression on cancer and inflammatory cells.[3, 12-15]

Traditional drug screening methods, and those employed in previous hA_3R drug discovery attempts, revolve around the use of a ligand's affinity as the selection criterion for further optimization in a so-called structure-affinity relationships (SAR) approach. In recent years, however, there has been emerging the realization that selecting ligands based on their affinity, an equilibrium parameter, does not necessarily predict *in vivo* efficacy. This is due to the dynamic conditions *in vivo*, that often are in contrast to the equilibrium conditions applied in *in vitro* assays.[16] In fact a ligand's kinetic properties may provide a better indication of how a ligand will perform *in vivo*.[17] Specifically, the parameter of residence time (RT) has been proposed as a more relevant selecting criterion. The RT reflects the

lifetime of the ligand-receptor complex and can be calculated as the reciprocal of the ligand's dissociation constant ($RT=1/k_{off}$).[18, 19]

Table 1. Binding Affinity and Kinetic Parameters of 1-benzyl-8-methoxy-3-propylpyrido[2,1-f]purine-2,4(1H,3H)-dione[23, 24]

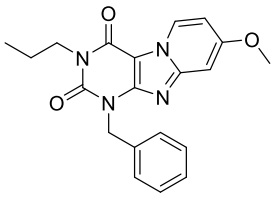

Compound	pK_i [a] ± SEM (mean K_i in nM)	KRI[b]	k_{on} [c] ($M^{-1}s^{-1}$)	k_{off} [d] (s^{-1})	RT [e] (min)
1	8.5 ± 0.02 (3.2)	0.99 (0.97; 1.0)	(8.5 ± 1.2) x 10^5	(3.2 ± 0.02) x 10^{-4}	52 ± 0.3

[a] pK_i ± SEM (n ≥ 3, average K_i value in nM), obtained at 25 °C from radioligand binding assays with [^{3}H]PSB-11 ([^{3}H]**34**) on human Adenosine A_3 receptors stably expressed on CHO cell membranes.

[b] KRI (n = 2, individual estimates in parentheses), obtained at 10 °C from dual-point competition association assays with [^{3}H]**34** on human Adenosine A_3 receptors stably expressed on CHO cell membranes.

[c] k_{on} ± SEM (n ≥ 3), obtained at 10 °C from competition association assays with [^{3}H]**34** on human Adenosine A_3 receptors stably expressed on CHO cell membranes.

[d] k_{off} ± SEM (n ≥ 3), obtained at 10 °C from competition association assays with [^{3}H]**34** on human Adenosine A_3 receptors stably expressed on CHO cell membranes.

[e] RT (min) = $1/(60*k_{off})$.

While the binding kinetics of some (labeled) hA_3R agonists have been studied,[20] this parameter has not been part of medicinal chemistry efforts for antagonists, i.e. yielding structure-kinetics relationships (SKR), next to SAR.[21] Therefore, in order to provide the first SKR analysis on the hA_3R, a highly potent and selective hA_3R antagonist scaffold was chosen. The pyrido[2,1-*f*]purine-2,4-dione template has been previously characterized with respect to affinity alone. In a Topliss approach[22] we had synthesized and characterized a number of highly potent and selective hA_3R antagonists.[23, 24] One of the reference antagonists (**1**) with good affinity and selectivity over other adenosine receptors is represented in **Table 1**. Using this compound as the starting point, we further selected and synthesized compounds to add to the library of pyrido[2,1-*f*]purine-2,4-dione derivatives. Using

radioligand displacement assays and competition association assays, we obtained affinity (K_i) and kinetic parameters (k_{on}, k_{off}, and RTs). This allowed a full SKR study alongside a more traditional SAR analysis. The findings provide information on the structural requirements for a favorable kinetic profile at the hA_3R and consequently may improve the *in vitro* to *in vivo* translation for hA_3R antagonists.

Results and discussion

Chemistry.

The synthesis approach shown in **Scheme 1** was adapted from Priego *et al.*[23, 24] Starting from the commercially available materials benzylurea (**3**), ethyl cyanoacetate and sodium methoxide 1-benzyl-6-amino-uracil (**4**) was synthesized in a 88% yield.[25] *In situ* dibromination of uracil **4** at the C^5 position by *N*-bromosuccinimide, followed by cyclisation with 4-methoxypyridine gave the pyrido[2,1-*f*]purine-2,4-dione (**5**) in a one pot reaction. Final compounds **1**, **2** and **6**-**22** (as depicted in Table 1) were obtained, with yields varying in the range of 3-86%, by alkylating the N^3 position of **5** using a variety of alkyl, alkenyl and alkynyl bromides in acetonitrile and 1,8-diazabicyclo[5.4.0]undec-7-ene (DBU) as a base. Secondly, to be able to diversify on the N^1 (R_2) position, building block **23** had to be obtained. Full conversion of methylcyclopropyl compound **2** into the desired debenzylated **23** was realized by multiple additions of ammonium formate and $Pd(OH)_2$ at 80 °C in ethanol overnight. Due to poor solubility **23** was extracted with hot DMF and $Pd(OH)_2$ was removed by filtration, resulting in a quantitative yield. Finally various N^1 substituted benzyl (**24**-**32**) and phenethyl (**33**) derivatives (**Scheme 1**) were made starting from the respective benzyl- or phenethyl bromides in DMF with K_2CO_3 used as base.

Biological Evaluation.

All binding affinities of the pyrido[2,1-*f*]purine-2,4-dione derivatives were determined at 25 °C in a 2 hours incubation protocol. All compounds were able to concentration-dependently inhibit specific

[^{3}H]8-Ethyl-4-methyl-2-phenyl-(8*R*)-4,5,7,8-tetrahydro-1*H*- imidazo[2,1-*i*]-purin-5-one[26] ([^{3}H]PSB-11, **34**) binding to the human adenosine A_3 receptor and their affinities are listed in **Tables 1**, **2** and **3**. All compounds had (sub)nanomolar binding affinities ranging from 0.38 nM for compound **27** to 108 nM for compound **5**.

Scheme 1. Synthesis of 1,3-disubstituted-1*H*,3*H*-pyrido[2,1-*f*]purine-2,4-dione derivatives.

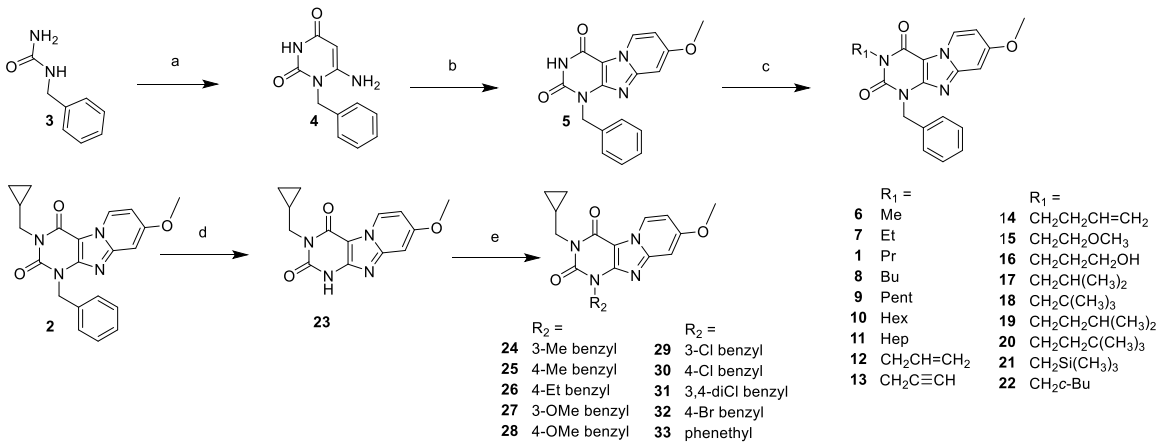

Reagents and conditions: **a**) ethyl cyanoacetate, NaOEt, EtOH, reflux, overnight; **b**) i) NBS, CH_3CN, 80 °C, 1h ii) 4-methoxypyridine, 80 °C, overnight; **c**) R_1-Br, DBU, CH_3CN, 80 °C, overnight; **d**) 20% $Pd(OH)_2$, ammonium formate, EtOH, reflux, overnight; **e**) R_2-Br, K_2CO_3, DMF, 40 °C overnight.

Subsequently, the human adenosine A_3 receptor ligands were screened in a so-called "dual-point" competition association assay,[27] allowing for the semi-quantitative estimation of the compounds' dissociation rates and therefore the compounds' RTs. The specific binding of [^{3}H]**34** was measured after 20 and 240 minutes in the absence and presence of a single concentration (i.e. 1 x IC_{50}) of unlabeled human adenosine A_3 receptor antagonists, which yielded their Kinetic Rate Index (KRI). A long RT compound shows a characteristic "overshoot" followed by a steady decrease in specific binding until a new equilibrium is reached; in such a case the KRI value is greater than unity. Conversely, a ligand with a fast dissociation rate is represented by a more shallow curve, yielding a KRI value smaller than one when dividing the binding at t_1 by the binding at t_2. The KRI values in the series ranged from 0.38 to 4.06 (**Table 1**, **2** and **3**).

Table 2. Binding Affinities and Kinetic Parameters of Pyrido[2,1-*f*]purine-2,4-dione Derivatives with Modification on *N*-3 Position (R_1 group)

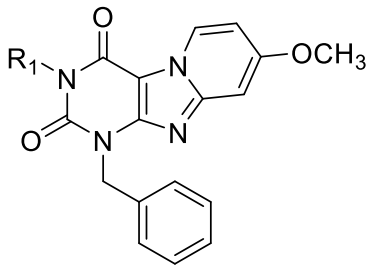

Compd.	R_1	pK_i [a] ± SEM (mean K_i in nM)	KRI[b]	k_{on} [c] ($M^{-1}s^{-1}$)	k_{off} [d] (s^{-1})	RT [e] (min)
5	H	7.0 ± 0.02 (108)	0.38 ± 0.12	(5.3 ± 1.5) x10^5	(1.4 ± 0.5) x 10^{-2}	2.2 ± 1.4
6	CH_3	7.7 ± 0.1 (20.8)	0.54 (0.52; 0.55)	n.d.[f]	n.d.	n.d.
7	CH_2CH_3	8.0 ± 0.1 (10.7)	0.80 (0.85; 0.75)	n.d.	n.d.	n.d.
8	$CH_2CH_2CH_2CH_3$	8.8 ± 0.1 (1.5)	1.29 (1.27; 1.31)	n.d.	n.d.	n .d.
9	$CH_2CH_2CH_2CH_2CH_3$	8.5 ± 0.02 (3.5)	1.11 (0.98; 1.24)	(1.1 ± 0.1) x 10^6	(6.0 ± 0.5) x 10^{-4}	28 ± 2.2
10	$CH_2CH_2CH_2CH_2CH_2CH_3$	8.6 ± 0.1 (2.8)	2.18 (2.15; 2.21)	(2.3 ± 1.0) x 10^5	(8.2 ± 1.3) x 10^{-5}	213 ± 35
11	$CH_2CH_2CH_2CH_2CH_2CH_2CH_3$	8.2 ± 0.2 (6.8)	4.06 (3.66; 4.46)	(4.2 ± 0.3) x 10^5	(6.2 ± 0.2) x 10^{-5}	278 ± 45
12	$CH_2CH{=}CH_2$	8.3 ± 0.1 (5.9)	0.72 (0.46; 0.99)	n.d.	n.d.	n.d.
13	$CH_2C{\equiv}CH$	8.4 ± 0.02 (4.3)	1.20 (1.16; 1.23)	n.d.	n.d.	n.d.
14	$CH_2CH_2CH{=}CH_2$	8.9 ± 0.1 (1.4)	1.23 (1.04; 1.41)	n.d.	n.d.	n.d.
15	$CH_2CH_2OCH_3$	7.7 ± 0.2 (23)	0.70 (0.70; 0.70)	(4.3 ± 0.8) x 10^5	(6.3 ± 0.7) x 10^{-4}	27 ± 2.6
16	$CH_2CH_2CH_2OH$	7.1 ± 0.1 (81)	1.04 ± 0.11	n.d.	n.d.	n.d.
17	$CH_2CH(CH_3)_2$	8.9 ± 0.02 (1.2)	1.64 ± 0.24	(7.8 ± 2.7) x 10^5	(2.0 ± 0.8) x 10^{-4}	148 ± 102
18	$CH_2C(CH_3)_3$	8.5 ± 0.1 (3.5)	1.73 ± 0.28	(5.5 ± 1.3) x 10^5	(1.1 ± 0.4) x 10^{-4}	250 ± 147
19	$CH_2CH_2CH(CH_3)_2$	8.5 ± 0.04 (3.5)	1.39 (1.23; 1.55)	n.d.	n.d.	n.d.
20	$CH_2CH_2C(CH_3)_3$	8.1 ± 0.02 (8.0)	0.95 (1.02; 0.87)	n.d.	n.d.	n.d.
21	$CH_2Si(CH_3)_3$	8.6 ± 0.03 (2.7)	1.36 (1.26; 1.45)	n.d.	n.d.	n.d.
2	$CH_2C_3H_5$	9.0 ± 0.02 (1.0)	2.68 ± 0.48	(2.8 ± 0.5) x 10^6	(6.0 ± 1.7) x 10^{-5}	315 ± 105
22	$CH_2C_4H_7$	8.6 ± 0.03 (2.7)	1.48 (1.66;1.30)	n.d.	n.d.	n.d.

[a] pK_i ± SEM (n ≥ 3, average K_i value in nM), obtained at 25 °C from radioligand binding assays with [^{3}H]**34** on human Adenosine A_3 receptors stably expressed on CHO cell membranes.

[b] KRI ± SEM (n = 3) or KRI (n = 2, individual estimates in parentheses), obtained at 10 °C from dual-point competition association assays with [^{3}H]**34** on human Adenosine A_3 receptors stably expressed on CHO cell membranes.

[c] k_{on} ± SEM (n ≥ 3), obtained at 10 °C from competition association assays with [^{3}H]**34** on human Adenosine A_3 receptors stably expressed on CHO cell membranes.

[d] k_{off} ± SEM (n ≥ 3), obtained at 10 °C from competition association assays with [^{3}H]**34** on human Adenosine A_3 receptors stably expressed on CHO cell membranes.

[e] RT (min) = $1/(60*k_{off})$.

[f] n.d. = not determined.

Compounds with a KRI value less than 0.7 or greater than 1.5 were selected for complete kinetic characterization through the use of a competition association assay with [^{3}H]**34** (**Figure 1A**). In order to obtain extensive Structure-Kinetics Relationships (SKR), close structural analogs (**9**, **28**, **29** and **30**) of **1** were also tested to obtain their association (k_{on}) and dissociation (k_{off}) rate constants. Association rate constants varied by 30-fold, ranging from (1.0 ± 0.1) x 10^5 $M^{-1}s^{-1}$ for antagonist **31** to (3.0 ± 0.3) x 10^6 $M^{-1}s^{-1}$ for antagonist **30** (**Table 3**)**.**

Interestingly, there was an approximately 290-fold difference in dissociation rate constants, reflecting the divergent KRI values. Antagonist **5** had the fastest dissociation rate constant of (1.4 ± 0.5) x 10^{-2} s^{-1} and thus the shortest RT of 2.2 min, while both antagonist **27** and **31** had the slowest dissociation rate constants of (4.7 ± 0.7) x 10^{-5} s^{-1} and (5.3 ± 1.5) x 10^{-5} s^{-1}, respectively, and thus the longest RTs of 376 min and 391 min, respectively. Of note, the long RT antagonist **27** (**Figure 1A**)

Table 3. Binding Affinities and Kinetic Parameters of Pyrido[2,1-*f*]purine-2,4-dione Derivatives with Modification at R_2

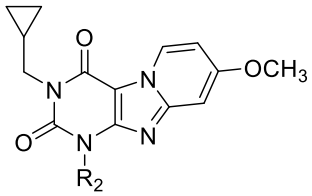

Compd.	R_2	pK_i [a] ± SEM (mean K_i in nM)	KRI[b]	k_{on} [c] (M^{-1} s^{-1})	k_{off} [d] (s^{-1})	RT [e] (min)
2	benzyl	9.0 ± 0.02 (1.0)	2.68 ± 0.48	(2.8 ± 0.5) x 10^6	(6.0 ± 1.7) x 10^{-5}	315 ± 105
24	3-CH_3-benzyl	8.8 ± 0.02 (1.5)	1.18 (1.18; 1.17)	n.d.[f]	n.d.	n.d.
25	4-CH_3-benzyl	9.0 ± 0.1 (0.92)	1.15 (1.03; 1.27)	n.d.	n.d.	n.d.
26	4-CH_2CH_3-benzyl	9.2 ± 0.04 (0.71)	0.81 (0.82; 0.79)	n.d.	n.d.	n.d.
27	3-OCH_3-benzyl	9.4 ± 0.03 (0.38)	2.24 (2.32; 2.15)	(4.8 ± 0.2) x 10^5	(4.7 ± 0.7)x 10^{-5}	376 ± 58
28	4-OCH_3-benzyl	8.9 ± 0.01 (1.4)	1.39 (1.22; 1.55)	(4.8 ± 0.1) x 10^5	(7.8 ± 2.0) x 10^{-5}	250 ± 72
29	3-Cl-benzyl	8.3 ± 0.02 (4.9)	0.89 (1.06; 0.72)	(8.2 ± 1.3) x 10^5	(4.7 ± 0.7) x 10^{-4}	36 ± 5.5
30	4-Cl-benzyl	8.9 ± 0.01 (1.2)	1.11 (1.02; 1.20)	(3.0 ± 0.3) x 10^6	(8.2 ± 0.2) x 10^{-4}	20 ± 0.5
31	3,4-dichlorobenzyl	8.3 ± 0.01 (5.3)	3.12 (3.49; 2.75)	(1.0 ± 0.1) x 10^5	(5.3 ± 1.5) x 10^{-5}	391 ± 137
32	4-Br-benzyl	8.9 ± 0.1 (1.2)	1.19 (1.30; 1.08)	n.d.	n.d.	n.d.
33	phenethyl	8.1 ± 0.04 (7.7)	1.09 (1.21; 0.97)	n.d.	n.d.	n.d.

[a] pK_i ± SEM (n ≥ 3, average K_i value in nM), obtained at 25 °C from radioligand binding assays with [^{3}H]**34** on human Adenosine A_3 receptors stably expressed on CHO cell membranes.

[b] KRI ± SEM (n = 3) or KRI (n = 2, individual estimates in parentheses), obtained at 10 °C from dual-point competition association assays with [^{3}H]**34** on human Adenosine A_3 receptors stably expressed on CHO cell membranes.

[c] k_{on} ± SEM (n ≥ 3), obtained at 10 °C from competition association assays with [^{3}H]**34** on human Adenosine A_3 receptors stably expressed on CHO cell membranes.

[d] k_{off} ± SEM (n ≥ 3), obtained at 10 °C from competition association assays with [^{3}H]**34** on human Adenosine A_3 receptors stably expressed on CHO cell membranes.

[e] RT (min) = 1/(60*k_{off})

[f] n.d. = not determined.

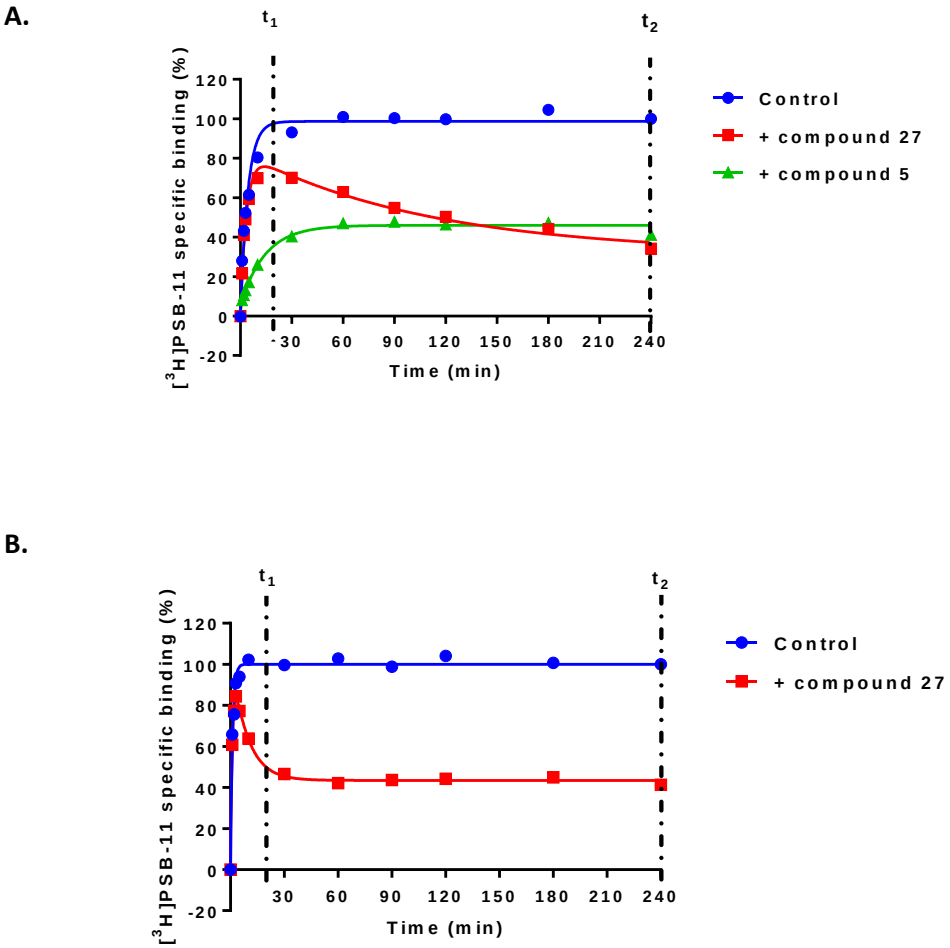

Figure 1: (**A**) Representative competition association assay curves of [^{3}H]**34** in the absence (control) or presence of a long residence time compound **27** and a short residence time compound **5**. Experiments were performed at 10 °C using the compound's respective IC_{50} value at the hA_3R. (**B**) Competition association curves of [^{3}H]**34** in the absence (control) or presence of long residence time compound **27**. Experiments were performed at 25 °C using the compound's respective IC_{50} value at the hA_3R. t_1 is the radioligand binding at 20 min, while t_2 is the radioligand binding at 240 min.

displayed a typical "overshoot" in the competition association curve, indicative of a slower dissociation than the radiolabeled probe [^{3}H]**34,** while the short RT antagonists, exemplified by antagonist **5** (**Figure 1A**) presented more shallow, gradually ascending curves. There was a good correlation between the negative logarithm of the antagonists' dissociation rate constants and their KRI values derived from the kinetic screen (**Figure 2A**), which confirmed that a compound's KRI value

is a good predictor for its dissociation rate constant. Notably, the experimental temperatures in the kinetic assays were lower than in the equilibrium displacement assays (25 °C vs 10 °C), because kinetic studies performed at 25 °C were compromised by the nature of the compounds tested. This is shown in **Figure 1B**, where the "overshoot" of long RT antagonist **27** happened before the t_1 checkpoint of 20 min, which did not happen at 10 °C. A significant correlation was also observed between the antagonist affinities (K_i values) determined in equilibrium displacement experiments and their kinetic K_D values derived from competition association experiments (**Figure 2B**), despite the differences in assay temperature (25 °C vs 10 °C). Interestingly, the kinetic association rate constants (k_{on}) did not show any significant correlation with affinity (**Figure 2C**), whilst the dissociation rate constants (k_{off}) had a fair correlation with affinity (**Figure 2D**).

The representative long RT and short RT antagonists (**27** and **5**) were selective for the hA_3 receptor when compared to other adenosine receptors (i.e. human adenosine A_1 and A_{2A} receptor, **Table S1**). These two antagonists (**27** and **5**) with comparable association rate constants but distinct dissociation rate constants (or RTs) were further analyzed in a [^{35}S]GTPγS binding assay in which we studied the (in)surmountable antagonism induced by the two compounds (**Figure 3**).

Moreover, a k_{on}-k_{off}-K_D "kinetic map" (**Figure 4**) was constructed based on the compounds' divergent affinities (expressed as kinetic K_D values) and kinetics parameters, yielding a division of these antagonists into three different sub-categories: antagonists that show similar k_{off} values (< 2-fold) but due to differing k_{on} values (> 28-fold) have different K_D values (~100-fold, Group A); antagonists that display similar K_D values (< 10-fold) despite showing divergent k_{off} and k_{on} values (17-fold and 30-fold, Group B); antagonists with similar k_{on} values (< 5-fold), but due to differing k_{off} values (~290-fold) have different K_D values (> 110-fold, Group C). Additionally, we applied molecular modeling to compare the binding behavior in some molecular detail of several antagonists with similar affinities (**2** vs **10**; **31** vs **29** or **30**) (**Figure 5**).

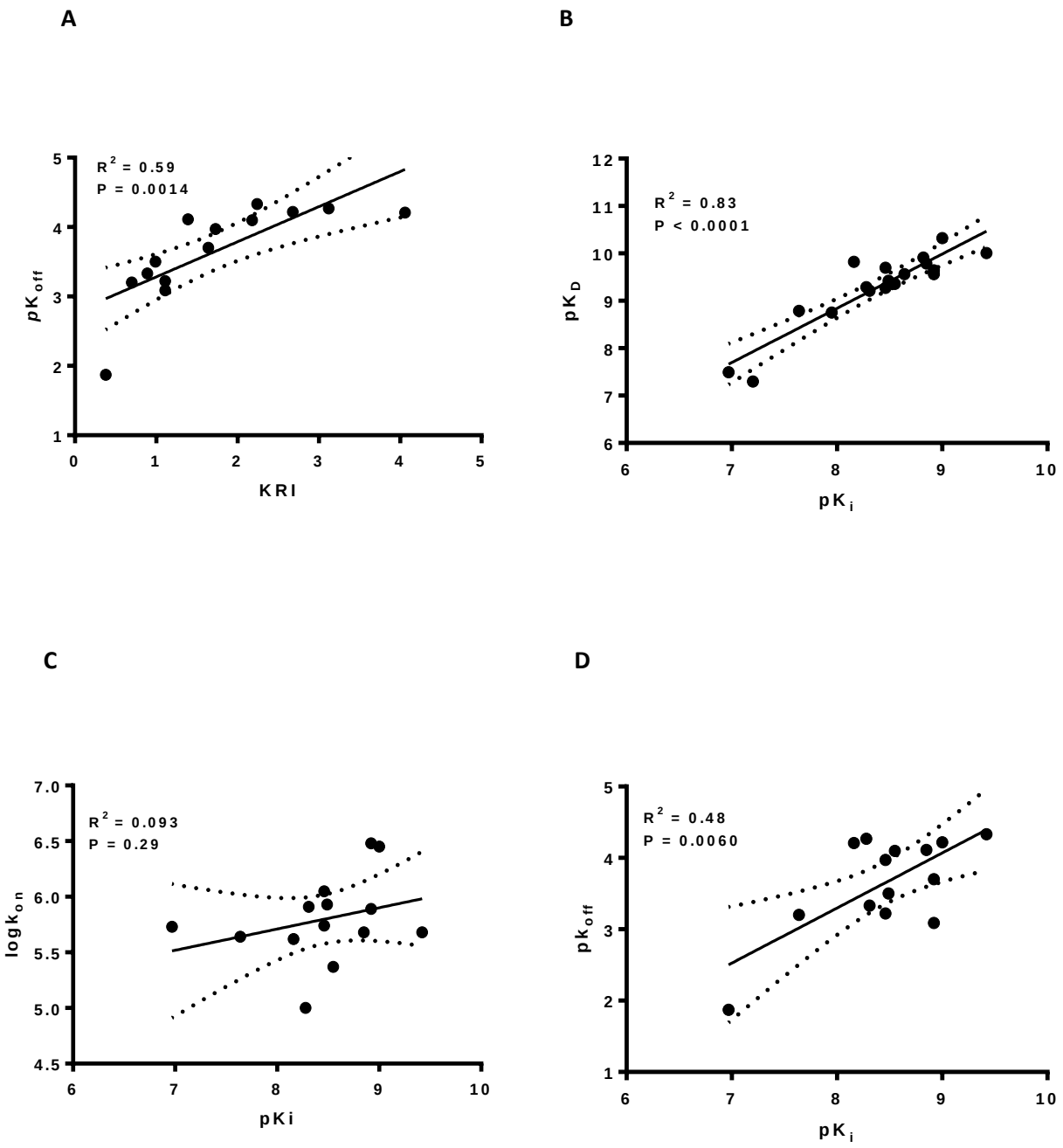

Figure 2: The correlations between the negative logarithm of the human adenosine A_3 receptor antagonists' dissociation rates (pk$_{off}$) and their kinetic rate index (KRI) (**A**), the human adenosine A_3 receptor antagonists' affinity (pK$_i$) and their "kinetic K$_D$" (pK$_D$) (**B**), association rate constants (logk$_{on}$) (**C**), dissociation rate constants (pk$_{off}$) (**D**). The central line corresponds to the linear regression of the data, the dotted lines represent the 95% confidence intervals for the regression. Data used in these plots are detailed in **Tables 1** - **3**. Data are expressed as mean from at least three independent experiments.

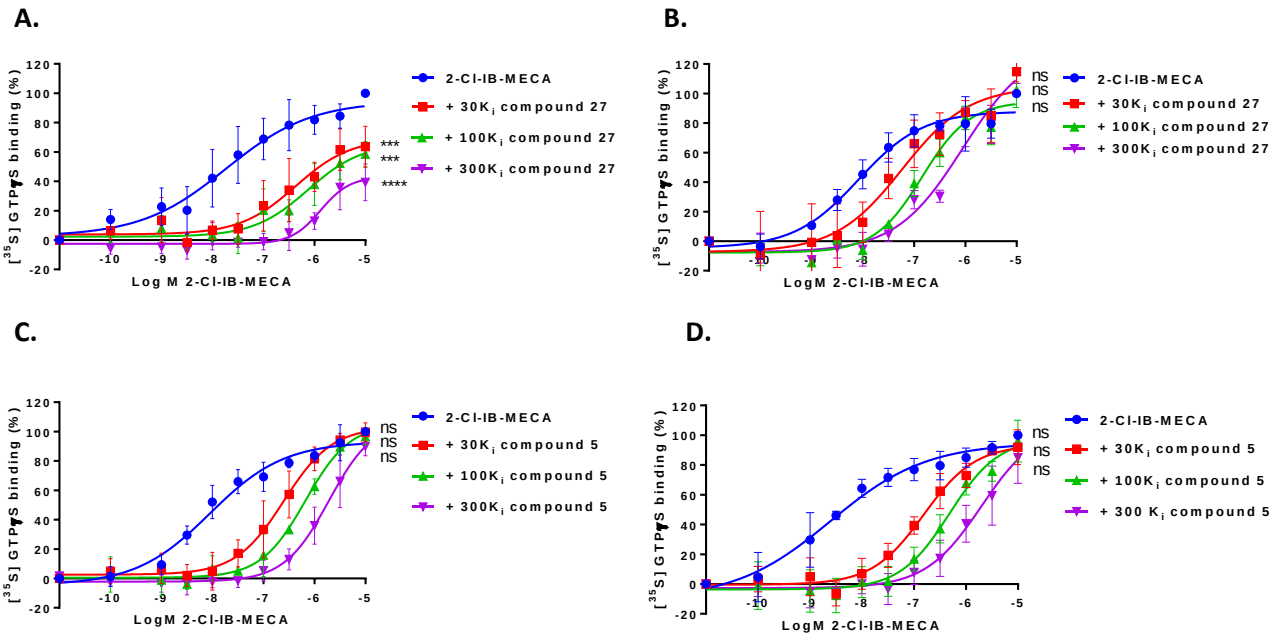

Figure 3: 2-Cl-IB-MECA-stimulated [^{35}S] GTPγS binding to hA_3R stably expressed on CHO cell membranes (25 °C) in the absence or presence of long-residence-time antagonist **27** (**A** and **B**, normalized and combined, n ≥3), or short-residence-time antagonist **5** (**C** and **D**, normalized and combined, n ≥3). Antagonist **27** (**A**), **5** (**C**) were incubated for 60 min prior to the challenge of the hA_3R agonist 2-Cl-IB-MECA, at a concentration ranging from 0.1 nM to 10 µM, for another 30 min. Antagonist **27** (**B**), **5** (**D**) were coincubated with 2-Cl-IB-MECA, at the same concentration range, for 30 min. The agonist curves were generated in the presence of increasing concentrations of antagonists, namely 30-, 100-, 300-fold their respective K_i values. Curves were fitted to a four parameter logistic dose-response equation. Data is from at least three independent experiments performed in duplicate, normalized according to the maximal response (100%) produced by 2-Cl-IB-MECA alone. The shift in agonist EC_{50} values was determined to perform Schild analyses. Two-way ANOVA with Dunnett's post-test was applied for the comparison of E_{max} by agonist control, * $p < 0.05$, ** $p < 0.01$, *** $p < 0.001$, **** $p < 0.0001$, **** $p < 0.0001$, ns for not significant.

Structure-Affinity Relationships (SAR) and Structure-Kinetics relationships (SKR).

According to previous studies from our group,[23, 24] methoxy-substitution at the C^8 position (**Table 1**) of the pyrido[2,1-*f*]purine-2,4-dione scaffold yielded selective hA_3R antagonists with good affinity (3.2 nM for **1** as a reference compound). From our preliminary studies, this methoxy-group appeared important for slow dissociation (**1** vs Compound **S2** from **Figure S1**, **Table S2**). Due to the nanomolar affinity and close-to-unity KRI value of **1**, it was treated as the starting point of this SAR and SKR study, having, on further analysis, an association rate constant of (8.5 ± 1.2) x 10^5 $M^{-1}s^{-1}$ and a

dissociation rate constant of (3.2 ± 0.02) x 10^{-4} s^{-1} (RT = 52 min). Next, we decided to investigate R_1 substitutions (**Table 2**), beginning with antagonist **5** (R_1 = H).

*The substitutions at R_1 (**Table 2**).*

Firstly, an increase in alkyl chain length was investigated, indicating an elongated carbon chain had a cumulative effect on KRI (**5**, **6**, **7**, **8**, **10**, **11)**, with the exception of antagonist **9** (KRI values from 0.38 to 4.06). One could point to a possible correlation between lipophilicities and dissociation rate constants (and consequently RTs) to explain this trend (**Figure S2A**). However, with all of the antagonists kinetically characterized, no such correlation was observed (**Figure S2B**). Therefore other reasons should be taken into account as to why elongating the carbon chain has such a profound effect on the ligand's dissociation rate. The role of membrane-drug interactions in determining the pharmacological profile is a possible reason, especially the role long carbon tails have in such interactions.[28] Interesting to point out is the affinity of antagonist **11** which, had a traditional lead selection process taken place, would most likely have resulted in the elimination of this compound due the more favorable affinity and hydrophilic properties of its shorter carbon chain counterparts (**8** or **9**) (affinities: 6.8 nM vs 1.5 nM or 3.5 nM, KRI values: 4.06 vs 1.29 or 1.11). This would have overlooked the efficacy this compound could offer due to its longer residence time.

Secondly, the presence of a more rigid substitution of the R_1 group of saturated equivalents (antagonists **1** and **8)** led to antagonists **12** and **14**, with similar improvement in the affinity pairs (**12** and **14**: 5.9 nM and 1.4 nM; **1** and **8**: 3.2 nM and 1.5 nM) and KRI values (**12** and **14**: 0.72 and 1.23; **1** and **8**: 0.99 and 1.29). Further rigidification with alkyne (**13**) rather than alkene **(12)** maintained affinities (4.3 nM vs 5.9 nM) and increased KRI values (1.20 vs 0.72). This alkyne could be the starting point for a further study on "click-chemistry" for introducing e.g., fluorescent tags.[29-31]

Thirdly, the introduction of a polar atom or group in antagonist **15** or **16**, respectively, led to a decrease in affinity compared to their non-polar counterpart **1** (23 nM or 81 nM vs 3.2 nM). The

changes in KRI values between antagonist **1** and its polar counterparts **15** and **16** can be considered minor (0.99 vs 0.70 and 1.04). Of note, by comparing affinities and kinetic profiles of polar antagonist **15** with its non-polar equivalent **1**, we found the polarity at the "lipophilic carbon chain" resulted in slower association (k_{on} of (4.3 ± 0.8) x 10^5 $M^{-1}s^{-1}$ vs (8.5 ± 1.2) x 10^5 $M^{-1}s^{-1}$) but faster dissociation (k_{off} of (6.3 ± 0.7) x 10^{-4} s^{-1} vs (3.2 ± 0.02) x 10^{-4} s^{-1}), with a concomitant decrease in affinity (23 nM vs 3.2 nM).

Moreover, the bulkiness of the substituents was studied with branched carbon side chains (**17, 18, 19, 20** and **21**) or aliphatic rings (**2** and **22**). As to the branched carbon side chains, compound affinities remained in the nanomolar range, while in terms of KRI values, 2-carbon-linker branched side chains (**17** and **18**) caused larger KRI values than those of either their linear counterparts (**8** and **9**) or 3-carbon-linear branched side chains (**19** and **20**) (**17:** 1.64 vs 1.29 or 1.39; **18:** 1.73 vs 1.11 or 0.95). Although the association rate constants of **17** and **18** were similar to other antagonists in Table 2, the dissociation rate constants suggest their branched side chains have an extra "anchoring" effect, compared with the linear counterparts. For example, the k_{off} of **18** with a 5-carbon branched side chain was quite similar to **10** or **11** having a 6 or 7-carbon linear side chain ((1.1 ± 0.4) x 10^{-4} s^{-1} vs (8.2 ± 1.3) x 10^{-5} s^{-1} or (6.2 ± 0.2) x 10^{-5} s^{-1}). The presence of a slightly less polar but larger silicon atom (**21**) instead of carbon (**18**) made the KRI value decrease (1.36 vs 1.73), although the affinity remained virtually the same (2.7 nM vs 3.5 nM).

Interestingly, another reported analogue (**2**)[23] of compound **1**, with cyclopropylmethyl substitution at the R_1 group, led to unique kinetic parameters, i.e. a combination of a fast association rate constant ((2.8 ± 0.5) x 10^6 $M^{-1}s^{-1}$ vs (8.5 ± 1.2) x 10^5 $M^{-1}s^{-1}$) and a slow dissociation rate constant ((6.0 ± 1.7) x 10^{-5} s^{-1} vs (3.2 ± 0.02) x 10^{-4} s^{-1}), although the affinities of **2** and **1** were similar (1.0 ± 0.03 nM vs 3.2 ± 0.1 nM, respectively). The RT of compound **2** was the longest in **Table 2** with 315 min. For the antagonist with cyclobutylmethyl (**22**), affinity (2.7 nM vs 1.0 nM) and KRI value (1.48 vs 2.68) were lower than for compound **2**.

Although the dissociation rate constants of the antagonists in **Table 2** varied greatly depending on the R_1 substituent, the association rate constants were more similar (within 5-fold). Association rate constants are often reasoned to be caused by a diffusion limited process whereby the collision rate of ligand and receptor determines the rate of ligand-receptor complex formation.[32] When no conformational changes are required for the receptor and ligand to bind and when taking into account the proportion of the receptor responsible for binding, this sets the association rate constant at observed limits of around 10^7 $M^{-1}s^{-1}$.[33] As the association rate constants for all R_1 substituted compounds were slower than the diffusion limit by at least 3.5 fold (**2**), we hypothesize target engagement for R_1 substituted antagonists is more hampered than imposed by the diffusion limit.

*The substitutions at R_2-group (**Table 3**).*

From **Table 2** we learned that cyclopropylmethyl-substituted antagonist **2** exhibited a kinetic profile as a long RT compound whilst showing the affinity previously reported.[23] As a result, this compound became the starting point for our exploration of the substitutions (*R_2-group*) on the aromatic ring.

Introduction of a non-polar alkyl substituent on antagonist **2**'s benzyl ring (**24, 25, 26**), resulted in a decrease in KRI values (from 2.68 to 0.81), while slight variations in affinity were observed. Then, introduction of a polar methoxy substituent on antagonist **2**'s benzyl ring, led to mixed results with a small decrease in RT at *para*-position, and a slight increase in RT at *meta*-position in **28** (250 min vs 315 min) and **27** (376 min vs 315 min), respectively. In particular, the long residence time for **27** in combination with its sub-nanomolar affinity (0.38 nM), made this compound stand out in the series.

Next, halogen substitutions on antagonist **2**'s benzyl ring were examined. Apparently, the position of halogen substitution is important for affinity as *para*-substitution in antagonist **30** and **32** yielded similar affinity compared to **2** (1.2 nM vs 1.2 nM vs 1.0 nM). The one compound with *meta*-substitution, **29,** showed a 5-fold decrease in affinity compared to **2** (4.9 nM vs 1.0 nM). Dichloro-

substituted compound **31** had the largest KRI value (3.12) among the halogen-substituted antagonists; the *para*-bromo substituted compound **32** was similar in this respect to *para*-chloro substituted **30** (1.19 vs 1.11). In a full competition association experiment we determined the rate constants for **31**, and learned it had the longest RT of all compounds kinetically characterized (391 min), concomitant with the slowest association rate constant of the compounds kinetically characterized ((1.0 ± 0.1) x 10^5 $M^{-1}s^{-1}$). Previous theoretical studies have indicated the strength of halogen bonding can be increased through the introduction of electron withdrawing groups onto halobenzenes.[34] Such would be the case for **31** where the additional chloro substituent forms a stronger halogen bonding interaction with the R_2 binding pocket. Introducing a phenethyl (**33**) rather than benzyl substituent (**2**) led to a decrease in affinity (7.7 nM vs 1.0 nM), whilst the KRI value was also strongly affected (1.09 vs 2.68). This observation parallels our previous findings that the binding pocket for the R_2 substituent is of limited size.[23]

Functional Assay.

Following kinetic characterization, a long (**27**) and a short (**5**) RT compound were chosen for functional characterization in a [^{35}S]GTPγS binding assay, also because for these two compounds the k_{on} values were similar ((4.8 ± 0.2) x 10^5 $M^{-1}s^{-1}$ vs (5.3 ± 1.5) x 10^5 $M^{-1}s^{-1}$). This difference allowed a possible link to be made between RTs and efficacies.

Pretreatment of hA_3 receptor membranes with increasing concentrations of the long RT antagonist **27**, before stimulation by the A_3 receptor agonist 2-Cl-IB-MECA, induced insurmountable antagonism. In other words, the 2-Cl-IB-MECA concentration-effect curves were shifted to the right with a concomitant decrease in the maximal response (**Figure 3A**). Conversely, the short RT antagonist **5** displayed surmountable antagonism, shifting 2-Cl-IB-MECA's curves to the right without affecting its maximum effect (**Figure 3B**).

Table 4. Functional activity of hA_3 receptor antagonists from [^{35}S]GTPγS binding assays

Ligands	RT[a] (min)	Preincubation pA_2[b]	Preincubation Schild slope[b]	Coincubation pA_2[b]	Coincubation Schild slope[b]	Mode of antagonism
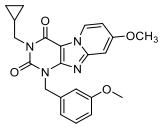 **27**	376 ± 58	N.A.[c]	N.A.	8.9 ± 0.3	0.9 ± 0.2	Competitive insurmountability
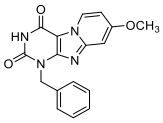 **5**	2.2 ± 1.4	6.8 ± 0.4	1.0 ± 0.3	7.2 ± 0.4	1.0 ± 0.2	Competitive surmountability

[a] RTs were obtained from Tables **1** and **2**.

[b] Obtained from Schild analyses.

[c] N.A.: not applicable.

In this experimental set-up, the Schild-slope of **5** generated from Schild-plots was close to unity (**Table 4**), and the compound's pA_2 value was comparable with its pK_i value (6.8 ± 0.4 vs 7.0 ± 0.02). We also performed co-incubation experiments with these antagonists in the presence of 2-Cl-IB-MECA. In this experimental set-up, all antagonists produced a rightward shift of the 2-Cl-IB-MECA concentration-effect curves without a suppression of the maximal response (**Figure 3C** and **D**). Notably, the Schild-slopes of both long and short RT antagonists (**27** and **5**) were close to unity (0.9 ± 0.2 for **27**, 1.0 ± 0.2 for **5**, **Table 4**). In addition, the pA_2 value of **5** was comparable with the result from the pre-incubation condition (7.2 ± 0.4 vs 6.8 ± 0.4, **Table 4**), and the pA_2 value of **27** was also in agreement with its pK_i value (8.9 ± 0.3 vs 9.4 ± 0.03).

Kinetic Map.

Using the association (k_{on}) and dissociation (k_{off}) rate constants obtained from competition association experiments (**Tables 1**-**3**), a kinetic map (**Figure 4**) was constructed by plotting these values on the *y*-axis and *x*-axis, respectively. The dashed diagonal parallel lines represent the kinetically derived K_D values ($K_D = k_{off}/k_{on}$). Out of this map three subgroups emerged. Group A represents compounds that exhibit similar k_{off} values, but with vastly different k_{on} values. As a consequence a diverse range of K_D values was observed. Previous SKR studies have primarily focused on optimizing dissociation rates and RTs for predicting *in-vivo* efficacy and creating a kinetically favorable ligand. Yet recently, there has been greater acknowledgment of the important role that the association rate constants may play in determining the efficacy of a drug as the result of increased rebinding or increased drug-target selectivity.[19] A kinetic map would thus allow for the selection of compounds with appropriate RTs whilst exploring the role of association rate constants in determining efficacy by choosing a rapidly or slowly associating compound, i.e. **2** or **31** ($(2.8 \pm 0.5) \times 10^6$ $M^{-1}s^{-1}$ vs $(1.0 \pm 0.1) \times 10^5$ $M^{-1}s^{-1}$). Group B displays ligands that exhibit a narrow range of affinity (K_D: 0.1 nM - 1 nM), yet a wide range of k_{off} values that result in RTs ranging from 20 min to 391 min. This information would have gone unnoticed in a traditional SAR hit-to-lead approach and would most likely have led to the selection of high affinity compounds not in possession of a potentially efficacy promoting long residence time. Thus, combining SAR with SKR aspects in lead optimization would allow the selection of not only potent but also long RT compounds through the drug development pipeline. Lastly group C represents compounds that present similar k_{on} values but due to differing k_{off} values show considerable differences in affinities (K_D). This illustrates the differences that were observed in the binding kinetics of the R_1 and R_2 substituents, as group C mainly consists of R_1 substituents (non-cyclopropylmethyl substituents), whilst group A mainly consists of R_2 substituents (cyclopropylmethyl substituents). This difference also suggests a different mode of receptor-ligand interaction during the binding process of the two ligand groups.

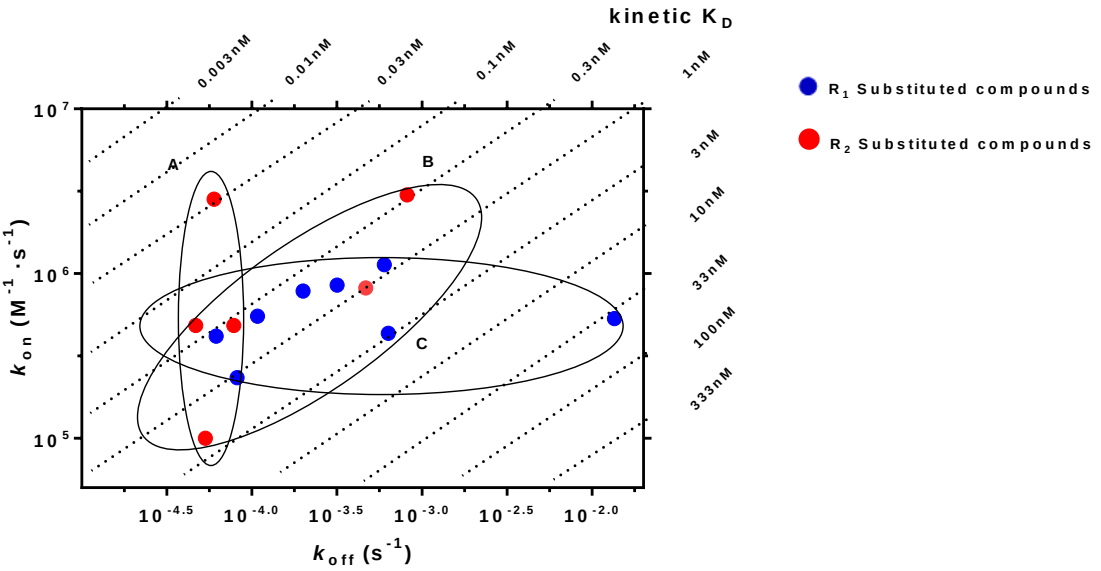

Figure 4: Kinetic map (*y* axis: k_{on} in $M^{-1} \cdot s^{-1}$, *x* axis: k_{off} in s^{-1}) of all compounds that were kinetically characterized in this study. k_{on} and k_{off} values were obtained through competition association assays performed at the hA_3R. The kinetically derived affinity ($K_D = k_{off}/k_{on}$) is represented through diagonal parallel lines. Group A: compounds that show similar k_{off} values but due to differing k_{on} values have different K_D values. Group B: compounds that display similar K_D values despite showing divergent k_{off} and k_{on} values. Group C: compounds with similar k_{on} values, but due to differing k_{off} values have different K_D values.

Altogether, the construction of a kinetic map allows for a more detailed categorization of compounds' affinities as dictated by their kinetic rate constants. In previous studies, such a separation has explained the different therapeutic effects molecules exhibit highlighting the benefits of such an in-depth analysis.[35, 36]

Given the putative link between RT and clinical efficacy, it may be postulated that the lack of hA_3R antagonists progressing from preclinical trials is due to insufficient selection criteria employed in these initial phases of hA_3R drug screening. As previously reported, hA_3R antagonists are reasoned to be beneficial in the treatment of Chronic Obstructive Pulmonary Disease (COPD).[37] For this indication, a number of antagonists are available that act at the muscarinic M_3 receptor.[38] For these therapeutics their dosing regime and thus duration of action have been linked to their RT. For example, aclidinium which requires a twice daily dosing regimen, exhibits a much shorter RT than tiotropium that in turn requires only once daily dosing.[16] This extended duration of action that

enables long-lasting efficacy and practical dosing regimens at the muscarinic M_3 receptor is thought to be a beneficial feature in the treatment of chronic illnesses.[39, 40] As hA_3R antagonists can be used to treat chronic COPD but also a number of other chronic disorders, we could imagine that considering the ligand's kinetic profile early in the drug screening process, would reduce the likelihood of failure due to insufficient efficacy in future clinical trials. Perhaps when selecting hA_3R antagonists with a favorable long RT, i.e. the group A in the kinetic map, will we see the therapeutic potential of the hA_3R fulfilled.

Computational studies.

Finally, we decided to further investigate the ligand-receptor interactions using a homology model of the adenosine A_3 receptor, based on the crystal structure of the adenosine A_{2A} receptor (PDB: 4EIY)[41]. WaterMap calculations were applied to try and explain the variance in kinetic profiles of different ligands by unfavorable hydration[42, 43].

Antagonist **2** (in black stick representation) was docked in the homology model. As a first step it was placed inside the transmembrane bundle, with the tricyclic ring system surrounded by TM3, TM6 and EL2. Hydrogen bonding was constrained between the amide-hydrogen ($-NH_2$, δ^+) from Asn250$^{6.55}$ and the carbonyl-oxygen (-C=O, δ^-) at the C^4-position of the pyrido[2,1-*f*]purine-2,4-dione scaffold (**Figure 5**, left). In order to compare differences between the ligands, an "apo" WaterMap of the hA_3 receptor was generated. Hydration sites shown as red and orange spheres represent positions where "unstable" water molecules are found. Antagonist **10** (hexyl-substitution), with comparable k_{off} ($(8.2 \pm 1.3) \times 10^{-5}$ s^{-1} vs $(6.0 \pm 1.7) \times 10^{-5}$ s^{-1}) to **2** but 10-fold slower k_{on} ($(2.3 \pm 1.0) \times 10^5$ $M^{-1}s^{-1}$ vs $(2.8 \pm 0.5) \times 10^6$ $M^{-1}s^{-1}$), was docked with two different binding modes in the same binding site (**Figure 5**, up-right, cyan and grey sticks). We found additional unstable waters (8, 11, 22 in **Figure 5**, up-right) surrounding the lipophilic substituents of the compounds, which could be explained as hindrance when the antagonist is associating with the binding site.

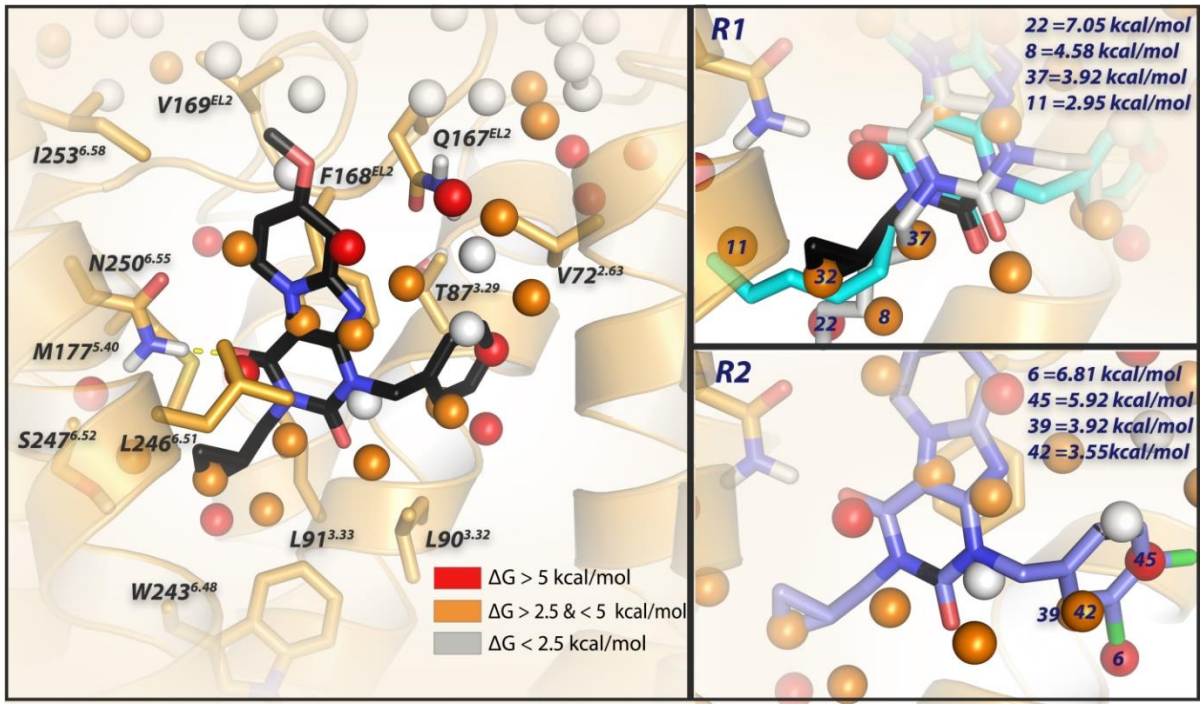

Figure 5. Docking of antagonist **2** into the binding site of the homology model of the adenosine A_3 receptor based on the crystal structure of the adenosine A_{2A} receptor (PDB: 4EIY).[41] Antagonist **2** is represented by black sticks, and residues within 5 Å of **2** are visualized as orange sticks. The protein is represented by orange ribbons. Ligand and residues atoms color code: red = oxygen, blue = nitrogen, white = hydrogen. The overlay of consecutively numbered hydration sites (colored spheres; for color code, see below) were calculated by WaterMap **(Left)**. Hydration sites shown as red and orange spheres represent positions were "unstable" water molecules can be found, which should be displaced by antagonist **2**. White spheres symbolize "stable" water molecules, which are in exchange with the bulk solvent. Two different binding modes are represented for antagonist **10** (cyan and grey sticks), which shows that the flexible hexyl chain can displace different hydration sites (8 for grey and 11 for cyan). For the key hydration sites (8, 11, 22, 32, 37) surrounding the lipophilic "tails", calculated ΔG values (in kcal/mol) with respect to bulk solvent are shown **(Up-right)**. Hydration sites 6, 39, 42 and 45 are proposed to be displaced by the 3,4 di-chloro substituents of **31**; calculated ΔG values (in kcal/mol) with respect to bulk solvent are shown **(Down-right)**.

The same WaterMap was used to investigate the kinetic profile of antagonist **31**. Indeed, hydration sites 6, 39, 42 and 45 are proposed to be displaced by the 3,4-dichloro substituent. Thus, both the association and dissociation of **31** were slowed down by these unstable waters. For the association process, the lipophilic 3,4-dichloro moiety has difficulty in approaching the occupied unstable hydration sites ((1.0 ± 0.1) x 10^5 $M^{-1}s^{-1}$, slowest k_{on} in the whole series); the same lipophilic 3,4-dichloro substituent seems to provide more stabilization to the receptor-ligand complex, thus hampering the dissociation process ((5.3 ± 1.5) x 10^{-5} s^{-1}, slowest k_{off} in the whole series).

Interestingly, by removing a single chloro atom at either the 3- or 4- position on the benzyl-ring (**30** or **29**), association and dissociation rate constants became faster by approximately 10-fold. Although the differences in their k_{on} and k_{off} values were modest (2-3 fold), the unstable hydration sites may prevent the 4-chloro-substituted antagonist **30** from reaching the hydration sites 6, 39 and 42 that interact with the 3-Cl substituent; consequently, both its association and dissociation rate constants were faster than of the 3-chloro-substituted counterpart **29** (k_{on}: (3.0 ± 0.3) x 10^6 $M^{-1}s^{-1}$ vs (8.2 ± 1.3) x 10^5 $M^{-1}s^{-1}$; k_{off}: (8.2 ± 0.2) x 10^{-4} s^{-1} vs (4.7 ± 0.7) x 10^{-4} s^{-1}).

Conclusions

We have demonstrated that, next to affinity, additional knowledge of target binding kinetics is useful for selecting and developing new hA_3R antagonists in the early phase of drug discovery. By introducing proper substituents at the N^3 position or the N^1 benzyl ring of a series of pyridopurinediones, divergences in kinetic profiles were observed, while almost all compounds had high and often similar affinity. Two representative ligands (**5** and **27**) were tested in [^{35}S]GTPγS binding assays, confirming the link between their RTs and their (in)surmountable antagonism. According to these findings, a k_{on}-k_{off}-K_D kinetic map was constructed and subsequently the antagonists were divided into three sub-groups. Additionally, we also performed a computational modelling study that sheds light on the crucial interactions (including with water molecules) for both the association and dissociation kinetics of this family of antagonists. It should be mentioned that the kinetic parameters were derived at the hA_3R, which may be different in e.g., rodents used in advanced animal models. Still, this study suggests that favorable long RTs would be a proper indicator in the development of hA_3R antagonists for chronic inflammatory conditions, e.g. COPD.

Experimental section

Chemistry. All solvents and reagents were purchased from commercial sources and were of analytical grade. Distilled water will be referred to as H_2O. TLC analysis was performed to monitor

the reactions, using Merck silica gel F_{254} plates. Grace Davison Davisil silica column material (LC60A, 30–200 µm) was used to perform column chromatography. Microwave reactions were performed in an Emrys Optimizer (Biotage AB, formerly Personal Chemistry). ^{1}H and ^{13}C NMR spectra were recorded on a Bruker DMX-400 (400 MHz) spectrometer, using tetramethylsilane as internal standard. Chemical shifts are reported in δ (ppm) and the following abbreviations are used: s, singlet; d, doublet; dd, double doublet; t, triplet; m, multiplet. The analytical purity of the final compounds is 95% or higher and was determined by high-performance liquid chromatography (HPLC) with a Phenomenex Gemini 3 µm C18 110A column (50 x 4.6 mm, 3 µm), measuring *UV* absorbance at 254 nm. The sample preparation and HPLC method was as follows: 0.3–0.6 mg of compound was dissolved in 1 mL of a 1:1:1 mixture of CH_3CN/H_2O/t-BuOH and eluted from the column within 15 min at a flow rate of 1.3 mL/min. The elution method was set up as follows: 1–4 min isocratic system of H_2O/CH_3CN/1% TFA in H_2O, 80:10:10; from the 4th min a gradient was applied from 80:10:10 to 0:90:10 within 9 min, followed by 1 min of equilibration at 0:90:10 and 1 min at 80:10:10. Liquid chromatography–mass spectrometry (LC–MS) analyses were performed using a Thermo Finnigan Surveyor—LCQ Advantage Max LC–MS system and a Gemini C18 Phenomenex column (50 x 4.6 mm, 3 µm). The elution method was set up as follows: 1–4 min isocratic system of H_2O/CH_3CN/1% TFA in H_2O, 80:10:10; from the 4th min a gradient was applied from 80:10:10 to 0:90:10 within 9 min, followed by 1 min of equilibration at 0:90:10 and 1 min at 80:10:10.

*1-Benzyl-8-methoxy-1H,3H-pyrido[2,1-f]purine-2,4-dione (**5.**)*[24] 6-Amino-1-benzyluracil (**4**) [25] (10.8 g, 49.7 mmol, 1.00 eq.) was suspended in CH_3CN (370 mL). *N*-bromosuccinimide (17.7 g, 99.4 mmol, 2.00 eq.) was added to the suspension and the mixture was heated at 80 ^{o}C for 1 hour, after which full conversion was shown by TLC (1:9 CH_3OH/CH_2Cl_2 + 3% triethylamine). Subsequently 4-methoxypyridine (15.1 mL, 149.2 mL, 3.00 eq.) was added and the mixture was heated at 80 ^{o}C during 10 hours. Full consumption of the bromo intermediate was shown by TLC (1% CH_3OH/CH_2Cl_2). A precipitate was formed overnight at RT which was collected by filtration and washed with diethyl

ether. This yielded the desired compound as a white solid (10.2 g, 31.6 mmol, 64%). ^{1}H NMR (400MHz, DMSO-d6) δ: 11.11 (s br, 1H), 8.72 (d, *J* = 7.2 Hz, 1H), 7.39-7.29 (m, 4H), 7.28-7.22 (m, 2H), 6.91 (dd, *J* = 7.2, 2.0 Hz, 1H), 5.19 (s, 2H), 3.89 (s, 3H) ppm. NMR was according to literature data.[24]

General procedure for the preparation of N^3-substitited 1-benzyl-8-methoxy-1*H*,3*H*-pyrido[2,1-*f*]purine-2,4-diones (1, 2, 6-22).[24] The compounds were synthesized using the procedure described by *Priego et al.*,[24] but 5 eq. of the alkyl halide was used instead of 1.5 eq. and the reaction mixture was heated to 80 °C overnight in all cases. The pure compounds were obtained by silica column chromatography using a mixture of petroleum ether/ethyl acetate (2:1) as eluent, if not otherwise stated.

*1-Benzyl-8-methoxy-3-propyl-1H,3H-pyrido[2,1-f]purine-2,4-dione (**1**).[24]* The pure product was obtained by column chromatography using petroleum ether/ethyl acetate (1:1) as eluent, yielding a white solid 113 mg, 0.31 mmol, 60%. ^{1}H NMR (400MHz, $CDCl_3$) δ: 8.83 (d, *J* = 7.2 Hz, 1H), 7.54 (d, *J* = 7.2 Hz, 2H), 7.34-7.25 (m, 3H), 6.98 (d, *J* = 2.0 Hz, 1H), 6.74 (dd, *J* = 7.6, 2.8 Hz, 1H), 5.37 (s, 2H), 4.02 (t, *J* = 7.6 Hz, 2H), 3.92 (s, 3H), 1.74 (sextet, *J* = 7.6 Hz, 2H), 0.99 (t, *J* = 7.6 Hz, 3H) ppm.[24] MS $[ESI+H]^+$: calcd for $C_{20}H_{20}N_4O_3$, 364.15; found, 365.0.

*1-Benzyl-3-(cyclopropylmethyl)-8-methoxypyrido[2,1-f]purine-2,4(1H,3H)-dione (**2**).[23]* The pure product was obtained by column chromatography using a mixture of 2% CH_3OH/CH_2Cl_2 as eluent, yielding a white solid, 1.51 g, 3.98 mmol, 86%. ^{1}H NMR (400MHz, $CDCl_3$) δ: 8.82 (d, J = 7.2 Hz, 1H), 7.54 (d, J = 7.2 Hz, 2H), 7.33-7.23 (m, 3H), 6.97 (d, J = 2.4 Hz, 1H), 6.73 (dd, J = 8.4, 2.4 Hz, 1H), 5.37 (s, 2H), 3.94 (d, J = 7.4 Hz, 2H), 3.92 (s, 3H), 1.35-1.25 (m, 1H), 0.47-0.44(m, 4H) ppm. MS $[ESI+H]^+$: calcd for $C_{21}H_{20}N_4O_3$, 376.15; found, 376.9.

*1-Benzyl-8-methoxy-3-methylpyrido[2,1-f]purine-2,4(1H,3H)-dione (**6**).* Reaction was performed in a sealed tube and 50 eq. of methyl iodide was used. The residue was purified by silica column chromatography eluting with a petroleum ether/ethyl acetate (1:1) mixture, yielding a white solid,

25 mg, 0.074 mmol, 15%. ^{1}H NMR (400MHz, $CDCl_3$) δ: 8.83 (d, *J* = 7.6 Hz, 1H), 7.54 (d, *J* = 7.2 Hz, 2H), 7.33-7.24 (m, 3H), 6.99 (d, *J* = 2.4 Hz, 1H), 6.75 (dd, *J* = 7.6, 2.4 Hz, 1H), 5.37 (s, 2H), 3.93 (s, 3H), 3.45 (s, 3H) ppm. MS $[ESI+H]^+$: calcd for $C_{18}H_{16}N_4O_3$, 336.12; found, 337.2.

*1-Benzyl-3-ethyl-8-methoxypyrido[2,1-f]purine-2,4(1H,3H)-dione (**7**).* The pure product was obtained by column chromatography using petroleum ether/ethyl acetate (1:1) as eluent, yielding a white solid, 58 mg, 0.17 mmol, 33%. ^{1}H NMR (400MHz, $CDCl_3$) δ: 8.83 (d, *J* = 7.2 Hz, 1H), 7.54 (d, *J* = 7.2 Hz, 2H), 7.33-7.24 (m, 3H), 6.98 (d, *J* = 2.0 Hz, 1H), 6.74 (dd, *J* = 7.6, 2.8 Hz, 1H), 5.36 (s, 2H), 4.12 (q, *J* = 7.2 Hz, 2H), 3.92 (s, 3H), 1.28 (t, J = 7.2 Hz, 3H) ppm. MS $[ESI+H]^+$: calcd for $C_{19}H_{18}N_4O_3$, 350.14; found, 351.0.

*1-Benzyl-3-butyl-8-methoxypyrido[2,1-f]purine-2,4(1H,3H)-dione (**8**).* Purified by column chromatography using petroleum ether/EtOAc (3:1), yielding a white solid 10 mg, 0.026 mmol, 5%. ^{1}H NMR (400MHz, $CDCl_3$) δ: 8.83 (d, *J* = 7.6 Hz, 1H), 7.54 (d, *J* = 6.8 Hz, 2H), 7.24-7.33 (m, 3H), 6.98 (d, *J* = 2.4 Hz, 1H), 6.74 (dd, *J* = 7.4, 2.6 Hz, 1H), 5.36 (s, 2H), 4.04 (t, *J* = 7.6 Hz, 2H), 3.93 (s, 3H), 1.70-1.64 (m, 2H), 1.40 (sextet, *J* = 3.6 Hz, 2H), 0.95 (t, *J* = 7.2 Hz, 3H) ppm. MS $[ESI+H]^+$: calcd for $C_{21}H_{22}N_4O_3$, 378.17; found, 378.9.

*1-Benzyl-8-methoxy-3-pentyl-1H,3H-pyrido[2,1-f]purine-2,4-dione (**9**).* White solid, 110 mg, 0.28 mmol, yield 56%. ^{1}H NMR (400MHz, $CDCl_3$) δ: 8.83 (d, *J* = 7.6 Hz, 1H), 7.56 (d, *J* = 7.2 Hz, 2H), 7.34-7.25 (m, 3H), 6.97 (d, *J* = 2.0 Hz, 1H), 6.74 (dd, *J* = 7.6, 2.8 Hz, 1H), 5.37 (s, 2H), 4.05 (t, *J* = 7.6 Hz, 2H), 3.93 (s, 3H), 1.72-1.66 (m, 2H), 1.39-1.37 (m, 4H), 0.91 (t, *J* = 7.2 Hz, 3H) ppm. MS $[ESI+H]^+$: calcd for $C_{22}H_{24}N_4O_3$, 392.18; found, 393.1.

*1-Benzyl-3-hexyl-8-methoxypyrido[2,1-f]purine-2,4(1H,3H)-dione (**10**).* White solid, 90 mg, 0.22 mmol, yield 44%. ^{1}H NMR (400MHz, $CDCl_3$) δ: 8.83 (d, *J* = 7.2 Hz, 1H), 7.55 (d, *J* = 6.8 Hz, 2H), 7.34-7.25 (m, 3H), 6.98 (d, *J* = 2.0 Hz, 1H), 6.74 (dd, *J* = 7.6, 2.4 Hz, 1H), 5.37 (s, 2H), 4.05 (t, *J* = 7.6 Hz, 2H),

3.92 (s, 3H), 1.69 (pentet, *J* = 7.6 Hz, 2H), 1.40-1.26 (m, 6H), 0.89 (t, *J* = 7.2 Hz, 3H) ppm. MS $[ESI+H]^+$: calcd for $C_{23}H_{26}N_4O_3$, 406.20; found, 407.1.

*1-Benzyl-3-heptyl-8-methoxypyrido[2,1-f]purine-2,4(1H,3H)-dione (**11**).* Column chromatography using a mixture of petroleum ether/ethyl acetate (3:1) as eluent yielded 131 mg of the pure product as white solid, 0.31 mmol, 62%. 1H NMR (400MHz, $CDCl_3$) ^1H NMR (400MHz, CDCl3) δ: 8.80 (d, *J* = 7.6 Hz, 1H), 7.54 (d, *J* = 6.8 Hz, 2H), 7.32-7.25 (m, 3H), 6.95 (d, *J* = 2.4 Hz, 1H), 6.71 (dd, *J* = 7.2, 2.4 Hz, 1H), 5.35 (s, 2H), 4.03 (t, *J* = 7.6, 2H), 3.90 (s, 3H), 1.67 (pentet, *J* = 7.6 Hz, 2H), 1.38-1.26 (m, 8H), 0.87 (t, *J* = 7.2 Hz, 3H) ppm. MS $[ESI+H]^+$: calcd for $C_{24}H_{48}N_4O_3$, 420.22; found, 421.2.

*3-Allyl-1-benzyl-8-methoxypyrido[2,1-f]purine-2,4(1H,3H)-dione (**12**).* Purified by column chromatography using petroleum ether/ethyl acetate (1:1) as eluent, yielding a white solid, 73 mg, 0.20 mmol, 40%. ^1H NMR (400MHz, $CDCl_3$) δ: 8.82 (d, *J* = 7.6 Hz, 1H), 7.55 (d, *J* = 7.2 Hz, 2H), 7.34-7.25 (m, 3H), 6.99 (d, *J* = 2.0 Hz, 1H), 6.75 (dd, *J* = 7.6, 2.4 Hz, 1H), 6.02-5.92 (m, 1H), 5.38 (s, 2H), 5.29 (dd, *J* = 17.2, 1.2 Hz, 1H), 5.20 (d, *J* = 10.0 Hz, 1H), 4.68 (d, *J* = 5.6 Hz, 2H), 3.93 (s, 3H) ppm. MS $[ESI+H]^+$: calcd for $C_{20}H_{18}N_4O_3$, 362.14; found, 363.0.

*1-Benzyl-8-methoxy-3-(prop-2-yn-1-yl)pyrido[2,1-f]purine-2,4(1H,3H)-dione (**13**).* The pure product was obtained by column chromatography using petroleum ether/ethyl acetate (1:1) as eluent, yielding a white solid, 60 mg, 0.17 mmol, 3%. ^1H NMR (400MHz, $CDCl_3$) δ: 8.82 (d, *J* = 7.2 Hz, 1H), 7.57 (d, *J* = 6.8 Hz, 2H), 7.36-7.26 (m, 3H), 6.99 (d, *J* = 2.4 Hz, 1H), 6.76 (dd, *J* = 7.2, 2.4 Hz, 1H), 5.38 (s, 2H), 4.83 (d, *J* = 2.4 Hz, 2H), 3.94 (s, 3H), 2.19 (t, *J* = 2.4 Hz, 1H) ppm. MS $[ESI+H]^+$: calcd for $C_{20}H_{16}N_4O_3$, 360.12; found, 361.1.

*1-Benzyl-3-(but-3-en-1-yl)-8-methoxypyrido[2,1-f]purine-2,4(1H,3H)-dione (**14**).* White solid, 18 mg, 0.05 mmol, yield 10%. ^1H NMR (400MHz, $CDCl_3$) δ: 8.84 (d, *J* = 7.6 Hz, 1H), 7.54 (d, *J* = 7.2 Hz, 2H), 7.35-7.28 (m, 3H), 7.00 (d, *J* = 2.4 Hz, 1H), 6.77 (dd, *J* = 7.6, 2.4 Hz, 1H), 5.91-5.84 (m, 1H), 5.39 (s,

2H), 5.08 (dd, *J* = 16.8, 1.2 Hz, 1H), 5.02 (d, *J* = 10.4, 1H), 4.15 (t, *J* = 7.2 Hz, 2H), 3.95 (s, 3H), 2.48 (q, *J* = 7.2 Hz, 2H) ppm. MS $[ESI+H]^+$: calcd for $C_{21}H_{20}N_4O_3$, 376.15; found, 376.9.

*1-Benzyl-8-methoxy-3-(2-methoxyethyl)-1H,3H-pyrido[2,1-f]purine-2,4-dione (**15**).* Purified by column chromatography using a mixture of 2% CH_3OH in CH_2Cl_2 yielded the product as a white solid, 70 mg, 0.18 mmol, 37%. ^1H NMR (400MHz, $CDCl_3$) δ: 8.83 (d, *J* = 7.2 Hz, 1H), 7.54 (d, *J* = 6.8 Hz, 2H), 7.33-7.24 (m, 3H), 6.98 (d, *J* = 2.4 Hz, 1H), 6.74 (dd, *J* = 7.6, 2.4 Hz, 1H), 5.36 (s, 2H), 4.30 (t, *J* = 6.0 Hz, 2H), 3.93 (s, 3H), 3.68 (t, *J* = 6.0 Hz, 2H), 3.36 (s, 3H) ppm. MS $[ESI+H]^+$: calcd for $C_{20}H_{20}N_4O_3$, 380.15; found, 380.8.

*1-Benzyl-3-(3-hydroxypropyl)-8-methoxypyrido[2,1-f]purine-2,4(1H,3H)-dione (**16**).* Purified by column chromatography using a mixture of petroleum ether/EtOAc (1:2), followed by recrystallization from CH_3OH/EtOAc. Yield: white solid, 106 mg, 0.28 mmol, 28%. ^1H NMR (400MHz, $CDCl_3$) δ: 8.80 (d, *J* = 7.2 Hz, 1H), 7.53 (d, *J* = 7.6 Hz, 2H), 7.33-7.24 (m, 3H), 6.99 (d, *J* = 2.4 Hz, 1H), 6.76 (dd, *J* = 7.6, 2.4 Hz, 1H), 5.37 (s, 2H), 4.22 (t, *J* = 6.0 Hz, 2H), 3.93 (s, 3H), 3.53 (t, *J* = 5.6 Hz, 2H), 1.92 (pentet, *J* = 5.6 Hz, 2H) ppm. MS $[ESI+H]^+$: calcd for $C_{20}H_{20}N_4O_3$, 380.15; found, 380.9.

*1-Benzyl-3-isobutyl-8-methoxypyrido[2,1-f]purine-2,4(1H,3H)-dione (**17**).* White solid, 0.08 mmol, 29 mg, yield 15%. ^1H NMR (400MHz, $CDCl_3$) δ: 8.86 (d, *J* = 7.2 Hz, 1H), 7.55 (d, *J* = 7.2 Hz, 2H), 7.33-7.28 (m, 3H), 7.00 (d, *J* = 2.0 Hz, 1H), 6.76 (dd, *J* = 7.6, 2.4 Hz, 1H), 5.39 (s, 2H), 3.95 (s, 3H), 3.92 (d, *J* = 7.6 Hz, 2H), 2.22 (nonet, *J* = 7.2 Hz, 1H), 0.97 (d, *J* = 6.8 Hz, 6H) ppm. MS $[ESI+H]^+$: calcd for $C_{21}H_{22}N_4O_3$, 378.17; found, 379.0.

*1-Benzyl-8-methoxy-3-(3-neopentyl)-1H,3H-pyrido[2,1-f]purine-2,4-dione (**18**).* Purified by column chromatography using a mixture of 1% CH_3OH in CH_2Cl_2 as eluent, yielding the product as a white solid, 0.025 mmol, 20mg, 5%. ^1H NMR (400MHz, $CDCl_3$) δ: 8.84 (d, *J* = 7.2 Hz, 1H), 7.52 (d, *J* = 7.2 Hz, 2H), 7.32-7.25 (m, 3H), 6.98 (d, *J* = 2.4 Hz, 1H), 6.73 (dd, *J* = 7.2, 2.4 Hz, 1H), 5.37 (s, 2H), 3.99 (s, 2H), 3.92 (s, 3H), 0.98 (s, 9H) ppm. MS $[ESI+H]^+$: calcd for $C_{22}H_{24}N_4O_3$, 392.18; found, 393.0.

*1-Benzyl-3-isopentyl-8-methoxypyrido[2,1-f]purine-2,4(1H,3H)-dione (**19**).* Yield: white solid, 104 mg, 0.26 mmol, 53%. ^{1}H NMR (400MHz, $CDCl_3$) δ: 8.83 (d, *J* = 7.2 Hz, 1H), 7.53 (d, *J* = 7.2 Hz, 2H), 7.33-7.24 (m, 3H), 6.98 (d, *J* = 2.4 Hz, 1H), 6.74 (dd, *J* = 7.6, 2.4 Hz, 1H), 5.36 (s, 2H), 4.08-4.04 (m, 2H), 3.93 (s, 3H), 1.69 (nonet, *J* = 6.8 Hz, 1H), 1.59-1.53 (m, 2H), 0.98 (d, *J* = 6.4 Hz, 6H) ppm. MS $[ESI+H]^+$: calcd for $C_{22}H_{24}N_4O_3$, 392.18; found, 393.1.

*1-Benzyl-3-(3,3-dimethylbutyl)-8-methoxy-pyrido[2,1-f]purine-2,4(1H,3H)-dione (**20**).* Yield: white solid, 81 mg, 0.20 mmol, 40%. ^{1}NMR (400MHz, $CDCl_3$) δ: 8.84 (d, *J* = 7.6 Hz, 1H), 7.55 (d, *J* = 7.2, 2H), 7.35-7.27 (m, 3H), 6.98 (d, *J* = 2.4 Hz, 1H), 6.74 (dd, *J* = 7.2, 2.4 Hz, 1H), 5.38 (s, 2H), 4.12-4.08 (m, 2H), 3.93 (s, 3H), 1.61-1.57 (m, 2H), 1.04 (s, 9H) ppm. MS $[ESI+H]^+$: calcd for $C_{23}H_{26}N_4O_3$, 406.20; found, 407.1.

*1-Benzyl-8-methoxy-3-((trimethylsilyl)methyl)pyrido[2,1-f]purine-2,4(1H,3H)-dione (**21**).* White solid, 137 mg, 0.34 mmol, yield 67%. ^{1}H NMR (400MHz, $CDCl_3$) δ: 8.84 (d, *J* = 7.2 Hz, 1H), 7.50 (d, *J* = 6.8 Hz, 2H), 7.32-7.24 (m, 3H), 6.98 (d, *J* = 2.4 Hz, 1H), 6.73 (d, *J* = 7.2, 2.4 Hz, 1H), 5.39 (s, 2H), 3.93 (s, 3H), 3.64 (s, 2H), 0.08 (s, 9H) ppm. MS $[ESI+H]^+$: calcd for $C_{21}H_{24}N_4O_3Si$, 408.16; found, 409.2.

*1-Benzyl-3-(cyclobutylmethyl)-8-methoxypyrido[2,1-f]purine-2,4(1H,3H)-dione (**22**).* White solid, 90 mg, 0.23 mmol, yield 46%. ^{1}H NMR (400MHz, $CDCl_3$) δ: 8.82 (d, *J* = 7.2 Hz, 1H), 7.53 (d, *J* = 7.2 Hz, 2H), 7.33-7.13 (m, 3H), 6.69 (d, *J* = 1.8 Hz, 1H), 6.73 (dd, *J* = 7.2, 2.4 Hz, 1H), 5.35 (s, 2H), 4.11 (d, *J* = 7.6 Hz, 2H), 3.92 (s, 3H), 2.83-2.72 (m, 1H), 2.05-1.95 (m, 2H), 1.90-1.79 (m, 4H) ppm. MS $[ESI+H]^+$: calcd for $C_{22}H_{22}N_4O_3$, 390.17; found, 391.2.

*3-(Cyclopropylmethyl)-8-methoxypyrido[2,1-f]purine-2,4(1H,3H)-dione (**23**).*[23] Prepared following a slightly modified procedure described by Priego et al. In total 4 portions of 8 eq. of ammonium formate (after 0, 2, 4 and 6 hours) and 3 portions of 0.15 eq. of 20% $Pd(OH)_2$ (0, 4 and 6 hours) were added, after which full conversion was reached after overnight reflux visualized by TLC (3% CH_3OH/CH_2Cl_2). The reaction mixture was filtered over Celite and the residue extracted 5 times with

hot DMF. The combined organic layer was concentrated *in vacuo* which resulted in a quantitative yield. ^{1}H-NMR in accordance to data in literature.[23]

General procedure for the preparation of N^1-substitited-3-cyclopropylmethyl-8-methoxy-1*H*,3*H*-pyrido[2,1-*f*]purine-2,4-diones (24-33).[23] The compounds were synthesized according to the procedure described by *Priego et al.*[2] Purification by silica column chromatography using an eluent mixture of petroleum ether/ethyl acetate (3:1) yielded the pure final products.

3-(Cyclopropylmethyl)-8-methoxy-1-(3-methylbenzyl)pyrido[2,1-f]purine-2,4(1H,3H)-dione ***(24)****.* White solid, 79 mg, 0.20 mmol, yield 57%. ^{1}H NMR (400MHz, $CDCl_3$) δ: 8.84 (d, *J* = 7.2 Hz, 1H), 7.36 (s, 2H), 7.22 (t, *J* = 7.6 Hz, 1H), 7.09 (d, *J* = 7.6 Hz, 1H), 6.99 (d, *J* = 2.4 Hz, 1H), 6.75 (dd, *J* = 7.2, 2.4 Hz, 1H), 5.36 (s, 2H), 3.97 (d, *J* = 7.2 Hz, 2H), 3.94 (s, 3H), 2.34 (s, 3H), 1.37-1.31 (m, 1H), 0.52-0.45 (m, 4H) ppm. MS $[ESI+H]^+$: calcd for $C_{22}H_{22}N_4O_3$, 390.17; found, 391.0.

*3-(Cyclopropylmethyl)-8-methoxy-1-(4-methylbenzyl)pyrido[2,1-f]purine-2,4(1H,3H)-dione (****25****).*[23]

3-(Cyclopropylmethyl)-1-(4-ethylbenzyl)-8-methoxypyrido[2,1-f]purine-2,4(1H,3H)-dione ***(26)****.* White solid, 43 mg, 0.11 mmol, yield 21%. ^{1}H NMR (400MHz, $CDCl_3$) δ: 8.82 (d, *J* = 7.6 Hz, 1H), 7.48 (d, *J* = 8.0 Hz, 2H), 7.14 (d, *J* = 8.0 Hz, 2H), 6.98 (d, *J* = 2.0 Hz, 1H), 6.73 (dd, *J* = 7.2, 2.4 Hz, 1H), 5.34 (s, 2H), 3.95-3.93 (m, 5H), 2.60 (q, *J* = 7.6 Hz, 2H), 1.34-1.28 (m, 1H), 1.19 (t, *J* = 7.6 Hz, 3H), 0.50-0.42 (m, 4H) ppm. MS $[ESI+H]^+$: calcd for $C_{23}H_{24}N_4O_3$, 404.18; found, 405.2.

3-(Cyclopropylmethyl) -8-methoxy-1-(3-methoxybenzyl)pyrido[2,1-f]purine-2,4(1H,3H)-dione ***(27)****.* White solid, 20 mg, 0.049 mmol, yield 14%. ^{1}H NMR (400MHz, $CDCl_3$) δ: 8.83 (d, *J* = 7.6 Hz, 1H), 7.23 (t, *J* = 8.0 Hz, 1H), 7.15-7.10 (m, 2H), 6.97 (d, *J* = 1.6 Hz, 1H), 6.80 (dd, *J* = 8.4, 2.4 Hz, 1H), 6.74 (dd, *J* = 7.6, 2.4 Hz, 1H), 5.35 (s, 2H), 3.96-3.92 (m, 5H), 3.77 (s, 3H), 1.35-1.28 (m, 1H), 0.50-0.45 (m, 4H) ppm. MS $[ESI+H]^+$: calcd for $C_{22}H_{22}N_4O_4$, 406.16; found, 406.9.

*3-(Cyclopropylmethyl)-8-methoxy-1-(4-methoxybenzyl)pyrido[2,1-f]purine-2,4(1H,3H)-dione (****28****).*[23]

*1-(3-Chlorobenzyl)-3-(cyclopropylmethyl)-8-methoxypyrido[2,1-f]purine-2,4(1H,3H)-dione (**29**).*[23]

*1-(4-Chlorobenzyl)-3-(cyclopropylmethyl)-8-methoxypyrido[2,1-f]purine-2,4(1H,3H)-dione (**30**).*[23]

*3-(Cyclopropylmethyl)-1-(3,4-dichlorobenzyl)-8-methoxypyrido[2,1-f]purine-2,4(1H,3H)-dione (**31**).*[23]

*1-(4-Bromobenzyl)-3-(cyclopropylmethyl)-8-methoxypyrido[2,1-f]purine-2,4(1H,3H)-dione (**32**).* White solid, 22 mg, 0.048 mmol, yield 14%. ^{1}H NMR (400MHz, $CDCl_3$) δ: 8.85 (d, *J* = 7.2 Hz, 1H), 7.46 (s, 4H), 6.99 (d, *J* = 1.6 Hz, 1H), 6.87 (dd, *J* = 7.2, 2.0 Hz, 1H), 5.33 (s, 2H), 3.99-3.85 (m, 5H), 1.34-1.24 (m, 1H), 0.50-0.44 (m, 4H) ppm. MS $[ESI+H]^+$: calcd for $C_{21}H_{19}N_4O_3$, 454.06; found, 455.0.

*3-(Cyclopropylmethyl) -8-methoxy-1-phenylethylpyrido[2,1-f]purine-2,4(1H,3H)-dione (**33**).* White solid, 112 mg, 0.29 mmol, yield 82%. ^{1}H NMR (400MHz, $CDCl_3$) δ: 8.81 (d, *J* = 7.2 Hz, 1H), 7.35-7.25 (m, 4H), 7.20 (t, *J* = 7.2 Hz, 1H), 6.96 (d, *J* = 2.4 Hz, 1H), 6.73 (dd, *J* = 7.2, 2.4 Hz, 1H), 4.40 (t, *J* = 8.0 Hz, 2H), 3.95-3.90 (m, 5H), 3.12 (t, *J* = 8.0 Hz, 2H), 1.32-1.23 (m, 1H), 0.49-0.40 (m, 4H) ppm. MS $[ESI+H]^+$: calcd for $C_{22}H_{22}N_4O_3$, 390.17; found, 391.0.

Biology. *Chemicals and Reagents.* [^{3}H]8-Ethyl-4-methyl-2-phenyl-(8*R*)-4,5,7,8-tetrahydro-1*H*-imidazo[2,1-*i*]-purin-5-one[26] ([^{3}H]**34**, specific activity 56 Ci·mmol^{-1}) was a gift from Prof. C.E. Müller (University of Bonn, Germany). Unlabeled **34** was purchased from Tocris Ltd. (Abingdon, UK). 5'-*N*-ethylcarboxamidoadenosine (NECA) was purchased from Sigma-Aldrich (Steinheim, Germany). Adenosine deaminase (ADA) was purchased from Boehringer Mannheim (Mannheim, Germany). Bicinchoninic acid (BCA) and BCA protein assay reagents were purchased from Pierce Chemical Company (Rockford, IL, USA). Chinese hamster ovary cells stably expressing the human adenosine A_3 receptor ($CHOhA_3$) were a gift from Dr. K-N Klotz (University of Würzburg, Germany). All other chemicals were obtained from standard commercial sources and were of analytical grade.

Cell Culture and Membrane Preparation. Chinese Hamster Ovary (CHO) cells, stably expressing the human adenosine A_3 receptor ($CHOhA_3$), were cultured and membranes were prepared and stored

as previously described[44]. Protein determination was done through use of the bicinchoninic acid (BCA) method[45].

Radioligand Displacement Assay. Membrane aliquots containing ~15 µg of $CHOhA_3$ protein were incubated in a total volume of 100 µL assay buffer (50 mM Tris-HCl, 5 mM $MgCl_2$, supplemented with 0.01% CHAPS and 1 mM EDTA, pH 7.4) at 25 °C for 120 min. Displacement experiments were performed using 6 concentrations of competing antagonist in the presence of a final concentration of ~10 nM [^{3}H] **34**. At this concentration, total radioligand binding did not exceed 10% of that added to prevent ligand depletion. Nonspecific binding (NSB) was determined in the presence of 100 µM NECA. Incubation was terminated by rapid filtration performed on 96-well GF/B filter plates (Perkin Elmer, Groningen, the Netherlands), using a PerkinElmer Filtermate-harvester (Perkin Elmer, Groningen, the Netherlands). After drying the filter plate at 50 °C for 30 min, the filter-bound radioactivity was determined by scintillation spectrometry using the 2450 MicroBeta^2 Plate Counter (Perkin Elmer, Boston, MA).

Radioligand association and dissociation assays. Association experiments were performed by incubating membrane aliquots containing ~15 µg of $CHOhA_3$ membrane in a total volume of 100 µL of assay buffer at 10 or 25 °C with ~10 nM [^{3}H] **34**. The amount of radioligand bound to the receptor was measured at different time intervals during a total incubation of 120 min. Dissociation experiments were performed by preincubating membrane aliquots containing ~15 µg of protein in a total volume of 100 µL of assay buffer at 10 or 25 °C for 60 min. After the preincubation, radioligand dissociation was initiated by the addition of 5 µl 100 µM unlabeled NECA. The amount of radioligand still bound to the receptor was measured at various time intervals for a total of 120 min to ensure that full dissociation from hA_3 receptor was reached. Incubations were terminated and samples were obtained as described under *Radioligand Displacement Assay*.

Radioligand Competition Association Assay. The binding kinetics of unlabeled ligands were quantified using the competition association assay based on the theoretical framework by Motulsky

and Mahan.[46] The competition association assay was initiated by adding membrane aliquots (15 µg/well) at different time points for a total of 240 min to a total volume of 100 µl of assay buffer at 10 °C or 25 °C with ~10 nM [^{3}H] **34** in the absence or presence of a single concentration of competing hA_3R antagonists (i.e. at their IC_{50} value). Incubations were terminated and samples were obtained as described under *Radioligand Displacement Assay*. The "dual-point" competition association assays were designed as described previously,[27] where in this case the two time points were selected at 20 (t_1) and 240 min (t_2).

[^{35}S] GTPγS Binding Assay. The assays were performed by incubating 15 µg of homogenized $CHOhA_3$ membranes in a total volume of 80 µl assay buffer (50 mM Tris-HCl buffer, 5 mM $MgCl_2$, 1 mM EDTA, 0.05% BSA and 1 mM DTT, pH 7.4) supplemented with 1 µM GDP and 5 µg saponin. The assays were performed in a 96-well plate format, where DMSO stock solutions of the compounds were added using a HP D300 Digital Dispenser (Tecan, Männedorf, Switserland). The final concentration of organic solvent per assay point was ≤0.1%. In all cases, the basal level of [^{35}S] GTPγS binding was measured in untreated membrane samples, whereas the maximal level of [^{35}S] GTPγS binding was measured by treatment of the membranes with 10 µM 2-Cl-IBMECA. For the insurmountability experiments, membrane preparations were pre-incubated with or without antagonists (30-, 100-, 300-fold Ki values) for 60 min at 25 °C, prior to the addition of 2-Cl-IBMECA (10 µM to 0.1 nM) and 20 µl [^{35}S] GTPγS (final concentration ~0.3 nM), after which incubation continued for another 30 min at 25 °C. For the surmountability (control) experiments, antagonists and 2-Cl-IBMECA were co-incubated with [^{35}S] GTPγS for 30 min at 25 °C. For all experiments, incubations were terminated and samples were obtained as described under *Radioligand Displacement Assay*, by using GF/B filters (Whatman International, Maidstone, UK).

Data Analysis. All experimental data were analyzed using the nonlinear regression curve fitting program GraphPad Prism 6.0 (GraphPad Software, Inc., San Diego, CA). From displacement assays, IC_{50} values were obtained by non-linear regression analysis of the displacement curves. The obtained

IC_{50} values were converted into K_i values using the Cheng-Prusoff equation to determine the affinity of the ligands.[47] The observed association rates (k_{obs}) derived from both assays were obtained by fitting association data using one phase exponential association. The dissociation rates were obtained by fitting dissociation data to a one phase exponential decay model. The k_{obs} values were converted into association rate constants (k_{on}) using the equation $k_{on} = (k_{obs} – k_{off})/[L]$, where [L] is the amount of radioligand used for the association experiments. The association and dissociation rates were used to calculate the kinetic K_D using the equation $K_D = k_{off}/k_{on}$. Association and dissociation rate constants for unlabeled compounds were calculated by fitting the data into the competition association model using "kinetics of competitive binding":[46]

$$K_A = k_1[L]\cdot 10^{-9} + k_2$$

$$K_B = k_3[I]\cdot 10^{-9} + k_4$$

$$S = \sqrt{(K_A - K_B)^2 + 4\cdot k_1 \cdot k_3 \cdot L \cdot I \cdot 10^{-18}}$$

$$K_F = 0.5(K_A + K_B + S)$$

$$K_S = 0.5(K_A + K_B - S)$$

$$Q = \frac{B_{\max} \cdot k_1 \cdot L \cdot 10^{-9}}{K_F - K_S}$$

$$Y = Q \cdot \left(\frac{k_4 \cdot (K_F - K_S)}{K_F \cdot K_S} + \frac{k_4 - K_F}{K_F} e^{(-K_F \cdot X)} - \frac{k_4 - K_S}{K_S} e^{(-K_S \cdot X)}\right)$$

where k_1 is the k_{on} of the radioligand ($M^{-1}s^{-1}$), k_2 is the k_{off} of the radioligand (s^{-1}), L is the radioligand concentration (nM), I is the concentration of the unlabeled competitor (nM), X is the time (s) and Y is the specific binding of the radioligand (DPM). The control curve (without competitor) from competition association assays generates the k_1 value and the k_2 value was obtained from *Radioligand association and dissociation assays*. With that the k_3, k_4 and B_{max} can be calculated, where k_3 represents the k_{on} ($M^{-1}s^{-1}$) of the unlabeled ligand, k_4 stands for the k_{off} (s^{-1})of the unlabeled ligand and B_{max} equals the total binding (DPM). All competition association data were globally fitted. The residence time (RT, in min) was calculated using the equation $RT = 1/(60*k_{off})$, as k_{off} values are expressed in s^{-1}. [^{35}S] GTPγS binding curves were analyzed by nonlinear regression using "log

(agonist) vs response-variable slope" to obtain potency, inhibitory potency or efficacy values of agonists and inverse agonists/antagonists (EC_{50}, IC_{50} or E_{max}, respectively). In the (in)surmountability assays, Gaddum/Schild EC_{50} shift equations were used to obtain Schild-slopes and pA_2 values; statistical analysis of two-way ANOVA with Tukey's post-test was applied. All experimental values obtained are means of at least three independent experiments performed in duplicate, unless stated otherwise. R^2 and *P* values were calculated using the GraphPad Prism linear regression analysis function. Log*P* (log partition coefficient) values were calculated using Chemdraw Professional 15.0 (Cambridge Soft, Perkin Elmer, Waltham Mass).

Computational studies. A ligand optimized homology model of the hA_3R was generated, following a similar approach as has been used before[48] and using the Maestro software package (Schroedinger Inc, New York). In short: first different homology models were constructed based on the high resolution crystal structure of the adenosine A_{2A} receptor (PDB: 4EIY),[41] and using a sequence alignment from GPCRDB.[49, 50] In the subsequent steps we iteratively optimized the model using Prime.[51-53] During every step the best model was selected based on enrichment (BEDROC-160.9 and ROC). For this we used a set of 100 diverse antagonists from ChEMBL[54] obtained by "Cluster Molecules".[55] We matched 50 decoys to every ligand ionization state, using the DUD-e web service.[56] The final model used here showed excellent enrichment (BEDROC-160.9: 0.55 ROC: 0.80). We introduced a long residence time ligand, **2**, in the putative ligand binding site using Induced fit docking,[57] with H-bond constraints on Asn250$^{6.55}$. Based on this we generated a WaterMap[42, 43] of the apo state of the receptor. Other ligands were docked using core-constrained docking (using the core of **2** as constraints). Figures were rendered using PyMol.[58]

References

1. Meyerhof, W.; Müller-Brechlin, R.; Richter, D. Molecular cloning of a novel putative G-protein coupled receptor expressed during rat spermiogenesis. *FEBS Lett.* **1991,** 284, 155-160.

2. Fredholm, B. B.; IJzerman, A. P.; Jacobson, K. A.; Klotz, K.-N.; Linden, J. International union of pharmacology. XXV. nomenclature and classification of adenosine receptors. *Pharmacol. Rev.* **2001,** 53, 527-552.
3. Jacobson, K. A.; Gao, Z.-G. Adenosine receptors as therapeutic targets. *Nat. Rev. Drug Discov.* **2006,** 5, 247-264.
4. Gessi, S.; Merighi, S.; Varani, K.; Leung, E.; Mac Lennan, S.; Borea, P. A. The A3 adenosine receptor: an enigmatic player in cell biology. *Pharmacol. Ther.* **2008,** 117, 123-140.
5. Jacobson, K. A.; Moro, S.; Kim, Y.-C.; Li, A.-H. A3 adenosine receptors: protective vs. damaging effects identified using novel agonists and antagonists. *Drug Dev. Res.* **1998,** 45, 113-124.
6. Shamama, N.; Luqman, A. K.; Zafar, M. A.; Seemi, F. B. Adenosine A3 receptor: a promising therapeutic target in cardiovascular disease. *Curr. Cardiol. Rev.* **2016,** 12, 18-26.
7. Koscsó, B.; Csóka, B.; Pacher, P.; Haskó, G. Investigational A3 adenosine receptor targeting agents. *Expert Opin. Invest. Drugs* **2011,** 20, 757-768.
8. Fishman, P.; Bar-Yehuda, S.; Synowitz, M.; Powell, J. D.; Klotz, K. N.; Gessi, S.; Borea, P. A. Adenosine receptors and cancer. *Handb. Exp. Pharmacol.* **2009**, 399-441.
9. Zhou, Y.; Schneider, D. J.; Blackburn, M. R. Adenosine signaling and the regulation of chronic lung disease. *Pharmacol. Ther.* **2009,** 123, 105-116.
10. Wilson, C. N.; Nadeem, A.; Spina, D.; Brown, R.; Page, C. P.; Jamal Mustafa, S. Adenosine receptors and asthma. *Handb. Exp. Pharmacol.* **2009**, 10.1007/1978-1003-1540-89615-89619_89611.
11. Wilson, C. N. Adenosine receptors and asthma in humans. *Br. J. Pharmacol.* **2008,** 155, 475-486.
12. Borea, P. A.; Varani, K.; Vincenzi, F.; Baraldi, P. G.; Tabrizi, M. A.; Merighi, S.; Gessi, S. The A3 adenosine receptor: history and perspectives. *Pharmacol. Rev.* **2015,** 67, 74-102.
13. Baraldi, P. G.; Cacciari, B.; Romagnoli, R.; Merighi, S.; Varani, K.; Borea, P. A.; Spalluto, G. A3 adenosine receptor ligands: history and perspectives. *Med. Res. Rev.* **2000,** 20, 103-128.
14. Baraldi, P. G.; Preti, D.; Borea, P. A.; Varani, K. Medicinal chemistry of A3 adenosine receptor modulators: pharmacological activities and therapeutic implications. *J. Med. Chem.* **2012,** 55, 5676-5703.
15. Hasko, G.; Linden, J.; Cronstein, B.; Pacher, P. Adenosine receptors: therapeutic aspects for inflammatory and immune diseases. *Nat. Rev. Drug Discov.* **2008,** 7, 759-770.
16. Guo, D.; Hillger, J. M.; IJzerman, A. P.; Heitman, L. H. Drug-target residence time—a case for G protein-coupled receptors. *Med. Res. Rev.* **2014,** 34, 856-892.
17. Cusack, K. P.; Wang, Y.; Hoemann, M. Z.; Marjanovic, J.; Heym, R. G.; Vasudevan, A. Design strategies to address kinetics of drug binding and residence time. *Bioorg. Med. Chem. Lett.* **2015,** 25, 2019-2027.
18. Copeland, R. A.; Pompliano, D. L.; Meek, T. D. Drug-target residence time and its implications for lead optimization. *Nat. Rev. Drug Discov.* **2006,** 5, 730-739.
19. Copeland, R. A. The drug-target residence time model: a 10-year retrospective. *Nat. Rev. Drug Discov.* **2016,** 15, 87-95.
20. Zeilinger, M.; Pichler, F.; Nics, L.; Wadsak, W.; Spreitzer, H.; Hacker, M.; Mitterhauser, M. New approaches for the reliable in vitro assessment of binding affinity based on high-resolution real-time data acquisition of radioligand-receptor binding kinetics. *EJNMMI Research* **2017,** 7, 22.
21. Guo, D.; Heitman, L. H.; IJzerman, A. P. Kinetic aspects of the interaction between ligand and G protein-coupled receptor: the case of the adenosine receptors. *Chem. Rev.* **2017,** 117, 38-66.
22. Topliss, J. G. A manual method for applying the Hansch approach to drug design. *J. Med. Chem.* **1977,** 20, 463-469.
23. Priego, E.-M.; Pérez-Pérez, M.-J.; von Frijtag Drabbe Kuenzel, J. K.; de Vries, H.; IJzerman, A. P.; Camarasa, M.-J.; Martín-Santamaría, S. Selective human adenosine A3 antagonists based on pyrido[2,1-f]purine-2,4-diones: novel features of hA3 antagonist binding. *ChemMedChem* **2008,** 3, 111-119.

24. Priego, E.-M.; von Frijtag Drabbe Kuenzel, J.; IJzerman, A. P.; Camarasa, M.-J.; Pérez-Pérez, M.-J. Pyrido[2,1-f]purine-2,4-dione derivatives as a novel class of highly potent human A3 adenosine receptor antagonists. *J. Med. Chem.* **2002,** 45, 3337-3344.
25. Kalla, R.; Perry, T.; Elzein, E.; Varkhedkar, V.; Li, X.; Ibrahim, P.; Palle, V.; Xiao, D.; Zablocki, J. Xanthine derivatives as a2b adenosine receptor antagonists. WO2004106337 A1, 2004.
26. Müller, C. E.; Diekmann, M.; Thorand, M.; Ozola, V. [3H]8-Ethyl-4-methyl-2-phenyl-(8R)-4,5,7,8-tetrahydro-1H-imidazo[2,1-i]-purin-5-one ([3H]PSB-11), a novel high-affinity antagonist radioligand for human A3 adenosine receptors. *Bioorg. Med. Chem. Lett.* **2002,** 12, 501-503.
27. Guo, D.; van Dorp, E. J. H.; Mulder-Krieger, T.; van Veldhoven, J. P. D.; Brussee, J.; IJzerman, A. P.; Heitman, L. H. Dual-point competition association assay: a fast and high-throughput kinetic screening method for assessing ligand-receptor binding kinetics. *J. Biomol. Screening* **2013,** 18, 309-320.
28. Vauquelin, G. Cell membranes… and how long drugs may exert beneficial pharmacological activity in vivo. *Br. J. Clin. Pharmacol.* **2016,** 82, 673-682.
29. Hu, M.-H.; Chen, X.; Chen, S.-B.; Ou, T.-M.; Yao, M.; Gu, L.-Q.; Huang, Z.-S.; Tan, J.-H. A new application of click chemistry in situ: development of fluorescent probe for specific G-quadruplex topology. *Sci. Rep.* **2015,** 5, 17202.
30. Kolb, H. C.; Sharpless, K. B. The growing impact of click chemistry on drug discovery. *Drug Discovery Today* **2003,** 8, 1128-1137.
31. Tian, H.; Fürstenberg, A.; Huber, T. Labeling and single-molecule methods yo monitor G protein-coupled receptor dynamics. *Chem. Rev.* **2017,** 117, 186-245.
32. Tummino, P. J.; Copeland, R. A. Residence time of receptor−ligand complexes and Its Effect on Biological Function. *Biochemistry* **2008,** 47, 5481-5492.
33. Smith, G. F. Medicinal chemistry by the numbers: the physicochemistry, thermodynamics and kinetics of modern drug design. In *Prog. Med. Chem.*, Lawton, G.; Witty, D. R., Eds. Elsevier B.V.: Burlington, **2009**; Vol. 48, p 1.
34. Wilcken, R.; Zimmermann, M. O.; Lange, A.; Joerger, A. C.; Boeckler, F. M. Principles and applications of halogen bonding in medicinal chemistry and chemical biology. *J. Med. Chem.* **2013,** 56, 1363-1388.
35. Markgren, P.-O.; Schaal, W.; Hämäläinen, M.; Karlén, A.; Hallberg, A.; Samuelsson, B.; Danielson, U. H. Relationships between structure and interaction kinetics for HIV-1 protease inhibitors. *J. Med. Chem.* **2002,** 45, 5430-5439.
36. Yu, Z.; van Veldhoven, J. P. D.; Louvel, J.; 't Hart, I. M. E.; Rook, M. B.; van der Heyden, M. A. G.; Heitman, L. H.; IJzerman, A. P. Structure–affinity relationships (SARs) and structure–kinetics relationships (SKRs) of Kv11.1 blockers. *J. Med. Chem.* **2015,** 58, 5916-5929.
37. Polosa, R.; Blackburn, M. R. Adenosine receptors as targets for therapeutic intervention in asthma and chronic obstructive pulmonary disease. *Trends Pharmacol. Sci.* **2009,** 30, 528-535.
38. Barnes, P. J. The role of anticholinergics in chronic obstructive pulmonary disease. *Am. J. Med. Supplements* **2004,** 117, 24-32.
39. Tashkin, D. P. Is a long-acting inhaled bronchodilator the first agent to use in stable chronic obstructive pulmonary disease? *Curr. Opin. Pulm. Med.* **2005,** 11, 121-128.
40. Cazzola, M.; Page, C. Long-acting bronchodilators in COPD: where are we now and where are we going? *Breathe* **2014,** 10, 110-120.
41. Liu, W.; Chun, E.; Thompson, A. A.; Chubukov, P.; Xu, F.; Katritch, V.; Han, G. W.; Roth, C. B.; Heitman, L. H.; IJzerman, A. P. Structural basis for allosteric regulation of GPCRs by sodium ions. *Science* **2012,** 337, 232-236.
42. Abel, R.; Young, T.; Farid, R.; Berne, B. J.; Friesner, R. A. Role of the active-site solvent in the thermodynamics of factor Xa ligand binding. *J. Am. Chem. Soc.* **2008,** 130, 2817-2831.
43. Young, T.; Abel, R.; Kim, B.; Berne, B. J.; Friesner, R. A. Motifs for molecular recognition exploiting hydrophobic enclosure in protein–ligand binding. *Proc. Natl. Acad. Sci. U. S. A.* **2007,** 104, 808-813.

44. Heitman, L. H.; Göblyös, A.; Zweemer, A. M.; Bakker, R.; Mulder-Krieger, T.; van Veldhoven, J. P. D.; de Vries, H.; Brussee, J.; IJzerman, A. P. A Series of 2,4-disubstituted quinolines as a new class of allosteric enhancers of the adenosine A3 receptor. *J. Med. Chem.* **2009,** 52, 926-931.
45. Smith, P. K.; Krohn, R. I.; Hermanson, G. T.; Mallia, A. K.; Gartner, F. H.; Provenzano, M. D.; Fujimoto, E. K.; Goeke, N. M.; Olson, B. J.; Klenk, D. C. Measurement of protein using bicinchoninic acid. *Anal. Biochem.* **1985,** 150, 76-85.
46. Motulsky, H. J.; Mahan, L. C. The kinetics of competitive radioligand binding predicted by the law of mass action. *Mol. Pharmacol.* **1984,** 25, 1-9.
47. Cheng, Y.-C.; Prusoff, W. H. Relationship between the inhibition constant (K_i) and the concentration of inhibitor which causes 50 percent inhibition (IC_{50}) of an enzymatic reaction. *Biochem. Pharmacol.* **1973,** 22, 3099-3108.
48. Louvel, J.; Guo, D.; Soethoudt, M.; Mocking, T. A.; Lenselink, E. B.; Mulder-Krieger, T.; Heitman, L. H.; IJzerman, A. P. Structure-kinetics relationships of Capadenoson derivatives as adenosine A 1 receptor agonists. *Eur. J. Med. Chem.* **2015,** 101, 681-691.
49. Isberg, V.; Mordalski, S.; Munk, C.; Rataj, K.; Harpsøe, K.; Hauser, A. S.; Vroling, B.; Bojarski, A. J.; Vriend, G.; Gloriam, D. E. GPCRdb: an information system for G protein-coupled receptors. *Nucleic Acids Res.* **2016,** 44, D356-D364.
50. Munk, C.; Isberg, V.; Mordalski, S.; Harpsøe, K.; Rataj, K.; Hauser, A.; Kolb, P.; Bojarski, A.; Vriend, G.; Gloriam, D. GPCRdb: the G protein-coupled receptor database–an introduction. *Br. J. Pharmacol.* **2016,** 173, 2195-2207.
51. Schrödinger, L. L. C., New York. *Schrödinger Release 2016-3: Prime*, 2016.
52. Jacobson, M. P.; Friesner, R. A.; Xiang, Z.; Honig, B. On the role of the crystal environment in determining protein side-chain conformations. *J. Mol. Biol.* **2002,** 320, 597-608.
53. Jacobson, M. P.; Pincus, D. L.; Rapp, C. S.; Day, T. J.; Honig, B.; Shaw, D. E.; Friesner, R. A. A hierarchical approach to all-atom protein loop prediction. *Proteins: Struct., Funct., Bioinf.* **2004,** 55, 351-367.
54. Gaulton, A.; Bellis, L. J.; Bento, A. P.; Chambers, J.; Davies, M.; Hersey, A.; Light, Y.; McGlinchey, S.; Michalovich, D.; Al-Lazikani, B. ChEMBL: a large-scale bioactivity database for drug discovery. *Nucleic Acids Res.* **2012,** 40, D1100-D1107.
55. Accelrys Software Inc. *Pipeline pilot version 9.2*, Scitegic: 2016.
56. Mysinger, M. M.; Carchia, M.; Irwin, J. J.; Shoichet, B. K. Directory of useful decoys, enhanced (DUD-E): better ligands and decoys for better benchmarking. *J. Med. Chem.* **2012,** 55, 6582-6594.
57. Sherman, W.; Day, T.; Jacobson, M. P.; Friesner, R. A.; Farid, R. Novel procedure for modeling ligand/receptor induced fit effects. *J. Med. Chem.* **2006,** 49, 534-553.
58. Schrödinger, L. L. C., New York. *The PyMOL molecular graphics system, version 1.8* 2016.

Supporting information

The binding affinities of short RT antagonist (**5**) and long RT antagonist (**27**) at human adenosine A_1 and A_{2A} receptors, the KRI values of pyrido[2,1-f]purine-2,4- dione derivatives without methoxy-substitution at C-8 position, the comparison with their methoxy-substituted counterparts, and the correlation between pkoff and Log P of the compounds.

1. Binding affinities of short RT antagonist (**5**) and long RT antagonist (**27**) at human adenosine A_1 and A_{2A} receptors.

Binding affinities of antagonist **5** at hA_1 and hA_{2A} receptors have been reported before,[1] whilst binding affinities of antagonist **27** at hA_1 and hA_{2A} receptors were determined as described previously.[2, 3] Percentage displacement of antagonists (n=2, average) or K_i ± SEM (nM, n=3) at human adenosine A_1 and A_{2A} receptors are listed in **Table S1**.

Table S1. Binding affinities of short RT antagonist (**5**) and long RT antagonist (**27**) at human adenosine A_1 and A_{2A} receptors.

Compound	hA_1 [a]	hA_{2A} [b]
5	49%[c]	10%[c]
27	209 ± 16	24%

[a] Displacement of [^{3}H]DPCPX from CHO cell membranes expressing the human adenosine A_1 receptor. Percentage displacement at 10 µM (n=2, average) or K_i ± SEM (nM, n=3).

[b] Displacement of [^{3}H]ZM241385 from HEK_{293} cell membranes expressing the human adenosine A_{2A} receptor. Percentage displacement at 10 (**5**) or 1 µM (**27**, n=2, average),

[c] Published data.[1]

2. The KRI values of pyrido[2,1-f]purine-2,4-dione derivatives without methoxy-substitution at C-8 position.

The KRI values of pyrido[2,1-f]purine-2,4-dione derivatives without methoxy-substitution at C-8 position were obtained as described under "*the 'dual-point' competition association assays*". Experiments were designed as described previously,[4] where in this case the two time points were selected at 20 (t_1) and 240 min (t_2). The results are listed in **Table S2**.

Table S2. Kinetic Parameters of Pyrido[2,1-*f*]purine-2,4-dione Derivatives without Methoxy-substitution at *C*-8 Position.

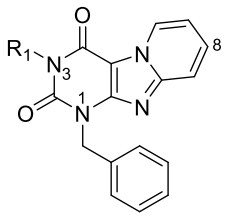

Compound	R_1	KRI[a]
S1	CH_2CH_3	0.61 (0.63,0.59)
S2	$CH_2CH_2CH_3$	0.59 (0.40,0.77)
S3	$CH_2CH(CH_3)_2$	0.88 (0.85,0.90)
S4	$CH_2CH{=}CH_2$	0.88 (0.79,0.96)
S5	$CH_2C{\equiv}CH$	1.16 ± 0.38
S6	$CH_2C_3H_5$	1.01 (1.08,0.93)

[a] KRI ± SEM (n = 3) or KRI (n = 2, individual estimates in parentheses), obtained at 10 °C from dual point competition association assays at 10 °C with [^{3}H]**34** on CHO cell membranes stably expressing the hA_3R.

3. The comparison between the KRI values of pyrido[2,1-f]purine-2,4-dione derivatives without methoxy-substitution at C-8 position and their methoxy-substituted counterparts The comparison is presented in **Figure S1**.

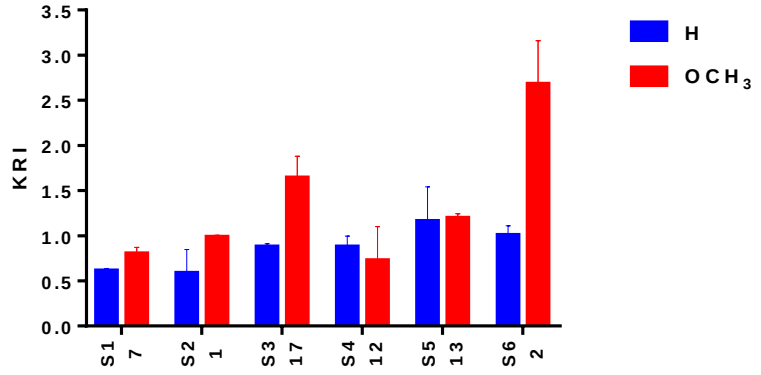

Figure S1: Comparison of KRI values of compounds with (red bars) and without (blue bars) *C*-8 methoxy substitution. KRI values obtained from dual point competition association assay on CHO cells stably expressing hA_3R at 10 °C. Each data point is the average of two or three independent experiments performed in duplicate.

4. The correlation between pk_{off} and LogP for antagonists.

Log*P* values were calculated using Chemdraw Professional 15.0 (Cambridge Soft, Perkin Elmer, Waltham, MA, USA). R^2 and *P* values were calculated using the GraphPad Prism linear regression analysis function. The correlations are presented in **Figure S2**.

A. **B.**

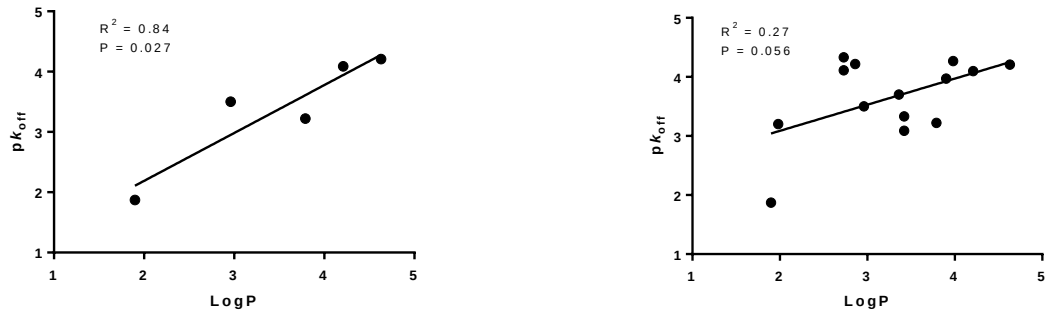

Figure S2: Correlation between pk_{off} and LogP for antagonists with an elongated carbon chain (**1, 5, 9, 10** and **11**) at the R_1 position (A), or for all antagonists (B), obtained from competition association assays.

References

1. Priego, E.-M.; von Frijtag Drabbe Kuenzel, J.; IJzerman, A. P.; Camarasa, M.-J.; Pérez-Pérez, M.-J. Pyrido[2,1-f]purine-2,4-dione derivatives as a novel class of highly potent human A3 adenosine receptor antagonists. *J. Med. Chem.* **2002,** *45*, 3337-3344.

2. Guo, D.; Xia, L.; van Veldhoven, J. P. D.; Hazeu, M.; Mocking, T.; Brussee, J.; IJzerman, A. P.; Heitman, L. H. Binding Kinetics of ZM241385 Derivatives at the human adenosine A_{2A} receptor. *ChemMedChem* **2014,** *9*, 752-761.

3. Xia, L.; de Vries, H.; IJzerman, A. P.; Heitman, L. H. Scintillation proximity assay (SPA) as a new approach to determine a ligand's kinetic profile. A case in point for the adenosine A_1 receptor. *Purinergic Signalling* **2016,** *12*, 115-126.

4. Guo, D.; van Dorp, E. J. H.; Mulder-Krieger, T.; van Veldhoven, J. P. D.; Brussee, J.; IJzerman, A. P.; Heitman, L. H. Dual-point competition association assay: a fast and high-throughput kinetic screening method for assessing ligand-receptor binding kinetics. *J. Biomol. Screening* **2013,** *18*, 309-320.

Chapter 5

A Binding Kinetics Study of Human Adenosine A3 Receptor Agonists

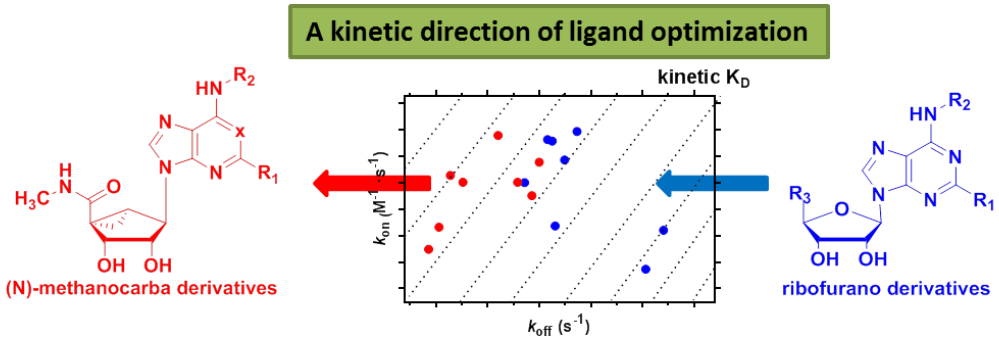

Lizi Xia, Athina Kyrizaki, Dilip K. Tosh, Tirsa T. van Duijl, Jacomina Cornelia Roorda, Kenneth A. Jacobson, Adriaan P. IJzerman, Laura H. Heitman

Adapted from: *Biochem. Pharmacol.* **2018** doi: 10.1016/j.bcp.2017.12.026. [Epub ahead of print]

About this chapter

The human adenosine A_3 (hA_3) receptor has been suggested as a viable drug target in inflammatory diseases and in cancer. So far, a number of selective hA_3 receptor agonists (e.g. IB-MECA and 2-Cl-IB-MECA) inducing anti-inflammatory or anticancer effects are under clinical investigation. Drug-target binding kinetics is increasingly recognized as another pharmacological parameter, next to affinity, for compound triage in the early phases of drug discovery. However, such a kinetics-driven analysis has not yet been performed for the hA_3 receptor. In this study, we first validated a competition association assay for adenosine A_3 receptor agonists to determine the target interaction kinetics. Affinities and Kinetic Rate Index (KRI) values of 11 ribofurano and 10 methanocarba nucleosides were determined in radioligand binding assays. Afterwards, 15 analogues were further selected (KRI <0.70 or KRI >1.35) for full kinetics characterization. The structure-kinetics relationships (SKRs) were derived and longer residence times were associated with methanocarba and enlarged adenine N^6 and C2 substitutions. In addition, from a k_{on}-k_{off}-K_D kinetic map we divided the agonists into three subgroups. A residence time "cliff" was observed, which might be relevant to (N)-methanocarba derivatives' rigid C2-arylalkynyl substitutions. Our findings provide substantial evidence that, next to affinity, additional knowledge of binding kinetics is useful for developing and selecting new hA_3R agonists in the early phase of the drug discovery process.

Introduction

The adenosine A_3 receptor is the youngest member discovered in the family of adenosine receptors (A_1, A_{2A}, A_{2B} and A_3), all of which belong to class A G protein-coupled receptors (GPCR).[1] Unlike the other subtypes, the adenosine A_3 receptor is endogenously activated by both adenosine and inosine.[2] Following agonist activation, the receptor causes a decrease in cAMP levels as it primarily couples to G_i protein. The adenosine A_3 receptor is widely distributed throughout the body, albeit at low expression levels, and its activation can affect numerous organs, tissues and systems. However, this receptor is overexpressed in inflammatory and cancer cells, reflecting its importance as a therapeutic target and biological marker in these tissues.[3, 4] Moreover, the adenosine A_3 receptor is rapidly internalized within 30 min after agonist exposure.[5, 6] It is unresolved whether receptor desensitization terminates agonist-induced signaling or if this signaling persists after internalization.[7]

Since agonists cause effects of anti-inflammation, cardioprotection and neuroprotection, numerous potent and selective agonists have been extensively studied and developed.[8-13] Most of these agonists are derivatives of adenosine, with substitutions on the adenine nucleobase or the ribose moiety. In particular, IB-MECA and 2-Cl-IB-MECA are two potent clinical candidates with excellent bioavailability and safety profiles. Selective hA_3 receptor agonists are being evaluated for the treatment of chronic inflammatory diseases (e.g., rheumatoid arthritis or psoriasis), neuropathic pain and cancer (i.e. hepatocellular carcinoma).[14-17]

Traditional drug discovery approaches mainly focus on affinity, a parameter that is defined under equilibrium conditions. However, it is emerging that selecting ligands based on their affinity alone, does not necessarily predict *in vivo* efficacy very well. This may be due to the dynamic conditions *in vivo*, that often are in contrast to the equilibrium conditions applied in *in vitro* assays.[18] In fact a ligand's kinetic properties may provide a better indication of how a ligand will perform *in vivo.*[19] Notably, the parameter of residence time (RT) has been proposed as a more relevant selection

criterion. The RT reflects the lifetime of the ligand-receptor complex and can be calculated as the reciprocal of the ligand's dissociation constant.[20, 21]

Although the binding kinetics of hA_3 receptor agonists are occasionally reported,[22, 23] a systematic kinetics analysis yielding structure-kinetics relationships (SKRs) has not been conducted. Therefore, we firstly validated the binding kinetics of the prototypical hA_3 receptor agonists (i.e. IB-MECA and 2-Cl-IB-MECA), using radioligand displacement and competition association assays. Then, two series of ribofurano and methanocarba ([3.1.0]bicyclohexane) adenosine derivatives were evaluated for both their affinity (K_i) and kinetics (kinetic rate index values, k_{on}, k_{off}, and RTs). This allowed a complete SKR analysis next to a more traditional SAR study. Afterwards, a retrospective evaluation linking residence times and *in vivo* efficacies was discussed. Last but not least, from a k_{on}-k_{off}-K_D kinetic map we divided the agonists into three subgroups, providing a possible direction for the further development of hA_3R agonists.

Method

Chemicals and reagents. [^{3}H]8-Ethyl-4-methyl-2-phenyl-(8*R*)-4,5,7,8-tetrahydro-1*H*- imidazo[2,1-*i*]-purin-5-one ([^{3}H]PSB-11, specific activity 56 Ci·mmol^{-1}) was obtained with the kind help of Prof. C.E. Müller (University of Bonn, Germany). 5'-*N*-methylcarboxamidoadenosine (MECA) was provided by one of the authors (KAJ). Unlabeled PSB-11, 1-deoxy-1-[6-[((3-Iodophenyl)methyl)amino]-9H-purin-9-yl]-N-methyl-β-D-ribofuranuronamide (IB-MECA), and 2-chloro-N^6-(3-iodobenzyl)-adenosine-5'-N-methyluronamide (2-Cl-IB-MECA) were purchased from Tocris Ltd. (Abingdon, UK). 5'-*N*-ethylcarboxamidoadenosine (NECA) was purchased from Sigma-Aldrich (Steinheim, Germany). LUF5501, LUF5505, LUF5500, LUF5506 and LUF5521 have been synthesized and described previously by de Zwart *et al*.[24]; LUF5595, LUF5586 and LUF5589 have been described by van Tilburg *et al*.[25]; MRS7140, MRS5980, MRS7154, MRS7549, MRS5655, MRS5679, MRS5698, MRS5644, MRS5667 and MRS7294 have been described by Tosh *et al*.[26-29], and MRS3558 by Tchilibon *et al*.[30]. Adenosine deaminase (ADA) was purchased from Boehringer Mannheim (Mannheim, Germany). Bicinchoninic

acid (BCA) and BCA protein assay reagents were purchased from Pierce Chemical Company (Rockford, IL, USA). Chinese hamster ovary (CHO) cells stably expressing the human adenosine A_3 receptor ($CHOhA_3$) were a gift from Dr. K-N Klotz (University of Würzburg, Germany). All other chemicals were obtained from standard commercial sources and were of analytical grade.

Cell culture and membrane preparation. $CHOhA_3$ cells were cultured and membranes were prepared and stored as previously described.[22] Protein determination was done through use of the bicinchoninic acid (BCA) method.[31]

Radioligand equilibrium displacement assays. Membrane aliquots containing ~15 µg of $CHOhA_3$ protein were incubated in a total volume of 100 µL assay buffer (50 mM Tris-HCl, 5 mM $MgCl_2$, supplemented with 0.01% CHAPS and 1 mM EDTA, pH 7.4) at 10 °C for 240 min. Displacement experiments were performed using 6 concentrations of competing agonist in the presence of a final concentration of ~10 nM [^{3}H]PSB-11. At this concentration, total radioligand binding did not exceed 10% of that added to prevent ligand depletion. Nonspecific binding (NSB) was determined in the presence of 100 µM NECA. Incubation was terminated by rapid filtration performed on 96-well GF/B filter plates (Perkin Elmer, Groningen, the Netherlands), using a PerkinElmer Filtermate-harvester (Perkin Elmer, Groningen, the Netherlands). After drying the filter plate at 50 ^oC for 30 min, the filter-bound radioactivity was determined by scintillation spectrometry using the 2450 MicroBeta^2 Plate Counter (Perkin Elmer, Boston, MA).

Radioligand competition association assays. The binding kinetics of unlabeled ligands were quantified using the competition association assay based on the theoretical framework by Motulsky and Mahan.[32] The competition association assay was initiated by adding membrane aliquots (15 µg/well) at different time points for a total of 240 min to a total volume of 100 µl of assay buffer at 10 °C with ~10 nM [^{3}H]PSB-11 in the absence or presence of a single concentration of competing hA_3 receptor agonists (i.e. at their IC_{50} value), and, in some experiments indicated, in the simultaneous presence of 1 mM GTP. Incubations were terminated and samples were obtained as described under

Radioligand Displacement Assay. The "dual-point" competition association assays were designed as described previously,[33] where in this case the two time points were selected at 20 min (t_1) and 240 min (t_2).

Data analysis. All experimental data were analyzed using the nonlinear regression curve fitting program GraphPad Prism 7.0 (GraphPad Software, Inc., San Diego, CA). From displacement assays, IC_{50} values were obtained by non-linear regression analysis of the displacement curves. The obtained IC_{50} values were converted into K_i values using the Cheng-Prusoff equation to determine the affinity of the ligands,[34] using a K_D value for the radioligand of 1.04 nM at 10 °C as determined from radioligand association and dissociation assays, as previously reported.[35] The residence time (RT, in min) was calculated using the equation RT = 1/(60 * k_{off})), as k_{off} is in s^{-1}. Association and dissociation rate constants for unlabeled compounds were calculated by fitting the data into the competition association model using "kinetics of competitive binding":

$$K_A = k_1[L]\cdot 10^{-9} + k_2$$

$$K_B = k_3[I]\cdot 10^{-9} + k_4$$

$$S = \sqrt{(K_A - K_B)^2 + 4\cdot k_1 \cdot k_3 \cdot L \cdot I \cdot 10^{-18}}$$

$$K_F = 0.5(K_A + K_B + S)$$

$$K_S = 0.5(K_A + K_B - S)$$

$$Q = \frac{B_{\max} \cdot k_1 \cdot L \cdot 10^{-9}}{K_F - K_S}$$

$$Y = Q \cdot \left(\frac{k_4 \cdot (K_F - K_S)}{K_F \cdot K_S} + \frac{k_4 - K_F}{K_F} e^{(-K_F \cdot X)} - \frac{k_4 - K_S}{K_S} e^{(-K_S \cdot X)}\right)$$

where k_1 is the k_{on} of the radioligand ($M^{-1}s^{-1}$), k_2 is the k_{off} of the radioligand (s^{-1}), L is the radioligand concentration (nM), I is the concentration of the unlabeled competitor (nM), X is the time (s) and Y is the specific binding of the radioligand (DPM). The control curve (without competitor) from competition association assays generates the k_1 value, and the k_2 value was obtained from previous radioligand association and dissociation assays.[35] With that the k_3, k_4 and B_{max} were calculated,

where k_3 represents the k_{on} ($M^{-1}s^{-1}$) of the unlabeled ligand, k_4 stands for the k_{off} (s^{-1}) of the unlabeled ligand and B_{max} equals the total binding (DPM). All competition association data were globally fitted.

Results

The effects of GTP on affinities and kinetics of the reference hA_3 receptor agonists IB-MECA and 2-Cl-IB-MECA

Firstly, we determined the effects of GTP (1 mM) on both the affinities and binding kinetics of the reference hA_3 receptor agonists IB-MECA and 2-Cl-IB-MECA. Under the two different assay conditions (i.e. in the absence or presence of GTP) the affinities of IB-MECA and 2-Cl-IB-MECA were significantly different (**Table 1**). We observed a rightward shift of the displacement curves in the presence of GTP (**Figure 1A**, closed symbols), representing an approx. 3–fold decrease in affinity for both compounds. Of note, under both experimental conditions, monophasic displacement curves were obtained with pseudo-Hill coefficients close to unity (**Table 1**).

Furthermore, there were significant differences between the kinetics of hA_3 receptor agonists tested in the absence or presence of 1 mM GTP. In the competition association assays without GTP, both IB-MECA and 2-Cl-IB-MECA produced a typical "overshoot", representative of a slower dissociation from the hA_3 receptor than the radioligand [^{3}H]PSB-11 (**Figure 1B**). This overshoot, however, disappeared in the experiments with GTP (**Figure 1C**). Thus, their KRI values were decreased from well-above-unity in the absence of GTP to close-to-unity in the presence of GTP. The k_{off} values of IB-MECA and 2-Cl-IB-MECA determined by the Motulsky-Mahan model[32] were (1.8 ± 0.2) x 10^{-4} s^{-1} and (7.2 ± 1.1) x 10^{-5} s^{-1} in the absence of GTP, respectively (**Table 1**), which were smaller than the corresponding values determined in the presence of GTP (IB-MECA: (8.5 ± 3.0) x 10^{-4} s^{-1}; 2-Cl-IB-MECA: (5.7 ± 1.5) x 10^{-4} s^{-1}, **Table 1**). Consequently, the calculated RTs in the absence of GTP were longer than the values derived when GTP was present (IB-MECA: 95 min vs 20 min; 2-Cl-IB-MECA 231 min vs 29 min, **Table 1**). Last but not least, the k_{on} values of these two agonists determined under the

two assay conditions were similar. Therefore, in order to define a more agonist-relevant receptor interaction, we decided to use the competition association assay in the absence of GTP for the determination of the affinities and the binding kinetics of other unlabeled hA_3 receptor agonists in the remainder of the study.

Table 1. The effects of GTP (1 mM) on the affinities and kinetics of hA_3 receptor agonists IB-MECA and 2-Cl-IB-MECA.

Agonists	pK_i (mean K_i in nM)[a]	Hill Slope[a]	KRI[b]	k_{on} (M^{-1} s^{-1})[c]	k_{off} (s^{-1})[d]	RT (min)[e]	Kinetic K_D (mean pK_D)[f]
no GTP							
IB-MECA	8.5 ± 0.07 *** (2.9)	-0.94 ± 0.05 ns	1.55 ± 0.07 **	(5.9 ± 0.9) x 10^5 ns	(1.8 ± 0.2) x 10^{-4} ns	95 ± 13 *	0.30 ± 0.06 (9.5)
2-Cl-IB-MECA	8.5 ± 0.1* (3.5)	-0.85 ± 0.21 ns	2.02 ± 0.06 ***	(4.0 ± 0.5) x 10^5 ns	(7.2 ± 1.1) x 10^{-5} *	231 ± 34 *	0.18 ± 0.04 (9.7)
+ 1 mM GTP							
IB-MECA	8.0 ± 0.02 (11)	-0.99 ± 0.07	0.99 ± 0.08	(4.5 ± 2.5) x 10^5	(8.5 ± 3.0) x 10^{-4}	20 ± 7	1.9 ± 1.2 (8.7)
2-Cl-IB-MECA	8.0 ± 0.08 (10)	-1.1 ± 0.1	1.07 ± 0.07	(4.0 ± 2.3) x 10^5	(5.7 ± 1.5) x 10^{-4}	29 ± 8	1.4 ± 0.9 (8.9)

[a] pKi ± SEM (n ≥ 3, mean K_i value in nM), obtained from radioligand binding assays with [^{3}H]PSB-11 on the hA_3 receptor stably expressed on CHO cell membranes.

[b] KRI ± SEM (n = 3) obtained from dual-point competition association assays with [^{3}H]PSB-11 on the hA_3 receptor stably expressed on CHO cell membranes.

[c] k_{on} ± SEM (n ≥ 3), obtained from competition association assays with [^{3}H]PSB-11 on the hA_3 receptor stably expressed on CHO cell membranes.

[d] k_{off} ± SEM (n ≥ 3), obtained from competition association assays with [^{3}H]PSB-11 on the hA_3 receptor stably expressed on CHO cell membranes.

[e] RT = 1/(60*k_{off}); RT is expressed in min, whereas k_{off} is expressed in s^{-1}.

[f] $K_D = k_{off}/k_{on}$

Student's t-test was applied for the comparison of values of pK_i, KRI, k_{on}, k_{off}, RT obtained in the absence vs presence of GTP (1 mM) in the assay conditions, ***p < 0.0005, **p < 0.005, * p < 0.05, ns for not significant

A.

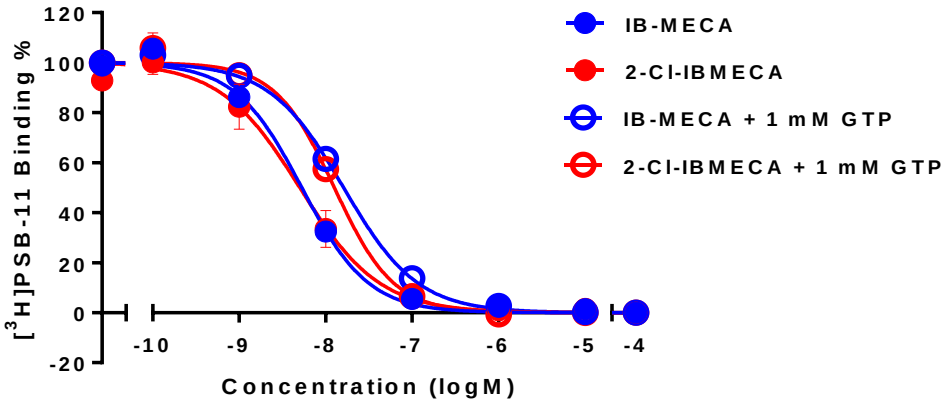

B.

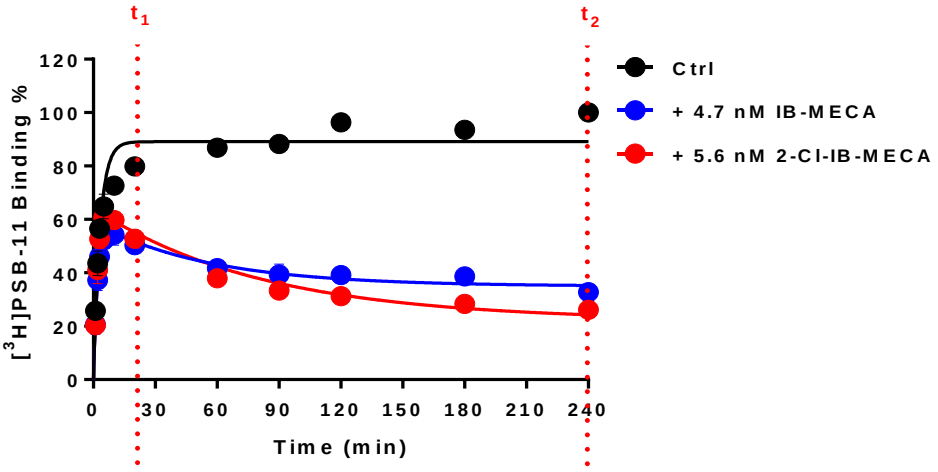

C.

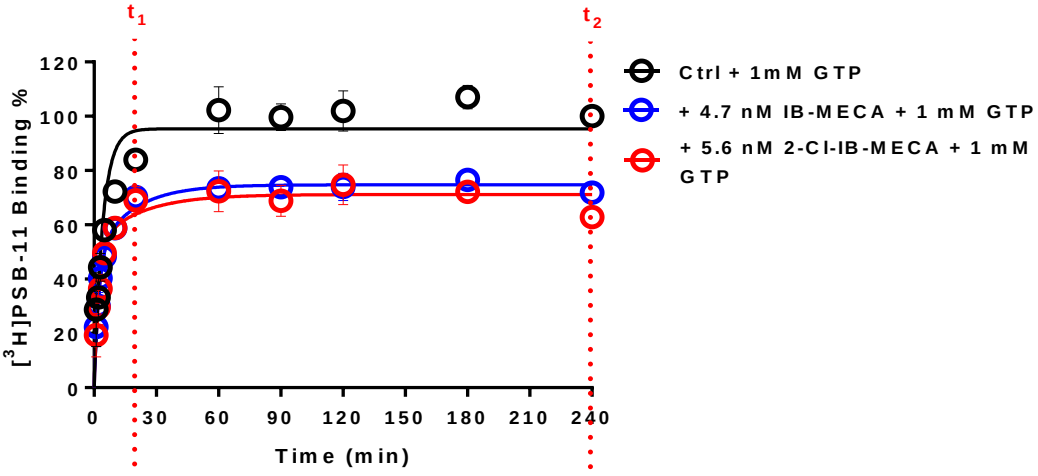

Figure 1: Displacement of specific [^{3}H]PSB-11 binding from the recombinant hA_3 receptor stably expressed on CHO cell membranes by IB-MECA and 2-Cl-IB-MECA in the absence (closed symbols) or presence of 1 mM GTP (open symbols) (**A**); [^{3}H]PSB-11 competition association experiments in the absence (**B**) or presence (**C**) of 1 mM GTP with IB-MECA (blue) or 2-Cl-IB-MECA (red). Combined graphs are shown from at least three experiments performed in duplicate (see **Table 1** for pK_i values and kinetic parameters). Note, t_1, t_2 are indicated, which are the two time points used in KRI determinations.

Binding affinity (K_i) of hA_3 receptor agonists

The binding affinities of 22 human A_3 receptor agonists in total were determined in equilibrium radioligand displacement studies. All agonists were able to concentration-dependently inhibit specific [^{3}H]PSB-11 binding to the human A_3 receptor and their affinities are listed in **Tables 2** and **3**. The agonists displayed moderate to high binding affinities, ranging from 82 nM for agonist MRS5679 to 0.72 nM for agonist MRS5980, while the reference agonists IB-MECA and 2-Cl-IB-MECA had an affinity of 2.9 and 3.5 nM, respectively.

Kinetic Rate Index (KRI) values of hA_3 receptor agonists

Subsequently, these hA_3 receptor agonists were screened in what is termed a "dual-point" competition association assay. The specific binding of [^{3}H]PSB-11 was measured after 20 and 240 minutes in the absence and presence of a single concentration (i.e. IC_{50}) of unlabeled hA_3 receptor agonists, which yielded their Kinetic Rate Index (KRI). The KRI values of the hA_3 receptor agonists ranged from 0.64 (LUF5501) to 5.56 (MRS5679) (**Tables 2** and **3**). Agonists with a KRI value larger than unity are considered to have a slower dissociation rate, and thus a longer RT, than the radioligand used, i.e. [^{3}H]PSB-11, and *vice versa.* Agonists having KRI values below 0.70 (LUF5501 and LUF5505) or above 1.35 (LUF5521, IBMECA to LUF5595, LUF5589, MRS7140, MRS5980, and MRS7154 to MRS5667) were selected for further kinetic profiling.

Table 2. Binding Affinities and Kinetic Parameters (KRI, k_{on}, k_{off}, RT and K_D) for ribofurano derivatives as hA_3 receptor agonists.

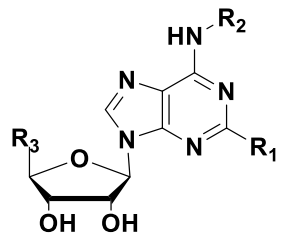

Agonists	R_1	R_2	R_3	pKi (mean K_i in nM) [a]	KRI [b]	k_{on} ($M^{-1}s^{-1}$) [c]	k_{off} (s^{-1}) [d]	RT (min) [e]	Kinetic K_D (mean pK_D)[f]
LUF5501	H	-Ph-3-Cl	$-CH_2OH$	7.5 ± 0.02 (31)	0.64 (0.53; 0.75)	(1.7 ± 0.2) x 10^5	(1.6 ± 0.2) x 10^{-3}	10 ± 1.3	9.2 ± 1.4 (8.0)
LUF5505	H	-Ph-3-Br	$-CH_2OH$	7.1 ± 0.1 (78)	0.65 (0.63; 0.66)	(8.8 ± 1.4) x 10^4	(1.1 ± 0.04) x 10^{-3}	16 ± 0.6	12 ± 1.9 (7.9)
LUF5500	H	-Ph-4-Cl	$-CH_2OH$	7.3 ± 0.03 (51)	0.98 (0.95; 1.01)	N.D.	N.D.	N.D.	N.D.
LUF5506	H	-Ph-4-I	$-CH_2OH$	7.6 ± 0.08 (29)	0.99 (0.98; 1.00)	N.D.	N.D.	N.D.	N.D.
LUF5521	H	-Ph-4-I	$-CONHCH_2CH_3$	7.9 ± 0.06 (14)	2.06 ± 0.82	(1.9 ± 0.3) x 10^5	(1.4 ± 0.1) x 10^{-4}	117 ± 12	0.76 ± 0.13 (9.1)
MECA	H	$-CH_2Ph$	$-CONHCH_3$	7.4 ± 0.04 (42)	1.24 ± 0.09	N.D.[h]	N.D.	N.D.	N.D.

IB-MECA[g]	H	-CH_2Ph-3-I	-$CONHCH_3$	8.5 ± 0.07 (2.9)	1.55 ± 0.07	(5.9 ± 0.9) x 10^5	(1.8 ± 0.2) x 10^{-4}	95 ± 13	0.30 ± 0.06 (9.5)
2-Cl-IB-MECA[g]	-Cl	-CH_2Ph-3-I	-$CONHCH_3$	8.5 ± 0.1 (3.5)	2.02 ± 0.06	(4.0 ± 0.5) x 10^5	(7.2 ± 1.1) x 10^{-5}	231 ± 34	0.18 ± 0.04 (9.7)
LUF5595	-Cl	-CH_2Ph-3-I	-$CH_2OC_3H_5$	8.5 ±0.09 (3.2)	1.37 (1.39; 1.35)	(9.6 ± 3.1) x 10^5	(2.3 ± 1.0) x 10^{-4}	72 ± 30	0.24 ± 0.13 (9.6)
LUF5586	H	-CH_2Ph-3-I	-$CH_2OCH_2CH_3$	8.6 ± 0.04 (2.8)	1.30 (1.30; 1.29)	N.D.	N.D.	N.D.	N.D.
LUF5589	-Cl	-CH_2Ph-3-I	-$CH_2OCH_2CH_3$	8.7 ± 0.08 (2.2)	1.66 ± 0.21	(8.4 ± 0.7) x 10^5	(1.2 ± 0.3) x 10^{-4}	138 ± 37	0.14 ± 0.04 (9.8)
MRS7294	-C≡C-C_4H_2S-5-Cl	-CH_3	-CH_2OH	8.4 ± 0.05 (3.7)	1.63 (1.50; 1.75)	(8.2 ± 3.8) x 10^5	(1.3 ± 0.2) x 10^{-4}	125 ± 14	0.16 ± 0.02 (9.8)

[a] pKi ± SEM (n ≥ 3, mean K_i value in nM), obtained from radioligand binding assays with [^{3}H]PSB-11 on the hA_3 receptor stably expressed on CHO cell membranes.

[b] KRI ± SEM (n = 3) or KRI (n1,n2) (n = 2), obtained from dual-point competition association assays with [^{3}H]PSB-11 on the hA_3 receptor stably expressed on CHO cell membranes.

[c] k_{on} ± SEM (n ≥ 3), obtained from competition association assays with [^{3}H]PSB-11 on the hA_3 receptor stably expressed on CHO cell membranes.

[d] k_{off} ± SEM (n ≥ 3), obtained from competition association assays with [^{3}H]PSB-11 on the hA_3 receptor stably expressed on CHO cell membranes.

[e] RT = 1/(60 * k_{off}); RT is expressed in min, whereas k_{off} is expressed in s^{-1}.

[f] $K_D = k_{off}/k_{on}$, expressed in nM

[g] values taken from **Table 1**

[h] N.D. = not determined

Table 3. Binding Affinities and Kinetic Parameters (KRI, k_{on}, k_{off}, RT and K_D) for (N)-methanocarba derivatives as hA_3 receptor agonists.

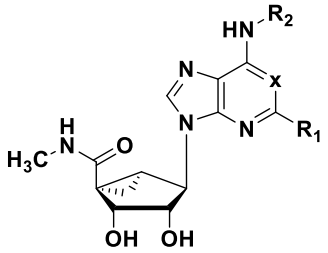

Agonists	X	R_1	R_2	pKi (mean K_i value in nM) [a]	KRI [b]	k_{on} ($M^{-1}s^{-1}$) [c]	k_{off} (s^{-1}) [d]	RT (min) [e]	Kinetic K_D (mean pK_D)[f]
MRS7294 [g]	N	-C≡C-C_4H_2S-5-Cl	-CH_3	8.4 ± 0.05 (3.7)	1.63 (1.50; 1.75)	(8.2 ± 3.8) x 10^5	(1.3 ± 0.2) x 10^{-4}	125 ± 14	0.16 ± 0.02 (9.8)
MRS5980	N	-C≡C-C_4H_2S-5-Cl	-CH_3	9.2 ± 0.09 (0.72)	1.97 (1.87; 2.06)	(9.0 ± 2.3) x 10^5	(4.0 ± 1.0) x 10^{-5}	417 ± 104	0.044 ± 0.016 (10.4)
MRS7140	C	-C≡C-C_4H_2S-5-Cl	-CH_3	8.3 ± 0.08 (5.2)	1.94 (1.82; 2.07)	(3.2 ± 1.2) x 10^5	(8.5 ± 0.3) x 10^{-5}	196 ± 8	0.27 ± 0.10 (9.6)
MRS7154	N	-C≡C-C_4H_2S-5-Cl	-$CH_2CH_2CH_3$	8.7 ± 0.06 (2.2)	1.67 (1.75; 1.59)	(4.0 ± 0.7) x 10^5	(6.2 ± 1.2) x 10^{-5}	270 ± 51	0.15 ± 0.04 (9.8)
MRS3558	N	-Cl	-CH_2Ph-3-Cl	9.1 ± 0.2 (1.0)	1.49 (1.33; 1.64)	(5.7 ± 0.8) x 10^5	(1.0 ± 0.2) x 10^{-4}	167 ± 39	0.18 ± 0.05 (9.8)

MRS5655	N	-C≡C-Ph	-CH_2Ph-3-Cl	8.5 ± 0.09 (3.6)	2.58 (2.05; 3.12)	(4.0 ± 0.8) x 10^5	(1.8 ± 0.3) x 10^{-5}	909 ± 165	0.046 ± 0.013 (10.3)
MRS5644	N	-C≡C-Ph	-CH_3	8.6 ± 0.01 (2.4)	2.42 (2.28; 2.56)	(4.5 ± 1.8) x 10^5	(1.4 ± 0.2) x 10^{-5}	1205 ± 174	0.031 ± 0.013 (10.5)
MRS5698	N	-C≡C-(3,4-di-F-Ph)	-CH_2Ph-3-Cl	8.1 ± 0.2 (9.4)	4.21 (3.75; 4.67)	(1.3 ± 0.4) x 10^5	(8.5 ± 0.7) x 10^{-6}	1961 ± 154	0.068 ± 0.020 (10.2)
MRS5679	N	-C≡C-(4-biphenyl)	-CH_2Ph-3-Cl	7.1 ± 0.05 (82)	5.56 (6.00; 5.11)	undefined	undefined	undefined	undefined
MRS5667	N	-C≡C-(4-biphenyl)	-CH_3	8.3 ± 0.05 (4.6)	3.34 (3.14; 3.55)	(1.8 ± 0.3) x 10^5	(1.1 ± 0.3) x 10^{-5}	1563 ± 464	0.058 ± 0.020 (10.2)

[a] pKi ± SEM (n ≥ 3, mean K_i value in nM), obtained from radioligand binding assays with [^{3}H]PSB-11 on the hA_3 receptor stably expressed on CHO cell membranes.

[b] KRI ± SEM (n = 3) or KRI (n1,n2) (n = 2), obtained from dual-point competition association assays with [^{3}H]PSB-11 on the hA_3 receptor stably expressed on CHO cell membranes.

[c] k_{on} ± SEM (n ≥ 3), obtained from competition association assays with [^{3}H]PSB-11 on the hA_3 receptor stably expressed on CHO cell membranes.

[d] k_{off} ± SEM (n ≥ 3), obtained from competition association assays with [^{3}H]PSB-11 on the hA_3 receptor stably expressed on CHO cell membranes.

[e] RT = 1/(60 * k_{off}); RT is expressed in min, whereas k_{off} is expressed in s^{-1}.

[f] $K_D = k_{off}/k_{on}$, expressed in nM

[g] MRS7294 has a ribofurano ring (see also **Table 2**).

Binding kinetics of selected hA_3 receptor agonists using the competition association assay

Next, the kinetic binding parameters of selected agonists that had either low or high KRI values were determined using the competition association assay with [^{3}H]PSB-11. Association rate constants varied by only 11-fold, ranging from (8.8 ± 1.4) x 10^4 $M^{-1}s^{-1}$ for LUF5505 to (9.6 ± 3.1) x 10^5 $M^{-1}s^{-1}$ for LUF5595 (**Tables 2** and **3**). There was a more pronounced 188-fold difference in dissociation rate constants, in line with the divergent KRI values (LUF5501: (1.6 ± 0.2) x 10^{-3} s^{-1} vs MRS5698: (8.5 ± 0.7) x 10^{-6} s^{-1}). The shortest RT agonist, LUF5501, presented a gradually ascending curve in the competition association assays (**Figure 2A**). Of note, the dissociation of MRS5679**,** with the largest KRI value (5.56), was determined as very slow and not readily quantitated under the current method. The very prominent "overshoot" in the competition association curve was already indicative of a much slower dissociation rate than [^{3}H]PSB-11 (**Figure 2B**). Notably, a significant correlation between the negative logarithm of the dissociation rate constants for the selected agonists and their KRI values derived from the kinetic assays was obtained (**Figure 3A**), which confirmed that a compound's KRI value is a good predictor for its dissociation rate constant. Besides, a significant correlation was also observed between the agonist affinities (pK_i values) determined in equilibrium displacement experiments and their pK_D values ("kinetic K_D values") derived from competition association experiments, although the pK_D values were on average one log unit higher than the pK_i values (**Figure 3B**). As to the kinetic rate constants (k_{on} or k_{off}) of the hA_3 receptor agonists, their association rate constants showed a better correlation with affinity than their dissociation rate constants (**Figure 3C** and **3D**). Furthermore, a k_{on}-k_{off}-K_D "kinetic map" (**Figure 4**) was constructed based on the compounds' divergent affinities (expressed as kinetic K_D values) and rate constants, yielding a division of these agonists into three different sub-categories: agonists that show k_{off} values in a lower range but due to divergent k_{on} values have various K_D values (Group A); agonists that show k_{off} values in a median range but due to divergent k_{on} values (although smaller than in Group A) have different K_D values (Group B); and two agonists that have relatively poor affinity due to larger k_{off} values and smaller k_{on} values (Group C).

A.

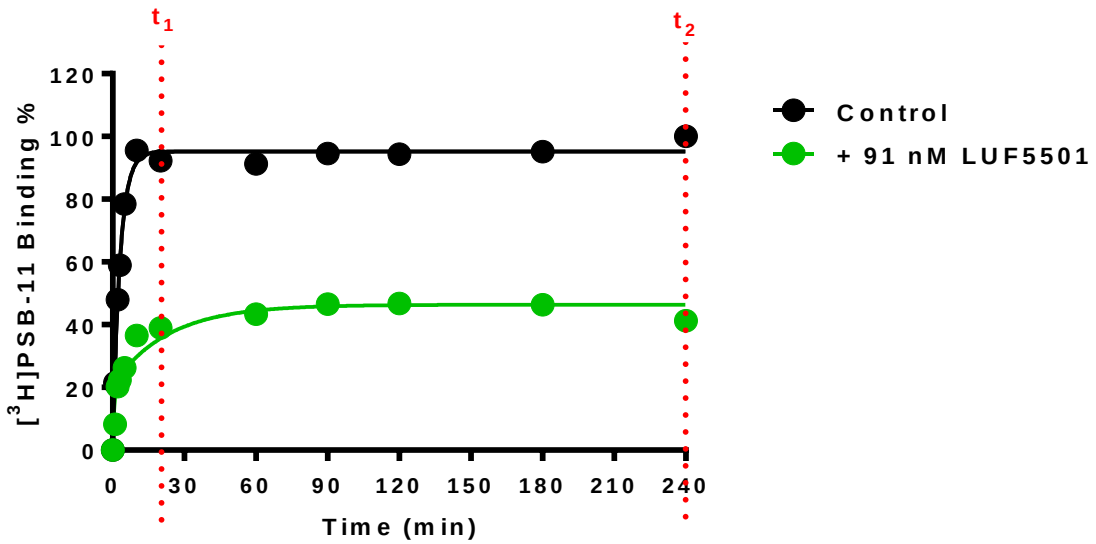

B.

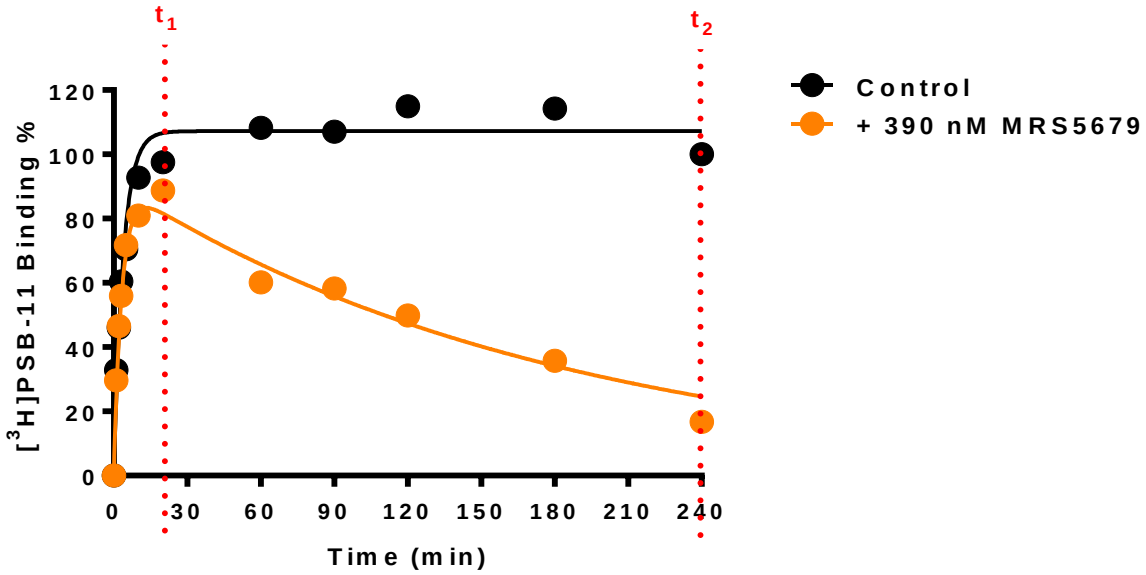

Figure 2: Competition association experiments with [^{3}H]PSB-11 binding to the recombinant hA_3 receptor stably expressed on CHO cell membranes (10 °C) in the absence or presence of unlabeled short-residence-time agonist LUF5501 (**A**), or long-residence-time agonist MRS5679 (**B**). Representative graphs are shown from one experiment performed in duplicate. Note, t_1, t_2 are indicated, which are the two time points used in KRI determinations.

A.

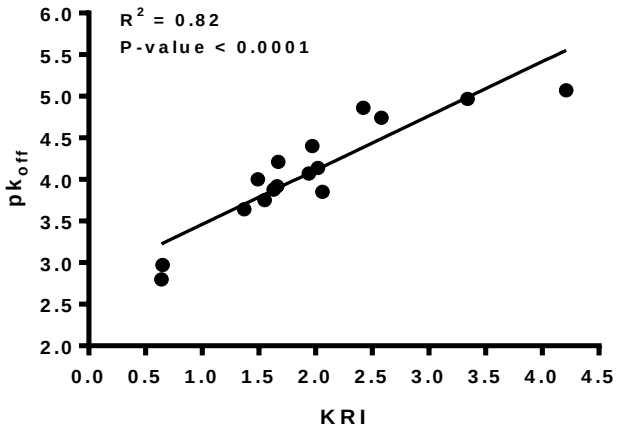
R² = 0.82
P-value < 0.0001
pkoff
KRI
6.0
5.5
5.0
4.5
4.0
3.5
3.0
2.5
2.0
0.0 0.5 1.0 1.5 2.0 2.5 3.0 3.5 4.0 4.5

B.

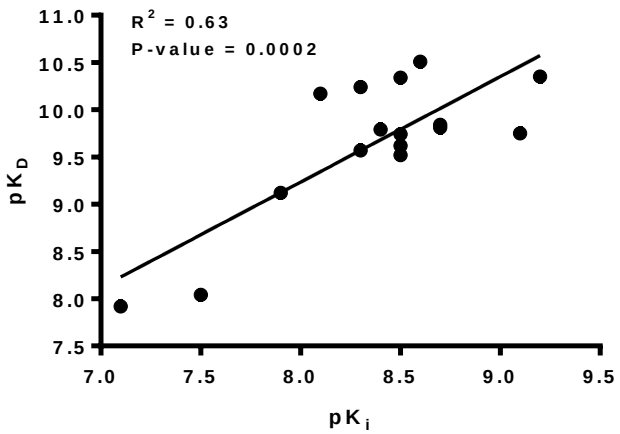
R² = 0.63
P-value = 0.0002
pKD
pKi
11.0
10.5
10.0
9.5
9.0
8.5
8.0
7.5
7.0 7.5 8.0 8.5 9.0 9.5

C.

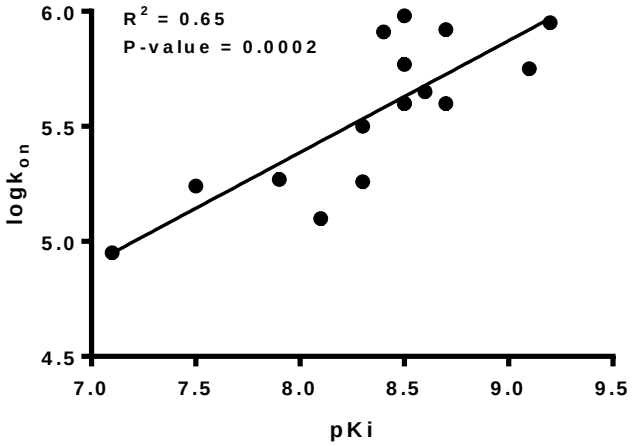
R² = 0.65
P-value = 0.0002
logkon
pKi
6.0
5.5
5.0
4.5
7.0 7.5 8.0 8.5 9.0 9.5

D.

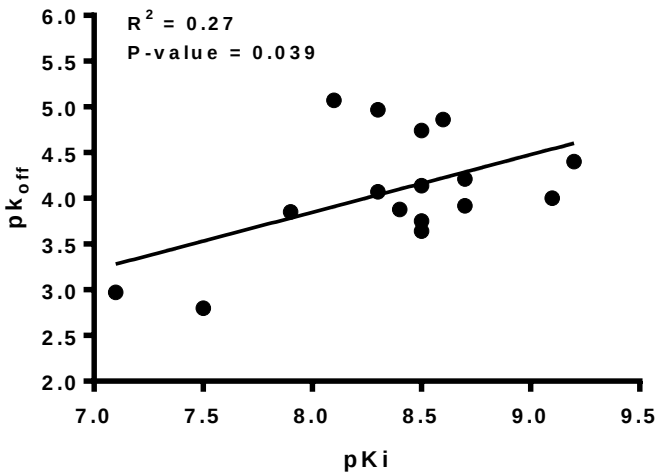

Figure 3: The correlations between the negative logarithm of each hA_3 receptor agonist dissociation rate constants (pk_{off}) and the kinetic rate index (KRI) (**A**), the A_3 receptor agonist affinity (pK_i) and the "kinetic K_D" (pK_D) (**B**), logarithm of association rate constants ($logk_{on}$) (**C**) and negative logarithm of dissociation rate constants (pk_{off}) (**D**). Data used in these plots are detailed in **Tables 2** and **3**.

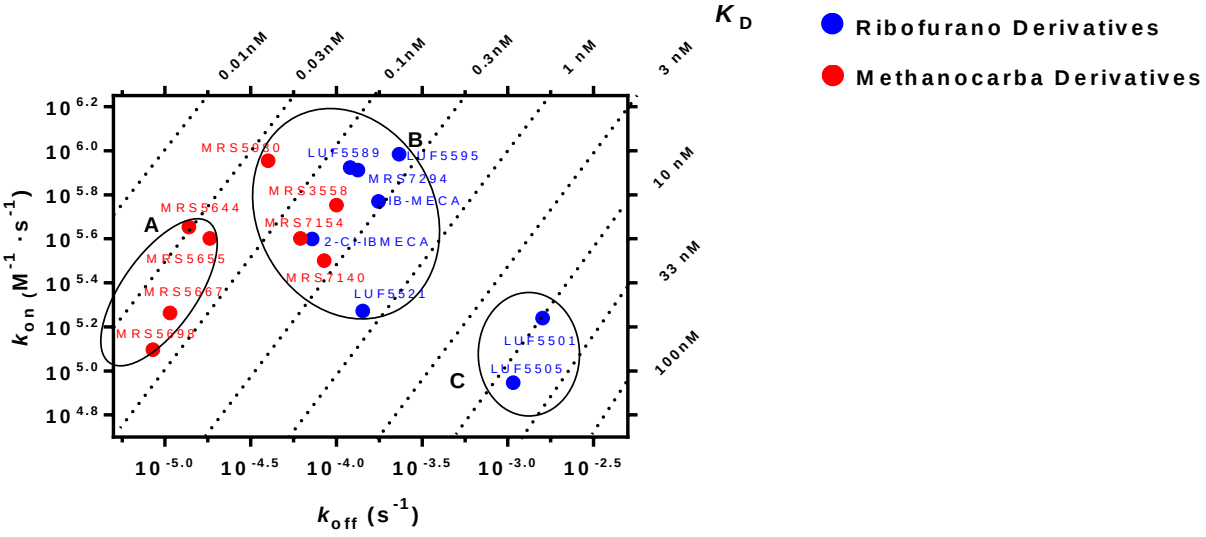

Figure 4: Kinetics map (y axis: k_{on} in $M^{-1}{\cdot}s^{-1}$, x axis: k_{off} in s^{-1}) of all compounds that were kinetically characterized in this study. k_{on} and k_{off} values were obtained through competition association assays. The kinetically derived affinity ($K_D = k_{off}/k_{on}$) is represented through diagonal parallel lines. The ribofurano derivatives are colored in blue, and the methanocarba derivatives are colored in red.

Structure−Affinity Relationships (SAR) and Structure−Kinetics Relationships (SKR) of hA_3 receptor agonists

First, a series of hA_3R agonists with either a natural or 5'-modified ribose moiety was investigated (**Table 2**). LUF5501-LUF5506 have an intact ribofurano moiety and a halogen substitution at the N^6 phenyl group of the core scaffold. 3-Chlorophenyl substitution (LUF5501) provided somewhat better affinity than 3-bromophenyl (LUF5505) or 4-chlorophenyl (LUF5500) substitution (31 nM vs 78 nM; 31 nM vs 51 nM, respectively). The affinity of the 4-iodophenyl substituted derivative (LUF5506) was similar to LUF5501 (31 nM vs 29 nM). Meanwhile, their KRI values showed that halogen substitution at *meta*-position led to lower KRI values than those at *para*-position of the phenyl ring. The KRI values of LUF5501 and LUF5505 were at the lower end (< 0.7) with 0.64 and 0.65, respectively. The full-curve competition association experiments confirmed their similar fast dissociation rates (LUF5501: (1.6 ± 0.2) x 10^{-3} s^{-1}; LUF5505: (1.1 ± 0.04) x 10^{-3} s^{-1}). Worthy of note, LUF5501 proved to have the shortest RT (10 min) among the entire selection of compounds.

When the 5'-hydroxymethylene group (LUF5506) was substituted by an ethylcarboxamide (-$CONHCH_2CH_3$, LUF5521), affinity (14 nM vs 29 nM) and particularly the KRI increased (2.06 vs 0.99). The association and dissociation rates of LUF5521 were (1.9 ± 0.3) x 10^5 $M^{-1}s^{-1}$ and (1.4 ± 0.1) x 10^{-4} s^{-1}, respectively, and its RT was calculated as 117 min.

We then examined benzyl substitutions at the N^6 position of the core scaffold, with a methylcarboxamide (-$CONHCH_3$) modification of the 5'-position on the ribofuran moiety (MECA, IB-MECA and 2-Cl-IBMECA). MECA had an affinity of 42 nM with a KRI value of 1.24. When iodine was introduced at the 3-position of the benzyl ring, yielding IB-MECA, affinity was strongly increased (2.9 nM vs 42 nM) as well as the KRI value (1.55 vs 1.24); with a further chlorine atom substitution at the *C*-2 position on the core scaffold (2-Cl-IBMECA) there was no further increase in affinity (3.5 nM vs 2.9 nM), but its KRI value increased significantly (2.02 vs 1.55), which is the largest value in this series (**Table 2**). For IB-MECA and 2-Cl-IBMECA, the association rate constants were similar ((5.9 ± 0.9) x

10^5 $M^{-1}s^{-1}$ vs (4.0 ± 0.5) x 10^5 $M^{-1}s^{-1}$) , however 2-Cl-IBMECA had a slower dissociation rate ((7.2 ± 1.1) x 10^{-5} s^{-1} vs (1.8 ± 0.2) x 10^{-4} s^{-1}) as had been immanent already from their KRI values. The RTs of IB-MECA and 2-Cl-IBMECA were calculated from their dissociation rate constants as 95 min and 231 min, respectively.

Interestingly, when the amide at the 5'-position on the ribofurano ring of 2-Cl-IBMECA was changed to an ether function (-$CH_2OC_3H_5$, LUF5595), both association ((9.6 ± 3.1) x 10^5 $M^{-1}s^{-1}$ vs (4.0 ± 0.5) x 10^5 $M^{-1}s^{-1}$) and dissociation (2.3 ± 1.0) x 10^{-4} s^{-1} vs (7.2 ± 1.1) x 10^{-5} s^{-1}) became faster, even though the compound was still a slowly dissociating agonist compared with the radioligand (KRI: 1.37).

Finally, the effect of the 2-Cl substitution was further confirmed in the comparison between LUF5586 and LUF5589. Their affinities were similar (2.8 nM vs 2.2 nM), but with 2-Cl, LUF5589 had a higher KRI than LUF5586 (1.66 vs 1.30), and the RT of LUF5589 was determined as 138 min. In addition, a larger substituent at the *C*-2 position (MRS7294) was tolerated with respect to both affinity and kinetics, at least in combination with a small N^6-methyl substituent.

Table 3 summarizes our findings on the series of ring-rigidified methanocarba derivatives that maintain a receptor-preferred North (N) conformation, with the flexible ribose-substituted MRS7294 included once more to allow a comparison. MRS7294, MRS5980, MRS7140, MRS7158 and MRS7154 share a common fragment ((5-chlorothiophen-2-yl)ethynyl) at the *C*-2-position (R_1 group). MRS7294, the agonist with unmodified ribofuran moiety, served as the starting of the analysis, which had both high affinity (3.7 nM) and a large KRI value (1.63). By competition association experiments its association and dissociation rates were determined as (8.2 ± 3.8) x 10^5 ($M^{-1}s^{-1}$) and (1.3 ± 0.2) x 10^{-4} s^{-1}, respectively; its RT was calculated as 125 min. When the ribofurano ring was changed by the methanocarba moiety (MRS5980), the affinity increased to the sub-nanomolar range (0.72 nM vs 3.7 nM) and its KRI value also increased largely (1.97 vs 1.63). The full-curve competition association experiments showed that MRS5980's association rate was slightly faster ((9.0 ± 2.3) x 10^5 $M^{-1}s^{-1}$ vs (8.2 ± 3.8) x 10^5 $M^{-1}s^{-1}$ for the respective rate constants), but its dissociation rate was much slower

((4.0 ± 1.0) x 10^{-5} s^{-1} vs (1.3 ± 0.2) x 10^{-4} s^{-1}) than its ribose-equivalent. The RT of MRS5980 was 417 min. When the nitrogen atom at the *N-1*-position was replaced by a carbon atom (MRS7140), the affinity remained high (5.2 nM), and its kinetics profile was not much altered compared with MRS5980 (k_{on}: (3.2 ± 1.2) x 10^5 $M^{-1}s^{-1}$ vs (9.0 ± 2.3) x 10^5 $M^{-1}s^{-1}$; k_{off}: (8.5 ± 0.3) x 10^{-5} s^{-1} vs (4.0 ± 1.0) x 10^{-5} s^{-1}). Changing the mono-methyl substitution at the N^6 position (MRS5980) for di-methyl substitution (MRS7158), severely compromised both affinity and KRI value (618 nM vs 0.72 nM; 0.93 vs 1.97). When mono-substitution at the N^6 position (MRS7140) was extended to n-propyl (MRS7154), affinity remained high (2.2 nM), like the KRI value (1.67); both association and dissociation rates of MRS7154 were quite similar to MRS5980 (k_{on}: (4.0 ± 0.7) x 10^5 $M^{-1}s^{-1}$ vs (9.0 ± 2.3) x 10^5 $M^{-1}s^{-1}$; k_{off}: (6.2 ± 1.2) x 10^{-5} s^{-1} vs (4.0 ± 1.0) x 10^{-5} s^{-1}), with RTs of 270 min and 417 min, respectively.

The methanocarba derivatives MRS3558, MRS5655, MRS5679 and MRS5698 share their R_2 groups (3-chlorobenzyl substitution). When the 2-Cl substituent of MRS3558 was replaced by the bulky and rigid phenylethynyl (MRS5655), the affinity decreased from 1.0 nM (MRS3558) to 3.6 nM (MRS5655), while the KRI value increased, however (1.49 vs 2.58). In the competition association assays the association rate constants of MRS3558 and MRS5655 were similar ((5.7 ± 0.8) x 10^5 $M^{-1}s^{-1}$ vs (4.0 ± 0.8) x 10^5 $M^{-1}s^{-1}$), while the dissociation rate constants were 5.6-fold different ((1.0 ± 0.2) x 10^{-4} s^{-1} vs (1.8 ± 0.3) x 10^{-5} s^{-1}), leading to a RT for MRS5655 of 909 min. When the phenylethynyl of MRS5655 was 3,4-di-fluorinated as in MRS5698, the affinity was reduced from 3.6 nM (MRS5655) to 9.4 nM (MRS5698), whilst the KRI value increased significantly from 2.58 (MRS5655) to 4.21 (MRS5698), with both slower association and dissociation rate constants (k_{on}: (4.0 ± 0.8) x 10^5 $M^{-1}s^{-1}$ vs (1.3 ± 0.4) x 10^5 $M^{-1}s^{-1}$; k_{off}: (1.8 ± 0.3) x 10^{-5} s^{-1} vs (8.5 ± 0.7) x 10^{-6} s^{-1}), thus extending RT from 909 min to 1961 min. Furthermore, when the phenylethynyl fragment of MRS5655 was expanded to a 4-biphenylethynyl substitution on the R_1 group (MRS5679), the affinity suffered from 3.6 nM (MRS5655) to 82 nM (MRS5679); however, its KRI value increased dramatically from 2.58 to 5.56. This high value rendered the determination of the kinetics profile of MRS5679 impossible. Obviously,

from all these compounds we learned there can be a clear dichotomy between affinity and residence time.

When the benzyl substitutions at the N^6 position (R_2 in **Table 3**) were replaced by a simple monomethyl (i.e. MRS5655 to MRS5644; MRS5679 to MRS5667), their binding affinities to hA_3 receptors were not compromised (MRS5655/MRS5644: 3.6 nM vs 2.4 nM) or even increased (MRS5679/MRS5667: 82 nM vs 4.6 nM), and so were the kinetics profiles of MRS5655 and MRS5644. The KRI values of MRS5679 and MRS5667 were both at the higher end (5.56 and 3.34).

Discussion

Effects of GTP on agonist binding to the human adenosine A_3 receptor

In the current study, the binding interactions of unlabeled hA_3 receptor agonists were determined in radioligand binding experiments with the reference tritiated antagonist [^{3}H]PSB-11. The favorable binding characteristics of this radioligand served us particularly well in the competition association experiments where robust binding over time could still be measured in the presence of unlabeled ligands, essential for the calculation of the association and dissociation rate constants. It is well known that antagonists occupy a GPCR irrespective of whether it is coupled to a G protein, whereas agonists prefer the G protein-coupled state of the receptor [36]. Addition of GTP to the incubation mixture induces an uncoupling between receptor and available G protein, which leads to a lower apparent receptor affinity for agonists. We confirmed this behavior in our equilibrium displacement experiments, in which the two reference agonists IB-MECA and 2-Cl-IB-MECA had a 3-4-fold lower affinity in the presence of GTP (**Figure 1A**, **Table 1**). Interestingly, all displacement curves had pseudo-Hill coefficients of approx. unity (**Table 1**), suggesting that the agonists recognized one receptor state in both the presence and absence of GTP, most likely a G protein-coupled state (no GTP) or an uncoupled state (with GTP). We then determined the agonist binding kinetics for the two

states in subsequent competition association assays by measuring these in the absence or presence of GTP (**Figure 1B**). Interestingly, the association rate constants were identical for the two states (**Table 1**). Apparently, the ligand, when approaching the receptor from the extracellular side, is insensitive to the coupling status at the intracellular G protein interface. However, the dissociation kinetics proved to be (significantly) different between the states, up to 8-fold for 2-Cl-IB-MECA (**Table 1**), suggesting that dissociating from the receptor is influenced by the absence or presence of the G protein. We then performed further experiments in the absence of GTP, as we felt that for the case of the hA_3 receptor this experimental condition provides us information on the more relevant high-affinity agonist binding state of the receptor. The mathematical modeling provided by Motulsky and Mahan[32] does not allow the calculation of two receptor states with corresponding kinetic parameters. Hence, in a number of cases similar to ours it was decided to include GTP in the assays. For the adenosine A_1 receptor, we included GTP in our assays, forcing the receptor to be in one lower affinity, G protein-uncoupled state only; with this restriction, the kinetic parameters of agonists were determined as conveniently as antagonists.[37] Likewise, the team of Charlton included GTP in kinetic assays on the muscarinic M_3 receptor.[38] On the other hand, GTP was excluded in assays on the adenosine A_{2A} receptor, as agonist affinity at this protein is insensitive to GTP in both equilibrium and kinetics assays.[39]

Methodological aspects of the radioligand binding assays

To ensure an accurate and robust kinetic quantification, experiments were performed at 10 ^{o}C, as reported and documented previously.[35] Initially, a so-called dual-point competition association assay yielding KRI values for the hA_3 receptor was performed as a "kinetic screening campaign" to increase throughput in comparison to the traditional, more elaborate, competition association experiments.[35] Although fast kinetics of agonist binding (e.g. LUF5501, **Figure 2A**) was determined accurately at a relatively low temperature, the kinetics of one agonist with obviously very slow dissociation

characteristics (MRS5679**, Figure 2B**) could not be reliably determined with the Motulsky-Mahan equations. Meanwhile, its large KRI value (5.56) undoubtedly reflects its slow dissociation.

Besides the significant correlation between the agonists' KRI values and dissociation rate constants (**Figure 3A**), the equilibrium K_i and kinetic K_D values were also well correlated (**Figure 3B**). Despite this correlation there are large discrepancies in values between the equilibrium affinities (K_i) and kinetic K_D values. In general, the kinetic pK_D values are higher than pK_i values, with differences from 0.5 to 2.1 log-unit (LUF5501 and MRS5698), whilst the short RT agonists have smaller differences than long RT agonists. This phenomenon suggests that the affinities determined in the radioligand displacement studies may not reflect the true affinity of the compounds as many of them have residence times much longer than the (already long) incubation time of 240 min. In fact, this points to a general caveat in end-point assays in which the equilibrium characteristics of the probe, e.g., a radiolabeled or fluorescently tagged compound, determine the assay protocol without further consideration of the same characteristics of the unlabeled ligands to be tested.

Furthermore, there was a significant correlation between k_{on} (k_3) and affinity values (K_i) of the agonists, but no relationship was found between k_{off} (k_4) and K_i (**Figure 3C** and **3D**). Such correlation between affinity and on-rates has been reported in the case of other GPCR [40] and ion channels.[41, 42] However, in the current study, variations in association rate constants were approximately 10-fold ($logk_{on}$: 5.0 to 6.0), much smaller than at the other targets mentioned above. In addition, all the association rates were well below the diffusion limit of around 10^7 $M^{-1}s^{-1}$, which had been observed previously for membrane-bound proteins.[43]

Ligand optimization based on Structure−Kinetics Relationships (SKR)

All the agonists examined in the current study have been reported, and the riboside MRS7294 was most recently disclosed as a hA_3 receptor agonist.[28] Most ribofurano derivatives (**Table 2**) had been synthesized and tested as early as 1994.[44] The (N)-methanocarba derivatives (**Table 3**) were explored

more recently, showing generally improved affinities over the earlier compounds.[26-29] Although most of these compounds have been described in the context of structure-affinity relationships (SARs), we reasoned that an extensive structure−kinetics relationships (SKRs) analysis is warranted since kinetic profiles are emerging indicators of *in vivo* functional efficacy.[18, 20, 21, 45]

In the series of ribofurano derivatives (**Table 2**), the most outstanding agonist with respect to residence time was 2-Cl-IB-MECA (231 min). The underlying chemical features that prolonged the residence time in the ribofurano series are: i) a chlorine atom at the C2 position (R_1 in **Table 2**, IB-MECA vs 2-Cl-IB-MECA**,** 95 min vs 231 min; LUF5586 vs LUF5589 in KRI: 1.30 vs 1.66), ii) a bulky *meta*-iodobenzyl substitution at the N^6 position of the adenine nucleobase (R_2 in **Table 2**, MECA vs IB-MECA in KRI: 1.24 vs 1.55), and iii) an amide modification at the 5' position (R_3 in **Table 2**, 2-Cl-IB-MECA vs LUF5595: 231 min vs 72 min; LUF5506 vs LUF5521 in KRI: 0.99 vs 2.06). Interestingly, slow dissociation kinetics of agonists can be maintained by introducing an extended linear side chain at the C2 position and removing the bulky substituent at the N^6 position (i.e. N^6-Me analogue MRS7294 in RT: 125 min). The kinetic behavior of another known reference agonist, 2-(1-hexynyl)-N-methyladenosine (HEMADO), also confirmed this observation from comparison with other research.[45, 46]

More impressive kinetics were observed in the methanocarba series. From a previous study it was concluded that a possible H-bond interaction between the amide modification at the original 5' position (-$CONHCH_3$) and residues in the binding pocket of the hA_3 receptor was a key feature of agonist kinetics.[47] Comparing the kinetics of ribofurano MRS7294 and its methanocarba equivalent MRS5980 provides evidence the conformational-constrained (N)-methanocarba moiety as a ribofurano ring substitute adds to the slow dissociation of MRS5980, suggesting this rigid ring system fits even better in the ligand binding pocket. Additionally, the N1 atom on the adenine core is contributing to slow dissociation (1-deza MRS7140 vs MRS5980 in RT: 196 min vs 417 min). The N^6 position in the methanocarba series (R_2 substituent) accepted a small methyl group as avidly as the

larger *n*-propyl (MRS5980 vs MRS7154) and 3-chlorobenzyl substituent (MRS5644 vs MRS5655), with respect to both affinity and kinetics. Apparently, differences in lipophilicity between the N^6-substituents did not seem to matter either. Data for the R_1 (C2 position) substituent were already commented on in the Results section. It is noteworthy that the 3,4-difluorophenyl fragment contributed to a long residence time of MRS5698, quite similar to the 2,4-difluorophenyl fragment we encountered in A_{2A} receptor antagonists displaying long residence time.[48]

So far the human A_3 receptor has not been crystallized yet, although its most homologous relative, the adenosine A_1 receptor, has.[49] Homology models of the A_3 receptor have been constructed, and their relevance has been recently reviewed and discussed.[50] It appeared that the interaction of the extended and rigid 2-arylethynyl groups at the C-2 position (as in e.g., MRS5679 and MRS5644) with the A_3 receptor required an outward movement of TM2. Although the agonists' path of binding to or dissociation from the A_3 receptor is unknown, one could speculate that such reorganization of TM2 "locks" the C2-substituted agonist. This reasoning stems from a molecular dynamics simulation and site-directed mutation study of the ligand dissociation pathway from the human adenosine A_{2A} receptor,[51] for which we used a high resolution crystal structure.[52] It taught us there may be a lid adjacent to the ligand binding pocket retaining the ligand for some time before the compound leaves the receptor. A follow-up study revealed that ligand dissociation correlated with the strength of the salt-bridge between His264 in EL3 and Glu169 in EL2.[53] It would be interesting to learn whether a similar mechanism exists for the A_3 receptor.

Retrospective evaluation of selected agonists with complete kinetic profiles

IB-MECA (RT = 95 min) and 2-Cl-IB-MECA (RT = 231 min) are two reference full agonists for the hA_3 receptor. Despite numerous reports about their controversial cardioprotection,[54, 55] they have been taken into a series of clinical trials: for IB-MECA, in total 12 completed or planned trials have been reported related to inflammatory conditions (e.g., keratoconjunctivitis sicca, rheumatoid arthritis, psoriasis, uveitis); for 2-Cl-IB-MECA, four trials have been registered for liver diseases (e.g.,

hepatocellular carcinoma, hepatitis C).[56, 57] Intuitively one would expect that long residence time hA_3 receptor agonists could be beneficial in chronic diseases, for instance to allow once daily dosing.

More recently, the neuroprotective effect provided by hA_3 receptor agonists has been receiving attention.[11, 58] A number of agonists have been designed and evaluated both in *in vitro* and *in vivo* functional experiments, especially for the treatment of chronic neuropathic pain.[26, 27, 29] MRS5698 in particular, having the longest residence time (1961 min) from our research, has been studied extensively in various pre-clinical animal models of neuropathic pain.[59-61] We, however, hesitate to link the binding kinetics profile of MRS5698 with its *in vivo* effects, also because issues such as pharmacokinetics and species differences (human/rodent) may play an important but yet unknown role.

The adenosine A_3 receptor has a peculiar and rapid desensitization/internalization profile in cultured cells.[6] However, the fast desensitization after A_3 agonist exposure under in vitro conditions does not generalize to *in vivo* pain models. MRS5698 maintained full efficacy over a five-day period, with the drug administered either by daily injection or by an implanted mini-pump to provide a steady state plasma concentration.[55] Prolonged MRS5698 exposure in the rat did not reduce its efficacy, as would be expected from agonist-induced desensitization alone. Thus, additional studies of agonist occupancy of the receptor and subsequent receptor processing are warranted to further explore this interesting target for combatting neuropathic pain.

Kinetic Map

Using the association (k_{on}) and dissociation (k_{off}) rate constants obtained from competition association experiments (**Tables 2** and **3**), a kinetic map (**Figure 4**) was constructed by plotting these values on the y-axis and x-axis, respectively. The dashed diagonal parallel lines represent the kinetically derived K_D values ($K_D = k_{off}/k_{on}$). Out of this map three subgroups emerged, which were divided according to k_{off} values: Group A < Group B < Group C. Obviously, Group A and C are solely

composed of methanocarba derivatives (**Figure 4**, red) and ribofurano derivatives (**Figure 4**, blue), respectively. Group B is a mixture of these two compound classes, with the methanocarba derivatives mainly displaying smaller k_{off} values. Thus, rigidifying the ribose ring with the bicyclic group consistently prolonged the dissociation time. This general division indicates a different mode of receptor-ligand interaction during the binding and unbinding process of the two ligand groups. It also seems there is a clear residence-time "cliff" between Groups A (having one rigid C2-phenylethynyl or 4-biphenylethynyl group with or without one enlarged N^6-benzyl group) and B (having multiple enlarged adenine substituents) in the kinetic map.

In each subgroup, agonists exhibit k_{off} values in a similar range, but have different k_{on} values. As a consequence, variation in K_D values in each group was observed (Group A: ~10-fold; Group B: ~100-fold; Group C: ~3-fold). Previous SKR studies have primarily focused on optimizing dissociation rates and residence times for designing a kinetically favorable ligand. Yet recently, there has been increasing acknowledgement of the important role association rate constants may play in determining the efficacy of a drug as the result of increased rebinding or increased drug-target selectivity.[21, 62] A kinetic map would thus allow for the selection of compounds with appropriate residence times whilst exploring the role of association rate constants.

In summary, an agonist-related competition association assay at the hA_3 receptor was validated, and a series of ribofurano and methanocarba derivatives were kinetically profiled for the first time. A k_{on}-k_{off}-K_D kinetic map was constructed and subsequently the agonists with complete kinetic profile were divided into three sub-groups based on their residence times. Longer residence times were associated with methanocarba (vs. ribose) and enlarged adenine N^6 and C-2 (rigid arylalkynyl) substitutions. We identified agonists with very long residence times, but these may not be the most therapeutically favorable for treating various conditions in view of the fast desensitization of the receptor. Although far from definitive, this study suggests that proper residence times, not

necessarily longer than target turnover time, may be vital parameters in the development of hA_3R agonists for therapeutic use.

References

1. Meyerhof, W.; Müller-Brechlin, R.; Richter, D. Molecular cloning of a novel putative G-protein coupled receptor expressed during rat spermiogenesis. *FEBS Lett.* **1991,** *284*, 155-160.
2. Cortés, D.; Guinzberg, R.; Villalobos-Molina, R.; Piña, E. Evidence that endogenous inosine and adenosine-mediated hyperglycaemia during ischaemia–reperfusion through A_3 adenosine receptors. *Auton. Autacoid Pharmacol.* **2009,** *29*, 157-164.
3. Madi, L.; Ochaion, A.; Rath-Wolfson, L.; Bar-Yehuda, S.; Erlanger, A.; Ohana, G.; Harish, A.; Merimski, O.; Barer, F.; Fishman, P. The A_3 adenosine receptor is highly expressed in tumor versus normal cells: potential target for tumor growth inhibition. *Clin. Cancer Res.* **2004,** *10*, 4472-4479.
4. Ochaion, A.; Bar-Yehuda, S.; Cohen, S.; Barer, F.; Patoka, R.; Amital, H.; Reitblat, T.; Reitblat, A.; Ophir, J.; Konfino, I.; Chowers, Y.; Ben-Horin, S.; Fishman, P. The anti-inflammatory target A_3 adenosine receptor is over-expressed in rheumatoid arthritis, psoriasis and Crohn's disease. *Cell. Immunol.* **2009,** *258*, 115-122.
5. Palmer, T. M.; Stiles, G. L. Identification of threonine residues controlling the agonist-dependent phosphorylation and desensitization of the rat A_3 adenosine receptor. *Mol. Pharmacol.* **2000,** *57*, 539-545.
6. Klaasse, E. C.; IJzerman, A. P.; de Grip, W. J.; Beukers, M. W. Internalization and desensitization of adenosine receptors. *Purinergic Signalling* **2008,** *4*, 21-37.
7. Gessi, S.; Merighi, S.; Varani, K.; Leung, E.; Mac Lennan, S.; Borea, P. A. The A_3 adenosine receptor: an enigmatic player in cell biology. *Pharmacol. Ther.* **2008,** *117*, 123-140.
8. Shamama, N.; Luqman, A. K.; Zafar, M. A.; Seemi, F. B. Adenosine A_3 receptor: a promising therapeutic target in cardiovascular disease. *Curr. Cardiol. Rev.* **2016,** *12*, 18-26.
9. Borea, P. A.; Varani, K.; Vincenzi, F.; Baraldi, P. G.; Tabrizi, M. A.; Merighi, S.; Gessi, S. The A_3 adenosine receptor: history and perspectives. *Pharmacol. Rev.* **2015,** *67*, 74-102.
10. Antonioli, L.; Csóka, B.; Fornai, M.; Colucci, R.; Kókai, E.; Blandizzi, C.; Haskó, G. Adenosine and inflammation: what's new on the horizon? *Drug Discovery Today* **2014,** *19*, 1051-1068.
11. Fishman, P.; Bar-Yehuda, S.; Liang, B. T.; Jacobson, K. A. Pharmacological and therapeutic effects of A_3 adenosine receptor (A_3AR) agonists. *Drug Discovery Today* **2012,** *17*, 359-366.
12. Müller, C. E.; Jacobson, K. A. Recent developments in adenosine receptor ligands and their potential as novel drugs. *Biochim. Biophys. Acta, Biomembr.* **2011,** *1808*, 1290-1308.
13. Koscsó, B.; Csóka, B.; Pacher, P.; Haskó, G. Investigational A_3 adenosine receptor targeting agents. *Expert Opin. Invest. Drugs* **2011,** *20*, 757-768.
14. Salvemini, D.; Jacobson, K. A. Highly selective A_3 adenosine receptor agonists relieve chronic neuropathic pain. *Expert Opin. Ther. Pat.* **2017,** *27*, 967.
15. Fishman, P.; Cohen, S. The A_3 adenosine receptor (A_3AR): therapeutic target and predictive biological marker in rheumatoid arthritis. *Clin. Rheumatol.* **2016,** *35*, 2359-2362.
16. Cohen, S.; Stemmer, S. M.; Zozulya, G.; Ochaion, A.; Patoka, R.; Barer, F.; Bar-Yehuda, S.; Rath-Wolfson, L.; Jacobson, K. A.; Fishman, P. CF102 an A_3 adenosine receptor agonist mediates anti-tumor and anti-inflammatory effects in the liver. *J. Cell. Physiol.* **2011,** *226*, 2438-2447.
17. Jacobson, K. A.; Merighi, S.; Varani, K.; Borea, P. A.; Baraldi, S.; Aghazadeh Tabrizi, M.; Romagnoli, R.; Baraldi, P. G.; Ciancetta, A.; Tosh, D. K.; Gao, Z.-G.; Gessi, S. A_3 adenosine receptors as

modulators of inflammation: from medicinal chemistry to therapy. *Med. Res. Rev.*, 10.1002/med.21456.
18. Guo, D.; Hillger, J. M.; IJzerman, A. P.; Heitman, L. H. Drug-target residence time—a case for G protein-coupled receptors. *Med. Res. Rev.* **2014,** *34*, 856-892.
19. Cusack, K. P.; Wang, Y.; Hoemann, M. Z.; Marjanovic, J.; Heym, R. G.; Vasudevan, A. Design strategies to address kinetics of drug binding and residence time. *Bioorg. Med. Chem. Lett.* **2015,** *25*, 2019-2027.
20. Copeland, R. A.; Pompliano, D. L.; Meek, T. D. Drug-target residence time and its implications for lead optimization. *Nat. Rev. Drug Discovery* **2006,** *5*, 730-739.
21. Copeland, R. A. The drug-target residence time model: a 10-year retrospective. *Nat. Rev. Drug Discovery* **2016,** *15*, 87-95.
22. Heitman, L. H.; Göblyös, A.; Zweemer, A. M.; Bakker, R.; Mulder-Krieger, T.; van Veldhoven, J. P. D.; de Vries, H.; Brussee, J.; IJzerman, A. P. A series of 2,4-disubstituted quinolines as a new class of allosteric enhancers of the adenosine A_3 receptor. *J. Med. Chem.* **2009,** *52*, 926-931.
23. Gessi, S.; Varani, K.; Merighi, S.; Morelli, A.; Ferrari, D.; Leung, E.; Baraldi, P. G.; Spalluto, G.; Borea, P. A. Pharmacological and biochemical characterization of A_3 adenosine receptors in Jurkat T cells. *Br. J. Pharmacol.* **2001,** *134*, 116-126.
24. de Zwart, M.; de Groote, M.; van der Klein, P. A. M.; van Dun, S.; Bronsing, R.; von Frijtag Drabbe Künzel, J. K.; IJzerman, A. P. Phenyl-substituted N^6-phenyladenosines and N^6-phenyl-5′-N-ethylcarboxamidoadenosines with high activity at human adenosine A_{2B} receptors. *Drug Dev. Res.* **2000,** *49*, 85-93.
25. van Tilburg, E. W.; van der Klein, P. A. M.; von Frijtag Drabbe Künzel, J.; de Groote, M.; Stannek, C.; Lorenzen, A.; IJzerman, A. P. 5'-O-alkyl ethers of N,2-substituted adenosine derivatives: partial agonists for the adenosine A_1 and A_3 receptors. *J. Med. Chem.* **2001,** *44*, 2966-2975.
26. Tosh, D. K.; Finley, A.; Paoletta, S.; Moss, S. M.; Gao, Z.-G.; Gizewski, E. T.; Auchampach, J. A.; Salvemini, D.; Jacobson, K. A. In vivo phenotypic screening for treating chronic neuropathic pain: modification of C2-arylethynyl group of conformationally constrained A_3 adenosine receptor agonists. *J. Med. Chem.* **2014,** *57*, 9901-9914.
27. Tosh, D. K.; Crane, S.; Chen, Z.; Paoletta, S.; Gao, Z.-G.; Gizewski, E.; Auchampach, J. A.; Salvemini, D.; Jacobson, K. A. Rigidified A_3 adenosine receptor agonists: 1-deazaadenine modification maintains high in vivo efficacy. *ACS Med. Chem. Lett.* **2015,** *6*, 804-808.
28. Tosh, D. K.; Janowsky, A.; Eshleman, A. J.; Warnick, E.; Gao, Z.-G.; Chen, Z.; Gizewski, E.; Auchampach, J. A.; Salvemini, D.; Jacobson, K. A. Scaffold repurposing of nucleosides (adenosine receptor agonists): enhanced activity at the human dopamine and norepinephrine sodium symporters. *J. Med. Chem.* **2017,** *60*, 3109-3123.
29. Tosh, D. K.; Deflorian, F.; Phan, K.; Gao, Z.-G.; Wan, T. C.; Gizewski, E.; Auchampach, J. A.; Jacobson, K. A. Structure-guided design of A_3 adenosine receptor-selective nucleosides: combination of 2-arylethynyl and bicyclo[3.1.0]hexane substitutions. *J. Med. Chem.* **2012,** *55*, 4847-4860.
30. Tchilibon, S.; Joshi, B. V.; Kim, S.-K.; Duong, H. T.; Gao, Z.-G.; Jacobson, K. A. (*N*)-methanocarba 2,N^6-disubstituted adenine nucleosides as highly potent and selective A_3 adenosine receptor agonists. *J. Med. Chem.* **2005,** *48*, 1745-1758.
31. Smith, P. K.; Krohn, R. I.; Hermanson, G. T.; Mallia, A. K.; Gartner, F. H.; Provenzano, M. D.; Fujimoto, E. K.; Goeke, N. M.; Olson, B. J.; Klenk, D. C. Measurement of protein using bicinchoninic acid. *Anal. Biochem.* **1985,** *150*, 76-85.
32. Motulsky, H. J.; Mahan, L. C. The kinetics of competitive radioligand binding predicted by the law of mass action. *Mol. Pharmacol.* **1984,** *25*, 1-9.
33. Guo, D.; van Dorp, E. J. H.; Mulder-Krieger, T.; van Veldhoven, J. P. D.; Brussee, J.; IJzerman, A. P.; Heitman, L. H. Dual-point competition association assay: a fast and high-throughput kinetic screening method for assessing ligand-receptor binding kinetics. *J. Biomol. Screening* **2013,** *18*, 309-320.

34. Cheng, Y.-C.; Prusoff, W. H. Relationship between the inhibition constant (K_I) and the concentration of inhibitor which causes 50 per cent inhibition (IC_{50}) of an enzymatic reaction. *Biochem. Pharmacol.* **1973,** *22*, 3099-3108.
35. Xia, L.; Burger, W. A. C.; van Veldhoven, J. P. D.; Kuiper, B. J.; van Duijl, T. T.; Lenselink, E. B.; Paasman, E.; Heitman, L. H.; IJzerman, A. P. Structure–affinity relationships and structure–kinetics relationships of pyrido[2,1-f]purine-2,4-dione derivatives as human adenosine A_3 receptor antagonists. *J. Med. Chem.* **2017,** *60*, 7555-7568.
36. Sprang, S. R. Cell signalling: binding the receptor at both ends. *Nature* **2011,** *469*, 172-173.
37. Xia, L.; de Vries, H.; IJzerman, A. P.; Heitman, L. H. Scintillation proximity assay (SPA) as a new approach to determine a ligand's kinetic profile. A case in point for the adenosine A_1 receptor. *Purinergic Signalling* **2016,** *12*, 115-126.
38. Sykes, D. A.; Dowling, M. R.; Charlton, S. J. Exploring the mechanism of agonist efficacy: a relationship between efficacy and agonist dissociation rate at the muscarinic M_3 receptor. *Mol. Pharmacol.* **2009,** *76*, 543-551.
39. Guo, D.; Mulder-Krieger, T.; IJzerman, A. P.; Heitman, L. H. Functional efficacy of adenosine A_{2A} receptor agonists is positively correlated to their receptor residence time. *Br. J. Pharmacol.* **2012,** *166*, 1846-1859.
40. Doornbos, M. L. J.; Cid, J. M.; Haubrich, J.; Nunes, A.; van de Sande, J. W.; Vermond, S. C.; Mulder-Krieger, T.; Trabanco, A. A.; Ahnaou, A.; Drinkenburg, W. H.; Lavreysen, H.; Heitman, L. H.; IJzerman, A. P.; Tresadern, G. Discovery and kinetic profiling of 7-aryl-1,2,4-triazolo[4,3-a]pyridines: positive allosteric modulators of the metabotropic glutamate receptor 2. *J. Med. Chem.* **2017,** *60*, 6704–6720.
41. Yu, Z.; van Veldhoven, J. P. D.; Louvel, J.; 't Hart, I. M. E.; Rook, M. B.; van der Heyden, M. A. G.; Heitman, L. H.; IJzerman, A. P. Structure–affinity relationships (SARs) and structure–kinetics relationships (SKRs) of Kv11.1 blockers. *J. Med. Chem.* **2015,** *58*, 5916-5929.
42. Yu, Z.; IJzerman, A. P.; Heitman, L. H. K(v)11.1 (hERG)-induced cardiotoxicity: a molecular insight from a binding kinetics study of prototypical K(v)11.1 (hERG) inhibitors. *Br. J. Pharmacol.* **2015,** *172*, 940-955.
43. Smith, G. F. Medicinal chemistry by the numbers: the physicochemistry, thermodynamics and kinetics of modern drug design. In *Progress in Medicinal Chemistry*, Lawton, G.; Witty, D. R., Eds. Elsevier B.V.: Burlington, **2009**; Vol. *48*, p 1.
44. Gallo-Rodriguez, C.; Ji, X.-d.; Melman, N.; Siegman, B. D.; Sanders, L. H.; Orlina, J.; Fischer, B.; Pu, Q.; Olah, M. E.; van Galen, P. J. M.; Stiles, G. L.; Jacobson, K. A. Structure − activity relationships of N^6-benzyladenosine-5′-uronamides as A_3-selective adenosine agonists. *J. Med. Chem.* **1994,** *37*, 636-646.
45. Guo, D.; Heitman, L. H.; IJzerman, A. P. Kinetic aspects of the interaction between ligand and G protein-coupled receptor: the case of the adenosine receptors. *Chem. Rev.* **2017,** *117*, 38-66.
46. Klotz, K.-N.; Falgner, N.; Kachler, S.; Lambertucci, C.; Vittori, S.; Volpini, R.; Cristalli, G. [^{3}H]HEMADO— a novel tritiated agonist selective for the human adenosine A_3 receptor. *Eur. J. Pharmacol.* **2007,** *556*, 14-18.
47. Auchampach, J. A.; Gizewski, E. T.; Wan, T. C.; de Castro, S.; Brown, G. G.; Jacobson, K. A. Synthesis and pharmacological characterization of [^{125}I]MRS5127, a high affinity, selective agonist radioligand for the A_3 adenosine receptor. *Biochem. Pharmacol.* **2010,** *79*, 967-973.
48. Guo, D.; Xia, L.; van Veldhoven, J. P. D.; Hazeu, M.; Mocking, T.; Brussee, J.; IJzerman, A. P.; Heitman, L. H. Binding kinetics of ZM241385 derivatives at the human adenosine A_{2A} receptor. *ChemMedChem* **2014,** *9*, 752-761.
49. Glukhova, A.; Thal, D. M.; Nguyen, A. T.; Vecchio, E. A.; Jörg, M.; Scammells, P. J.; May, L. T.; Sexton, P. M.; Christopoulos, A. Structure of the adenosine A_1 receptor reveals the basis for subtype selectivity. *Cell* **2017,** *168*, 867-877.
50. Ciancetta, A.; Jacobson, K. Structural Probing and Molecular Modeling of the A_3 Adenosine Receptor: A Focus on Agonist Binding. *Molecules* **2017,** 22, 449.

51. Guo, D.; Pan, A. C.; Dror, R. O.; Mocking, T.; Liu, R.; Heitman, L. H.; Shaw, D. E.; IJzerman, A. P. Molecular basis of ligand dissociation from the adenosine A_{2A} receptor. *Mol. Pharmacol.* **2016,** *89*, 485-491.
52. Liu, W.; Chun, E.; Thompson, A. A.; Chubukov, P.; Xu, F.; Katritch, V.; Han, G. W.; Roth, C. B.; Heitman, L. H.; IJzerman, A. P.; Cherezov, V.; Stevens, R. C. Structural basis for allosteric regulation of GPCRs by sodium ions. *Science* **2012,** *337*, 232-236.
53. Segala, E.; Guo, D.; Cheng, R. K. Y.; Bortolato, A.; Deflorian, F.; Doré, A. S.; Errey, J. C.; Heitman, L. H.; IJzerman, A. P.; Marshall, F. H.; Cooke, R. M. Controlling the Dissociation of Ligands from the Adenosine A_{2A} Receptor through Modulation of Salt Bridge Strength. *J. Med. Chem.* **2016,** 59, 6470-6479.
54. Xu, Z.; Jang, Y.; Mueller, R. A.; Norfleet, E. A. IB-MECA and cardioprotection. *Cardiovasc. Drug Rev.* **2006,** *24*, 227-238.
55. Ge, Z.-D.; Peart, J. N.; Kreckler, L. M.; Wan, T. C.; Jacobson, M. A.; Gross, G. J.; Auchampach, J. A. Cl-IB-MECA [2-chloro-N^6-(3-iodobenzyl)adenosine-5′-*N*-methylcarboxamide] reduces ischemia/reperfusion injury in mice by activating the A_3 adenosine receptor. *J. Pharmacol. Exp. Ther.* **2006,** *319*, 1200-1210.
56. National center for biotechnology information. Pubchem compound database; CID=123683, https://pubchem.ncbi.nlm.nih.gov/compound/123683 (accessed June 30, 2017).
57. National center for biotechnology information. PubChem compound database; CID=3035850, https://pubchem.ncbi.nlm.nih.gov/compound/3035850 (accessed June 30, 2017).
58. Chen, Z.; Janes, K.; Chen, C.; Doyle, T.; Bryant, L.; Tosh, D. K.; Jacobson, K. A.; Salvemini, D. Controlling murine and rat chronic pain through A_3 adenosine receptor activation. *FASEB J.* **2012,** *26*, 1855-1865.
59. Carlin, J. L.; Tosh, D. K.; Xiao, C.; Piñol, R. A.; Chen, Z.; Salvemini, D.; Gavrilova, O.; Jacobson, K. A.; Reitman, M. L. Peripheral adenosine A_3 receptor activation causes regulated hypothermia in mice that is dependent on central histamine H_1 receptors. *J. Pharmacol. Exp. Ther.* **2016,** *356*, 474-482.
60. Little, J. W.; Ford, A.; Symons-Liguori, A. M.; Chen, Z.; Janes, K.; Doyle, T.; Xie, J.; Luongo, L.; Tosh, D. K.; Maione, S.; Bannister, K.; Dickenson, A. H.; Vanderah, T. W.; Porreca, F.; Jacobson, K. A.; Salvemini, D. Endogenous adenosine A_3 receptor activation selectively alleviates persistent pain states. *Brain* **2015,** *138*, 28-35.
61. Ford, A.; Castonguay, A.; Cottet, M.; Little, J. W.; Chen, Z.; Symons-Liguori, A. M.; Doyle, T.; Egan, T. M.; Vanderah, T. W.; De Konnick, Y.; Tosh, D. K.; Jacobson, K. A.; Salvemini, D. Engagement of the GABA to KCC2 signaling pathway contributes to the analgesic effects of A_3AR agonists in neuropathic pain. *J. Neurosci.* **2015,** *35*, 6057-6067.
62. de Witte, W. E. A.; Danhof, M.; van der Graaf, P. H.; de Lange, E. C. M. In vivo target residence time and kinetic selectivity: the association rate constant as determinant. *Trends Pharmacol. Sci.* **2016,** *37*, 831-842.

Chapter 6

Scintillation proximity assay (SPA) as a new approach to determine a ligand's kinetic profile. A case in point for the adenosine A_1 receptor

Lizi Xia, Henk de Vries, Adriaan P. IJzerman and Laura H. Heitman

Adapted from: *Purinergic Signalling*, **2016** 12(1):115–126

About this chapter

Scintillation Proximity Assay (SPA) is a radio-isotopic technology format used to measure a wide range of biological interactions, including drug-target binding affinity studies. The assay is homogeneous in nature, as it relies on a "mix and measure" format. It does not involve a filtration step to separate bound from free ligand as is the case in a traditional receptor-binding assay.

For G protein-coupled receptors (GPCR), it has been shown that optimal binding kinetics, next to a high affinity of a ligand, can result in more desirable pharmacological profiles. However, traditional techniques to assess kinetic parameters tend to be cumbersome and laborious. We thus aimed to evaluate whether SPA can be an alternative platform for real-time receptor-binding kinetic measurements on GPCR.

To do so we first validated the SPA technology for equilibrium binding studies on a prototypic class A GPCR, the human adenosine A_1 receptor (hA_1R). Differently to classic kinetic studies, the SPA technology allowed us to study binding kinetic processes almost real-time, which is impossible in the filtration assay. To demonstrate the reliability of this technology for kinetic purposes, we performed so-called competition association experiments. The association and dissociation rate constants (k_{on} and k_{off}) of unlabeled hA_1R ligands were reliably and quickly determined, and agreed very well with the same parameters from a traditional filtration assay performed simultaneously.

In conclusion, SPA is a very promising technique to determine the kinetic profile of the drug-target interaction. Its robustness and potential for high-throughput may render this technology a preferred choice for further kinetic studies.

Introduction

Scintillation Proximity Assays (SPA) are a bead-based assay technology for radioligand binding studies in drug research.[1, 2] The technology is homogeneous in nature, as it relies on a "mix and measure" format and avoids a filtration step to separate bound from unbound radiolabeled ligand as is the case in a traditional receptor-binding assay.[3] SPA technology, therefore, allows the rapid and convenient assay of a wide range of molecular interactions in a homogeneous system.[4, 5] With the help of a suitable radiolabeled probe the affinity of a compound for its drug target, such as G Protein-Coupled Receptors (GPCR), can be determined fast and reliably by SPA technology.[6-9] Nowadays in industry, SPA technology is routinely used for radioligand binding assays to determine ligand affinity in drug screening applications where high throughput is required.[10]

Alongside classical affinity parameters such as IC_{50} and K_i values, drug-target binding kinetics, in particular the receptor-ligand residence time (RT), is emerging as an additional parameter to assess the therapeutic potential of drug candidates with respect to drug efficacy and safety.[11-14] Consequently, there is an increasing awareness of the importance of measuring the kinetics of drug−target interactions. In the research field of GPCR a number of structure-kinetics relationship (SKR) studies have been published that suggest that for educated compound triage for further studies binding kinetics should be included in the decision process.[15-17] Therefore, a fast and trustful approach to determine kinetic parameters is urgently required.

By definition, the RT is inversely proportional to the ligand dissociation-rate constant (k_{off}). This rate constant together with the association-rate constant (k_{on}) can both be retrieved from appropriate kinetic experiments following the principles laid out by Motulsky and Mahan.[18] In that publication so-called competition association experiments are described, which are conventionally performed in the form of filtration assays. In this format the method consumes a great amount of radioligand, membrane protein and other materials. Besides, the tediousness and limited throughput of the kinetic assay are impediments to obtain k_{on} and k_{off} values for series of ligands efficiently.

So far there have been quite a few attempts to improve the efficiency of kinetic screening. For example, an insurmountable effect of slowly dissociating ligands in a functional IP-1 assay in SPA format on the neurokinin-1 (NK_1) receptor has been described.[19] In this case the costly functional methodology only allowed for the qualitative screening of the slowly dissociating ligands. Another kinetic screening approach in the form of SPA technology took the observation of a K_i (leftward) shift [20] over time as proof for slowly dissociating compounds from different GPCR.[6, 7] Although SPA technology was used in both studies, they were essentially equilibrium binding assays with long incubation times (10 h in gonadotropin-releasing hormone (GnRH) receptor,[6] and 5 h in human CCR5 receptor [7]) that were inevitable to determine the kinetic effects with a read-out that was rather qualitative.

Recently, a method called dual-point competition association assay that enables the relatively fast kinetic screening of series of compounds was introduced by Guo *et al*.[21] By measuring radioligand binding at two different time points in the absence or presence of unlabeled competitors, the kinetic rate index (KRI) was obtained. Although both fast and slowly dissociating ligands can be characterized and discriminated with this index, it is still a rather qualitative measure, as the k_{on} (k_3) and k_{off} (k_4) values of the unlabeled ligands cannot be obtained. Thus, the resolution of a kinetic comparison for SKR through KRI values is not as high as with full kinetic parameters.[17]

The true benefit of SPA technology relies in its separation-free approach, which could allow almost continuous kinetic measurements over time. Previously, a kinetic study of radioligand association and dissociation by SPA technology has been reported for the inositol trisphosphate receptor ($InsP_3R$), a Ca^{2+} channel, and it indeed confirmed that SPA is a useful technique to determine fast k_{on} and k_{off} values that might have been difficult to obtain using traditional methods.[22] However, SPA technology as a format to study the kinetics of radioligand binding to GPCR has not been reported in literature in any detail.

Therefore in the present study we aimed to fill this gap by converting a filtration-based kinetic radioligand binding assay to an SPA format, using a prototypical GPCR, the human adenosine A_1 receptor (hA_1R), as an example. We firstly validated the SPA technology for equilibrium binding studies by comparing it to traditional filtration assays performed simultaneously. In these experiments both hA_1R agonists and antagonists were tested, and their affinity determined with SPA technology was similar to the affinity determined in a filtration assay. In subsequent kinetic studies, the SPA technology was of great benefit, as it allowed us to follow radioligand binding over time in a single well, which is impossible in the filtration assay. We further demonstrated that advantage in the most laborious of all kinetic assays, the competition association experiment. The association and dissociation rate constants of unlabeled ligands for hA_1R were reliably and quickly determined and agreed very well with the same parameters in a traditional filtration assay performed in parallel.

Methods

Chemicals and reagents. [^{3}H]-1,3-Dipropyl-8-cyclopentyl-xanthine ([^{3}H]-DPCPX, specific activity 113.4 Ci·mmol^{-1}) was purchased from ARC, Inc. (St. Louis, MO). The Wheat Germ Agglutinin-Polyvinyl toluene (WGA-PVT) SPA beads (RPNQ0001) were purchased from PerkinElmer (Waltham, MA). Adenosine deaminase (ADA) was purchased from Boehringer Mannheim (Mannheim, Germany). 1,3-Dipropyl-8-cyclopentylxanthine (DPCPX, a selective hA_1R antagonist),[23] 8-cyclopentyl-3-*N*-[3-((3-(4-fluorosulphonyl)benzoyl)-oxy)-propyl]-1-*N*-propyl-xanthine (FSCPX, an irreversible hA_1R antagonist),[24] 2-chloro-N^6-cyclopentyladenosine (CCPA, a specific hA_1R agonist),[25] N^6-Cyclopentyladenosine (CPA, a specific hA_1R agonist [25]), 5'-*N*-ethylcarboxamidoadenosine (NECA, a non-selective agonist for adenosine receptors)[26] and guanosine-5'-triphosphate (GTP) were purchased from Sigma (St. Louis, MO). BCA (Bicinchoninic acid) protein assay kit was obtained from Pierce Chemical Company (Rockford, IL). LUF5834 (a hA_1R partial agonist) was synthesized in our laboratory as described previously.[27] Chinese hamster ovary (CHO) cells stably expressing the hA_1R

were obtained from Prof. Steve Hill (University of Nottingham, UK). All other chemicals were of analytical grade and obtained from standard commercial sources.

Cell culture and membrane preparation. CHO cells stably expressing hA_1R were grown in Ham's F12 medium containing 10% ($v \cdot v^{-1}$) normal adult bovine serum, streptomycin (100 $\mu g \cdot mL^{-1}$), penicillin (100 $IU \cdot mL^{-1}$), and G418 (0.4 $mg \cdot mL^{-1}$) at 37 °C in 5% CO_2. Cells were subcultured twice weekly at a ratio of 1:20 on 10-cm ø culture plates. For membrane preparation, cells were subcultured 1:10 and then transferred to 15-cm ø plates. Cells grown to 80% to 90% confluency were detached from plates by scraping them into 5 mL phosphate-buffered saline (PBS), collected, and centrifuged at 700 g (3 000 rpm) for 5 min. Cell pellets derived from 30 plates were pooled and resuspended in 20 mL of ice-cold 25 mM Tris-HCl buffer (pH 7.4). An UltraThurrax (Heidolph Instruments, Schwabach, Germany) was used to homogenize the cell suspension. Membranes and the cytosolic fraction were separated by centrifugation at 100 000 g (31 000 rpm) in a Beckman Optima LE-80K ultracentrifuge (Beckman Coulter, Fullerton, CA) at 4 °C for 20 min. The pellet was resuspended in 15 mL of the Tris-HCl buffer, and the homogenization and centrifugation step was repeated. Tris-HCl buffer (10 mL, pH 7.4) was used to resuspend the pellet, and ADA was added (0.8 $IU \cdot mL^{-1}$) to break down endogenous adenosine. Membranes were stored in 250 µL aliquots at -80 °C. Concentrations of membrane protein were measured using the BCA method.[28]

Radioligand displacement experiments. The displacement experiments were performed using 10 concentrations of competing ligands in 25 µL of assay buffer (For antagonists: 50 mM Tris-HCl [pH 7.4 at 25 °C]; for agonists: 50 mM Tris-HCl supplemented with 5 mM $MgCl_2$ [pH 7.4]) in the presence of another 25 µL of assay buffer with a final concentration of 2.4 nM [^{3}H]-DPCPX. At this concentration, total radioligand binding did not exceed 10% of that added to prevent ligand depletion. Nonspecific binding (NSB) was determined in the presence of 100 µM CPA. Each condition was measured in duplicate and at least 3 individual experiments were performed.

The SPA technology: A mixture of 5 μg protein membrane and 1 mg SPA bead was pre-coupled in a shaker (Vibrax VXR ,IKA) in a volume of 50 μL of assay buffer at room temperature for 30 min. Then together with the radioligand and competing ligands, the membrane-bead mixture was dispatched in an Isoplate-96 Microplate (Perkin Elmer, Groningen, the Netherlands), in a final reaction volume of 100 μL. The plate was incubated for 1 h inside the counting chamber of a 2450 MicroBeta^2 Plate Counter (Perkin Elmer, Groningen, the Netherlands) at the ambient temperature of 28 ^{o}C. The binding values were recorded in corrected counts per minute (CCPM).

The filtration assay: Membrane aliquots containing 5 μg protein were incubated together with the radioligand and competing ligands in a total volume of 100 μL assay buffer in a 96-well plate. After 1 h incubation at room temperature, the incubation was terminated by rapid vacuum filtration to separate the bound and free radioligand through 96-well GF/B filter plates using a PerkinElmer Filtermate-harvester (Perkin Elmer, Groningen, the Netherlands). Filters were subsequently washed three times with ice-cold wash buffer (50 mM Tris-HCl [pH 7.4], supplemented with 5 mM $MgCl_2$). After 30 min of dehydration of the filter plate at 50 ^{o}C, the filter-bound radioactivity was determined by scintillation spectrometry using the 2450 MicroBeta^2 Plate Counter. The binding values were recorded in both counts per minute (CPM) and disintegrations per minute (DPM).

Radioligand association and dissociation experiments. The SPA technology: The membrane-bead mixture was prepared as described under "Radioligand Displacement Experiments". Once the membrane-bead mixture was added to the wells of an Isoplate-96 Microplate, measurements of radioligand bound to the receptor were started immediately and continued every 30 sec for 1 h, using the 2450 MicroBeta^2 Plate Counter. Subsequently, radioligand dissociation was initiated by the addition of 10 μM unlabeled CPA. Another 1 h of measurements at every 30 sec was used to record the amount of radioligand still bound to the receptor. Samples were obtained as described under *Radioligand displacement experiments*.

The filtration assay: Association experiments were performed by incubating membrane aliquots containing 5 µg of protein in a total volume of 100 µL of assay buffer at 28 °C with 2.4 nM [^{3}H]-DPCPX. The amount of radioligand bound to the receptor was measured at different time intervals during a total incubation of 1 h. Dissociation experiments were performed by preincubating membrane aliquots containing 5 µg of protein in a total volume of 100 µL of assay buffer for 1 h. After the preincubation, radioligand dissociation was initiated by the addition of 10 µM unlabeled CPA. The amount of radioligand still bound to the receptor was measured at various time intervals for a total of 1 h to ensure that full dissociation from hA_1R was reached. Incubations were terminated and samples were obtained as described under *Radioligand Displacement Experiments*.

Competition association experiments. The binding kinetics of unlabeled ligands was quantified using the competition association assay based on the theoretical framework by Motulsky and Mahan.[18] In this experiment, one concentration of IC_{50} or three different concentrations of unlabeled competing ligands were tested—namely, at IC_{25}, IC_{50}, and IC_{75} determined from "Radioligand Displacement Experiments". For (partial) agonists, 1 mM of GTP was present in the agonist assay buffer to ensure that agonist binding only occurred to the uncoupled form of hA_1R.[13] The assay was performed by incubating in a total volume of 100 µL of assay buffer at 28 °C with 2.4 nM [^{3}H]-DPCPX.

The SPA technology: The membrane-bead mixture was prepared as described under "Radioligand Displacement Experiments". Once the membrane-bead mixture was added to the wells of an Isoplate-96 Microplate, measurements of radioligand bound to the receptor were started immediately and continued every 30 sec for 2 h, using the 2450 MicroBeta^2 Plate Counter. Samples were obtained as described under *Radioligand Displacement Experiments*.

The filtration assay: The competition association assay was initiated by adding membrane aliquots (5 µg per well) at different time points for a total of 2 h in the absence or presence of competing ligand. Incubations were terminated and samples were obtained as described under *Radioligand Displacement Experiments*.

Data analysis. All values obtained are means of at least three independent experiments performed in duplicate. All experimental data were analyzed by using GraphPad Prism 6 (GraphPad Software, Inc., San Diego, CA), as in the description of previous work from our research group,[21] including the following analysis: IC_{50} values obtained from competition displacement binding data were converted to K_i values using the Cheng-Prusoff equation [29], the k_{on} and k_{off} values for radiolabeled and unlabeled ligands were fitted and calculated, and the k_{on} and k_{off} values were used to calculate residence times (in min) and kinetic dissociation binding constants (kinetic K_D).

Results

The affinity (K_i) of hA_1R ligands in displacement experiments.

The affinities of several hA_1R ligands were determined by displacement experiments formatted with SPA technology or as filtration assays. The tested hA_1R ligands showed concentration-dependent inhibition of specific [^{3}H]-DPCPX binding, and the data of antagonists (DPCPX, FSCPX) or partial agonist (LUF5834) were best fitted to a one-state competition model, while the data of full agonists (CCPA, NECA) were best fitted with a two-state receptor model. Affinities of all ligands determined by both SPA technology and filtration assay are shown in **Table 1.** All compounds showed high affinities, with those of antagonists and partial agonist in the nanomolar range. The agonists displayed high, nanomolar affinity for the so-called high affinity state, and lower, submicromolar affinity for the low affinity state. The affinities of the hA_1R ligands from these equilibrium experiments were in good agreement between SPA technology and filtration assay (**Figure 1**). Due to the irreversible binding characteristics of FSCPX only its "apparent" affinity could be determined, which was subsequently included in the correlation.

Table 1. Comparison of the affinity of representative hA_1R antagonists and (partial) agonists obtained from displacement studies of specific [^{3}H]-DPCPX binding from hA_1R membranes by SPA technology or filtration assay, respectively. Values are means ± s.e.m of at least three independent experiments performed in duplicate. For full agonists CCPA and NECA, displacement curves were best analyzed with a two-state model, yielding K_i values for a high affinity state and a low affinity state of the receptor.

Compound	SPA K_i (nM)	Filtration K_i (nM)
FSCPX	0.9 ± 0.02[a]	1.6 ± 0.1[a]
DPCPX	4.3 ± 0.4	3.3 ± 0.3
LUF5834	6.2 ± 0.5	4.3 ± 0.6
CCPA	7.0 ± 1.1 (high)	8.3 ± 3.8 (high)
	861 ± 156 (low)	1010 ± 159 (low)
NECA	8.0 ± 2.3 (high)	7.8 ± 3.8 (high)
	282 ± 80 (low)	301 ± 39 (low)

[a] "Apparent" affinity of this irreversibly binding antagonist.

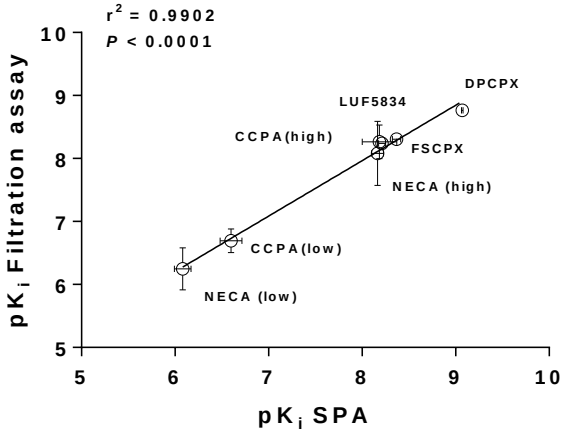

Figure 1: Correlation of the negative logarithm of hA_1R ligands' affinity (pK_i) determined by SPA and in a filtration assay Agonists: CCPA, NECA, LUF5834; Antagonist: DPCPX, FSCPX.

The association (k_{on}) and dissociation rate constants (k_{off}) of [^{3}H]-DPCPX at hA_1R.

Receptor association and dissociation rates of [^{3}H]-DPCPX were directly determined in classic radioligand association and dissociation experiments with either SPA technology or filtration assays. In both assay formats, the binding of [^{3}H]-DPCPX approached equilibrium after approximately 15 min

(**Figure 2**), indicating a relative fast k_{on} of 0.40 ± 0.05 $nM^{-1} \cdot min^{-1}$ by SPA technology and 0.24 ± 0.03 $nM^{-1} \cdot min^{-1}$ by filtration.

A.

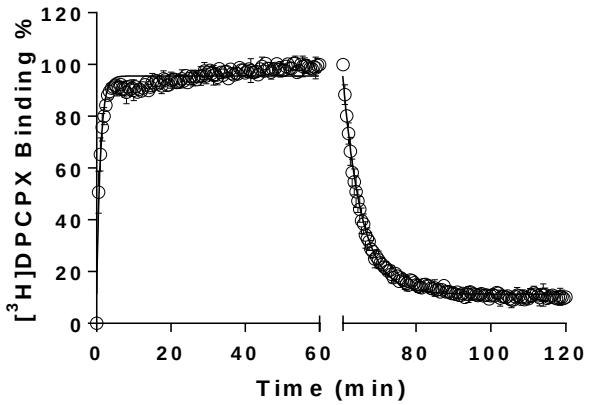

B.

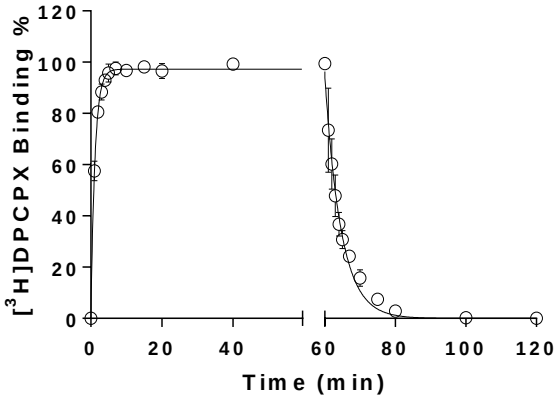

Figure 2: Association and dissociation kinetics of [^{3}H]-DPCPX (2.4 nM) to and from hA_1R stably expressed on CHO cell membranes (28 °C), measured in SPA technology (n=3, combined and normalized, **Fig. 2A**) or filtration assay (n=3, combined and normalized, **Fig. 2B**). 10 µM CPA was used as a displacer to initiate the dissociation. Association data was fitted in Prism 6 using one-phase exponential association. Dissociation data was fitted using one-phase exponential decay.

Binding of the radioligand was reversible after the addition of 10 µM CPA and complete dissociation was reached after approximately 25 min (**Figure 2**). The k_{off} of [^{3}H]-DPCPX from the hA_1R was 0.20 ± 0.02 min^{-1} with SPA technology and 0.25 ± 0.01 min^{-1} in the filtration assay (**Table 2**). The kinetic K_D

(k_{off}/k_{on}) of [^{3}H]-DPCPX was 0.50 ± 0.08 nM (SPA) and 1.04 ± 0.14 nM (filtration) (**Table 2**). The residence time (RT, $1/k_{off}$) of [^{3}H]-DPCPX was calculated as 5.0 ± 0.5 or 4.0 ± 0.2 min, determined by SPA or filtration, respectively.

Table 2. Comparison of the kinetic rates of [^{3}H]-DPCPX obtained from classic kinetic association and dissociation experiments from hA_1R membranes at 28 °C by SPA assay and filtration assay. Values are means ± s.e.m of three independent experiments performed in duplicate. Equations used are as follows: $k_{on} = (k_{obs} - k_{off})/[[^3H]\text{-DPCPX}]$; Kinetic $K_D = k_{off}/k_{on}$; $RT = 1/k_{off}$. RT is residence time.

[^{3}H]-DPCPX	SPA	Filtration
k_{on} ($nM^{-1} \cdot min^{-1}$)	0.40 ± 0.05	0.24 ± 0.03
k_{off} (min^{-1})	0.20 ± 0.02	0.25 ± 0.01
Kinetic K_D (nM)	0.50 ± 0.08	1.0 ± 0.1
RT (min)	5.0 ± 0.5	4.0 ± 0.2

The Competition Association Assay at hA_1R.

With the established k_{on} (k_1) and k_{off} (k_2) values of [^{3}H]-DPCPX binding from classic association and dissociation experiments, k_{on} (k_3) and k_{off} (k_4) values of unlabeled DPCPX were determined by fitting the values based on the mathematical model as previously described (see **Methods**). Three different concentrations of unlabeled DPCPX, lower than (IC_{25}), equal to and higher than (IC_{75}) its IC_{50} value, were tested (**Figure 3**). Its k_{on} and k_{off} values determined by this competition association method were 0.72 ± 0.16 $nM^{-1} \cdot min^{-1}$ and 0.50 ± 0.01 min^{-1} by SPA (**Figure 3A** and **Table 3**) or 0.19 ± 0. 04 $nM^{-1} \cdot min^{-1}$ and 0.27 ± 0.03 min^{-1} by filtration (**Figure 3B** and **Table 3**), which were in good accordance with the k_1 and k_2 values determined in the classic association and dissociation experiments (**Table 2 and Figure 2**). Since the kinetic K_D values and affinities (K_i) obtained from the different equilibrium and kinetic experiments are well comparable (**Tables 1**-**3**) this further verified that the competition association assay by SPA technology could be accurately used to determine the binding kinetics of unlabeled A_1R ligands.

We then used FSCPX, an irreversibly binding hA_1R antagonist, as a further validation tool. In the competition association assay FSCPX displayed an “overshoot” in the association curve indicating a

negligible dissociation, which was observed in both SPA (**Figure 4A**) and filtration assay (**Figure 4B**). Its k_{on} and k_{off} values determined by the competition association method were 0.0047 ± 0.0007 $nM^{-1}\cdot min^{-1}$ and 0.0064 ± 0.0013 min^{-1} by SPA or 0.0019 ± 0.0003 $nM^{-1}\cdot min^{-1}$ and 0.0060 ± 0.0020 min^{-1} by filtration (**Table 3**).

Table 3. Comparison of the kinetic rate constants, residence times (RT) and kinetic K_D values of representative hA_1R antagonists and (partial) agonists obtained from competition association experiments to hA_1R expressed on CHO cell membranes at 28 °C by SPA assay and filtration assay. For (partial) agonists LUF5834, CCPA and NECA, 1 mM GTP was present in the assay. The k_{on} (k_3), k_{off} (k_4) values of the unlabeled compounds were determined in [^{3}H]-DPCPX (2.4 nM) competition association experiments. RTs and kinetic K_Ds were determined in the same manner as described in **Table 2**.

Cmpd.	SPA				Filtration assay			
	k_{on} ($nM^{-1}\cdot min^{-1}$)	k_{off} (min^{-1})	RT (min)	Kinetic K_D (nM)	k_{on} ($nM^{-1}\cdot min^{-1}$)	k_{off} (min^{-1})	RT (min)	Kinetic K_D (nM)
FSCPX	0.0047 ± 0.0007	0.0064 ± 0.0013	156 ± 31	1.4 ± 0.3	0.0019 ± 0.0003	0.0060 ± 0.0020	167 ± 56	3.2 ± 0.4
DPCPX	0.72 ± 0.16	0.50 ± 0.01	2.0 ± 0.1	0.69 ± 0.15	0.19 ± 0. 04	0.27 ± 0.03	3.7 ± 0.4	1.4 ± 0.1
LUF5834	0.13 ± 0.05	0.50 ± 0.05	2.0 ± 0.1	3.9 ± 1.5	0.062 ± 0.006	0.23 ± 0.03	4.4 ± 0.5	3.7 ± 0.5
CCPA	0.0094 ± 0.0022	0.73 ± 0.04	1.4 ± 0.1	78 ± 19	0.016 ± 0.002	1.5 ± 0.03	0.68 ± 0.01	92 ± 9
NECA	0.0014 ± 0.0004	0.54 ± 0.06	1.9 ± 0.02	386 ± 36	0.0012 ± 0.0001	0.60 ± 0.04	1.7 ± 0.1	500 ± 8

The other unlabeled ligands included the hA_1R partial agonist LUF5834 and full agonists CCPA and NECA. Their k_{on} and k_{off} values were determined in both SPA and filtration assays, in the presence of 1 mM GTP (**Figures 5-7** and **Table 3**). The current mathematical model does not allow the calculation of two receptor states with corresponding kinetic parameters; the inclusion of GTP in the assay forces the receptor to be in one lower affinity, G protein-uncoupled, state only. With this restriction the kinetic parameters of both partial and full agonists were determined as conveniently as the two antagonists (**Table 3**). The kinetic profiles (k_{on} and k_{off}) of all hA_1R ligands obtained by SPA were in good agreement with the results from filtration (**Figure 8A** and **8B**). Due to its irreversible binding

nature, FSCPX was not included in the correlation. The correlation between kinetic K_D values from either SPA or filtration assay was high too (**Figure 8C**). Finally, with data from all experiments at hand, we concluded that the equilibrium K_i and kinetic K_D values from both SPA technology and filtration assay were also highly correlated (**Figure 8D** and **8E**).

A.

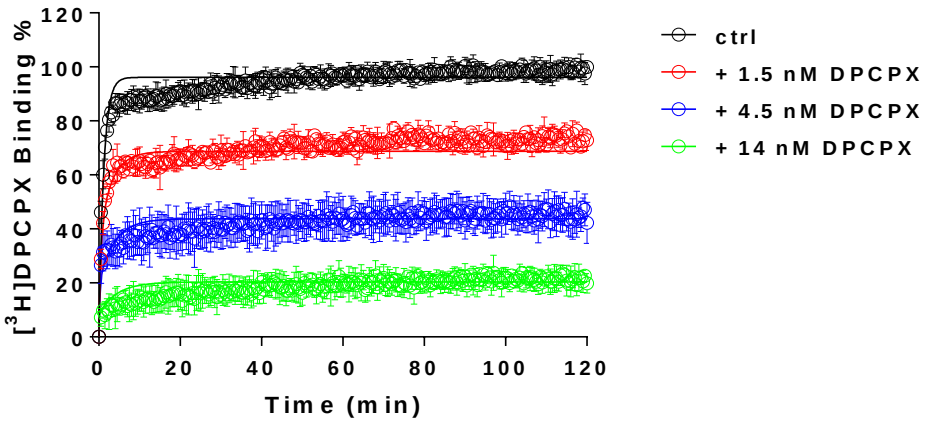

B.

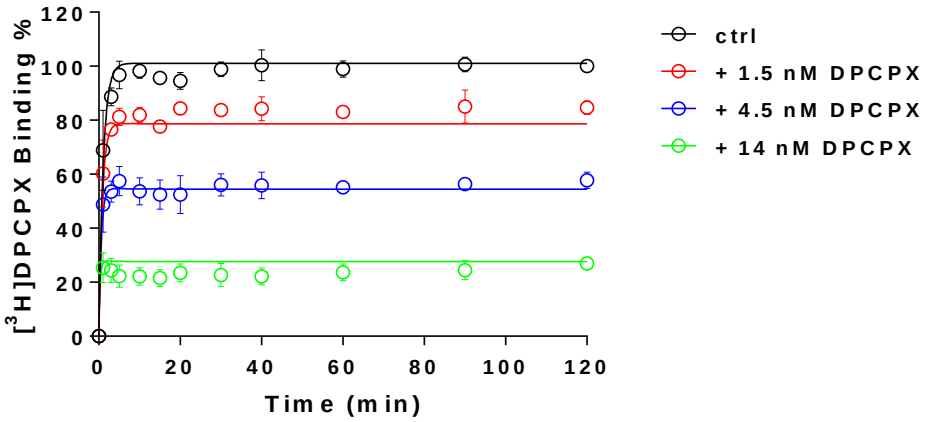

Figure 3: Competition association experiments with [^{3}H]-DPCPX binding to hA_1R stably expressed on CHO cell membranes (28 °C) in the absence or presence of 1.5 nM, 4.5 nM, and 14 nM of unlabeled DPCPX by SPA assay (n=4, combined and normalized, **Fig. 3A**) or classic filtration assay (n=3, combined and normalized, **Fig. 3B**)

A.

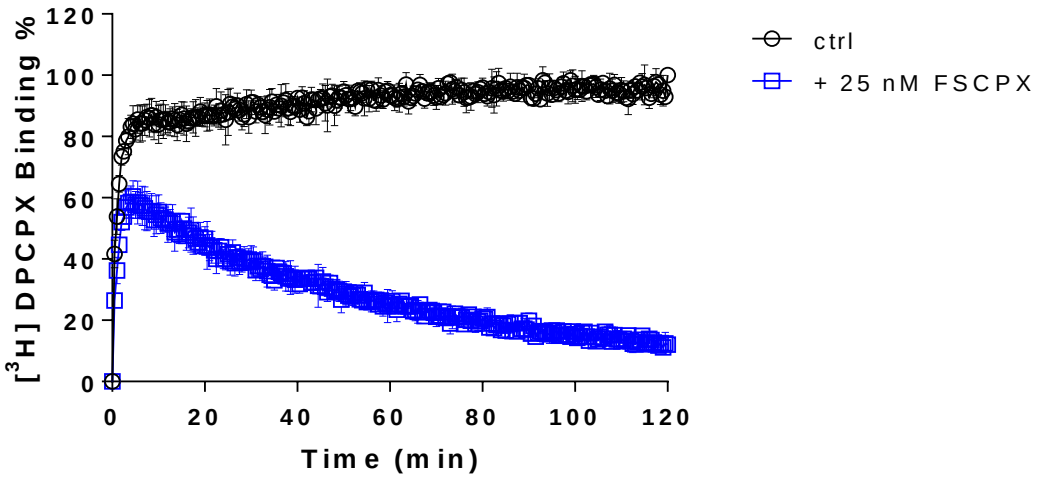

B.

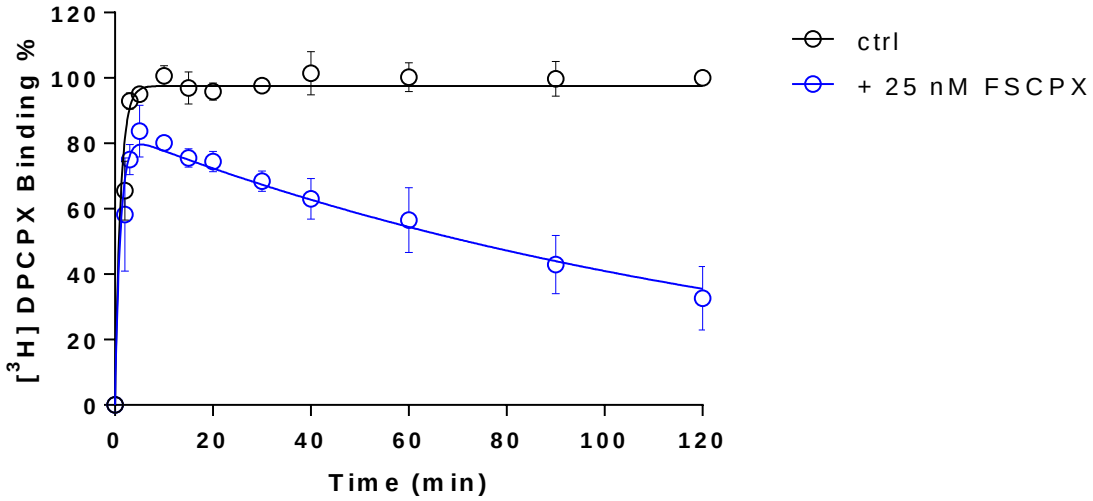

Figure 4: Competition association experiments with [^{3}H]-DPCPX binding to hA_1R stably expressed on CHO cell membranes (28 °C) in the absence or presence of 25 nM FSCPX, measured in SPA technology (n=4, combined and normalized, **Fig. 4A**) or filtration assay (n=3, combined and normalized, **Fig. 4B**).

A.

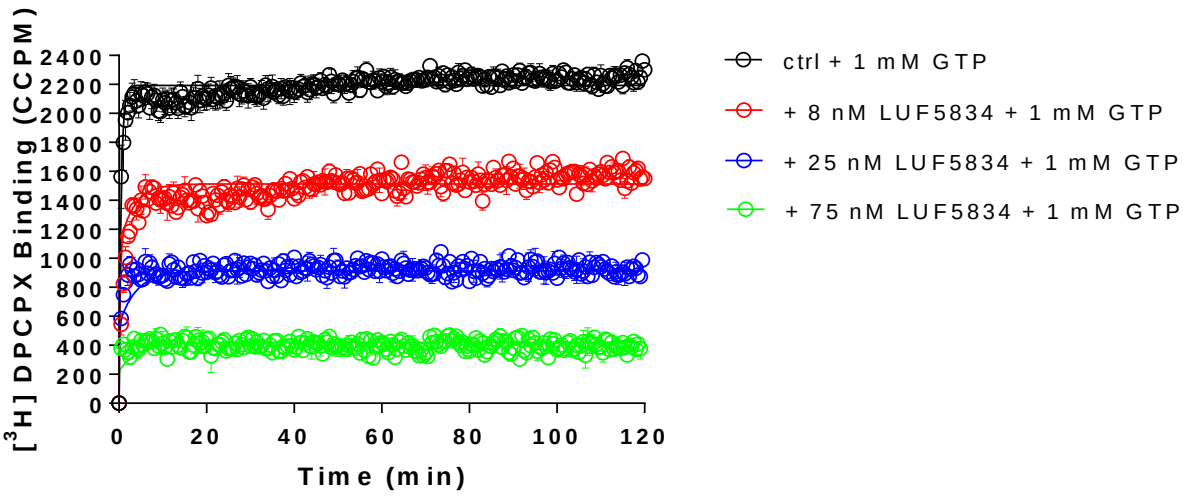

B.

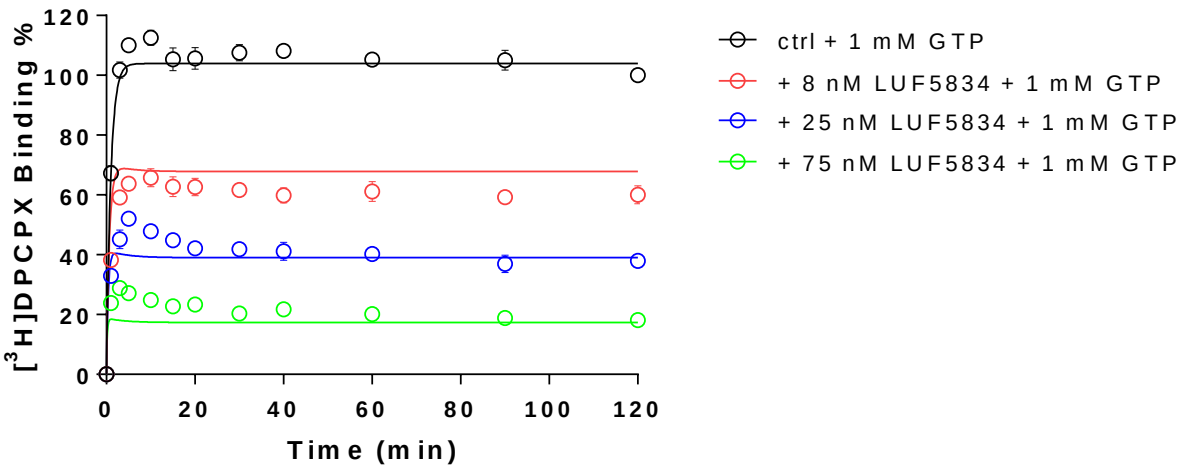

Figure 5: Competition association experiments with [^{3}H]-DPCPX binding to hA_1R stably expressed on CHO cell membranes (28 °C) in the absence or presence of 8 nM, 25 nM, and 75 nM of unlabeled LUF5834 by SPA technology (n=3, one representative experiment, **Fig. 5A**) or filtration assay (n=3, combined and normalized, **Fig. 5B**)

A.

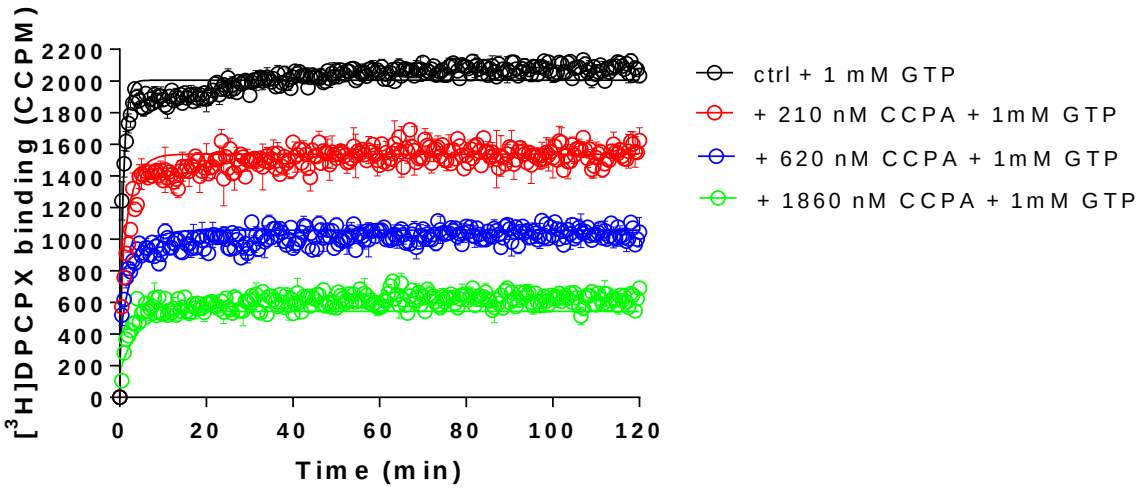

B.

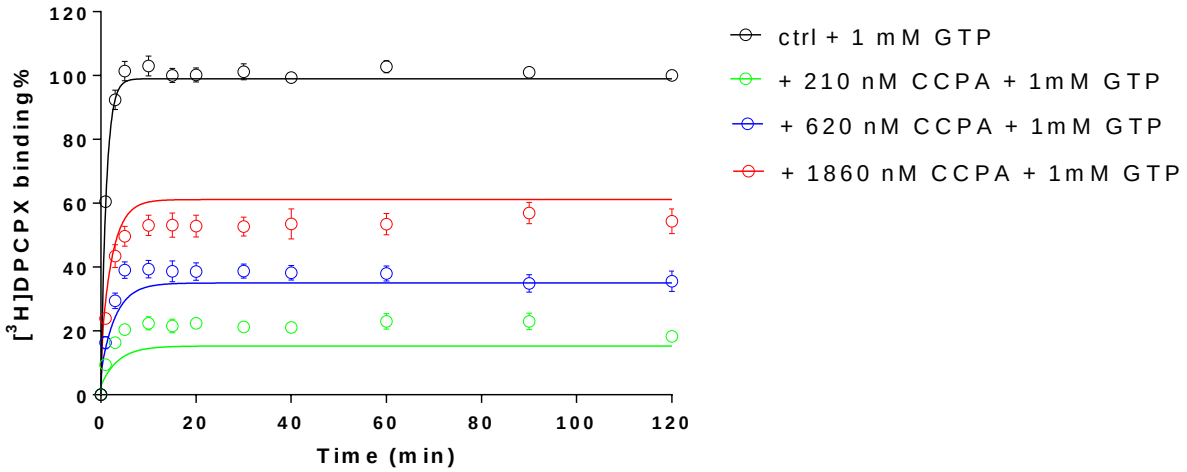

Figure 6: Competition association experiments with [^{3}H]-DPCPX binding to hA_1R stably expressed on CHO cell membranes (28 °C) in the absence or presence of 210 nM, 620 nM, and 1860 nM of unlabeled CCPA by SPA assay (n=3, one representative experiment, **Fig. 6A**) or filtration assay (n=3, combined and normalized, **Fig. 6B**)

A.

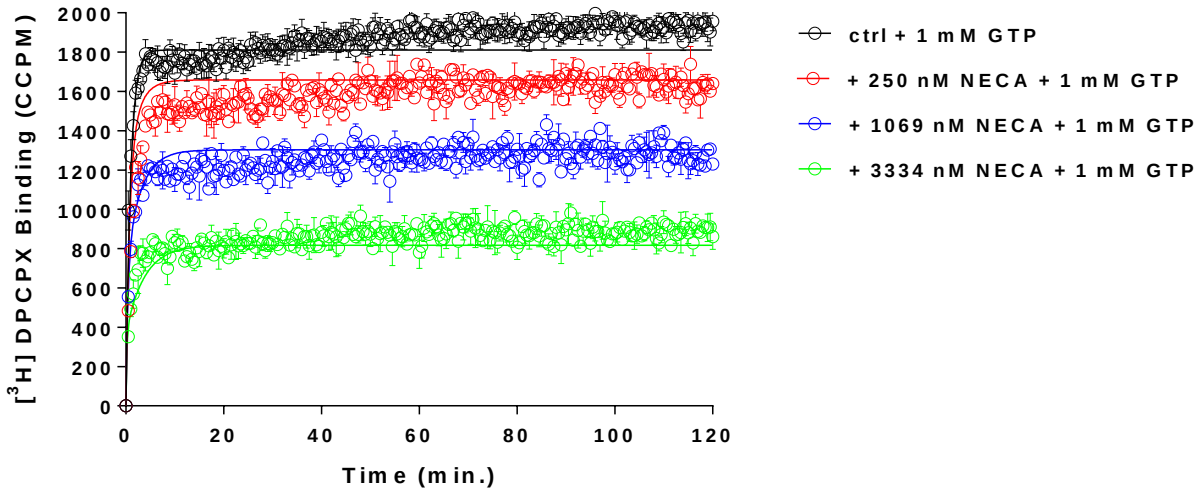

B.

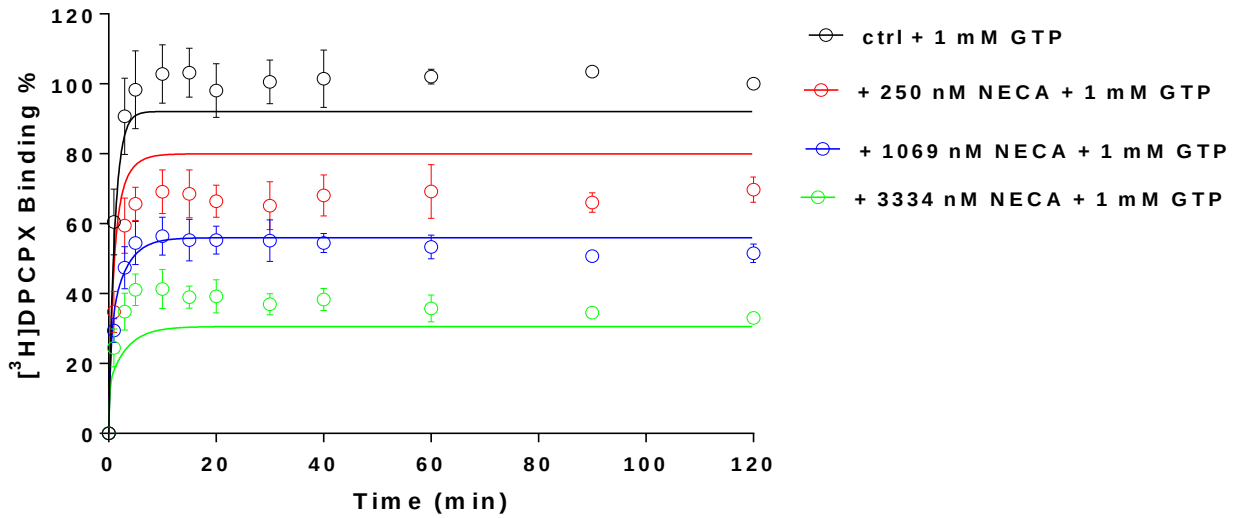

Figure 7: Competition association experiments with [^{3}H]-DPCPX binding to hA_1R stably expressed on CHO cell membranes (28 °C) in the absence or presence of 250 nM, 1069 nM, and 3334 nM of unlabeled NECA by SPA assay (n=3, one representative experiment, **Fig. 7A**) or filtration assay (n=3, combined and normalized, **Fig. 7B**).

A. B.

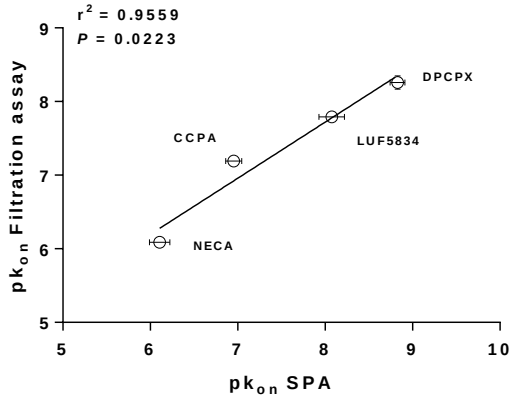

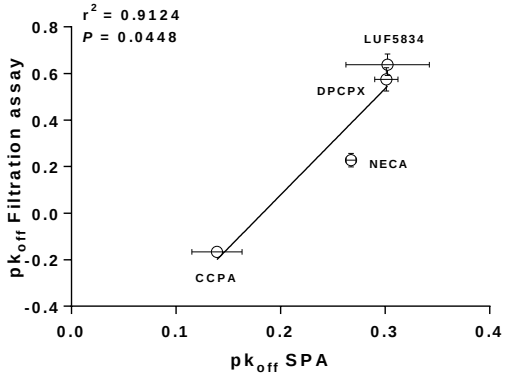

C.

D.

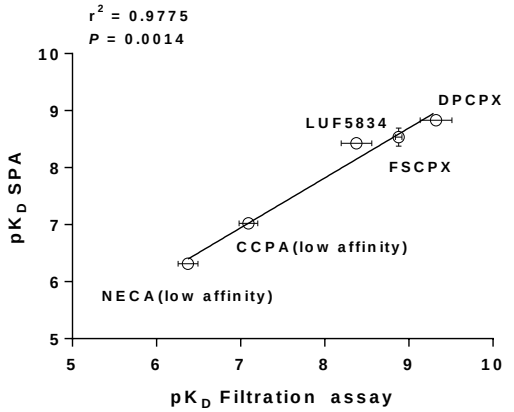

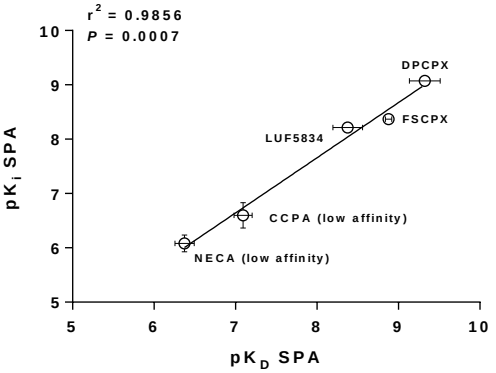

E.

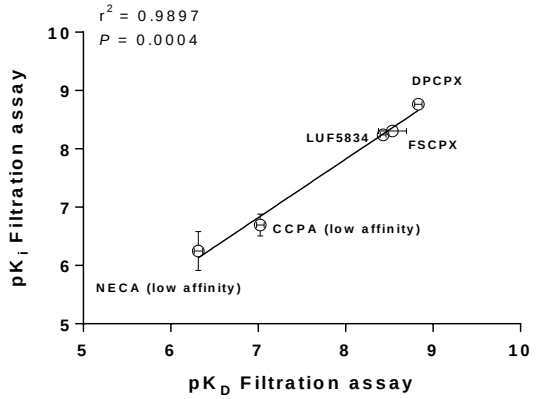

Figure 8: Correlation of the negative logarithm of hA_1R ligands' association rates (pk_{on}, **Fig. 8A**) and dissociation rates (pk_{off}, **Fig. 8B**) determined by SPA (*x*-axis) and filtration assay (*y*-axis). Agonists: CCPA, NECA, LUF5834; Antagonist: DPCPX. Correlation of the negative logarithm of hA_1R ligands' kinetic K_D (pK_D) determined by SPA (*y*-axis) and filtration (*x*-axis). For (partial) agonists LUF5834, CCPA and NECA only the low affinity state of the receptor was taken into account due to the presence of 1 mM GTP in the competition association experiments (**Fig. 8C**). Correlation of the negative logarithm of hA_1R ligands' affinity (pK_i) from displacement studies of specific [^{3}H]-DPCPX binding from hA_1R membranes and the negative logarithm of hA_1R ligands' kinetic K_D (pK_D) determined by SPA (**Fig. 8D**) and filtration (**Fig. 8E**). For (partial) agonists LUF5834, CCPA and NECA only the low

affinity state of the receptor was taken into account due to the presence of 1 mM GTP in the competition association experiments.

Discussion

In this study we developed and validated a method based on the principles of a scintillation proximity assay (SPA) for the determination of kinetic characteristics of GPCR ligands. The adenosine A_1 receptor was used as our workhorse, together with a number of reference ligands with divergent characteristics. In the following we discuss the benefits and relatively minor concerns of the approach.

Advantages of SPA technology.

We substituted a standard filtration assay by SPA technology to determine the kinetics of the drug-receptor interaction. In that setting the most obvious improvement is that the event of ligand association and dissociation to and from the receptor can be measured almost in real-time without washing steps which are indispensable in a filtration assay. This improvement brings the benefit of great efficiency in kinetic radioligand binding experiments.

For example, in the filtration format association and dissociation kinetics of [^{3}H]-DPCPX to and from hA_1R are determined separately, because it is impractical to perform both association and dissociation experiments in one 96-well plate. However in the SPA format only a single well is required to record such a full curve (**Figure 2**). This also brings impressively improved throughput in the competition association assay of unlabeled ligands with [^{3}H]-DPCPX as the radioligand. In an individual filtration experiment to measure competition association a whole 96-well plate is used, allowing for 2 duplicate curves from 3 different concentrations of unlabeled ligand and a control curve. However, with SPA only a few wells are required to obtain the same results, as is shown in Figs **3**-**7**. This is due to the 6-detector panel operating simultaneously in the counter, allowing a rich data collection of six wells simultaneously. On average, the duration of an n=3 competition association

experiment by SPA is reduced to 1-2 days from almost one week of practical work by filtration, with the additional benefit of much less bench time.

The SPA technology not only improved the speed and throughput of the kinetic radioligand binding experiments, but also provided more, more precise and more accurate data. The competition association experiment is based on the Motulsky-Mahan model for competition association, which requires a substantial number of data points for plotting curves and subsequent analysis. In other words, the more data points obtained, the more accurate k_{on} and k_{off} can be determined. The SPA technology enables to acquire a great number ('more') of data points, from one well rather than separate tubes ('more precise'). In this case of a 2-hour experiment, one well on a 96-well plate was sampled every 30 sec, yielding a total of 240 data points in one curve, while in the comparable filtration assay there are only a labor-intensive dozen or so (**Figure 3-7**). A further reason of concern in the filtration assay is that the separation step only differentiates bound from unbound ligand, irrespective of whether the binding process itself consists of several steps [7], or that weaker interactions are broken such that only a fraction of receptor-ligand complexes might be detected after washing [30]. In the absence of filtration steps SPA technology provides the possibility to collect this information without these caveats ('more accurate'). Lastly, overall financial expenses are favorable. Although the beads come at a price, the hugely reduced number of wells makes the experiment very cost-effective.

Differences in SPA technology from filtration assay.

SPA is a homogeneous bead-based technique, in which the receptor membrane protein is coupled with a certain type of SPA bead. Although there are several approaches to add SPA beads to the reaction (such as a precoupled format, a simultaneous addition ("T=0") format, or delayed addition format [10]), for kinetic experiments precoupling of the cell membranes with SPA beads is necessary. The convenience of doing so is that bead and membrane are treated as a single reagent, thus reducing the time to dispense an assay and there is no issue of membrane-bead diffusion. More

importantly, the membrane-bead ration needs to be optimized to generate a useful specific radioligand binding "window". In our case, 5 µg of hA_1R membrane protein was associated with 1 mg of WGA-PVT beads. Adding an excess of SPA beads would ensure that all the membrane is captured and a maximum signal is obtained, but the excess might equally contribute to an increased background signal [1]. It should be realized that besides normal non-specific binding (NSB) another background signal called non-proximity effect (NPE) may play a role. This was clearly observed in kinetic assays. The NPE is to describe that if a radioligand stays in close proximity, the bead would be activated irrespective of whether the radioligand is bound to the bead or membrane-bead mixture [2]. From **Figure 2A** it seems that [^{3}H]-DPCPX did not fully dissociate from the hA_1R as was the case in the filtration assay (**Figure 2B**), with an elevated baseline of approx. 10% of radioligand binding. This observation does not necessarily mean there was still 10% of [^{3}H]-DPCPX binding to the hA_1R, but rather indicates that some of the liberated [^{3}H]-DPCPX stayed in the proximity of the bead, yielding a weak signal.

In the SPA technology there is no need to add liquid scintillation fluid after harvesting as in filtration assays. As a consequence the typical CPM-DPM conversion from the spectrometer's counting efficiency as a result of quenching cannot be done [31-33]. As all events take place at the surface of the SPA bead [2] the light emitting process cannot be quenched. A further different and unique aspect of SPA technology and corresponding equipment is that samples are monitored from both top and bottom and a count is only a count when top and bottom detectors both record the light quant within a certain amount of time. It is possible that a light quant is emitted in the top of the well by dispersion by the beads, while this quant is not seen by the bottom detector. The counter has the possibility to make a correction for this and therefore the CPM measured with SPA are referred to as CCPM which stands for "corrected" CPM (the x-axis of **Figure 5A, 6A** and **7A**) [33].

Challenges for SPA technology.

Despite the many benefits of using SPA technology there are also challenges in SPA radioligand binding studies. As mentioned above, the higher background signal of SPA consists of NSB and/or NPE. The NPE can be reduced by centrifuging the beads or allowing them to settle prior to counting, and by increasing the volume of the assay, but all these work-around solutions are either not feasible or impractical in kinetic radioligand binding experiments.

Secondly, although not much of an issue in our current experiments, the window of specific binding may need further consideration. Along this vein one may try different SPA beads. There are two basic types of SPA beads: one is composed of plastic-based polyvinyltoluene (PVT), the other is silica-based yttrium silicate (Ysi). In general, PVT beads are bigger in size, in a regular ball shape, but lighter, while Ysi beads are crystal amorphous solids, which are heavier [2, 10]. Although in our case of the hA_1R we chose the PVT beads, it was recently reported that two types of Ysi beads were used for radioligand binding studies on the adenosine A_{2A} receptor [34,35].Apart from the above mentioned beads designed for photomultiplier tube/well-based counters, there is another type of yttrium based beads optimized for sensitive imaging-based detectors, the red-shifted yttrium oxide (YO) SPA bead. Both Ysi and YO SPA beads have been reported to enable HTS and to improve the filtration method [36,37]. It would be also interesting to use those Ysi beads to perform the radioligand binding kinetic studies.

Thirdly, even in a fast operation the first 30 seconds of ligand association or dissociation cannot be recorded, as it takes time to have the spectrometer place the detectors above the wells and measure scintillations [7]. This is not an issue in our case of the hA_1R, but it can be crucial with fastly associating ligands. This could be improved by using an automatic injection module inside the counter, although this is currently not provided. Last, the temperature inside the counting chamber is fixed and slightly higher than room temperature (in our experiments the temperature was 28±1 ^{o}C). In a typical filtration assay kinetic radioligand binding experiments can be performed at lower or higher temperatures according to the characteristics of the radioligand – target interaction. Although in

some scintillation counters it is possible to adjust temperature from 19 °C to 35 °C [34], a broader choice of assay temperatures would be highly advantageous.

Conclusion

We reported a rapid and reliable technique, the scintillation proximity assay (SPA) technology, for kinetic radioligand binding studies on a prototypic GPCR, the human adenosine A_1 receptor (hA_1R). The SPA technology was of great benefit, as it monitored the event of radioligand binding in a single well in almost real time, which is impossible in traditional filtration assays. Even in the otherwise most laborious of all kinetic assays, the competition association assay, the kinetic profiles (k_{on} and k_{off}) of unlabeled ligands for the hA_1R were reliably and quickly determined, and agreed very well with the same parameters in a filtration assay performed simultaneously. In conclusion SPA is a very promising technique to determine the kinetic profiles of the drug-target interaction in the early phase of drug discovery. Its robustness and potential high-throughput may render this technology a preferred choice for further kinetic studies.

References

1. Harder, D.; Fotiadis, D. Measuring substrate binding and affinity of purified membrane transport proteins using the scintillation proximity assay. Nat. Protoc. 2012, 7, 1569-1578.
2. Glickman, J. F.; Schmid, A.; Ferrand, S. Scintillation Proximity Assays in High-Throughput Screening. Assay Drug Dev. Technol. 2008, 6, 433-455.
3. Bosworth, N.; Towers, P. Scintillation proximity assay. Nature 1989, 341, 167-168.
4. Hart, H. E.; Greenwald, E. B. Scintillation-Proximity Assay of Antigen—Antibody Binding Kinetics: Concise Communication. J. Nucl. Med. 1979, 20, 1062-1065.
5. Udenfriend, S.; Gerber, L. D.; Brink, L.; Spector, S. Scintillation proximity radioimmunoassay utilizing 125I-labeled ligands. Proc. Natl. Acad. Sci. U. S. A. 1985, 82, 8672-8676.
6. Heise, C. E.; Sullivan, S. K.; Crowe, P. D. Scintillation Proximity Assay as a High-Throughput Method to Identify Slowly Dissociating Nonpeptide Ligand Binding to the GnRH Receptor. J. Biomol. Screening 2007, 12, 235-239.
7. Swinney, D. C.; Beavis, P.; Chuang, K.-T.; Zheng, Y.; Lee, I.; Gee, P.; Deval, J.; Rotstein, D. M.; Dioszegi, M.; Ravendran, P.; Zhang, J.; Sankuratri, S.; Kondru, R.; Vauquelin, G. A study of the

molecular mechanism of binding kinetics and long residence times of human CCR5 receptor small molecule allosteric ligands. Br. J. Pharmacol. 2014, 171, 3364-3375.
8. Chao, J.; Taveras, A. G.; Chao, J.; Aki, C.; Dwyer, M.; Yu, Y.; Purakkattle, B.; Rindgen, D.; Jakway, J.; Hipkin, W.; Fosetta, J.; Fan, X.; Lundell, D.; Fine, J.; Minnicozzi, M.; Phillips, J.; Merritt, J. R. C(4)-alkyl substituted furanyl cyclobutenediones as potent, orally bioavailable CXCR2 and CXCR1 receptor antagonists. Bioorg. Med. Chem. Lett. 2007, 17, 3778-3783.
9. Mikami, T.; Ochi, Y.; Suzuki, K.; Saito, T.; Sugie, Y.; Sakakibara, M. 5-Amino-6-chloro-N-[(1-isobutylpiperidin-4-yl)methyl]-2-methylimidazo[1,2-α]pyridine-8-carboxamide (CJ-033,466), a Novel and Selective 5-Hydroxytryptamine 4 Receptor Partial Agonist: Pharmacological Profile in Vitro and Gastroprokinetic Effect in Conscious Dogs. J. Pharmacol. Exp. Ther. 2008, 325, 190-199.
10. Auld DS, F. M., Kahl SD, et al. Receptor Binding Assays for HTS and Drug Discovery. In Assay Guidance Manual [Internet], Sittampalam GS, C. N., Nelson H, et al., Ed. Bethesda (MD): Eli Lilly & Company and the National Center for Advancing Translational Sciences, 2012.
11. Tummino, P. J.; Copeland, R. A. Residence time of receptor−ligand complexes and Its Effect on Biological Function. Biochemistry 2008, 47, 5481-5492.
12. Guo, D.; Hillger, J. M.; Ijzerman, A. P.; Heitman, L. H. Drug-Target Residence Time—A Case for G Protein-Coupled Receptors. Med. Res. Rev. 2014, 34, 856-892.
13. Sykes, D. A.; Dowling, M. R.; Charlton, S. J. Exploring the Mechanism of Agonist Efficacy: A Relationship between Efficacy and Agonist Dissociation Rate at the Muscarinic M3 Receptor. Mol. Pharmacol. 2009, 76, 543-551.
14. Guo, D.; Mulder-Krieger, T.; Ijzerman, A. P.; Heitman, L. H. Functional efficacy of adenosine A2A receptor agonists is positively correlated to their receptor residence time. Br. J. Pharmacol. 2012, 166, 1846-1859.
15. Vilums, M.; Zweemer, A. J. M.; Yu, Z.; de Vries, H.; Hillger, J. M.; Wapenaar, H.; Bollen, I. A. E.; Barmare, F.; Gross, R.; Clemens, J.; Krenitsky, P.; Brussee, J.; Stamos, D.; Saunders, J.; Heitman, L. H.; Ijzerman, A. P. Structure–Kinetic Relationships—An Overlooked Parameter in Hit-to-Lead Optimization: A Case of Cyclopentylamines as Chemokine Receptor 2 Antagonists. J. Med. Chem. 2013, 56, 7706-7714.
16. Guo, D.; Xia, L.; van Veldhoven, J. P. D.; Hazeu, M.; Mocking, T.; Brussee, J.; Ijzerman, A. P.; Heitman, L. H. Binding Kinetics of ZM241385 Derivatives at the Human Adenosine A2A Receptor. ChemMedChem 2014, 9, 752-761.
17. van Veldhoven, J. P. D.; Liu, R.; Thee, S. A.; Wouters, Y.; Verhoork, S. J. M.; Mooiman, C.; Louvel, J.; Ijzerman, A. P. Affinity and kinetics study of anthranilic acids as HCA2 receptor agonists. Bioorganic & Medicinal Chemistry 2015, 23, 4013-4025.
18. Motulsky, H. J.; Mahan, L. C. The kinetics of competitive radioligand binding predicted by the law of mass action. Mol. Pharmacol. 1984, 25, 1-9.
19. Morriello, G. J.; Chicchi, G.; Johnson, T.; Mills, S. G.; DeMartino, J.; Kurtz, M.; Tsao, K. L. C.; Zheng, S.; Tong, X.; Carlson, E.; Townson, K.; Wheeldon, A.; Boyce, S.; Collinson, N.; Rupniak, N.; DeVita, R. J. Fused tricyclic pyrrolizinones that exhibit pseudo-irreversible blockade of the NK1 receptor. Bioorg. Med. Chem. Lett. 2010, 20, 5925-5932.
20. Ehlert, F. J.; Roeske, W. R.; Yamamura, H. I. Mathematical Analysis of the Kinetics of Competitive Inhibition in Neurotransmitter Receptor Binding Assays. Mol. Pharmacol. 1981, 19, 367-371.
21. Guo, D.; Dorp, E. J. H. v.; Mulder-Krieger, T.; Veldhoven, J. P. D. v.; Brussee, J.; IJzerman, A. P.; Heitman, L. H. Dual-Point Competition Association Assay A Fast and High-Throughput Kinetic Screening Method for Assessing Ligand-Receptor Binding Kinetics. J. Biomol. Screening 2013, 18, 309-320.
22. Berry J, P.-J. M., Killian B. Use of Scintillation Proximity Assay to Measure Radioligand Binding to Immobilized Receptors Without Separation of Bound from Free Ligand. In Receptor Binding Techniques, AP, D., Ed. Humana Press: 2012; Vol. 897, pp 79-94.
23. Martinson, E. A.; Johnson, R. A.; Wells, J. N. Potent adenosine receptor antagonists that are selective for the A1 receptor subtype. Mol. Pharmacol. 1987, 31, 247-252.

24. Muijlwijk-Koezen, J. E. v.; Timmerman, H.; der Sluis, R. P. v.; van de Stolpe, A. C.; Menge, W. M. P. B.; Beukers, M. W.; van der Graaf, P. H.; de Groote, M.; Ijzerman, A. P. Synthesis and use of FSCPX, an irreversible adenosine A1 antagonist, as a 'Receptor Knock-Down' tool. Bioorg. Med. Chem. Lett. 2001, 11, 815-818.
25. Klotz, K.-N.; Lohse, M.; Schwabe, U.; Cristalli, G.; Vittori, S.; Grifantini, M. 2-Chloro-N6-[3H]cyclopentyladenosine ([3HCCPA) —a high affinity agonist radioligand for A1 adenosine receptors. Naunyn-Schmiedeberg's Arch. Pharmacol. 1989, 340, 679-683.
26. Cusack, N. J.; Hourani, S. M. O. 5'-N-ethylcarboxamidoadenosine: a potent inhibitor of human platelet aggregation. Br. J. Pharmacol. 1981, 72, 443-447.
27. Beukers, M. W.; Chang, L. C. W.; von Frijtag Drabbe Künzel, J. K.; Mulder-Krieger, T.; Spanjersberg, R. F.; Brussee, J.; Ijzerman, A. P. New, Non-Adenosine, High-Potency Agonists for the Human Adenosine A2B Receptor with an Improved Selectivity Profile Compared to the Reference Agonist N-Ethylcarboxamidoadenosine. J. Med. Chem. 2004, 47, 3707-3709.
28. Smith, P. K.; Krohn, R. I.; Hermanson, G. T.; Mallia, A. K.; Gartner, F. H.; Provenzano, M. D.; Fujimoto, E. K.; Goeke, N. M.; Olson, B. J.; Klenk, D. C. Measurement of protein using bicinchoninic acid. Anal. Biochem. 1985, 150, 76-85.
29. Cheng Y, P. W. Relationship between the Inhibition Constant (K1) and the Concentration of Inhibitor which Causes 50 Percent Inhibition (I50) of an Enzymatic Reaction. Biochem. Pharmacol. 1973, 22, 3099–3108.
30. Hoffmann, C.; Castro, M.; Rinken, A.; Leurs, R.; Hill, S. J.; Vischer, H. F. Ligand Residence Time at GPCRs - Why We Should Take Our Time to Study It. Mol. Pharmacol. 2015, 88, 552-560.
31. Horrocks, D. Scintilation solutions. In Applications of liquid scintillation counting, Academic Press: New York etc., 1974; pp 35-68.
32. Horrocks, D. Liquid Scintillation Counters and Multiplier Phototubes. In Applications of liquid scintillation counting, Academic Press: New York etc., 1974; pp 69-89.
33. Kahl SD, S. G., Weidner J. Calculations and Instrumentation used for Radioligand Binding Assays. . In Assay Guidance Manual [Internet], Sittampalam GS, C. N., Nelson H, et al., Ed. Bethesda (MD): Eli Lilly & Company and the National Center for Advancing Translational Sciences, 2012.
34. Bocquet, N.; Kohler, J.; Hug, M. N.; Kusznir, E. A.; Rufer, A. C.; Dawson, R. J.; Hennig, M.; Ruf, A.; Huber, W.; Huber, S. Real-time monitoring of binding events on a thermostabilized human A2A receptor embedded in a lipid bilayer by surface plasmon resonance. Biochim. Biophys. Acta, Biomembr. 2015, 1848, 1224-1233.

Chapter 7

Conclusions and Future Perspectives

About this chapter

In this thesis, the binding kinetics of ligands to several human GPCR, i.e. cannabinoid receptor 1 (hCB_1), adenosine A_1 and A_3 (hA_1 and hA_3) receptors, were studied to provide a better and multi-faceted understanding of drug-target interactions. In this concluding chapter, new insights are elaborated on, and suggestions for future investigations in this research area are outlined.

Conclusions from this thesis

Binding kinetics (i.e. knowledge of association and dissociation rate constants of ligands binding to and unbinding from their target) are gaining importance in the early phases of drug discovery. Therefore, throughout all the chapters of this thesis, we have characterized the binding kinetics of several series of compounds on different GPCR (i.e. hCB_1, hA_1 and hA_3). Firstly, binding kinetics of 1,2-diarylimidazol-4-carboxamide derivatives and 1-(4,5-diarylthiophene-2-carbonyl)-4-phenylpiperidine-4-carboxamide derivatives as hCB_1 receptor antagonists have been investigated in **Chapters 2** and **3**, respectively. Secondly, for the hA_3 receptor, both antagonists (i.e. pyrido[2,1-f]purine-2,4-dione derivatives) and agonists (i.e. ribofurano and (N)-methanocarba derivatives) have been subjected to kinetic characterization (**Chapters 4** and **5**). Lastly, the binding kinetics of a few reference agonists and antagonists for the hA_1 receptor that were obtained through a novel methodology have been compared with results stemming from traditional filtration assays (**Chapter 6**).

First of all the spectrum of their kinetics, especially the residence times (RTs), varied significantly, although experimental conditions (e.g., temperature) were different. We found that the shortest RT antagonist at hCB_1 receptor was rimonabant (14 min at 30 ^{o}C, from **Chapter 2** and **3**), the drug that was withdrawn from the market. The longest RT antagonist is a 1-(4,5-diarylthiophene-2-carbonyl)-4-phenylpiperidine-4-carboxamide derivative (**Chapter 3**) with a RT of 2222 min (>36h at 30 ^{o}C). Another reported example of a ligand with such a rare long-lasting RT is tiotropium, a M_3 muscarinic receptor antagonist.[1] In the case of the hA_3 receptor antagonists (**Chapter 4**), divergent RTs from 2.2 min to 391 min at 10 ^{o}C were obtained; under similar experimental conditions the hA_3 receptor agonists (**Chapter 5**) presented a greater range of RTs, from 10 min to 1961 min (>30h). In addition, the RTs variation (from 0.68 min to 167 min) of hA_1 receptor reference ligands was also significant (**Chapter 6**), which were obtained at 28 ^{o}C. We speculate that variation in ligand dissociation rate constants may be due to the following three aspects: 1) the nature of the receptors (i.e. lipid hCB_1R vs hA_1 and hA_3R); 2) different GPCR conformations (inactive state vs active, G protein-bound state); 3)

the ligand's class-related binding mode (two series of hCB_1R antagonists or two series of hA_3R agonists).

Interestingly, in the current thesis all the determined association rate constants are significantly below the so-called diffusion limit (i.e. 10^7 $M^{-1}s^{-1}$)[2]. This observation indicates that target engagement for ligands is more hampered than imposed by the diffusion limit alone. Specifically, the association rate constants of hA_1 receptor ligands varied substantially (by 100-fold), which was similar to a previous report.[3] In contrast, for hCB_1 receptor and hA_3 receptor ligands, the differences in association rate constants were less pronounced, approximately 5- to 30-fold, respectively. Interestingly, we found that hA_3 receptor agonists' association rate constants, albeit not that divergent, correlated significantly with their affinities. Such correlation between affinities and on-rates has been reported in the case of other GPCR[4] and ion channels.[5, 6] It is therefore necessary to examine both association and dissociation rate constants of a ligand for better ligand optimization.

Multiple binding kinetics assays have been performed in the present thesis. Especially, the radioligand competition association assay based on the Motulsky-Mahan model served as a working horse throughout all the research topics.[7] Indeed, it turned out to be a good approach for the quantitative measurement of unlabeled ("cold") ligands' binding kinetics. However, this assay's low-throughput and the (safety) restrictions imposed by labeled ("hot") ligands hamper its application in the kinetic profiling and concomitant structure kinetics relationships (SKR) studies. In the initial "kinetics screening" phase we adopted a simplified in-house validated competition association assay;[3] by sampling only two assay (time) points per ligand. With that a kinetic rate index (KRI) value was determined as a semi-quantitative descriptor for a ligand's dissociation rate. This relative high-throughput assay could be generally applied for kinetics studies at diverse drug targets. This screening assay does have limitations, namely 1) it provides kinetics information on the dissociation rate only, and, 2) the resolution of KRI values is not high enough for detailed SKRs, unlike full kinetic parameters.[8] In **Chapter 6** of this thesis, we developed and validated a kinetic scintillation proximity

assay (SPA), a homogenous technology with a "mix and measure" format, allowing monitoring of radioligand binding over time in a single well, from which association and dissociation rate constants of unlabeled ligands were reliably and quickly determined. Since this assay technology brings the benefit of greater efficiency in kinetic radioligand binding experiments, it can be of general use for kinetics studies at other drug targets as well.[4] One drawback of this technology is that the temperature of the microplate counter cannot be controlled (i.e. in our lab it was fixed at 28 ± 1 °C), preventing some targets from being kinetically investigated currently. In contrast, with a typical filtration assay, kinetic radioligand binding experiments can be performed at virtually any temperature, which allows for assay temperature optimization according to the characteristics of the radioligand—target interaction. Thus the SPA technology would greatly benefit from a counting device with temperature setting.

Last but not least, this thesis provides substantial evidence that studying SKR is of great importance in the early phases of drug discovery. We have provided quite a few examples of ligands within the same chemical scaffold with very similar affinities that present very divergent binding kinetics. Thus detailed SKR analysis is able to offer added value to the traditional SAR. This can be exemplified by one of the hCB_1 receptor antagonists, 14d (**Chapter 2**). On the basis of its high, picomolar affinity alone 14d seems a potent lead, but its close-to-unity KRI value indicates this may not be the case. Another example from **Chapter 4**: hA_3 receptor antagonist 9 with a pKi = 8.5 would be considered a better ligand than antagonist 11 with a pKi = 8.2, according to traditional SAR. However, their RTs are 28 min and 278 min, respectively, making antagonist 11 kinetically favorable. Thus, ignorance of the RT (by solely focusing on affinity) may lead to discontinuation of a compound that would likely perform better *in vivo*. Importantly the hA_3 receptor agonist MRS5698 has been confirmed an interesting candidate lead compound for neuropathic pain, which might (in retrospect) be due to its optimal binding kinetics as shown in Chapter 5 (RT = 1961 min). Hence, the strategic combination of SAR and SKR analyses results in a better understanding of a ligand-receptor interaction, which comprises not only the equilibrium state but also metastable intermediates and/or transition states

during the course of ligand association and dissociation. This strategy may be generally applied for efficient drug design and provide improved drug candidates.

Future perspectives

Opportunities for binding kinetics on hCB_1 receptor.

The challenge in the development of hCB_1R antagonists/inverse agonists as antiobesity drugs is their poor safety profile. Our strategy has been described in **Chapters 2** and **3**: a potent hCB_1R antagonist should not only be periphery-selective but also have a slow dissociation profile from the receptor. There might be other strategies as well. One approach is developing an allosteric modulator, aiming to "fine-tune" the pharmacological activity of the endogenous orthosteric agonists.[9] In this case, a negative allosteric modulator (NAM) would be aimed for,[10] potentially having certain advantages over orthosteric ligands, like an increased target selectivity and the ability to maintain the spatial and temporal signaling profile of the endogenous ligands.[11-13] Existing (positive) allosteric modulators such as ORG27569 tend to act as non-competitive antagonists in functional assays. The reason why is not entirely clear, but may be due to increased receptor desensitization induced by the compound,[11] also indicating that there is no clear cut between allosteric and orthosteric efficacy, as observed in previous research.[14, 15] Thus, development of a true NAM and a subsequent NAMs-hCB_1 binding kinetics study may provide additional ligand-receptor information, yielding a better understanding of a NAM's mechanism of action and, possibly, NAMs as drug candidates.

Another direction is developing neutral hCB_1R antagonists to avoid some side effects because since the withdrawal of rimonabant the scientific community has been debating the compound's inverse agonism in this respect.[16, 17] Some of the compounds reduced peripheral nervous system (PNS) disorders. However, no improvement in reducing CNS side effects was observed, which might be due to the fact that their bioavailability was not restricted to the periphery.[18, 19] Another possible explanation might be that inverse agonism with respect to G protein-independent pathways (e.g., β-

arrestin recruitment) was neglected,[20] i.e. the neutral antagonists developed so far were not neutral with respect to all relevant signaling pathways. To date, the concept of biased signaling has gained increasing attention in the GPCR field,[21, 22] and the first evidence is mounting that binding kinetics can have a profound impact on this phenomenon.[23, 24]

Opportunities for binding kinetics on hA_3 receptor.

There is no doubt that the hA_3 receptor possesses tremendous therapeutic potential and clinical indications, due to its overexpression on cancer and inflammatory cells.[25-29] However, the hA_3 receptor has a peculiar and rapidly changing expression profile in cultured cells.[30] Moreover, certain hA_3 receptor ligands have been described as cytoprotective or cytotoxic merely depending on the concentration employed, highlighting the difficulties that arise when one aims to characterize hA_3 receptor compounds.[31,32] Such observed "dichotomy" in different therapeutic applications might be significantly influenced by both ligand RTs and desensitization/internalization-related receptor vulnerability (i.e. receptor-turnover): would such rapid receptor turnover off-set some agonist's long RT? For instance, IB-MECA (with a RT of 95 min at 10 °C, in **Chapter 5**) has been proven safe and well tolerated but its anti-inflammatory effect may be hampered by its relatively quick onset of internalization of about 35 min – 60 min at 37 °C by different cellular assays. [33, 34] For other longer RT antagonists and agonists as determined in the current thesis (e.g., MRS5698), further cellular investigation is required, since knowledge of binding kinetics and the effect this has on internalization/desensitization will help to determine which kinetic profile is needed for an hA_3 receptor ligand to display a beneficial therapeutic profile.

Another interesting, but complicating factor may be hA_3 receptor homodimerization. This has recently been well illustrated by fluorescently labelled ligand-receptor binding kinetics studies on intact cells.[35-37] A ligand's binding kinetics on the hA_3 receptor dimer is significantly different from its binding interaction with the receptor monomer; as a result, its concomitant functional effect could

be profoundly influenced. It would be of great interest to test our hA_3 receptor ligands in such a system and provide binding kinetics profiles for receptor dimers as well.

General opportunities in binding kinetics for GPCR and beyond.

- Assays and technologies for binding kinetics.

A comprehensive overview of biochemical and biophysical assays and technologies for assessing ligand-receptor binding kinetics was described in a recently published review (**Table 1**).[38] Currently, the most recognized and most straightforward kinetic profiling approach is applying a radioligand binding filtration assay using membrane proteins, as described throughout the current thesis. Although this method is sensitive and selective, it suffers from constraints imposed by the probe: a) high affinity, b) optimal/fixed experimental temperature (in most cases below physiological 37 °C), c) optimal/fixed incubation duration, d) quantification of competing ligands. In the (near) future better kinetic assays and technologies will be the standard such as a real-time homogeneous assay enabling high-throughput measurements, as exemplified by scintillation proximity assays (SPA) in **Chapter 6.** On the other hand, a few emerging non-radioactive assays (TR-FRET, BRET and SPR) indeed have advantages of real-time measurement of target binding kinetics, even in a high-throughput capacity. However, there are still quite a few disadvantages, such as the use of modified ligands (probes) or targets, fixed temperatures, and half-lives of fluorescent emission (photo bleaching). Advantages and disadvantages of the current techniques to measure drug-target binding kinetics are summarized in **Table 1**.

Table 1. Emerging experimental methods for kinetic profiling. Adapted and modified from ref. 38.

Assays and Technologies	General Performance (in steps)	Advantages	Disadvantages
Radioligand binding	1. Add radioligand (and cold ligand, not shown);	Good sensitivity and selectivity,	Radioactivity, limited throughput,

(filtration) 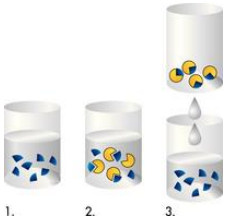 	2. Incubate with target for different period of time; 3.Harvest receptor/ligand complex on filter and count.	Non-engineered, wild-type receptor a universal tool	time-consuming, labor-intensive
Scintillation proximity assay (SPA) 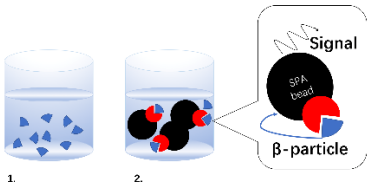 	1.Add radioligand (and cold ligand, not shown); 2.Incubate with precoupled target SPA-bead complex and count.	High-throughput, homogenous, real-time measurement, accurate and precise measurement	Radioactivity, fixed temperature, limited choices of beads
Time-resolved fluorescence resonance energy transfer (TR-FRET) 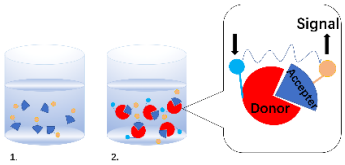 	1. Add probe (and ligand of interest, not shown); 2. Add target (as “Donor”) and record signal	Non-radioactive, high-throughput, homogenous, real-time measurement	Fluorescently labeled receptor and ligand, fixed temperature, photo bleaching.
Bioluminescence resonance energy transfer (BRET) 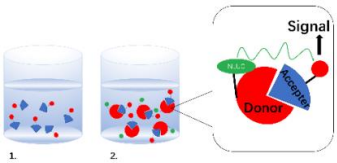 	1. Add probe (and ligand of interest, not shown); 2. Add target (as “Donor”) and record signal	Non-radioactive, high-throughput, homogenous, real-time measurement	Luminescent enzyme tagged receptor, fluorescently labeled ligand
Surface plasmon resonance (SPR) 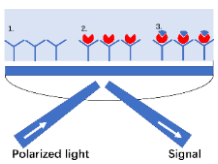 	1. Immobilize antibody; 2. Capture target; 3. Add ligand of interest and record signal	Non-radioactive, real-time measurement	Immobilized receptor (in large amounts), medium throughput

- From binding kinetics to functional dynamics

According to the medical definitions from the Merriam-Webster Dictionary, “kinetics” literally means the rate of change in a system effected by forces upon motions,[39] whilst “dynamics” describes “forces and their relation primarily to the motion but sometimes also to the equilibrium of bodies”.[40] In other words, *kinetics* emphasizes rates (e.g., ligands with a fast or slow association/dissociation to/from receptors); *dynamics* focuses on patterns of changes in systems (e.g., receptors, signaling pathways, cells, full bodies) after impact from external forces (e.g., all kinds of interactions), and such changes include equilibrium. Thus, there is a causal relation between “kinetics” and “dynamics”. Likewise, this entire thesis hypothesizes that, in GPCR, binding kinetics, more specifically RTs, are indispensable parameters to gauge dynamic functional effects.

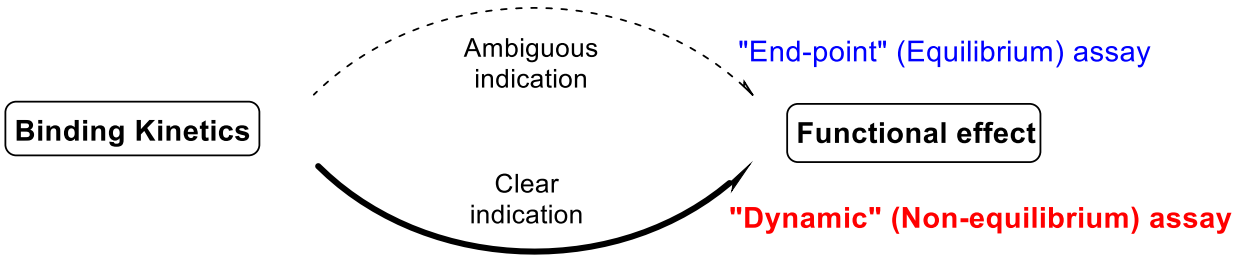

Figure 1. “Dynamic” functional assays are required for better translation of binding kinetics, as opposed to the currently much applied end-point functional assays.

Indeed, a positive correlation between agonist efficacy and residence time has been observed in case of the muscarinic acetylcholine M_3 receptor[41] and adenosine A_{2A} receptor.[42] In contrast, no such correlation was observed for the adenosine A_1 receptor.[43] There is a high chance that the effects of binding kinetics may not be perfectly depicted in classic functional assays under equilibrium conditions (e.g., with respect to E_{max}). For instance, E_{max} induced by an agonist can be dynamic over time.[44] Besides, receptor turnover (e.g., hA_3R has a peculiar and rapid desensitization/internalization profile in cultured cells[30]) may further complicate such dynamic processes. For antagonist’s binding

kinetics, insurmountability assays have been described as functional confirmation in this thesis (**Chapters 2, 3** and **4**). Such assays require complicated validation and optimization steps, especially for a long RT antagonist, where different preincubation times can lead to both insurmountable and surmountable effects, which also indicates the existence of functional dynamics. Therefore, dynamics of the functional effect shall be taken into account for further investigations. A simple rationale is presented below (**Figure 1**).

Methods for measuring and quantifying individual signaling pathways in real-time (e.g., G_{α}-protein, β-arrestin, cAMP) are emerging, which depict dynamic functional effects at a specific signaling pathway.[11, 45, 46] Moreover, binding kinetics-driven functional dynamics has been described as "apparent biased signalling".[23] However, the reported methods are performed under distinct experimental conditions due to practical reasons (e.g., temperature, cell type, sampling methods), questioning the robustness of these apparent bias observations. Quite recently, a proximity labeling technique called "APEX" (affinity purification coupled with mass spectrometry) has been introduced which may provide new insights into the kinetics of GPCR signaling.[47] Not only does it enlarge the signaling network,[48] but it also offers high time resolution into GPCR signaling in living cells.[49] In this way the dynamics of multiple signaling pathways can be carefully demonstrated and accurately quantified. Last but not least, by combining such detailed dynamic assessment technology with morphological label-free technology (e.g., xCELLigence™), better insights in cell signaling can be translated from binding kinetics.

- Motulsky-Mahan model, the perfect one?

Throughout the thesis, the Motulsky-Mahan model has been the mathematic foundation for the quantification of binding kinetics.[50] This model has been applied as an "Occam's razor" by simplifying the ligand-target interaction as a single and reversible binding interaction. Indeed such simplification is sufficient for unlabeled (cold) reversible ligands that competitively bind with the radioligand to the same target binding site. However, there are a few issues in its practical application. One example

are GPCR agonists which are able to bind more than one receptor conformation (e.g. active state and inactive state). Another example are bitopic ligands which might bind a target in different orientations.[51] Thus, kinetic quantification of GPCR agonists, irreversible binders and bitopic ligands faces difficulties when applying the Motulsky & Mahan model. In the future, more and more quantification-driven investigations of ligand-receptor binding kinetics, from both theoretical and experimental perspectives, shall be performed to further understand the mechanism of any ligand-target interaction.

- "The great divide" between *in vitro* binding kinetics and *in vivo* pharmacokinetics (PK) and pharmacodynamics (PD)

Although most of the current studies in this thesis have not been translated to *in vivo* studies (except for some ligands from **Chapter 5** by others [52]), one of the more outspoken differences between most *in vitro* and *in vivo* studies is the experimental temperature. Some slowly dissociating ligands were identified in *vitro* at temperatures (much) lower than mammals' body temperature (i.e. 37 ^{o}C), thus, their binding kinetic parameters in *vivo* will be (much) faster. Of note, the ranking of a series of drug candidates should not be changed under such temperature maneuver by translation from *in vitro* to *in vivo.* Still, a slowly dissociating ligand only leads to long-lasting *in vivo* effects, when its dissociation rate from the target exceeds the rate of free drug elimination from the effect compartment (**Figure 2**), ensuring pharmacodynamics (PD) outlasts pharmacokinetics (PK).[53]

Another overlooked pharmacological effect is target rebinding (**Figure 2)**, which means that a freshly dissociated ligand re-associates to the same or neighboring target. Prominent rebinding might be an important factor in dictating the duration of a ligand's *in vivo* effect, even if a ligand-target complex's lifetime is short. In this thesis, the RT of rimonabant, a hCB_1 receptor antagonist, was determined to be 14 min (**Chapters 2** and **3**). However in a previous study its RT was reported to be much longer (>80 min) in intact cells, which was explained by its prominent target rebinding.[54] Thus, despite its

relatively short RT determined *in vitro,* one could speculate that *in vivo* the rimonabant-related CNS on-target toxicity could be unavoidable.

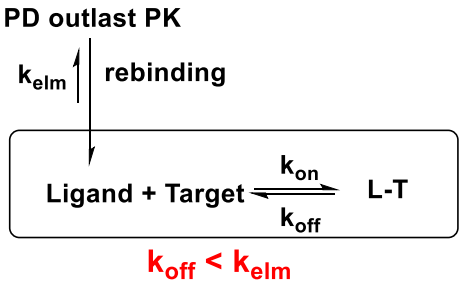

Figure 2. The binding kinetics *in vivo* is influenced by the rates of both free drug elimination (k_{elm}) from the effect compartment (the box) and rebinding. A slow dissociation rate (k_{off}) of a ligand exceeding its k_{elm} shall result in a long lasting *in vivo* effect, ensuring pharmacodynamics (PD) outlasts pharmacokinetics (PK). k_{on} is the association rate constant of a ligand to its target, k_{off} the dissociation rate constant.

Besides, recent theoretical studies on PK/PD has shown that such rebinding could persist by increased (local) concentrations of the drug, resulting from a high target association rate constant.[55, 56] On the other hand, an increased drug concentration can also lead to increased off-target binding and thus decreased selectivity.[56] Therefore, it is necessary to examine both association and dissociation rate constants of a ligand to its target for better translating *in vitro* binding kinetics to *in vivo* PK/PD. In this thesis, rimonabant has the slowest k_{on} among the antagonists tested in **Chapter 2**, but the fastest in **Chapter 3**, and thus is it appealing to further compare these antagonists' *in vivo* PK profile, concerning their rebinding and target occupancy. By combining data from different perspectives, the quality of the translation from *in vitro* to *in vivo* could be evaluated thoroughly.

Last but not least, species differences are another issue when translating *in vitro* findings to *in vivo* effects, which has been reported for both hCB_1 receptor and hA_3 receptors. [57-59] Thus, in binding kinetics, we suggest to perform an *in vitro* investigation of the "kinetic hits" in the species that will be used in later *in vivo* studies, next to obtaining data for the human receptor.[60] In this way, species variability can be predicted before the actual *in vivo* studies, and if needed, another lead compound can be selected which lacks these differences.

Final notes

The entire thesis evolves around the concept of ligand-receptor binding kinetics for the early phase of drug design and discovery. We extensively investigated this concept at two potential drug targets, the cannabinoid 1 receptor and adenosine A_3 receptor. We provide evidence that binding kinetics investigations on GPCR add indispensable information on these drug-target interactions. Besides, we propose that structure-kinetics relationship studies, next to the more traditional structure-affinity relationship studies, can improve the final decision and selection process of new chemical entities. Finally, we validated the scintillation proximity assay as a robust tool for high-throughput binding kinetics determination.

Hopefully, all findings from this thesis have brought new insights at a molecular understanding of ligand-receptor binding kinetics, and will offer suggestions for the design of better ligands with an appropriate kinetic profile, new technologies for rapid kinetic assessment, and ultimately suitable evaluation schemes for a better translation towards effective and safe drugs.

References

1. Casarosa, P.; Bouyssou, T.; Germeyer, S.; Schnapp, A.; Gantner, F.; Pieper, M. Preclinical evaluation of long-acting muscarinic antagonists: comparison of tiotropium and investigational drugs. *J. Pharmacol. Exp. Ther.* **2009,** *330*, 660-668.
2. Smith, G. F. Medicinal chemistry by the numbers: the physicochemistry, thermodynamics and kinetics of modern drug design. In *Progress in Medicinal Chemistry*, Lawton, G.; Witty, D. R., Eds. Elsevier B.V.: Burlington, **2009**; Vol. *48*, p 1.
3. Guo, D.; Dorp, E. J. H.; Mulder-Krieger, T.; Veldhoven, J. P. D.; Brussee, J.; IJzerman, A. P. Dual-point competition association assay: a fast and high-throughput kinetic screening method for assessing ligand-receptor binding kinetics. *J. Biomol. Screen* **2012,** *18*.
4. Doornbos, M. L. J.; Cid, J. M.; Haubrich, J.; Nunes, A.; van de Sande, J. W.; Vermond, S. C.; Mulder-Krieger, T.; Trabanco, A. A.; Ahnaou, A.; Drinkenburg, W. H.; Lavreysen, H.; Heitman, L. H.; IJzerman, A. P.; Tresadern, G. Discovery and kinetic profiling of 7-aryl-1,2,4-triazolo[4,3-a]pyridines: positive allosteric modulators of the metabotropic glutamate receptor 2. *J. Med. Chem.* **2017,** *60*, 6704–6720.
5. Yu, Z.; van Veldhoven, J. P. D.; Louvel, J.; 't Hart, I. M. E.; Rook, M. B.; van der Heyden, M. A. G.; Heitman, L. H.; IJzerman, A. P. Structure–affinity relationships (SARs) and structure–kinetics relationships (SKRs) of Kv11.1 blockers. *J. Med. Chem.* **2015,** *58*, 5916-5929.

6. Yu, Z.; IJzerman, A. P.; Heitman, L. H. K(v)11.1 (hERG)-induced cardiotoxicity: a molecular insight from a binding kinetics study of prototypical K(v)11.1 (hERG) inhibitors. *Br. J. Pharmacol.* **2015,** *172*, 940-955.
7. Motulsky, H. J.; Mahan, L. C. The kinetics of competitive radioligand binding predicted by the law of mass action. *Mol. Pharmacol.* **1984,** *25*, 1-9.
8. van Veldhoven, J. P. D.; Liu, R.; Thee, S. A.; Wouters, Y.; Verhoork, S. J. M.; Mooiman, C.; Louvel, J.; Ijzerman, A. P. Affinity and kinetics study of anthranilic acids as HCA_2 receptor agonists. *Bioorg. Med. Chem.* **2015,** *23*, 4013-4025.
9. Morales, P.; Goya, P.; Jagerovic, N.; Hernandez-Folgado, L. Allosteric modulators of the CB_1 cannabinoid receptor: a structural update review. *Cannabis and Cannabinoid Research* **2016,** *1*, 22-30.
10. Abood, M. E. Allosteric Modulators: a Side Door. *J. Med. Chem.* **2016,** *59*, 42-43.
11. Cawston, E. E.; Redmond, W. J.; Breen, C. M.; Grimsey, N. L.; Connor, M.; Glass, M. Real-time characterization of cannabinoid receptor 1 (CB_1) allosteric modulators reveals novel mechanism of action. *Br. J. Pharmacol.* **2013,** *170*, 893-907.
12. Cawston, E. E.; Connor, M.; Di Marzo, V.; Silvestri, R.; Glass, M. Distinct temporal fingerprint for cyclic adenosine monophosphate (cAMP) signaling of indole-2-carboxamides as allosteric modulators of the cannabinoid receptors. *J. Med. Chem.* **2015,** *58*, 5979-5988.
13. Kulkarni, P. M.; Kulkarni, A. R.; Korde, A.; Tichkule, R. B.; Laprairie, R. B.; Denovan-Wright, E. M.; Zhou, H.; Janero, D. R.; Zvonok, N.; Makriyannis, A.; Cascio, M. G.; Pertwee, R. G.; Thakur, G. A. Novel electrophilic and photoaffinity covalent probes for mapping the cannabinoid 1 receptor allosteric site(s). *J. Med. Chem.* **2016,** *59*, 44-60.
14. Laprairie, R. B.; Bagher, A. M.; Kelly, M. E. M.; Denovan-Wright, E. M. Cannabidiol is a negative allosteric modulator of the cannabinoid CB_1 receptor. *Br. J. Pharmacol.* **2015,** *172*, 4790-4805.
15. Baillie, G. L.; Horswill, J. G.; Anavi-Goffer, S.; Reggio, P. H.; Bolognini, D.; Abood, M. E.; McAllister, S.; Strange, P. G.; Stephens, G. J.; Pertwee, R. G.; Ross, R. A. CB1 Receptor Allosteric Modulators Display Both Agonist and Signaling Pathway Specificity. *Mol. Pharmacol.* **2013,** *83*, 322-338.
16. Pertwee, R. G. Inverse agonism and neutral antagonism at cannabinoid CB_1 receptors. *Life Sci.* **2005,** 76, 1307-1324.
17. Erdozain, A. M.; Diez-Alarcia, R.; Meana, J. J.; Callado, L. F. The inverse agonist effect of rimonabant on G protein activation is not mediated by the cannabinoid CB1 receptor: evidence from postmortem human brain. *Biochem. Pharmacol.* **2012,** 83, 260-268.
18. Storr, M. A.; Bashashati, M.; Hirota, C.; Vemuri, V. K.; Keenan, C. M.; Duncan, M.; Lutz, B.; Mackie, K.; Makriyannis, A.; Macnaughton, W. K.; Sharkey, K. A. Differential effects of CB_1 neutral antagonists and inverse agonists on gastrointestinal motility in mice. *Neurogastroenterol. Motil.* **2010,** *22*, 787-e223.
19. Tudge, L.; Williams, C.; Cowen, P. J.; McCabe, C. Neural effects of cannabinoid CB_1 neutral antagonist tetrahydrocannabivarin on food reward and aversion in healthy volunteers. *Int. J. Neuropsychopharmacol.* **2015,** *18*, pyu094.
20. Delgado-Peraza, F.; Ahn, K. H.; Nogueras-Ortiz, C.; Mungrue, I. N.; Mackie, K.; Kendall, D. A.; Yudowski, G. A. Mechanisms of biased *β*-arrestin-mediated signaling downstream from the cannabinoid 1 receptor. *Mol. Pharmacol.* **2016,** *89*, 618-629.
21. Kenakin, T. Functional selectivity and biased receptor signaling. *J. Pharmacol. Exp. Ther.* **2011,** *336*, 296-302.
22. Kenakin, T.; Christopoulos, A. Signalling bias in new drug discovery: detection, quantification and therapeutic impact. *Nat. Rev. Drug Discovery* **2013,** *12*, 205-216.
23. Klein Herenbrink, C.; Sykes, D. A.; Donthamsetti, P.; Canals, M.; Coudrat, T.; Shonberg, J.; Scammells, P. J.; Capuano, B.; Sexton, P. M.; Charlton, S. J.; Javitch, J. A.; Christopoulos, A.; Lane, J. R. The role of kinetic context in apparent biased agonism at GPCRs. *Nat. Commun.* **2016,** *7*, 10842.
24. Lane, J. R.; May, L. T.; Parton, R. G.; Sexton, P. M.; Christopoulos, A. A kinetic view of GPCR allostery and biased agonism. *Nat. Chem. Biol.* **2017,** *13*, 929-937.

25. Borea, P. A.; Varani, K.; Vincenzi, F.; Baraldi, P. G.; Tabrizi, M. A.; Merighi, S.; Gessi, S. The A_3 adenosine receptor: history and perspectives. *Pharmacol. Rev.* **2015,** *67*, 74-102.
26. Jacobson, K. A.; Gao, Z.-G. Adenosine receptors as therapeutic targets. *Nat. Rev. Drug Discovery* **2006,** *5*, 247-264.
27. Baraldi, P. G.; Cacciari, B.; Romagnoli, R.; Merighi, S.; Varani, K.; Borea, P. A.; Spalluto, G. A_3 adenosine receptor ligands: history and perspectives. *Med. Res. Rev.* **2000,** *20*, 103-128.
28. Baraldi, P. G.; Preti, D.; Borea, P. A.; Varani, K. Medicinal chemistry of A_3 adenosine receptor modulators: pharmacological activities and therapeutic implications. *J. Med. Chem.* **2012,** *55*, 5676-5703.
29. Hasko, G.; Linden, J.; Cronstein, B.; Pacher, P. Adenosine receptors: therapeutic aspects for inflammatory and immune diseases. *Nat. Rev. Drug Discovery* **2008,** *7*, 759-770.
30. Klaasse, E. C.; IJzerman, A. P.; de Grip, W. J.; Beukers, M. W. Internalization and desensitization of adenosine receptors. *Purinergic Signalling* **2008,** *4*, 21-37.
31. Jacobson, K. A.; Moro, S.; Kim, Y.-C.; Li, A.-H. A_3 adenosine receptors: protective vs. damaging effects identified using novel agonists and antagonists. *Drug Dev. Res.* **1998,** *45*, 113-124.
32. Gessi, S.; Merighi, S.; Varani, K.; Leung, E.; Mac Lennan, S.; Borea, P. A. The A_3 adenosine receptor: an enigmatic player in cell biology. *Pharmacol. Ther.* **2008,** *117*, 123-140.
33. Trincavelli, M. L.; Tuscano, D.; Cecchetti, P.; Falleni, A.; Benzi, L.; Klotz, K.-N.; Gremigni, V.; Cattabeni, F.; Lucacchini, A.; Martini, C. Agonist-induced internalization and recycling of the human A_3 adenosine receptors. *J. Neurochem.* **2000,** *75*, 1493-1501.
34. Stoddart, L. A.; Vernall, A. J.; Briddon, S. J.; Kellam, B.; Hill, S. J. Direct visualisation of internalization of the adenosine A_3 receptor and localization with arrestin3 using a fluorescent agonist. *Neuropharmacology* **2015,** *98*, 68-77.
35. Hill, S. J.; May, L. T.; Kellam, B.; Woolard, J. Allosteric interactions at adenosine A_1 and A_3 receptors: new insights into the role of small molecules and receptor dimerization. *Br. J. Pharmacol.* **2014,** *171*, 1102-1113.
36. Corriden, R.; Kilpatrick, L. E.; Kellam, B.; Briddon, S. J.; Hill, S. J. Kinetic analysis of antagonist-occupied adenosine-A_3 receptors within membrane microdomains of individual cells provides evidence of receptor dimerization and allosterism. *The FASEB Journal* **2014,** *28*, 4211-4222.
37. May, L. T.; Bridge, L. J.; Stoddart, L. A.; Briddon, S. J.; Hill, S. J. Allosteric interactions across native adenosine-A_3 receptor homodimers: quantification using single-cell ligand-binding kinetics. *The FASEB Journal* **2011,** *25*, 3465-3476.
38. Schuetz, D. A.; de Witte, W. E. A.; Wong, Y. C.; Knasmueller, B.; Richter, L.; Kokh, D. B.; Sadiq, S. K.; Bosma, R.; Nederpelt, I.; Heitman, L. H.; Segala, E.; Amaral, M.; Guo, D.; Andres, D.; Georgi, V.; Stoddart, L. A.; Hill, S.; Cooke, R. M.; De Graaf, C.; Leurs, R.; Frech, M.; Wade, R. C.; de Lange, E. C. M.; Ijzerman, A. P.; Müller-Fahrnow, A.; Ecker, G. F. Kinetics for drug discovery: an industry-driven effort to target drug residence time. *Drug Discovery Today* **2017,** *22*, 896-911.
39. Kinetics. https://www.merriam-webster.com/dictionary/kinetics#medicalDictionary
40. Dynamics. https://www.merriam-webster.com/dictionary/dynamics#medicalDictionary
41. Sykes, D. A.; Dowling, M. R.; Charlton, S. J. Exploring the mechanism of agonist efficacy: a relationship between efficacy and agonist dissociation rate at the muscarinic M_3 receptor. *Mol. Pharmacol.* **2009,** *76*, 543-551.
42. Guo, D.; Mulder-Krieger, T.; Ijzerman, A. P.; Heitman, L. H. Functional efficacy of adenosine A_{2A} receptor agonists is positively correlated to their receptor residence time. *Br. J. Pharmacol.* **2012,** *166*, 1846-1859.
43. Louvel, J.; Guo, D.; Agliardi, M.; Mocking, T. A. M.; Kars, R.; Pham, T. P.; Xia, L.; de Vries, H.; Brussee, J.; Heitman, L. H.; IJzerman, A. P. Agonists for the adenosine A_1 receptor with tunable residence time. A case for nonribose 4-amino-6-aryl-5-cyano-2-thiopyrimidines. *J. Med. Chem.* **2014,** *57*, 3213-3222.
44. Cheng, J.; McCorvy, J. D.; Giguere, P. M.; Zhu, H.; Kenakin, T.; Roth, B. L.; Kozikowski, A. P. Design and discovery of functionally selective serotonin 2C (5-HT_{2C}) receptor agonists. *J. Med. Chem.* **2016,** *59*, 9866-9880.

45. Bosma, R.; Moritani, R.; Leurs, R.; Vischer, H. F. BRET-based β-arrestin2 recruitment to the histamine H_1 receptor for investigating antihistamine binding kinetics. *Pharmacol. Res.* **2016,** 111, 679-687.
46. Michela, B.; Claudia, S.; Piero, A.; Diego Dal, B.; Catia, L.; Ajiroghene, T.; Rosaria, V.; Gabriella, M. Overview on radiolabel-free in vitro assays for GPCRs. *Mini-Rev. Med. Chem.* **2017,** *17*, 3-14.
47. Doerr, A. Biochemistry: GPCR interactions in space and time. *Nat. Methods* **2017,** *14*, 551-551.
48. Lobingier, B. T.; Hüttenhain, R.; Eichel, K.; Miller, K. B.; Ting, A. Y.; von Zastrow, M.; Krogan, N. J. An approach to spatiotemporally resolve protein interaction networks in living cells. *Cell 169*, 350-360.e312.
49. Paek, J.; Kalocsay, M.; Staus, D. P.; Wingler, L.; Pascolutti, R.; Paulo, J. A.; Gygi, S. P.; Kruse, A. C. Multidimensional tracking of GPCR signaling via peroxidase-catalyzed proximity labeling. *Cell* **2017,** *169*, 338-349.e311.
50. Motulsky, H. J.; Mahan, L. C. The kinetics of competitive radioligand binding predicted by the law of mass action. *Mol Pharmacol* **1984,** 25.
51. Wittmann, H.-J.; Strasser, A. Competitive association binding kinetic assays: a new tool to detect two different binding orientations of a ligand to its target protein under distinct conditions? *Naunyn-Schmiedeberg's Arch. Pharmacol.* **2017,** *390*, 595-612.
52. Jacobson, K. A.; Merighi, S.; Varani, K.; Borea, P. A.; Baraldi, S.; Aghazadeh Tabrizi, M.; Romagnoli, R.; Baraldi, P. G.; Ciancetta, A.; Tosh, D. K.; Gao, Z.-G.; Gessi, S. A3 Adenosine Receptors as Modulators of Inflammation: From Medicinal Chemistry to Therapy. *Medicinal Research Reviews* **2017**, 10.1002/med.21456.
53. Dahl, G.; Akerud, T. Pharmacokinetics and the drug–target residence time concept. *Drug Discovery Today* **2013,** *18*, 697-707.
54. Wennerberg, M.; Cheng, L.; Hjorth, S.; Clapham, J. C.; Balendran, A.; Vauquelin, G. Binding properties of antagonists to cannabinoid receptors in intact cells. *Fundam. Clin. Pharmacol.* **2011,** *25*, 200-210.
55. de Witte, W. E. A.; Vauquelin, G.; van der Graaf, P. H.; de Lange, E. C. M. The influence of drug distribution and drug-target binding on target occupancy: The rate-limiting step approximation. *European Journal of Pharmaceutical Sciences*.
56. de Witte, W. E. A.; Danhof, M.; van der Graaf, P. H.; de Lange, E. C. M. In vivo Target Residence Time and Kinetic Selectivity: The Association Rate Constant as Determinant. *Trends in Pharmacological Sciences* **2016,** 37, 831-842.
57. Gamage, T. F.; Farquhar, C. E.; Lefever, T. W.; Thomas, B. F.; Nguyen, T.; Zhang, Y.; Wiley, J. L. The great divide: separation between in vitro and in vivo effects of PSNCBAM-based CB_1 receptor allosteric modulators. *Neuropharmacology* **2017,** 125, 365-375.
58. Du, L.; Gao, Z.-G.; Paoletta, S.; Wan, T. C.; Gizewski, E. T.; Barbour, S.; van Veldhoven, J. P. D.; IJzerman, A. P.; Jacobson, K. A.; Auchampach, J. A. Species differences and mechanism of action of A3 adenosine receptor allosteric modulators. *Purinergic Signalling* **2017**.
59. Alnouri, M. W.; Jepards, S.; Casari, A.; Schiedel, A. C.; Hinz, S.; Müller, C. E. Selectivity is species-dependent: Characterization of standard agonists and antagonists at human, rat, and mouse adenosine receptors. *Purinergic Signalling* **2015,** *11*, 389-407.
60. Bot, I.; Ortiz Zacarías, N. V.; de Witte, W. E. A.; de Vries, H.; van Santbrink, P. J.; van der Velden, D.; Kröner, M. J.; van der Berg, D.-J.; Stamos, D.; de Lange, E. C. M.; Kuiper, J.; Ijzerman, A. P.; Heitman, L. H. A novel CCR_2 antagonist inhibits atherogenesis in apoE deficient mice by achieving high receptor occupancy. *Sci. Rep.* **2017,** *7*, 52.

Summary

The present thesis focuses on the pharmacological concept of drug-target interaction, which dates back to the beginning of modern pharmacology. In **Chapter 1**, a general introduction provides evidence that a traditional equilibrium metrics-based rationale (i.e. optimization of drug affinity leads to better efficacy and safety) is unable to prevent current high attrition rates in the early phase of drug discovery. In the past decade drug-target binding kinetics (i.e. association and dissociation rate constants, residence time) has been gaining more and more attention, which constitutes a paradigm shift to better predict parameters of drug efficacy and safety. We decided to investigate binding kinetics of G protein-coupled receptors (GPCR), since GPCR are involved in various critical physiological and pharmacological functions, being the target of about 30% of all drugs on the market. Both the human cannabinoid receptor 1 (hCB_1) and the human adenosine A_1 and A_3 (hA_1 and hA_3) receptors were chosen as prototypical GPCR as well as potential drug targets. Historical aspects of drug-target binding kinetics is also summarized in **Chapter 1**.

In **Chapters 2** and **3**, our binding kinetic study was focused on the human cannabinoid hCB_1 receptor, which is one of the "main actors" in the endocannabinoid system (ECS). In the particular case of obesity, the ECS, including the hCB_1 receptor, is overactive with increased levels of endocannabinoids in plasma, and in central and peripheral tissues. Therefore, blockade of the hCB_1 receptor is a potential approach for the treatment of obesity. Rimonabant, a hCB_1 receptor inverse agonist, was developed by Sanofi-Aventis and introduced on the market in Europe in 2006. However, it was quickly withdrawn from the market due to the risk of unacceptable psychiatric side effects. Although researchers have experienced many setbacks on this drug target, the intensive drug discovery efforts have never been terminated. In **Chapter 2**, we performed an extensive structure- kinetics relationship (SKR) study, in addition to a traditional structure-affinity relationship (SAR) analysis, on a series of 1,2-diarylimidazol-4-carboxamide derivatives developed as hCB_1 receptor antagonists. The compounds show high affinities and a diverse range of kinetic profiles at hCB_1 receptor. In **Chapter 3**, another series of 1-

(4,5-diarylthiophene-2-carbonyl)-4-phenylpiperidine-4-carboxamide derivatives, and rimonabant as a comparison were selected for SKR analysis and further molecular pharmacological investigation. This study shows that hCB_1 receptor antagonists can have very divergent kinetics (the difference in residence time in **Chapter 3** is 159-fold, while 18.5-fold in **Chapter 2**), which are not correlated to their equilibrium affinities. Furthermore, their dissociation rates appear to define their (*in vitro*) pharmacological effect. For both **Chapters 2** and **3**, based on the recently resolved hCB_1 receptor crystal structures, we propose that the differences in dissociation can be explained by a different binding mode of long residence time antagonists compared to short residence time antagonists (i.e. rimonabant) in which "unfavorable" water molecules are displaced. We learned that, next to affinity, additional knowledge of binding kinetics is useful for selecting new hCB_1 receptor antagonists in the early phases of drug discovery for the treatment of obesity.

Next, we explored binding kinetics on the human adenosine A_3 (hA_3) receptor in **Chapters 4** and **5**. The hA_3 receptor has been suggested as a viable drug target in inflammatory diseases and in cancer. So far, a number of selective hA_3 receptor agonists (e.g. IB-MECA and 2-Cl-IB-MECA) inducing anti-inflammatory or anticancer effects are under clinical investigation. In **Chapter 4**, we expand on a series of pyrido[2,1-*f*]purine-2,4-dione derivatives as hA_3 receptor antagonists, and many compounds showed high affinities and a diverse range of kinetic profiles. From a k_{on}-k_{off}-K_D kinetic map we divided the antagonists into three subgroups, providing a possible direction for the further development of hA_3R antagonists. Additionally, we performed a computational modelling study that sheds light on the crucial receptor interactions dictating the compounds' binding kinetics. In **Chapter 5** hA_3 receptor agonists are under binding kinetics investigation. We first validated a kinetic assay for agonists. Then, two series of ribofurano and methanocarba ([3.1.0]bicyclohexane) adenosine derivatives were evaluated for both their affinity and kinetics. Afterwards, a retrospective evaluation linking residence times and *in vivo* efficacies was discussed. Last but not least, from a k_{on}-k_{off}-K_D kinetic map we divided the agonists into three subgroups, providing a possible direction for the further development of hA_3R agonists.

In **Chapter 6**, the application of a novel radio-isotopic technology in binding kinetics is described for the human adenosine A_1 receptor. Compared to the classic radioligand binding experiment, its robustness and potential for high-throughput screening may render this technology a preferred choice for further kinetics studies.

In the last **Chapter 7**, the binding kinetics investigations described in this thesis provide a better and multi-faceted understanding of drug-target interactions, and future perspectives are outlined. Hopefully, all findings from this thesis have brought new insights at a molecular understanding of ligand-receptor binding kinetics, and will offer suggestions for the design of better ligands with an appropriate kinetic profile, new technologies for rapid kinetic assessment, and ultimately suitable evaluation schemes for a better translation towards effective and safe drugs.

Samenvatting

Samenvatting

Dit proefschrift richt zich op het farmacologische concept van drug/target interactie, dat teruggaat tot het begin van de moderne farmacologie. In **Hoofdstuk 1** geeft een algemene inleiding het bewijs dat een op traditionele evenwichts bepalingen gebaseerde redenering (optimalisatie van geneesmiddel-affiniteit leidt tot een betere werkzaamheid en veiligheid) niet in staat is om de huidige hoge uitval in de vroege ontwikkelingen fase van geneesmiddelen te voorkomen. In het afgelopen decennium heeft de bindingskinetiek van het geneesmiddel met het doelwit (met name de associatie- en dissociatiesnelheidsconstanten, en de verblijftijd) meer en meer aandacht gekregen, hetgeen een paradigma verschuiving is om parameters van effectiviteit en veiligheid van een geneesmiddel beter te voorspellen. We besloten om de bindingskinetiek van G-eiwit-gekoppelde receptoren (GPCR) te onderzoeken, aangezien GPCR betrokken zijn bij verschillende belangrijke fysiologische en farmacologische functies, en het doelwit zijn van ongeveer 30% van alle geneesmiddelen op de markt. Zowel de menselijke cannabinoïde receptor 1 (hCB_1) en de humane adenosine A_1- en A_3 (hA_1- en hA_3) -receptoren werden gekozen als prototypes voor een GPCR en als potentiële doelen voor geneesmiddelen. Historische aspecten van de bindingskinetiek van geneesmiddel en receptor worden ook samengevat in **Hoofdstuk 1**.

In **Hoofdstuk 2** en **3** was onze studie van de kinetiek van de binding gericht op de menselijke cannabinoïde hCB_1-receptor, een van de 'belangrijkste actieve onderdelen' van het endocannabinoïdesysteem (ECS). In het specifieke geval van obesitas is de ECS, inclusief de hCB_1-receptor, overactief met verhoogde niveaus van endocannabinoïden in plasma en in centrale en perifere weefsels. Daarom is blokkade van de hCB_1-receptor een potentiële benadering voor de behandeling van obesitas. Rimonabant, een inverse agonist voor de hCB_1-receptor, is ontwikkeld door Sanofi-Aventis en op de Europese markt geïntroduceerd in 2006. Het werd echter snel uit de handel genomen vanwege het risico van onaanvaardbare psychische bijwerkingen. Hoewel onderzoekers veel tegenslagen hebben ondervonden de ontwikkeling van dit medicijn, zijn de intensieve inspanningen

voor het ontdekken van geneesmiddelen nooit gestopt. In **Hoofdstuk 2** hebben we naast een traditionele structuur-affiniteitsrelatie (SAR) -analyse ook een uitgebreide structuur-kinetische relatie (SKR) studie uitgevoerd, betreffende een reeks 1,2-diarylimidazol-4-carboxamidederivaten ontwikkeld als hCB1-receptorantagonisten . De verbindingen vertonen hoge affiniteiten en een diverse reeks kinetische profielen bij de hCB_1-receptor. In **Hoofdstuk 3** werd een andere reeks 1- (4,5-diarylthiofeen-2-carbonyl) -4-fenylpiperidine-4-carboxamidederivaten en rimonabant als vergelijking geselecteerd voor SKR-analyse en verder moleculair farmacologisch onderzoek. Deze studie toont aan dat antagonisten voor de hCB1-receptor een zeer uiteenlopende kinetiek kunnen hebben (het verschil in verblijftijd in **Hoofdstuk 3** is 159-voudig, terwijl 18,5 in **Hoofdstuk 2**), die niet gecorreleerd zijn aan hun evenwichtsaffiniteiten. Bovendien lijken hun dissociatiesnelheden hun (in vitro) farmacologische effect te bepalen. Voor zowel **Hoofdstuk 2** als **Hoofdstuk 3**, gebaseerd op de recentelijk opgeloste kristalstructuren van de hCB_1-receptor, stellen we voor dat de verschillen in dissociatie verklaard kunnen worden door een andere bindingswijze van antagonisten met lange verblijftijd in vergelijking met antagonisten met een korte verblijftijd (zoals rimonabant) waarin "ongunstige " watermoleculen worden verplaatst. We hebben geleerd dat, naast affiniteit, aanvullende kennis van bindingskinetiek nuttig is voor het selecteren van nieuwe antagonisten voor de hCB_1-receptor in de vroege fasen van geneesmiddelontdekking voor de behandeling van obesitas.

Vervolgens hebben we bindingskinetiek onderzocht op de humane adenosine A_3 (hA_3) receptor in **Hoofdstuk 4** en **5**. De hA3-receptor is gesuggereerd als een bruikbaar doelwit voor geneesmiddelen bij ontstekingsziekten en bij kanker. Tot nu toe is een aantal selectieve hA_3-receptoragonisten (bijvoorbeeld IB-MECA en 2-Cl-IB-MECA) die ontstekingsremmende of antikanker effecten induceren, onder klinisch onderzoek. In **Hoofdstuk 4** gaan we dieper in op de eigenschappen van een reeks pyrido [2,1-f] purine-2,4-dion-derivaten als hA_3—antagonisten. Veel verbindingen vertoonden hoge affiniteiten en een breed scala aan kinetische profielen. Van een k_{on}-k_{off}-K_D-kinetische kaart verdeelden we de antagonisten in drie subgroepen, die een mogelijke richting voor de verdere ontwikkeling van hA_3R-antagonisten aangaven. Daarnaast hebben we een onderzoek met een computermodel

uitgevoerd dat licht werpt op de cruciale receptor interacties die de bindingskinetiek van de verbindingen veroorzaken. In **Hoofdstuk 5** is de bindings kinetiek van agonisten voor de hA_3-receptoronderzocht. We hebben eerst een kinetische test voor agonisten gevalideerd. Vervolgens werden twee reeksen van ribofurano en methanocarba ([3.1.0] bicyclohexaan) adenosinederivaten beoordeeld op zowel affiniteit als kinetiek. Daarna werd een retrospectieve evaluatie besproken die verblijftijden en in vivo-werkzaamheid koppelt. Last but not least, van een k_{on}-k_{off}-K_D kinetische kaart verdeelden we de agonisten in drie subgroepen, wat een mogelijke route voor de verdere ontwikkeling van hA_3R-agonisten biedt.

In **Hoofdstuk 6** wordt de toepassing van een nieuwe radio-isotopentechnologie in bindingskinetiek beschreven voor de humane adenosine A_1-receptor. In vergelijking met de klassieke radioligand-bindings assay, kan vanwege de robuustheid en het potentieel voor high-throughput screening aan deze technologie de voorkeur worden gegeven voor verdere kinetische studies.

In het laatste **Hoofdstuk 7** bieden de onderzoeken van de bindingskinetiek, die in dit proefschrift worden beschreven, een beter en veelzijdig begrip van interacties tussen geneesmiddelen en doelen (receptoren), en worden toekomstige perspectieven geschetst. Hopelijk hebben alle bevindingen uit dit proefschrift nieuwe inzichten opgeleverd in het moleculaire aspect van de ligand-receptor bindingskinetiek, en zullen ze suggesties bieden voor het ontwerp van betere liganden met een geschikt kinetisch profiel, nieuwe technologieën voor snelle kinetische beoordeling en uiteindelijk geschikte evaluatieschema's. voor een betere weg naar effectieve en veilige geneesmiddelen.

List of Publications

1: **Xia L**, Kyrizaki A, Tosh DK, van Duijl TT, Roorda JC, Jacobson KA, IJzerman AP, Heitman LH. A binding kinetics study of human adenosine A_3 receptor agonists. *Biochem Pharmacol.* 2018 Jan 3. doi:10.1016/j.bcp.2017.12.026.

2: **Xia L**, de Vries H, Lenselink EB, Louvel J, Waring MJ, Cheng L, Pahlén S, Petersson MJ, Schell P, Olsson RI, Heitman LH, Sheppard RJ, IJzerman AP. Structure-Affinity Relationships and Structure-Kinetic Relationships of 1,2-Diarylimidazol-4-carboxamide Derivatives as Human Cannabinoid 1 Receptor Antagonists. *J Med Chem.* 2017; 60(23): 9545-9564. doi: 10.1021/acs.jmedchem.7b00861.

3: **Xia L**, de Vries H, Yang X, Lenselink EB, Kyrizaki A, Barth F, Louvel J, Dreyer MK, van der Es D, IJzerman AP, Heitman LH. Kinetics of human cannabinoid 1 (CB_1) receptor antagonists: Structure-kinetics relationships (SKR) and implications for insurmountable antagonism. *Biochem Pharmacol.* 2017 Nov 2. doi: 10.1016/j.bcp.2017.10.014.

4: **Xia L,** Burger WAC, van Veldhoven JPD, Kuiper BJ, van Duijl TT, Lenselink EB, Paasman E, Heitman LH, IJzerman AP. Structure-Affinity Relationships and Structure-Kinetics Relationships of Pyrido[2,1-f]purine-2,4-dione Derivatives as Human Adenosine A_3 Receptor Antagonists. *J Med Chem.* 2017; 60(17): 7555-7568. doi: 10.1021/acs.jmedchem.7b00950.

5: Soethoudt M, Grether U, Fingerle J, Grim TW, Fezza F, de Petrocellis L, Ullmer C, Rothenhäusler B, Perret C, van Gils N, Finlay D, MacDonald C, Chicca A, Gens MD, Stuart J, de Vries H, Mastrangelo N, **Xia L**, Alachouzos G, Baggelaar MP, Martella A, Mock ED, Deng H, Heitman LH, Connor M, Di Marzo V, Gertsch J, Lichtman AH, Maccarrone M, Pacher P, Glass M, van der Stelt M. Cannabinoid CB_2 receptor ligand profiling reveals biased signalling and off-target activity. *Nat Commun.* 2017 Jan 3;8:13958. doi: 10.1038/ncomms13958.

6: **Xia L,** de Vries H, IJzerman AP, Heitman LH. Scintillation proximity assay (SPA) as a new approach to determine a ligand's kinetic profile. A case in point for the adenosine A_1 receptor. *Purinergic Signal.* 2016; 12(1): 115-26. doi: 10.1007/s11302-015-9485-0.

7: Massink A, Gutiérrez-de-Terán H, Lenselink EB, Ortiz Zacarías NV, **Xia L**, Heitman LH, Katritch V, Stevens RC, IJzerman AP. Sodium ion binding pocket mutations and adenosine A_{2A} receptor function. *Mol Pharmacol.* 2015; 87(2): 305-13. doi: 10.1124/mol.114.095737.

8: Louvel J, Guo D, Agliardi M, Mocking TA, Kars R, Pham TP, **Xia L**, de Vries H, Brussee J, Heitman LH, IJzerman AP. Agonists for the adenosine A_1 receptor with tunable residence time. A Case for nonribose

4-amino-6-aryl-5-cyano-2-thiopyrimidines. *J Med Chem.* 2014; 57(8): 3213-22. doi: 10.1021/jm401643m.

9: Guo D, **Xia L**, van Veldhoven JP, Hazeu M, Mocking T, Brussee J, IJzerman AP, Heitman LH. Binding kinetics of ZM241385 derivatives at the human adenosine A_{2A} receptor. *ChemMedChem*. 2014; 9(4): 752-61. doi: 10.1002/cmdc.201300474.

10: Gutiérrez-de-Terán H, Massink A, Rodríguez D, Liu W, Han GW, Joseph JS, Katritch I, Heitman LH, **Xia L**, IJzerman AP, Cherezov V, Katritch V, Stevens RC. The role of a sodium ion binding site in the allosteric modulation of the A_{2A} adenosine G protein-coupled receptor. Structure. 2013; 21(12): 2175-85. doi: 10.1016/j.str.2013.09.020.

11: **Xia L**, Zhou M, Xiao Y, Li G, Chen X, Zhang G. Chemical constituents from Helwingia japonica. Chinese Journal of Natural Medicines 2010; 8(1): 16-20. doi: 10.3724/sp.j.1009.2010.00016

12: Wu H, Lin W, **Xia L**, Luo Y, Chen X, Li G, Zhang G, Pan X. 'N-Stereogenic Quaternary Ammonium Salts' from L-Amino Acids: Synthesis, Separation, and Absolute Configuration 2009; 92(4): 677-88. doi: 10.1002/hlca.200800326

Curriculum Vitae

Lizi Xia was born in Luzhou, China, on 4th December 1983. In 2002, after graduating from Shi Shi High School (Chengdu, China), he started his university education at Xiangya School of Medicine, Central South University (Changshang, China), majoring in biopharmaceutical sciences. In 2006 he received a bachelor degree, and then he continued a joint master training in University of Science and Technology of China (USTC) and Chengdu Institute of Biology, Chinese Academy of Sciences (CIB-CAS), majoring in medicinal (natural product) chemistry. After he had graduated as "excellent student", he worked as a medicinal chemist for Shanghai ChemPartner (Chengdu). In the beginning of 2011, he decided to follow a second Master program abroad and move to Leiden University, the Netherlands. During this study he performed two internships at the Division of Medicinal Chemistry, Leiden Academic Centre for Drug Research, under the supervision of Prof. dr. Ad IJzerman, Dr. Johannes Brussee and Dr. Laura Heitman. Both internships were focused on drug-target binding kinetics, from the perspectives of medicinal chemistry as well as molecular pharmacology.

In 2013, Lizi Xia started his PhD training at Leiden University in the same division, under supervision of Prof. dr. Ad IJzerman and Dr. Laura Heitman. His PhD research was part of an Innovative Medicine Initiative (IMI) project named Kinetics for Drug Discovery (K4DD) in collaboration with 20 partners throughout Europe in academia and industry. This consortum was founded to improve the understanding of drug-target binding kinetics. Lizi Xia's research was focused on several G protein-coupled receptors (GPCR). Lizi Xia together with his supervisors developed several valuable collaborations within and beyond K4DD partners, where he experienced the multiple working styles in academia and industry. The fruitful results of his research are described in this thesis and were presented at many international conferences and during webinars. Lizi Xia has an ambition to apply the concept of binding kinetics in a broader setting, and eventually to make his contribution to drug discovery.

Acknowledgements

This thesis has not only been a work of the past four years, but also a fantastic travel log of the kinetic journey in my scientific career. In particular I would like to express my sincere appreciation to my promotors, Ad and Laura. Confucius said, “When I walk along with two others, they may serve me as my teachers.” I am extremely fortunate to have you both as my mentors and supervisors not just these four years, but ever since I came to Medicinal Chemistry many years ago. Ad, I admire you as an eminent scientist, brilliant group leader, as well as the most approachable mentor; your supervision is exactly the modern revelation of Confucius educational ideology, i.e. Education without Distinction. Laura, I got equal amount of inspiration from you and you were the catalyst for my transition from a chemist to a pharmacologist, in one way or another.

I would also like to thank my collaborators within and beyond K4DD for enabling this research and introducing me to many junior and senior passionate and talented scientists dedicating their life and energy to drug discovery. I have learned from you on how to collaborate with both pharmaceutical industry and academia.

Thirdly, I want to express my gratitude to my colleagues for all kinds of help and support. Particularly, I would like to thank Henk, who literally covered my pants when I was still a novice in binding assays. I want to thank Bart for all the beautiful computational work upon demanding request; to Julien, Jaco and Daan for all chemistry-related tasks. Especially, I must give great compliments to my master and bachelor students, Athina, Noortje, Tirsa, Wessel, Cornelia and Ellen, who were involved in parts of this thesis. I want to thank Andrea, Maarten, Xue and Zhiyi, for valuable suggestions regarding manuscript or rebuttal letter preparation.

Last but not least, I specially would like to thank my wife, Yuejiao, for her understanding, support and sacrifices. I particularly owe a great debt to my parents who I was not able to accompany. A PhD training is like a long journey creeping through a tunnel, and so I am deeply grateful to friends worldwide in two interest groups, Doctor Bier and Guokr, that I have been deeply involved in. You all

made my life colorful and enjoyable, and reminded me that the meaning of PhD goes beyond the pages of this thesis.